

**Pathological Mechanisms Underpinning Amelogenesis
Imperfecta in Mice Carrying an Amelogenin Mutation**

Nicola Jo Kingswell

Submitted in accordance with the requirements for the degree of
Doctor of Philosophy

The University of Leeds
Department of Oral Biology
Leeds Dental Institute
School of Medicine and Dentistry

July, 2015

The candidate confirms that the work submitted is his/her own, except where work which has formed part of jointly-authored publications has been included. The contribution of the candidate and the other authors to this work has been explicitly indicated below. The candidate confirms that appropriate credit has been given within the thesis where reference has been made to the work of others.

- Is the 32kDa Fragment the Functional Enamelin Unit in all Species? S.J. Brookes, N.J. Kingswell, M.J. Barron, M.J. Dixon, J. Kirkham, European Journal Oral Science, 2011: 119 (Supplement 1): 345-350

The candidate carried out the work reported in supplemental figure S4(c); and contributed to the writing and final approval of the manuscript.

- A mutation in the mouse Amelx tri-tyrosyl domain results in impaired secretion of amelogenin and phenocopies human X-linked amelogenesis imperfecta. Martin J. Barron, Steven J. Brookes, Jennifer Kirkham, Roger C. Shore, Charlotte Hunt, Aleksandr Mironov, Nicola J. Kingswell, Joanne Maycock, C. Adrian Shuttlecock, Michael J. Dixon, Human Molecular Genetics, April 2010 ; volume 19, number 7: 1230-47

The candidate contributed to dissection of samples, extraction of proteins and optimising the SDS PAGE and Western blot data reported. The candidate also sourced the sequence alignments, and contributed to the writing and final approval of the manuscript.

This copy has been supplied on the understanding that it is copyright material and that no quotation from the thesis may be published without proper acknowledgement.

Assertion of moral rights:

The right of Nicola Jo Kingswell to be identified as Author of this work has been asserted by her in accordance with the Copyright, Designs and Patents Act 1988.

Acknowledgements

I would like to thank my supervisors Professor Jennifer Kirkham and Dr Steven Brookes for their continual help, support and guidance. I would like to thank all the members of the Oral Biology department for their help over the last few years, with particular thanks to Mrs Claire Godfrey, Mr Adam Steel, Dr Sarah Myers, Dr Jo Maycock and Mrs Jackie Hudson.

Special thanks to colleagues at Manchester University including Professor Mike Dixon, Dr Martin Barron and Dr Adrian Shuttleworth.

This research has been funded by the Wellcome Trust. Without their funding, none of this work would have been possible.

Many thanks to my friends and family, for support, retail therapy and listening to me moan. Much appreciated. Special thanks to my Mum for always being there, no matter what.

I will always be eternally grateful for the support of the biotechnology team at Intertek Pharmaceutical Services Manchester. To my American friend, Jeff Beauchaine, for thinking sticks, moral support and proofreading. To Ashleigh Wake for her unwavering belief in me.

Thanks to Drew for all his love, understanding and patience. Love you.

This thesis is dedicated to my Dad, Charles Kingswell (1949-2004), whom I have inherited so much from. He'd have thought this was 'bizzo'!

Abstract

Mice carrying a Y64H amelogenin mutation phenotypically mimic human amelogenesis imperfecta. Affected ameloblasts are characterised by the presence of abnormal cytoplasmic vesicles of retained amelogenin. Protein-protein binding studies using recombinant wild type and Y64H amelogenin revealed that the mutation increased amelogenin-amelogenin binding. This may drive intracellular aggregation of Y64H amelogenin, explaining the abnormal retention. Intracellular protein aggregation causes ER stress which triggers the UPR. The UPR attempts to restore proteostasis but as a last resort triggers apoptosis. SEM of affected enamel showed initially secreted enamel is normal; coincident with UPR in pro-survival mode. The final outer enamel is abnormal; indicative of UPR induced ameloblast apoptosis. Q-RT-PCR was used to measure ER stress related gene expression in affected ameloblasts. Expression levels of ER stress genes increased but not significantly (significance was reached in later studies by others in the research consortium). Amelogenin expression was shown to be significantly reduced in affected ameloblasts; reduced protein expression being a known pro-survival tactic employed during ER stress.

A steady-state *in vitro* mineralisation system was used to examine the effect of the Y64H mutation on mineral nucleation by recombinant amelogenins in isolation or in conjunction with recombinant 32 kDa enamelin. Data showed that the Y64H mutation did not affect the nucleating potential suggesting that the pathological mechanism driving AI in affected mice is linked to ER stress rather than dysfunction of secreted amelogenin.

An unexpected finding was that the 32 kDa enamelin (much lauded in the literature as a functional species) may be unique to pig amelogenesis and its functional significance is therefore debateable

In summary, the mechanism driving AI in these mice is associated with intracellular ER stress. Extracellular dysfunction of mutated enamel proteins has been the focus of AI research but the involvement of ER stress provides additional therapeutic options for treating AI.

Table of Contents

Acknowledgements	iii
Abstract	iv
Table of Contents	v
List of Tables	ix
List of Figures	x
Chapter 1	19
Introduction	19
1.1 Biomineralisation.....	20
1.1.1 An introduction to biomineralisation	20
1.1.2 The chemistry of biomineralisation.....	21
1.1.3 The biology of biomineralisation.....	22
1.1.4 Biomineralisation in dental enamel.....	24
1.2 Structure and composition of the tooth.....	25
1.2.1 Overview of the structure of the tooth.....	25
1.2.2 Overview of enamel composition and structure.....	27
1.3 Tooth development.....	32
1.3.1 Embryological origins	32
1.3.2 Overview of amelogenesis	34
1.3.3 The ameloblasts and amelogenesis.....	34
1.3.4 Enamel matrix proteins.....	38
1.3.5 Non matrix proteins involved in enamel development	58
1.4. Inherited diseases of enamel	60
1.4.1. Amelogenesis Imperfecta.....	60
1.4.2 The Y64H amelogenin mutation in mice.....	61
1.4.2.1 Wild type and mutant (Y64H) mice teeth.....	61
1.4.3 Autosomal dominant amelogenesis imperfecta (ADAI)	68
1.4.4 Autosomal recessive amelogenesis imperfecta (ARAI).....	70
1.4.5 Other genes implicated in amelogenesis imperfecta	71
1.4.6 Syndromic and non-syndromic disease of enamel.....	72
AIMS AND OBJECTIVES	75
Chapter 2	77
General materials and methods	77
2.1 Recombinant protein production	77

2.1.1 Production of recombinant 32 kDa enamelin protein.....	77
2.1.2 Production of recombinant wild type and Y64H mutant amelogenin protein.....	78
2.2 <i>In vitro</i> mineral nucleation studies using recombinant amelogenin and enamelin proteins	85
2.2.1 Steady state agarose gel system	86
2.2.2 Phosphate assay.....	88
2.2.3 Scanning electron microscopy (SEM)	90
2.2.4 Energy dispersive X-ray (EDX) spectroscopy	91
2.2.5 Transmission electron microscopy (TEM)	91
2.3 Protein- protein binding assays	92
2.3.1 Production and labelling of recombinant proteins.....	92
2.3.2 Fluorescein labelling of recombinant amelogenin proteins	92
2.3.3 Bradford assay to determine protein concentration.....	93
2.3.4 Binding assays	93
2.4 Enamelin breakdown studies	95
2.4.1 Extraction of the enamel organ from rat incisors	95
2.4.2 Extraction of the enamel organ from pig molars.....	95
2.4.3 Preparation of enamel samples for enamelin breakdown studies	95
2.4.4 Western blotting of enamel proteins.....	96
2.4.5 Comparison of rat and pig enamelin protein breakdown	97
2.5 Quantitative PCR studies to compare the gene profiles of mice teeth containing the wild type or Y64H <i>Amelx</i> gene.....	98
2.5.1 Collection of mice teeth.....	98
2.5.2 RNA extraction	98
2.5.3 Confirmation of RNA purity.....	99
2.5.4 Transcription of RNA to cDNA.....	99
2.5.5 Confirmation of cDNA purity.....	100
2.5.6 Quantitative real time polymerase chain reaction (Q- RT-PCR)	101
2.6 Scanning electron microscopy (SEM) of mice incisors.....	105
Chapter 3.....	106
Results	106
3.1 Recombinant protein production	106
3.1.1 Recombinant amelogenin protein production	106

3.2 The ability of recombinant amelogenin and recombinant 32 kDa enamelin to nucleate mineral <i>in vitro</i> using a steady-state agarose gel system	111
3.2.1 Visual characterisation of nucleated mineral deposits at the gross level.....	111
3.2.2 Quantification of mineral deposition in agarose gels containing recombinant 32 kDa enamelin	116
3.2.3 Quantification of mineral deposition in agarose gels containing wild type of Y64H recombinant amelogenin.....	119
3.2.4 Quantification of nucleating potential of either wild type or Y64H recombinant amelogenin in combination with recombinant 32 kDa enamelin.....	120
3.2.5 Characterisation of nucleated mineral deposits using scanning electron microscopy (SEM).....	122
3.2.6 Characterisation of nucleated mineral deposits by energy dispersive X-ray spectroscopy (EDX).....	132
3.2.7 Characterisation of nucleated mineral deposits by transmission electron microscopy (TEM)	135
3.3 Studies of 32 kDa enamelin biochemistry in the developing enamel matrix.....	139
3.3.1 Characterisation of the enamelin proteome in secretory and maturation stage rat and pig enamel.....	140
3.3.2 The effect of continued proteolytic processing on the enamelin proteome in secretory stage rat enamel	142
3.3.3 Bioinformatics analysis of enamelin protein sequences across multiple species	144
3.4 Recombinant wild type and Y64H mutant amelogenin protein binding/aggregation studies	145
3.4.1 Adsorption and blocking of recombinant amelogenin proteins to microtitre plates	145
3.4.2 FITC-labelled protein binding	146
3.5 Q-RT-PCR of ER stress genes and amelogenin in wild type and Y64H mutant mice incisors.....	148
3.5.1 Comparison of the expression of ER stress genes in enamel organs of wild type and Y64H mutant amelogenin mice.	148
3.5.2 RNA extraction from mice enamel organs.....	148
3.5.3 Quantitative real time PCR of the transcribed cDNA.....	150
3.6 SEM analysis of Y64H mutant amelogenin mouse incisors	156
Chapter 4.....	162
General discussion.....	162

4.1 Effect of the Y64H mutation on the nucleating potential of amelogenin.....	163
4.2 Nucleation potential of wild type and Y64H mutant recombinant amelogenin	169
4.3 Nucleation potential of recombinant 32 kDa enamelin	169
4.4 Nucleation potential of 32 kDa enamelin in combination with either wild type or Y64H mutant recombinant amelogenin	171
4.5 The assumed role of the 32 kDa enamelin in amelogenesis	172
4.6 Is the 32 kDa enamelin required in amelogenesis?.....	174
4.7 Intracellular effect(s) of the Y64H amelogenin mutation on the ameloblast secretory pathway.....	177
4.8 Effect of the Y64H mutation on amelogenin-amelogenin interactions.....	179
4.9 ER stress, UPR and apoptosis in Y64H ameloblasts	182
4.9.1 Modulation of the UPR	189
4.9.1.1 The IRE1 Pathway	192
4.9.1.2 The PERK pathway	193
4.9.1.3 The ATF6 pathway.....	196
4.9.2 ER stress induced diseases	196
4.10 Scanning Electron Microscopy of wild type and Y64H amelogenin mutant mouse incisors.....	199
4.11 Summary.....	205
Future perspectives	209
Bibliography	212
List of Abbreviations.....	248
Appendix 1 Comparison of mineral nucleating systems.....	251
Appendix 2 Typical profile for Q-RT-PCR from the LightCycler.....	260
Appendix 3 Bioinformatics data for 290 enamelin sequences.....	269
Appendix 4 Posters.....	282

List of Tables

Table 1. CT values for all Mutant (M) and wild-type (WT) AMELX mice incisors for 6 genes. N/D = not detected.....	154
Table 2. Table to show comparison of common features of proteins that have been examined for hydroxyapatite nucleating potential. Note that the frequency of aspartic acid and glutamic acid invertebrate proteins is on average around 6% (Mann, 2001)	166

List of Figures

Figure 1. Diagram of the normal tooth (molar) showing the crown, root and gingival margin. (Ten Cate, 1998).....	25
Figure 2. Histology of developing tooth with enamel, dentine, ameloblasts, and pulp labelled. Tooth bud is in maturation/crown stage. Section of a non-erupted rabbit molar stained with H&E to show different tissue types.....	27
Figure 3. SEM of bovine enamel showing the arrangement of prismatic and interprismatic enamel. Prisms are in transverse section. (Image provided by S.J. Brookes).....	29
Figure 4. Scanning electron microscopy (SEM) image of mouse enamel showing prism decussation.....	29
Figure 5. Transmission electron microscopy (TEM) image of rat enamel crystals in exhibiting am hexagonal cross section. The crystals far left are visualised in longitudinal section (image provided by S.J. Brookes).....	30
Figure 6. Diagram of the different stages of tooth development. The initiation, bud, cap and bell stages are shown with the involvement of the different tissue and cell types at each stage.....	33
Figure 7. Extracellular processing of porcine 25 kDa amelogenin, showing the breakdown to 23 kDa and 20 kDa daughter proteins, and the further processing via the major and minor routes that generate TRAP and low molecular weight fragments (adapted from Brookes et al., 1995)	41
Figure 8. Extracellular processing of porcine enamelin protein showing molecular weights of the breakdown products, from the parent 186 kDa protein to the 32 kDa, 25 kDa and 34 kDa fragments. The 32 kDa breakdown product retains the post translational modifications of phosphorylation and glycosylation.	52
Figure 9. Schematic of the amelogenin gene, showing the genetic location of the identified mutations (g), the resulting protein mutation (p), and the clinical enamel phenotype.	61

Figure 10. Images showing the wild-type and Amelx mice incisors. Wild-type maxillary (panel A) and mandibular (panel B) incisors show smooth enamel, opalescent and orange/brown in colour. Panels C and D show the maxillary (C) and mandibular (D) incisors for heterozygous female mutant mice (Amelx^{X/Y64H}), illustrating patches of rough, chalky enamel. Panels E and F show the maxillary (E) and mandibular (F) incisors for hemizygous male mutant mice (Amelx^{Y/Y64H}), illustrating the whole of enamel surface as rough, opaque and chalky. The mutant mice teeth also show shortened incisors with irregular edges (C-F). Barron et al., 2010. Reproduced under Creative Commons Attribution License. Modified from figure 3 published in: 'A mutation in the mouse Amelx tri-tyrosyl domain results in impaired secretion of amelogenin and phenocopies human X-linked amelogenesis imperfecta' by Barron et al 2010 *Hum. Mol. Genet.* (2010) 19 (7): 1230-1247. Direct link: <http://www.ncbi.nlm.nih.gov/pubmed/20067920>.....64

Figure 11. The structures of tyrosine and histidine amino acids at physiological pH. 67

Figure 12. Hypoplastic enamel due to a mutation in the enamelin gene (photograph courtesy of Roger Shore)..... 69

Figure 13. Schematic diagram of the enamelin gene showing the genetic location of the identified mutations (g), the resulting protein mutation (p), and the clinical enamel phenotype. and the resulting enamel phenotype. 70

Figure 14: The amino acid sequence for the 32 kDa recombinant mouse enamelin. The amino acids in red and underlined are the sites of the post-translational modifications..... 77

Figure 15: Sequence for recombinant amelogenin protein purification. The same procedural steps were used for recombinant wild type and recombinant Y64H mutant amelogenin production..... 79

Figure 16. Schematic diagram of the Bio-Rad PrepCell 491 in action..... 82

Figure 17. Schematic diagram of the flow inside the Bio-Rad PrepCell 491..... 82

Figure 18. Exploded view of the modified dialysis cell used for the steady state agarose gel system. The end buffer reservoir chambers show the in/out ports in blue. A buffer reservoir is visible in each end piece. The central gel chamber piece shows the hole through the middle into which agarose gel is poured. 86

Figure 19. Diagram of a single steady state cell looking down onto the top of the cell. Buffers containing calcium and phosphate are circulated counter currently. The agarose gel in the central gel chamber is separated from the buffer reservoir chambers by dialysis membrane. Agarose gel is present in the centre portion only. Diagram provided by Ashley Firth, Department of Oral Biology.....	88
Figure 20. Picture of a dialysis cell fully assembled, post steady state run. Gel is present in the centre and white mineral precipitate is visible.....	90
Figure 21. Side view of the fully assembled dialysis cell after a steady state run. A band of white mineral precipitate is clearly visible in the centre gel.	90
Figure 22. Coomassie stained SDS-PAGE gel of various fractions of recombinant amelogenin protein obtained throughout the protein purification process. Molecular weight markers are displayed in the left hand lane. The cell lysate contained all the proteins recovered from the E.coli. The post His Trap column shows the protein recovered from the nickel chromatography His Trap column. "Post desalt" shows the protein recovered from the desalting column." Cleaved protein" shows the protein after it had been cleaved overnight at 4°C with HRV 3C. Note that cleavage was not 100% efficient with much of the protein remaining uncleaved. ...	107
Figure 23. Silver-stained SDS-PAGE gel showing fractions of cleaved recombinant amelogenin obtained by preparative SDS-PAGE. MW is the molecular weight ladder and starting protein is the partially cleaved sample. Every third fraction obtained from the prep-cell was run on the gel allowing the fractions containing cleaved protein only to be identified and pooled. Similar gels were obtained for the wild type and mutant amelogenin.	108
Figure 24. Mass spectrometry profile for recombinant wild type amelogenin showing a molecular weight of 20590 Daltons.	109
Figure 25. Mass spectrometry profile of recombinant Y64H mutant amelogenin showing a molecular weight of 20564 Daltons.	110
Figure 26. Panels A, B and C. Typical images of recovered agarose gel plugs showing recombinant 32 kDa enamelin nucleated mineral precipitation. Note the variability of mineral patterns obtained. Each panel represents the triplicates from a different steady-state assay run.	112
Figure 27. Panels A, B and C. Images for bands of mineral precipitation obtained when using 10 µg/mL PGA positive control as the nucleating agent. Variation in band thickness and patterns are evident. Each panel represents the triplicates from a different steady-state assay run.	113

Figure 28. Images for agarose gels containing 10 µg/mL PGA positive control as the mineral nucleator. Liesegang rings are evident.....	114
Figure 29. Panels A, B and C. Images obtained for negative control agarose gel plugs. It is clear that spontaneous nucleation occurred even in the absence of a nucleating agent.....	115
Figure 30. Typical standard curve data generated for phosphate analysis assay. Concentrations from 0 to 100 µM phosphate were used for the standard curve.....	116
Figure 31. Graph showing mean levels of phosphate precipitation for negative control, positive control and recombinant 32 kDa enamel in at various concentrations in the steady state agarose gel nucleation assay. Negative control (no nucleating agent) and positive control (10 µg/mL PGA) n=28, 1 µg/ml, 2.5 µg/ml and 5 µg/ml recombinant 32 kDa enamel n=6, 10 µg/ml recombinant 32 kDa enamel n=10. Statistical significance = p<0.05. Error bars for the standard deviations are also shown.	118
Figure 32. Graph showing the phosphate content of gels containing no added nucleating agent (negative control), 10 µg/mL PGA (positive control), 10 µg/mL recombinant wild type amelogenin or recombinant Y64H mutant amelogenin. Statistical significance = p<0.05. n=6. Error bars for the standard deviations are shown.....	119
Figure 33. Graph showing phosphate precipitated in negative control gels (no nucleating agent), positive control gels (10 µg/mL PGA) , gels containing 10 µg/mL recombinant wild type amelogenin + 5 µg/ml recombinant 32 kDa enamel in, 10 µg/mL recombinant Y64H mutant amelogenin + 5 µg/mL recombinant 32 kDa enamel in, and 5 µg/mL recombinant 32 kDa enamel in. N=6. Statistical significance = p<0.05. Standard deviations are shown.	121
Figure 34. SEM data for crystals nucleated in the presence of 10 µg/mL recombinant 32 kDa enamel in. Panel A shows the crystal morphology imaged at 24750 times magnification. Panel B shows the crystal morphology imaged at 66740 times magnification.....	123
Figure 35. SEM data for crystals nucleated in the presence of 5 µg/mL recombinant 32 kDa enamel in. Panel A shows the crystal morphology imaged at 12850 times magnification. Panel B shows the crystal morphology imaged at 50690 times magnification.....	124

Figure 36. SEM data for mineral crystals from the steady state agarose gel system nucleated in the presence of 2.5 µg/ml recombinant 32 kDa enamelin. Panel A shows the crystal morphology imaged at 24750 times magnification. Panel B shows the crystal morphology imaged at 89840 times magnification. Panel C shows the crystal morphology imaged at 25390 times magnification. Panel D shows the crystal morphology imaged at 65400 times magnification. Note the presence of clusters of small spheres in panels A and B. Panels C and D show smaller crystals exhibiting a different morphology.	126
Figure 37. SEM data for crystals nucleated in the presence of 1 µg/mL recombinant 32 kDa enamelin. Panel A shows the morphology of the crystals imaged at 24600 times magnification. Panel B shows the morphology of the crystals imaged at 64410 times magnification.....	127
Figure 38. SEM images for commercially available hydroxyapatite not exposed to the steady state agarose gel system. Panel A shows the commercially available hydroxyapatite imaged at 12850 times magnification. Panel B shows the commercially available hydroxyapatite imaged at 52850 times magnification.....	129
Figure 39. SEM data for the morphology of the mineral crystals nucleated in the presence of 10 µg/ml PGA recovered after 7 days exposure to the steady state agarose gel system. Panel A shows the crystals imaged at 12850 times magnification. Panel B shows the mineral crystals imaged at 51250 times magnification. Panel C shows the mineral crystals imaged at 24750 times magnification. Panel D shows the mineral crystals imaged at 67150 times magnification.	130
Figure 40. SEM data for mineral crystals recovered from the negative control agarose gels. These were agarose gel plugs without the addition of any recombinant protein or PGA, but that had been exposed to the mineralisation solutions in the steady state agarose gel system. Panel A shows the mineral crystals imaged at 10010 times magnification. Panel B shows the mineral crystals imaged at 68530 times magnification.	131
Figure 41. EDX data for commercially available hydroxyapatite (not exposed to the steady state agarose gel system). A Ca:P ratio of 1.52 was observed (within 10% of the theoretical value of 1.66 for pure hydroxyapatite).....	132
Figure 42. EDX data for agarose blank (agarose gel not exposed to mineralising solutions). Mean Ca:P from 5 steady state agarose gel runs = 0.60 ± 0.12.....	133
Figure 43. EDX data for negative control agarose gels (gels exposed to mineralising solutions). Mean Ca:P from 5 steady state agarose gel runs = 1.05 ± 0.32	133

- Figure 44. EDX data for the mineralised crystals nucleated in the presence of 10 µg/mL PGA positive control for 7 days at 37°C under steady state conditions. Mean Ca:P from 5 steady state agarose gel assay runs = 1.73 ± 0.12 (within 10% of theoretical value for hydroxyapatite)..... 134**
- Figure 45. EDX data for the mineralised crystals nucleated in the presence of 10 µg/mL recombinant 32 kDa enamelin protein for 7 days at 37°C under steady state conditions. Mean Ca:P from 5 steady state agarose gel assay 5 runs = 1.61 ± 0.03 (within 10% of theoretical value for hydroxyapatite)..... 134**
- Figure 46. TEM image of crystals nucleated in the presence of recombinant 32 kDa (5 µg/mL). Note the large, flat planar appearance of the crystals. The crystal at the bottom of the screen measures approximately 4 µm by 0.7 µm. Image taken at 28,000 times magnification. 135**
- Figure 47. TEM image of 2 overlapping crystals nucleated in the presence of recombinant 32 kDa enamelin (5 µg/mL). The smaller crystal measures approximately 0.4 µm by 1.3 µm and the larger crystal 0.7 µm by 1.6 µm. Image taken at 60,000 times magnification..... 136**
- Figure 48. TEM image of crystals nucleated in the presence of PGA (10 µg/mL) following incubation in the steady state agarose gel system. The crystal rosette has a diameter of approximately 2 µm. Image taken at 28,000 times magnification..... 137**
- Figure 49. TEM image of crystals nucleated in the presence of PGA (10 µg/ml) positive control recovered following incubation in the steady state agarose gel system. The top crystal has a maximum diameter of 3.5 µm. Image taken at 60,000 times magnification..... 137**
- Figure 50. Image of commercially available hydroxyapatite crystals. The crystals are more rod like with a length of approximately 0.2 µm. Image taken at 60,000 times magnification..... 138**
- Figure 51 Shows SDS-PAGE (top panels) of rat enamel from secretory through to the maturation stage and pig secretory enamel. The blue stained bands migrating below 25KDa are attributable to amelogenins. The corresponding western blots (bottom panels), probed with anti-enamelin antibody show higher molecular weight enamelin bands in the rat enamel samples. These bands migrate at around 70 kDa. In contrast, the pig secretory enamel contains a prominent enamelin band migrating at 32 kDa (marked *). The results indicate that rat amelogenesis does not involve the generation of a predominant 32 KDa enamelin molecule..... 141**

Figure 52. SDS PAGE and enamelin Western blot using anti-enamelin antibodies of rat secretory stage enamel matrix allowed to degrade over a period of 32 hours. Enamelin components shift to a lower molecular weight but no obvious 32 kDa species is generated.	143
Figure 53. Bioinformatics analysis of the amino acid sequences around the cleavage sites for generating the N terminus sequence cleavage site of enamelin (shown by blue line).	144
Figure 54. Bioinformatics analysis of the amino acid sequences around the cleavage sites responsible for generating the N C terminals of the 32 kDa enamelin in pig. The relevant cleavage sites in pig appear to be unique and are not shared by other species.	145
Figure 55. Results of FITC binding experiments showing 100 µg/mL of unlabelled wild type amelogenin, Y64H mutant amelogenin or BSA bound to a 96-well microtitre plate and interrogated with 100 µg/mL of either wild type or mutant FITC-labelled amelogenin. N =6. Standard deviation error bars are shown.	147
Figure 56. Image of an agarose gel of the extracted mouse tooth RNA. RNA markers are shown on the left, then the RNA for two wild-type mouse incisor enamel organs and then the RNA for two mutant mouse incisors.	149
Figure 57. Image of an agarose gel showing the cDNA PCR product achieved after performing RT-PCR on the RNA extracted from mice enamel organs using the Phire Hot-Start PCR kit from New England Biotech. Full-length amelogenin product at 540bp can be seen for both the wild type and Y64H mutant amelogenin cDNA.	150
Figure 58. Horizontal gel electrophoresis of q-RT-PCR amplicons from Wild-type amelogenin mice incisors enamel organs. BP= base pairs for the New England Biolabs low molecular weight DNA ladder.	151
Figure 59. Horizontal gel electrophoresis of q-RT-PCR amplicons from Y64H amelogenin mice incisors enamel organs. BP= base pairs for the New England Biolabs low molecular weight DNA ladder.	151
Figure 60. Agarose gel stained with Biotium Gel-red stain and viewed under UV light on GelDoc, showing RT-PCR product for extracted RNA with amelogenin forward and reverse primers.	152
Figure 61. Standard curve for <i>Gapdh</i> control. This curve is typical of the data obtained from the Light Cycler 4800 (see appendix for an example of the data obtained). The curve has an efficiency of 1.892 (expected value is approximately 2), a slope of -3.610, a Y Intercept of 31.52, with an error of 0.0203.	152

Figure 62. Typical graph generated by the LightCycler 4800 to show the CP values and amplification of samples. In this case, cDNA transcribed from mice carrying wild type <i>Amelx</i> is amplified for <i>Gapdh</i>.	153
Figure 63. Overall fold change ($\Delta\Delta$CT) for Y64H mutant amelogenin enamel organs compared to wild type amelogenin enamel organs (n=10) Grubbs outlier test applied. Student's two-tailed T test applied to determine upregulation and down-regulation to <i>gapdh</i> housekeeping control.	155
Figure 64. SEM image of a female wild type mouse incisor imaged at 450 times magnification. The decussating interlocking weave pattern of the enamel prisms emanating from the dentine layer is clear. The enamel layer is even in thickness at approximately 75 microns (shown with red arrow).	156
Figure 65. Higher magnification SEM image of the wild type female mouse incisor enamel layer shown in figure 63. The decussating interlocking weave pattern of the enamel prisms emanating from the dentine layer is clear.	157
Figure 66. SEM image of a section through an erupted mouse incisor of a female animal heterozygous for the Y64H amelogenin mutation. Imaged at 450 times magnification. The decussating interlocking weave pattern of the enamel prisms emanating from the dentine layer is clear in the inner enamel, but is lost in the outer enamel layer, shown by the red arrow. ...	157
Figure 67. Higher magnification SEM image of the section through the incisor from the Y64H mutant amelogenin heterozygous female mouse incisor enamel layer shown in figure 65. Note the interface between the normal decussating interlocking weave pattern of the enamel prisms and the abnormal outer enamel layer.	158
Figure 68. SEM image of a section through an incisor from a Y64H mutant amelogenin heterozygous female mouse. This image shows the pieces of the outer enamel structure have broken away leaving an uneven edge (shown with white arrows) suggesting the abnormal enamel is mechanically compromised during mastication.	159
Figure 69. SEM image of a section through an incisor from a Y64H mutant amelogenin homozygous male mouse imaged at 450 times magnification. The enamel layer (thickness shown with white arrows) is shown above the darker dentine layer, but the characteristic prism structure is not visible.	160
Figure 70. SEM image (times 1600 magnification) of the enamel layer for the male homozygous Y64H amelogenin mutant mouse incisor. The characteristic prism structure is not visible.	160

Figure 71. Structure of glutamate and aspartate polycarboxylate sequence.....	164
Figure 72. This figure shows the secretory ameloblast cells of a male Y64H mouse as seen by immunoelectron microscopy. The cytoplasm is abnormally engorged with vacuoles strongly immunoreactive for amelogenin (see black dots in the top right insert). The scale bar is 2 µm; N = nuclei. (Barron et al., 2010). Reproduced under Creative Commons Attribution License. Modified from figure 3 published in: 'A mutation in the mouse Amelx tri-tyrosyl domain results in impaired secretion of amelogenin and phenocopies human X-linked amelogenesis imperfecta' by Barron et al 2010 Hum. Mol. Genet. (2010)19 (7): 1230-1247. Direct link: http://www.ncbi.nlm.nih.gov/pubmed/20067920.....	178
Figure 73. Results of FITC binding experiments showing 100 µg/mL of unlabelled wild type amelogenin or Y64H mutant amelogenin bound to a 96-well microtitre plate and interrogated with 100 µg/mL of either wild type or mutant FITC-labelled amelogenin. N =6. Standard deviation error bars are shown. The cartoon below the graph depicts the hypothesis of the protein-protein interactions.....	181
Figure 74. Schematic diagram of protein synthesis, intracellular trafficking and secretion.....	183
Figure 75. In situ hybridisation: BiP protein in early secretory stage ameloblasts from wild type and Y64H affected female mice. The darker blue staining, indicates clear upregulated BiP expression in affected ameloblasts (arrowed). Reproduced under Creative Commons Attribution License. Modified from figure 3 published in: "Endoplasmic reticulum stress in amelogenesis imperfecta and phenotypic rescue using 4-phenylbutyrate"; by Brookes et al 2014 Hum. Mol. Genet. (2014) 23 (9): 2468-2480. Direct link: http://www.ncbi.nlm.nih.gov/pmc/articles/PMC3976337/).....	187
Figure 76. Diagram to show the protein receptors of the unfolded protein response (UPR) when the cell is in an unstressed state – UPR not activated.	190
Figure 77. Diagram to show the activation of the protein receptors in the unfolded protein response when the cell is in a stressed state – UPR activated.	191
Figure 78. Scanning electron microscopy image of a transverse section through a normal wild type mouse incisor (top panel). A corresponding schematic to show the progress of enamel formation is shown below (middle panel). Note that even in wild type ameloblasts some amelogenin misfolds and the UPR acts to promote cell survival. The UPR is active in wild type ameloblasts (Kubota et al., 2005).	201

Figure 79. Scanning electron microscopy image of a transverse section through a female heterozygous mutant mouse incisor (top panel). A corresponding schematic to show the progress of enamel formation is shown below (middle panel). Note that in affected ameloblasts misfolded amelogenin stimulates the UPR. Initially the UPR promotes cell survival and the initial enamel layer appears normal. With time, the continuing ER stress switches the UPR to promote apoptosis which leads to disruption of the ameloblast layer and malformation of the outer enamel layer. 203

Chapter 1

Introduction

This section is concerned with a review of the current literature pertaining to this thesis. With special reference to dental enamel it provides an introduction to the development of the teeth, the structures of the dental tissues, the process of biomineralisation, the role of the organic matrix and its proteins in biomineralisation, diseases due to protein mutations, and an overview of the crystalline structure of the minerals deposited during tooth enamel biomineralisation.

It is worthwhile to bear in mind the important factors driving research in the field of oral biology and dentistry. Although much is known about the development and formation of dental tissues in many species, including the underlying biochemical processes and genetics, there are still key questions that remain unanswered. The modern diet and lifestyle have shown that there are real requirements for alternative solutions for caries prevention and repair to the common practice of 'drilling and filling'. Achievements in material science and engineering have provided new synthetic materials for caries repair and fillings. Composite materials have become the normal solution for hard-wearing, long lasting and cosmetically pleasing dental fillers. However, could there be an opportunity to include biological materials to encourage enamel to self-repair? If so, which biological materials should, or even could be included to optimise repair of the dental enamel? Recently, self-assembling peptides that can infiltrate early caries lesions and form mineralising scaffolds have been shown to repair early lesions (Brunton et al., 2013). Understanding which of the enamel extracellular matrix proteins are important for mineral nucleation and growth, and the interplay between these proteins could provide further developments in caries lesion repair. This insight could be provided through the study of genetic diseases of mineralisation that effect normal enamel development. Though relatively rare, genetic diseases of enamel formation, amelogenesis imperfecta (AI), can have a major effect on wellbeing and quality of life for sufferers. Understanding the underlying genetic changes and the resulting structural changes in the enamel may shed light on the pathological mechanisms and processes driving AI. Such processes may be targets for drug interventions that allow AI to be treated while enamel is still developing. This thesis is concerned with a mouse model of AI; the genetic mutation involved being linked to the developing enamel matrix protein

amelogenin. The broad aim is to understand the role of amelogenin in amelogenesis in both normal wild type mice and mice suffering from AI linked to an amelogenin mutation.

1.1 Biomineralisation

1.1.1 An introduction to biomineralisation

Biomineralisation is the production of minerals by living organisms, often used to harden or lend mechanical strength to existing tissues. Examples include calcium phosphate in bones and teeth, silicates in algae, and carbonates in diatoms and invertebrates. Overall, the formation of biomineralised tissues in all species (algae, molluscs, mammals and birds) appears to be regulated by the same fundamental processes (Boskey, 2003). Organic molecules are often employed as 'templates' to initiate and control the biomineralisation process. In fact, biomineralisation is known to be under strict controls, but the precise processes involved are yet to be fully understood. There is plenty of evidence that extracellular matrix proteins in mineralised tissues play a major role in the precise location and morphology of mineral crystals (Zhu et al., 2007). The mineralised tissues of the human body vary enormously according to the crystal size and shape, arrangement of the crystals, distribution and amounts of trace ions, and the resulting physiochemical properties (such as solubility and porosity). These variations reflect the functional adaptations of these mineralised tissues (Boskey, 2003).

The evidence for biomineralisation goes back millions of years as demonstrated by the presence of fossils of bones and shells. Biomineralisation involves selecting, extracting and uptake of elements from a local environment, and, under strict biological rules, incorporating these elements into functional structures. It is an interdisciplinary study at the interface of chemistry, biology and material sciences, and impacts on palaeontology, sedimentology, dentistry and medicine. The incorporation of inorganic materials into organic tissues offers structural support and mechanical strength, but also aids protection, motion, cutting, buoyancy, grinding and storage (Mann, 2001; Lowenstam and Weiner, 1989; Simkiss and Wilbur, 1989).

The skeleton is an excellent example of an integrated biomineralisation machine. The structure and organisation of the skeletal tissues derive from a highly complex system, specially evolved to withstand mechanical stress. The biomineralisation of bone, dentine and dental enamel share many similarities, with specific differences for specialised structure and function. The skeletal tissues are

composed of calcium phosphate in the form of hydroxyapatite (HAP) ($\text{Ca}_{10}(\text{PO}_4)_6(\text{OH})_2$), along with proteins. Hydroxyapatite has a complex chemistry in biological systems because the mineral is not pure (non-stoichiometric), often being calcium deficient and enriched in carbonate (CO_3^{2-}) which replaces phosphate (PO_4^{3-}) ions in various lattice sites (Simkiss and Wilbur, 1989). Carbonate can also substitute for hydroxide ions (Barralet et al., 1998) and these substitutions of phosphate or hydroxide by carbonate in hydroxyapatite influence the crystallinity and crystal size. Bone is used by the body as a reservoir for phosphate, calcium and magnesium homeostasis (Palmer et al., 2008).

1.1.2 The chemistry of biomineralisation

Biomineralisation takes place in four biological sites: epicellular (cell wall), intercellular (in the spaces between cells), intracellular (inside cellular compartments) and extracellular (within or on a macromolecular framework outside the cell) (Lowestam, 1981). Most biologically controlled mineralisation processes occur in intracellular or extracellular sites.

There are four fundamental chemical factors governing biomineralisation; solubility, supersaturation, nucleation and crystal growth. A crucial factor in determining the thermodynamic conditions for precipitation is the solubility of the inorganic materials. The extent to which a solution is out of equilibrium is given by supersaturation, which also influences the rates of nucleation and growth. These four factors are chemically controlled in biomineralisation by co-ordinated ion transport and molecular-based promoters and inhibitors (Watabe, 1989).

Solubility refers to the number of moles of an inorganic salt that will dissolve in one litre of solvent at a given temperature. The solubility of an organic salt depends on the balance between crystal lattice energy and ion solvation and complexation in aqueous solution. Solubility is a key factor in the biological mineralisation of calcium phosphates such as hydroxyapatite. Ions such as sodium, magnesium, ammonium, potassium, iron, carbonate and fluoride are easily incorporated into the hydroxyapatite lattice structure (LeGeros 1991). They have a significant effect on hydroxyapatite solubility. An example of this is prevention of tooth enamel erosion by fluoride. Weak acids such as fruit acids in food and juices attack the hydroxyapatite crystals of enamel. If fluoride is present, the dissolved calcium and phosphate ions reprecipitate into the less soluble fluorapatite (FAP). Hydroxyl ions in the HAP lattice are substituted by fluoride ions as saliva is always supersaturated with respect to FAP (Larsen 1975). This substitution changes the mineral solubility

sufficiently to reduce enamel demineralisation and resist caries formation. The solubility product (K_{sp}) is a critical factor in determining the thermodynamic limit for the onset of inorganic precipitation. When the solubility product is less than the activity product (AP) of a solution then precipitation will occur until equilibrium is reached ($K_{sp}=AP$).

A solution is supersaturated when it contains molecules at a higher concentration than is normally possible under a given set of conditions. When a compound is at saturation there is a dynamic equilibrium between ions in the solid phase and ions in solution. At supersaturation, this equilibrium is shifted in the direction of the free ions in solution. Supersaturation can be achieved by chemical reactions, temperature changes, composition changes and changes in ionic activities. Biological systems can fine tune ion transport to achieve the correct supersaturation levels for biomineralisation (reviewed by Mann, 2001). Supersaturation is highly regulated in biology through the process of boundary organised biomineralisation. The activation energy and rate of nucleation are determined by the interfacial energy of the critical nucleus and the level of supersaturation. These factors can be biologically controlled in biomineralisation through the evolutionary design of organic matrices and the membrane regulation of ion concentration gradients (Addadi et al., 1985; Currey, 1984). Biological systems need to regulate supersaturation levels as increases in supersaturation lead to decreases in nucleation activation energy and therefore an increased rate of nucleation. This can cause a sudden 'runaway' in the crystallisation process and a pathological deposition of mineral. The presence of foreign particles, or a suitable surface, can cause increases in nucleation rates at any supersaturation level by so called heterogeneous nucleation. The nuclei are stabilised by attachment to these external substrates. Biological systems use heterogeneous nucleation and overcome any difficulties by regulating the activation energy for nucleation via interfacial interactions (Mann, 2007).

1.1.3 The biology of biomineralisation

Biomineralisation is controlled through the supramolecular organisation of organic templating molecules that determine the shape and size of the mineral deposits and the chemical mechanisms of their deposition (Weiner and Addadi, 1991). Structural control involves the preferential nucleation of a specific crystal face or axis by molecular recognition at the surface of an organic matrix. Morphogenesis involves a patterning process that gives rise to time-dependent

vectorial growth. This gives control over the complex formation of biominerals. Higher order structures are constructed by a series of integrated processes that extend across a range of length scales (Mann, 2001).

The organic matrix provides several functions. In some cases such as bone and dentine, it needs a mechanical design to provide strength and toughness for activity, so that the final biomineralised tissue is 'fit for purpose'. It needs to play a role in mineral passivation; stabilising minerals on the matrix surface. It needs to be involved in mineral nucleation; controlling the location and organisation of nucleation sites, and the structure and orientation of the mineral crystals. Finally the matrix needs to be involved in spatial delineation and organisation; portioning microenvironments to control mineral growth.

Even in the simplest support systems, the incorporation of mineral crystals into the macromolecular framework must be able to resist compression, bending and tension. Such a framework is usually designed to have the minimal amount of material to perform the appropriate function. There are many possible solutions to the actual mechanical structure of the organic matrix using this least-weight approximation, fine tuning of the final design will be performed by the stresses placed upon the matrices during and after synthesis. Matrix rigidity requires cross-linking of strands on connecting fibres or stacks of sheets. The mineral crystals will provide the necessary strength and hardness making the final biomineralised tissue suitable for its intended use.

The constituent macromolecules of organic matrices must be mostly hydrophobic. This is because they are produced in an aqueous environment and if they were not hydrophobic they would dissolve. However, for controlling biomineral nucleation, ions and hydrated species are necessary which would interact with this hydrophobic surface. A general model to encompass both the structural and functional activities of the matrix would be a structural framework of mostly hydrophobic molecules associated with anchored hydrophilic molecules to provide a nucleating surface. This model has been proposed from studies on mineralised extracellular tissues. Collagen, chitin and cellulose are well-documented framework macromolecules. Collagen in particular is key to biomineralisation in bone and dentine. The acidic macromolecules are more difficult to isolate so less information is known about them. They are defined as acidic due to the large numbers of aspartic acid and glutamic acid residues present, and also threonine and serine residues modified with phosphate groups. The acidic macromolecules are often glycoproteins; proteins with covalently linked polysaccharide side chains containing

sulphate and carboxylic acid residues. In bone and dentine, the framework macromolecule is collagen, and the acidic macromolecules include the glycoproteins; osteopontin and osteonectin, the proteoglycans chondroitin sulphate and keratin sulphate, gamma-carboxyglutamic acid (Gla)-containing proteins and osteocalcin. In dental enamel, the major framework protein macromolecule is amelogenin, and the acidic macromolecule is enamelin (Mann et al., 2001).

1.1.4 Biomineralisation in dental enamel

Mature dental enamel is the hardest substance in the human body due to its high mineral content (over 95% by weight) and it is a highly organised structure. The formation of enamel, the process known as amelogenesis, is the result of a highly orchestrated series of extracellular processes that control the nucleation, growth and organisation of forming mineral crystals. Vertebrate biomineralised tissues, such as tooth enamel, dentine, cementum and bone, all contain crystalline mineral with a similar chemical composition and atomic structure to hydroxyapatite (Margolis et al., 2006).

Biomineralisation in dental enamel obeys the underlying laws of chemistry and depends on the precipitation of the calcium phosphate mineral salts from biological fluids, supersaturated with respect to the mineral phase, followed by a period of subsequent crystal growth. As described previously this process is thought to be initiated and controlled by the extracellular matrix proteins. The ECM is presumed to provide the required stereochemical template that provides the initial nucleation site for mineral deposition whilst also serving to regulate and direct any subsequent crystal growth occurring (Addadi and Weiner, 1985).

Dental enamel, the main focus of this thesis, is unique in that the ECM is not a collagenous matrix like in bone, dentine and cementum but a specialised enamel matrix which orchestrates the process of enamel formation. The unique nature of the developing enamel proteins is reflected in the mature tissue itself as enamel is the most highly mineralised tissue in mammalian biology and in contrast to other mineralised tissues; it is acellular and cannot be naturally remodelled. It is assumed that enamel biomineralisation can act as a paradigm for biomineralisation in general (Currey, 1984; Mann, 2001).

1.2 Structure and composition of the tooth.

1.2.1 Overview of the structure of the tooth

The developing tooth is a useful tool for investigating the underlying processes involved in biomineralisation in mammalian systems. Biomineralisation in the tooth, as in all skeletal tissues, involves the ordered deposition and controlled growth of inorganic crystals on organic protein matrices to form tissues with specialised structures and functions. There are a number of components to human teeth that are ideal to for these investigations. Teeth comprise of three distinct mineralised tissues; enamel, dentine, and cementum, together with the non-mineralised pulp tissue (figure 1).

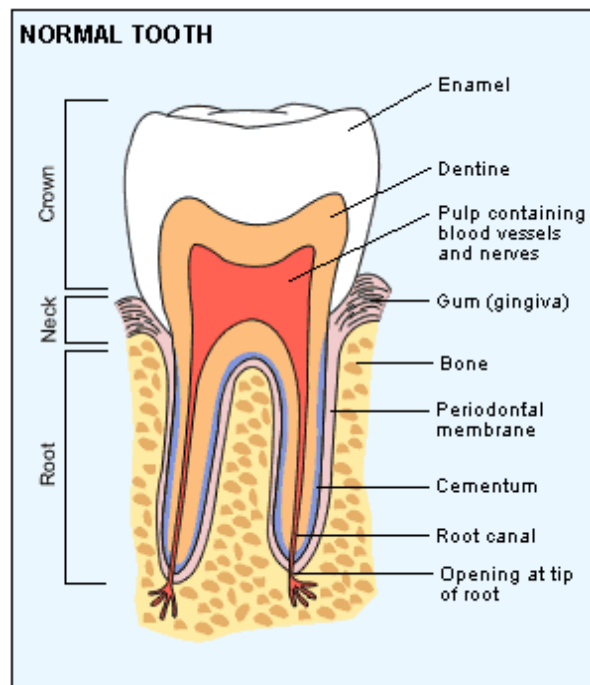


Figure 1. Diagram of the normal tooth (molar) showing the crown, root and gingival margin. (Ten Cate, 1998).

Enamel, the most highly mineralised tissue in the mammalian body, covers the crown, the exposed surface of the tooth and provides a hard surface for biting and chewing. Dentine, located underneath the enamel layer, is less mineralised than enamel but is a useful paradigm for bone construction. Dentine has tiny tubes (dentinal tubules) running from the pulp cavity outwards which are filled with the odontoblast processes. The dentinal tubules are also involved in pain sensation. Their exposure results in tooth sensitivity. In the centre of the tooth is the pulp cavity, which houses the dental pulp. The pulp is a soft tissue organ which includes the blood vessels to supply the tooth with nutrients to keep it alive, and nerves

which sense pressure and pain. The cementum covers the root dentine in the jaw and provides anchorage for the periodontal ligament to keep the tooth in place. (Bosshardt and Nanci, 1997; Berkovitz et al., 2009).

Though not part of the tooth, the periodontum consists of several different cell types, namely fibroblasts (cells that secrete the extracellular matrix and collagen of connective tissues), cementoblasts (cells that secrete cementum at the root of the tooth), osteoblasts (cells that secrete bone tissue), osteoclasts (cells that resorb bone tissue), macrophages (immune cells that engulf cell debris and foreign particles) and epithelial cells (cells that form the soft tissues). It is a connective tissue comprising of collagen, proteoglycans, glycoproteins and oxytalan (pre-elastin). The extracellular matrix (ECM) of the periodontum consists mainly of fibrils of type I collagen, typical of most soft connective tissues. The fibroblast cells secrete and degrade this ECM. Between the collagen fibrils is a ground substance composed of the proteoglycans, glycoproteins and other minor components. Islands of epithelial cells can be found within the periodontum. These are known as the 'cell rests of Malassez' and are remnants of the development processes of the tooth root (Ten Cate, 1998).

The development of the tooth is a multi-stage process during which teeth form from embryonic cells, and following the process of odontogenesis, erupt into the mouth. Many diverse species have teeth and the underlying processes for tooth development are largely conserved across all species. Enamel, dentine and cementum must all develop during the appropriate stage of development for healthy teeth. In humans, primary teeth start to form between 6 and 8 weeks *in utero* and the permanent dentition begins to form in the 20th week (Ash et al., 2003).

The tooth bud is an aggregation of cells, also referred to as the tooth germ, that eventually forms the tooth. The tooth bud consists of 3 parts; the enamel organ, the dental papillae and the dental follicle. The outer enamel epithelium, the inner enamel epithelium, stellate reticulum and the stratum intermedium all work together to make up the enamel organ. The inner enamel epithelium cells eventually form the ameloblast cells which secrete the enamel matrix proteins. The growth of the cervical loop cells into the surrounding tissues forms the Hertwig's epithelial root sheath (HERS) which determines the shape of the tooth root. The dental papillae encompass cells that eventually form the odontoblasts cells, the cells that form dentine. The junction between the dental papillae and the inner enamel epithelium, the dentine-enamel junction (DEJ) determines the shape of the crown. The dental follicle gives rise to the cementoblast cells that form the cementum of the tooth, the

osteoblast cells that form the alveolar bone around the roots, and the fibroblast cells that form the periodontal ligament. The cementum overlays the radicular dentine. The periodontal ligament connects the tooth to the alveolar bone (Ten Cate, 1998). A histological slide of the tissues and cells in a rabbit molar is shown in figure 2.

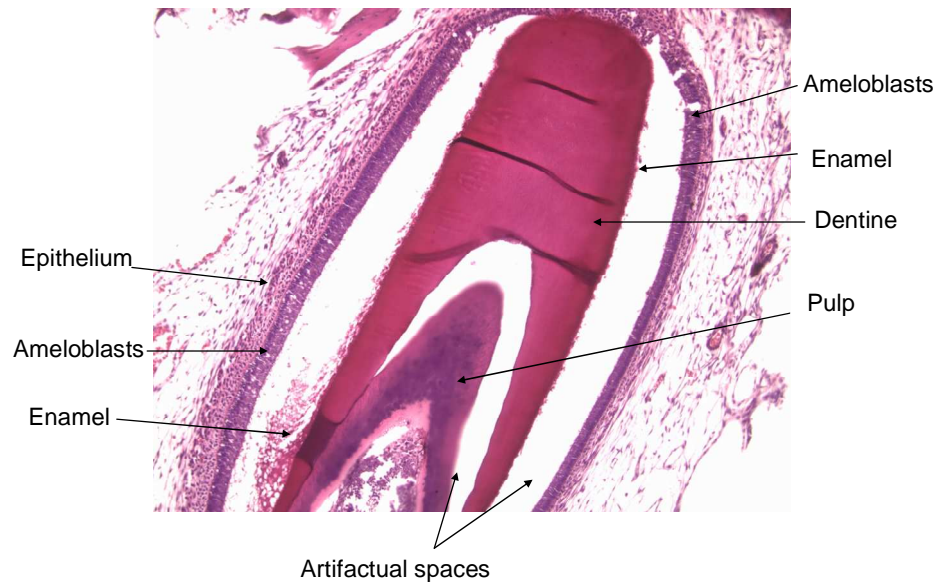


Figure 2. Histology of developing tooth with enamel, dentine, ameloblasts, and pulp labelled. Tooth bud is in maturation/crown stage. Section of a non-erupted rabbit molar stained with H&E to show different tissue types.

1.2.2 Overview of enamel composition and structure

Mature tooth enamel covers the visible parts of the erupted tooth in the mouth. It is not present on the roots of the teeth. Physically, tooth enamel is very hard and brittle. It relies on the underlying dentine for resilience. The microstructure of enamel has evolved to prevent fractures and shear within it. Enamel is translucent and the colour of the tooth is dictated by the dentine. Teeth appear to yellow with age due to the thinning of the enamel through wear allowing more of the dentine to be visible. Chemically, mature enamel is composed of 96-99% by weight hydroxyapatite mineral ($\text{Ca}_{10}(\text{PO}_4)_6\text{OH}_2$), a naturally occurring form of calcium apatite, with 3% water and 1% organic matter (non-collagenous protein) (Lowenstam and Weiner, 1989). The apatite minerals are a group of phosphate minerals formed and utilised in biological systems, defined by their high concentrations of OH^- ions (hydroxyapatite), F^- ions (fluoroapatite) or Cl^- ions

(chloroapatite) in the mineral crystal (Boivin 2007). Hydroxyapatite is the same mineral found in bone and dentine, although the hydroxyapatite crystals in enamel are much larger, elongated and less carbonated (Daculsi et al., 1984). The mineral content of dentine and bone is less at 65-70% by weight (Goldberg et al., 2011).

The composition of enamel is variable, between and within teeth, due to developmental factors and the effects of exposure in the mouth. Minor constituents of mature enamel typically include 3.0% w/w carbonate, 0.4 % w/w chloride, 0.2 % w/w magnesium, 0.01 % w/w fluoride and other trace elements (Elliot et al., 1994). The exact composition can vary with depth within the tissue. For example, from the surface towards the enamel-dentine junction, there is an increase in carbonate and magnesium concentration that parallels a decrease in crystallinity (Legfros et al., 1996). The concentration of fluoride, in contrast, is highest at the enamel surface and declines extremely rapidly with depth (Hallsworth and Weatherell, 1969). Margolis and Moreno (1990) calculated that up to 26% of hydroxyl ion sites are substituted by fluoride at the outer enamel surface. Developing enamel contains a high proportion of proteins which are progressively removed as the tissue matures, with the protein content dropping from approximately 20% in the developing enamel (Eastoe 1964) to less than 1% (Robinson et al., 1981; Simmer and Fincham, 1995) weight for weight. Fluoride is readily incorporated into hydroxyapatite, stabilising the lattice and reducing the solubility of the mineral phase (Cooper and de Leeuw, 2004).

It is difficult to accurately determine the percentage of water in enamel and its distribution between the mineral and organic phases. The mean values of these are usually given as 95% weight and 86% volume (Angmar et al., 1963), but have more recently been recalculated as 98% weight and 96% volume (Elliott et al., 1998). Water within enamel provides the medium for diffusion of ions in de- and re-mineralization, therefore knowledge of the volume fraction is fundamentally important. At the start of a caries lesion forming, there is a preferential loss of carbonate (Hallsworth et al., 1973) and magnesium (Hallsworth et al., 1972). Increased fluoride concentration is found in caries lesions (Hallsworth and Weatherell, 1969), with variably elevated levels (maximum detected 21,700 ppm) in the surface zone (Pearce et al., 1995). In mature enamel, magnesium-containing whitlockite crystals, identified by SEM and electron probe microanalysis, found in lamellae have been associated with dissolution and reprecipitation of mineral in caries (Kodaka et al., 1992).

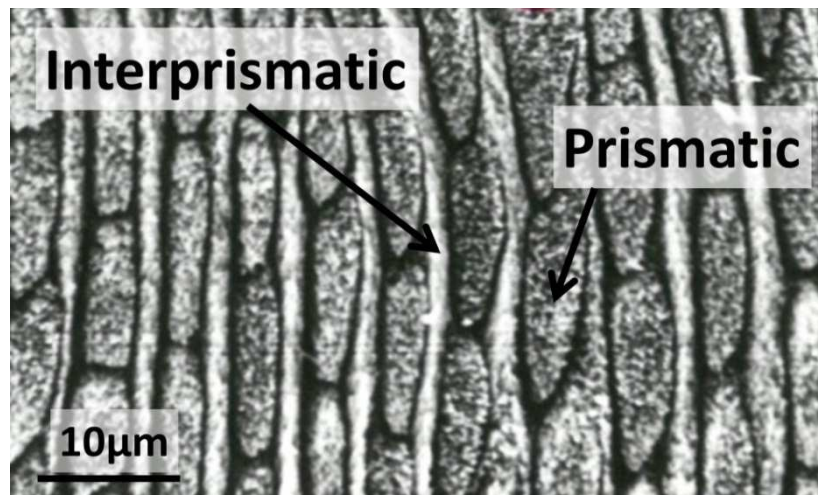


Figure 3. SEM of bovine enamel showing the arrangement of prismatic and interprismatic enamel. Prisms are in transverse section. (Image provided by S.J. Brookes).

In humans, the distinction between prismatic and interprismatic enamel is not as clear as in bovine enamel (figure 3), with the apical surfaces of the prisms being continuous with the apical surfaces of the interprismatic enamel.

In rodent incisor enamel, the prisms decussate with interprismatic enamel weaving between the ordered layers of prismatic enamel (figure 4). This structural difference may allow the rodent incisors to fracture at the biting edge along controlled fracture planes corresponding to the rows of decussating prisms running transversely across the incisor such that a sharp chisel like biting edge is maintained by wear.

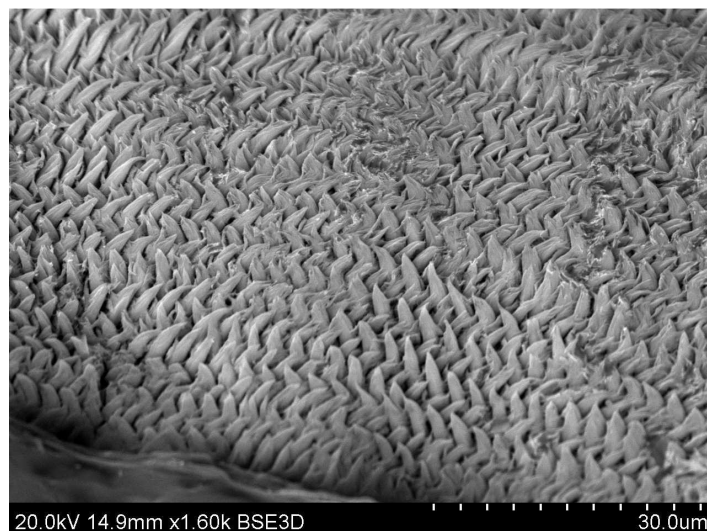


Figure 4. Scanning electron microscopy (SEM) image of mouse enamel showing prism decussation.

The developing hydroxyapatite crystals forming the prismatic and interprismatic enamel appear to have a roughly hexagonal cross-section (figure 5) with a width of 60-90 nm, thickness of 25-30 nm and a length that may span the entire enamel thickness unbroken (Arends & Jongebloed 1978; Kerebel et al., 1979).

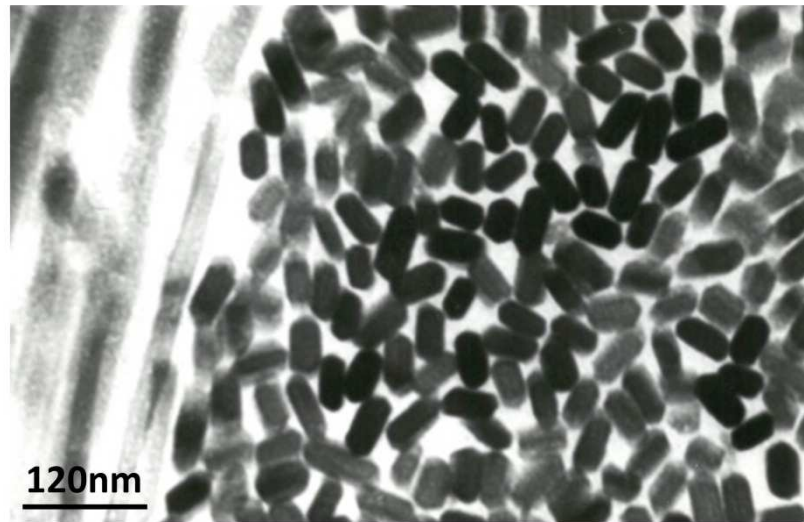


Figure 5. Transmission electron microscopy (TEM) image of rat enamel crystals in exhibiting am hexagonal cross section. The crystals far left are visualised in longitudinal section (image provided by S.J. Brookes).

That said, enamel crystal morphology is disputed and the hexagonal shape apparent when viewing enamel sections using TEM may be a shadowing artefact created by sections taken through rectangular crystals. In any event, the hydroxyapatite crystals of mature enamel tend to be less regular in appearance as they keep growing to fill all the available space and may have undergone repeated episodes of de- and re-mineralisation though the crystals are still arranged into prisms (Warshawsky et al., 1987).

The enamel forming ameloblasts secrete a proteinaceous extracellular matrix (ECM) on the dentine surface, and as they migrate away from the dentine the enamel matrix left behind partially mineralises with immature hydroxyapatite crystals which grow lengthwise in pursuit of the retreating ameloblasts (Garant, 2003). The amount of ECM secreted therefore defines the thickness of the mature tooth enamel. Enamel secretion is associated with circadian rhythms resulting in regular, daily cross-striations with a 5 μm periodicity in humans (Fitzgerald and Verveniolis, 1998). When viewed microscopically, these cross-striations run parallel to the long axis of the tooth. Many researchers have stated that these cross-

striations are a result of the metabolic activity of the ameloblasts over 24 hour periods (Risnes, 1986; Dean, 1987, 1989; Boyde 1989, 1990). Experiments using lab primates of known ages injected with markers have shown good correlation of the cross-striations with circadian rhythms and therefore a potential tool for determining age from crown formation (Mimura, 1939; Bromage, 1991; Dean, 1998; Smith, 2006), Despite this evidence, other researchers have claimed these correlations to be nothing more than a fluke and a source of error in determining age from teeth (Warshawsky et al, 1984; Mann et al., 1990). Analysis of the teeth from 5 children exhumed from a 19th Century London crypt was performed by Antonine et al., 2009. The age of the children was known but kept from the researchers. Microscopic analysis of the permanent dentition of the children showed that the formation of the cross-striations do follow circadian rhythms in the ameloblast cells, allowing the ages of the children to be correctly identified.

There are also less frequent incremental striations, the Striae of Retzius (SR), which appear as brown lines in the enamel when viewed microscopically. Where the SR terminate on the enamel surface, pits appear known as perikymata (Beynon and Dean, 1988). These are most noticeable on the surface enamel of canine teeth, and become less visible as the enamel is worn and smoothed. These grooves and pits have been used to try to determine times of crown formation, enamel growth patterns and even used in archaeology to try to determine the age of a human at death (Reid et al., 1998; Antoine et al., 2000; Reid and Ferrell, 2005). The SR appear at regular intervals, similar to the daily cross-striations, signifying changes in the ameloblasts activity. However, darker banding may occur when significant stress of illness has occurred, implying that the SR may also be affected by physiological strains, similar to the Andresen lines in dentine (Dean and Scandrett, 1996).

Mature enamel can resist acid attack due to the lack of organic material (Weatherall, 1975). This removal of the organic matrix leaves a strong, tough, inorganic surface for mastication, but also means that lost enamel tissue cannot regenerate as the ameloblasts completely disappear once the enamel has matured and erupted (Sasaki and Garant, 1986). In the mouth, the surface of enamel is in a constant flux of demineralisation and remineralisation. Consumption of acidic food or beverages such as fruit, juices and carbonated beverages or the presence of plaque acids produced by bacterial metabolism cause a reduction in mineral density due to demineralisation within the outer surface of the enamel. This can lead to erosion and caries respectively. The saliva contains mineral ions at supersaturated

levels and can remineralise the outer surface of enamel to some extent though lost tissue cannot be replaced (Ten Cate and Duijsters, 1982).

Once the ameloblasts stop secreting ECM, the ECM in the enamel is removed by proteases, creating space for the immature HAP crystallites to undergo secondary mineralisation and grow in width and thickness until the space is largely occluded by mineral (Bartlett et al., 2003). This is described in more detail later (See section 1.3.4)

1.3 Tooth development

1.3.1 Embryological origins

Teeth are ectodermally-derived organs, similar to hair, nails, scales and feathers, whose development relies on epithelial-mesenchymal interactions mediated by conserved signalling pathways present in other tissue developmental processes. Teeth develop as a combination of ectoderm and mesenchyme based upon continuous and dynamic reciprocal signalling interactions (Pipsa and Thesleff, 2003). The development of most ectodermal organs begins in the same way, with a thickening of the epithelium. This is the initiation stage, where in teeth, the dental placode forms. The epithelium then buds into the mesenchyme and neural-crest derived mesenchyme condenses around the epithelium. This is known as the bud stage. Many ectodermally-derived organs share similarity at the bud stage, with specificity elicited at the transition in the next stage (Jernvall and Fortelius, 2000). The inside of the tooth bud contains the stellate reticulum cells that secrete glycoaminoglycans (GAGs). As the GAGs are secreted, water is drawn in between the cells, stretching them apart. Cells of the stellate reticulum maintain contact with one another via desmosomes, giving them their unique star-shaped appearance as they are stretched apart (Yildirim, 2013). In teeth, the next stage is known as the cap stage. The cap is formed by growth and folding of the epithelium (Koussoulakou et al., 2009). Here the cervical loop is formed which will form the stem cell niche in continuously growing teeth, or the Hertwig's epithelial root sheath (HERS) in teeth with limited growth. The inner enamel epithelium (IEE) is formed inside the cap bordering the dental papillae, and consists of a layer of columnar cells. The outer enamel epithelium (OEE) covers the outer part of the cap and is a layer of cuboidal cells located on the periphery of the enamel organ (Marson et al, 2005). The next stage is the bell stage where more extensive growth and folding of the dental epithelium occurs. This folding corresponds to the final cusp pattern of the teeth, determining the function of the tooth. The stratum intermedium is a layer

of 2 to 3 cells in thickness between the inner enamel epithelium and the stellate reticulum. It is first seen early in the bell stage, at approximately 14 weeks *in utero*. The ameloblast cells differentiate from the IEE and the odontoblasts differentiate from the dental papillae. This differentiation is regulated by epithelium and mesenchyme interactions (D'Souza, 2002, Nanci, 2008,). At this stage, all structures are still part of the crown. The roots are formed during post-natal development. The cervical loops undergo structural changes, where the HERS fragments into a fenestrated network of epithelial cells named the Epithelial Rests of Malassez (ERM). See figure 6 for an overview of tooth embryological development.

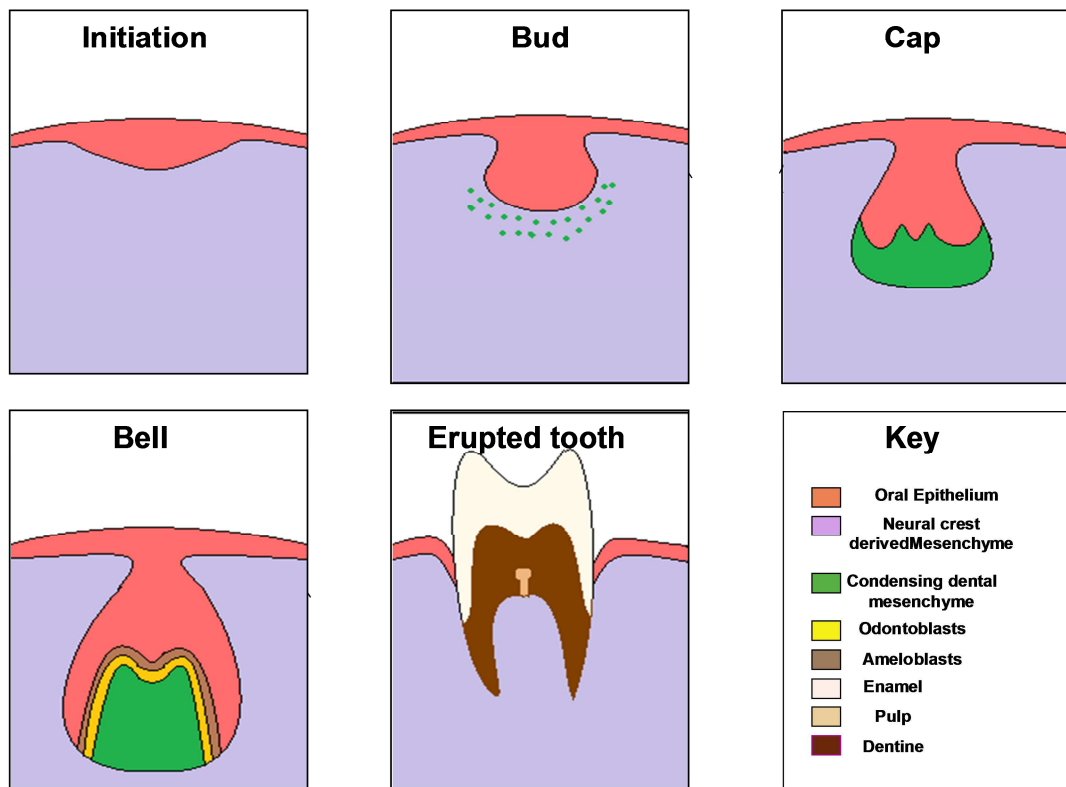


Figure 6. Diagram of the different stages of tooth development. The initiation, bud, cap and bell stages are shown with the involvement of the different tissue and cell types at each stage.

Defining these stages of tooth development is an attempt to describe changes that actually occur along a continuum. Development is not really divided into developmental “snap shots” and so it can be difficult, even histologically, to identify which stage of development a tooth is in. The dental papilla consists of the condensed ectomesenchymal cells, and is separated from the enamel organ by the

basal lamina. The dental follicle covers the enamel organ and dental papilla, and the dental follicle, dental papilla and the enamel organ are collectively known as the tooth germ. The dental papilla is the source of the pulp in a tooth, and the dental follicles differentiate to produce the odontoblasts cementoblasts, osteoblasts and fibroblasts (Yildirim, 2013).

1.3.2 Overview of amelogenesis

As described in the previous section, the development of the tooth requires epithelial – mesenchymal interactions, reciprocating between the differentiating odontoblasts of the dentine and the differentiating ameloblasts of the enamel organ (Ruch et al., 1995). The process whereby the ameloblast cells form the tooth enamel is known as amelogenesis and this section will describe that process. Ameloblasts only become fully functional after the first layer of dentine has formed and in turn it has been hypothesised by Nanci, 2008, that the ameloblasts may secrete growth factors or other proteins that influence the terminal differentiation of the odontoblast cells, possibly by interactions with the basement membrane.

During amelogenesis, ameloblasts pass through discrete development stages that correlate with the various stages of enamel formation. This occurs in 3 stages; the secretory stage, the transition stage, and the maturation stage.

1.3.3 The ameloblasts and amelogenesis

The ameloblast cells secrete extracellular enamel matrix proteins, such as amelogenin, enamelin and ameloblastin, which mineralise to form enamel (Simmer et al., 2010). The ameloblast cell morphology is changeable and dependent upon the stage of activity the cell is in. The ameloblast cell in the secretory stage is 4 µm in diameter and 70 µm in length while the ameloblast cell in the maturation stage is approximately 40 µm in length (Reith 1970). The secretory end of the ameloblast cells ends in a 6-sided pyramidal projection known as the Tomes' process, giving the ameloblast cells in the secretory stage a hexagonal appearance (Avery 2011). The angulation of the Tomes process determines the orientation of the enamel prisms. The ameloblasts form as a single layer on the newly formed dentine layer and progressively move away from the dentine, secreting enamel proteins into the space they leave behind as they progress. The ameloblast cells control the ionic and organic composition of the enamel by adjusting their secretory and resorbative

activities to maintain favourable conditions for biomineralisation (Berkowitz et al., 2009).

Once the first layer of dentine is formed, it induces the adjacent preameloblasts to complete their differentiation into ameloblasts and secrete enamel. The secretory ameloblasts are polarised, tall, columnar cells with Tomes' processes (conical shaped processes) at their distal ends. Tomes' processes interdigitate with the surface of the forming enamel giving it a picket fence appearance (Warshawsky et al., 1987). The Tomes' processes determine the orientation of the newly formed (nucleated) enamel hydroxyapatite crystals. The organelle content of the secretory ameloblasts is mainly protein synthesising organelles such as the Golgi complex and granular Endoplasmic Reticulum. Plentiful mitochondria and secretory granules are also present. Junctional complexes, tight junctions and desmosomes are present at the distal and proximal ends of the ameloblasts. Desmosomes and gap junctions are also present at the ameloblasts lateral surfaces. Towards the end of the secretory stage, the Tomes' processes are lost, and the last formed layers of enamel are prismless accordingly (Smith 1998). When ameloblasts are forming new enamel, their Golgi apparatus is extensive and occupies much of the supranuclear compartment (Nanci et al., 1993; Smith and Nanci, 1996). The secretory granules are directed to two spatially separate secretory sites, located on the Tomes' process, an apical extension. Here they release their contents constitutively to build up interprismatic and prism enamel (Nanci and Warshawsky, 1984).

It has been postulated that amelogenesis occurs in 5 distinct phases. Phase 1 is the secretory stage. Here the enamel proteins are synthesised, secreted and become partially mineralised (nucleation of the crystals, approximately 30% mineralised). Unlike other mineralised tissues such as bone or dentine, there is no non-mineralised 'pre-enamel' (Hu et al., 2007). The crystals are elongated but extremely thin in width and thickness and are supported by the matrix. During this stage the metalloproteinase 20 (MMP-20) is co-secreted which processes the enamel proteins to generate a complicated spectrum of discrete processing products. At some point protein secretion all but stops and the ameloblasts cease their migration. It has been hypothesised that the ameloblasts spend approximately 300 days in the secretory stage before moving into the maturation stage (phase 5) and begin degradation (Hillson, 1986).

Phase 2 is the assembly of amelogenin into nanospheres (covered in section 1.3.4.1.2) and phase 3 is the subsequent formation of elongated ribbon like crystallites (section 1.3.4.1.2).

Once the dental enamel reaches its full thickness, the ameloblasts enter a brief transitional stage. Their height is decreased, by approximately 50% to 40µm, and protein synthesising organelles are dramatically reduced in number (Smith and Nanci, 1996). The Tomes' processes are also removed (Reith, 1970). Many lysosomes and autophagic vacuoles are also present. The transition stage is characterised by a reduction in the ameloblast numbers, by as much as 50%, via apoptosis. Ameloblast morphology also changes, from that of secretory cells to that of one similar to epithelial cells involved in ion transport (Smith, 1998). This is the fourth phase and is characterised by the resorption of the organic matrix and its replacement with fluid.

The fifth phase is the maturation stage and is characterised by the loss of enamel ECM proteins and water, and by a massive influx of calcium and phosphate mineral ions, which provide for growth of hydroxyapatite crystals (96% mineralisation) (Berkowitz et al., 2002).. Ameloblasts now begin to secrete catalytic amounts of the serine protease kallikrein-4, which quickly degrades residual matrix proteins leaving behind the crystal architecture previously 'sketched out' in the secretory stage bathed in fluid (enamel fluid) (Tanabe, 1984). At the beginning of the maturation stage the crystals occupy about 30% of the tissue volume but the ameloblasts begin pumping mineral ions into the enamel fluid which promotes growth in width and thickness of the crystals until they eventually occlude more than 90% of the tissue volume in readiness for the tooth to erupt into the mouth (Robinson and Kirkham, 1986). Ultimately the ameloblasts atrophy and the cellular layer is lost entirely from the mature erupted tissue (Kim et al., 2008). Thus, throughout amelogenesis, ameloblast cells control the ionic and organic composition of the enamel by adjusting their secretory and resorptive activities to maintain favourable conditions for biomineralisation (Berkowitz et al., 2009). The maturation stage is the phase where most mineralisation occurs, though the exact timings and mechanisms in the process are not yet fully defined due to complexity of amelogenesis (Suga, 1989).

Unlike collagen based calcified tissues, such as bone, enamel matrix proteins are almost completely degraded by extracellular enzymes (Smith, 1998). This means that enamel achieves its high mineral content through a maturation process. The ameloblasts alter between two phenotypes depending on the morphology of

their distal ends. Numerous microvillae in the ameloblasts distal ends form either a ruffled end (RE), or an even, straight edge (SE). In the rat incisor, 60% of maturation ameloblasts are found in the ruffle-ended morphology, 20% are in the smooth-ended form, and twenty percent are transitional (Takano, 1995). The extracellular fluid related to the RE ameloblasts is acidic (as low as pH 5.8). The extracellular fluid in enamel related to the SE ameloblasts is of more neutral pH (pH 7.2). In rodent incisors, the SE ameloblasts are only present for a short duration (20% of cycle time), before they recreate the RE form. Some mammals have three cycles per day (RE – SE – RE, every 8 hours) (Avery, 2002). These two morphologies are grouped into alternating bands during maturation.

Ameloblasts lose their differentiation and become short, cuboidal cells which form a multi-layered structure with other layers of the dental organ, known as the reduced enamel epithelium (Sasaki, 1984). This structure remains on the surface of the newly formed dental enamel until the tooth erupts into the mouth. The reduced enamel epithelium separates the enamel from the dental sac, protecting it from contact with connective tissues in the dental sac. If contact between the newly secreted enamel and the dental sac accidentally occurs, the enamel can be resorbed at the contact area resulting in pitting, or the dental sac cells differentiate into cementoblasts and secrete cementum on the enamel surface. The reduced dental epithelium and the oral epithelium jointly form the dentinogingival junction (DGJ) of the erupting tooth.

The complete removal of the ECM in mature enamel is an interesting conundrum in itself. Is it possible that the enamel proteinases are so efficient that they remove all but a few very short peptides of the ECM to allow almost complete mineralisation of the enamel? It has been proposed that the ameloblast cells remove the enamel matrix as efficiently as they secrete it. It is likely that the processes of diffusion, pinocytosis and endocytosis cooperate to remove the ECM during enamel biomineralisation.

There is great variation between animal models with regards to enamel formation therefore a precise model for human enamel formation remains elusive (Boyde 1997). SEM, X-ray crystallography and position sensitive synchrotron X-ray diffraction of archeological human tooth samples at varying stages of enamel maturation have shown an inverse correlation between mineral content distribution and variations in crystallographic parameters as a function of maturation time. Mineral density homogeneity increases as the enamel matures while the crystallographic parameters are heterogeneous even in fully mature enamel. The

rate of mineral formation and mineral organisation are not equal in enamel. Full mineralisation of the enamel layer occurs earlier on maturation while the organisation of the crystallites is a slower process and continues for longer (Simmons et al., 2013).

1.3.4 Enamel matrix proteins

To recap, the enamel ECM consists of several different proteins, including the major ECM proteins amelogenin (approximately 90%), ameloblastin and enamelin and the minor ECM proteins including amelotin, the tuft proteins, sulphated proteins, biglycan, and the proteases enamelysin (matrix metalloprotease -20 – MMP-20) and kallikrein-4 (KLK-4) (Smith, 1998; Nanci, 2008).

Historically, the ameloblasts have been described as secreting two broad categories of ECM proteins; the amelogenins and the non-amelogenins (reviewed by Hu et al., 2005). The importance of the enamel matrix proteins in enamel development has been shown through a series of genetic studies. Both transgenic mice expressing mutated *amelx* (Paine et al., 2001, 2003) and *amelx* knockout mice (Gibson et al., 2001) exhibit major enamel structural defects resulting in reduced enamel thickness and altered prism structure. Identification of point mutations in enamelin and ameloblastin in amelogenesis imperfecta and gene knockout studies of enamelin and ameloblastin have shown that both are essential for enamel development (Fukumoto et al., 2004; Masuya et al., 2005; Poulter et al., 2014a and b).

1.3.4.1 Amelogenin

Developing tooth enamel contains about 30% protein by volume (Fukae et al., 1983) of which amelogenins comprises 90% (Hammarstrom 1997). The amelogenin gene exists on human X (*AMELX*) and Y (*AMELY*) chromosomes. *AMELX* and *AMELY* are 86% homologous and contain 7 exons though *AMELX* is expressed at levels 10 fold higher than that of *AMELY* (Salido et al., 1992).

To complicate matters, the amelogenin gene is subject to alternative mRNA splicing which generates several nascent amelogenins molecules that can be translationally modified by phosphorylation at serine 16 (they are not glycosylated) (Fincham et al., 1998). Most of the alternatively spliced variants are produced in small amounts (Bartlett and Simmer, 1999) and their significance remains unclear. Further heterogeneity is generated by extracellular proteolytic processing of nascent amelogenins by MMP-20 immediately following their secretion into the matrix. This produces a range of smaller proteins and peptides that form the bulk of the developing matrix. Full-length nascent amelogenin can be found in plenty in the

newly secreted, outermost enamel layer. Processing of the amelogenin results in smaller fragments being present in the older, deeper enamel layers (Fukae et al., 1980).

Newly secreted amelogenin has a molecular weight of 16-20 kDa (Smith and Nanci, 1996) depending on the species and the alternatively spliced isoform in question. SDS-PAGE studies show the molecular size to be higher than it actually is due to the high proline content (Termine et al., 1980). Using terminology based on relative molecular weights determined by SDS-PAGE, the newly secreted major amelogenin molecule prior to any processing is referred to as the '25 kDa parent amelogenin.' An alternative nomenclature for amelogenins is to use a prefix such as P for pig, M for mouse etc. and then a number corresponding to the number of amino acids contained in the protein. So, P173 would be the full length parent pig amelogenin of 173 residues. The corresponding mouse amelogenin would be M180 (mouse amelogenin contains an extra 7 amino acids).

Amelogenin primary structure consists of three domains:-

- 1) a highly conserved amino terminal sequence of 44-45 amino acids, that comprise the tyrosine rich amelogenin peptide (TRAP) containing 6 tyrosine residues, with 3 in the ATMP region
- 2) a central hydrophobic core of 100-130 residues rich in leucine, proline, histidine and glutamine
- 3) the amelogenin carboxyl-terminal peptide (ACP) which ends with the acidic hydrophilic teleopeptide sequence of 13 amino acids – WPATDKTKREEVD

Most of the 25 kDa parent amelogenin amino acid sequence (derived from cDNA and direct protein sequencing) for human, bovine, porcine, murine and rat is highly conserved between species (Lyngstadaas et al., 1990). This suggests great functional importance. There are additional residues present in the bovine x-linked amelogenin in exon 6, which appear to be derived from tandem duplication of DNA within exon 6 (Bonass et al., 1994). The 25 kDa parent amelogenin is the major amelogenin present in the outer secretory stage enamel (Fukae et al., 1980; Aoba et al., 1992A).

In pig, the 25 kDa parent amelogenin (P173) is rapidly degraded to give a range of products; these are shown in figure 7. Firstly, the C-terminal teleopeptide of 12 amino acids is cleaved, leaving a 23 kDa amelogenin of 161 residues (P161) (Yamakoshi et al., 1994).

With time the 23 kDa P161 amelogenin is processed from the C-terminal to give the 20 kDa P148 (Fukae et al., 1983; Aoba et al., 1992B; Yamakoshi et al., 1994). The 20 kDa amelogenin accumulates in the deeper enamel layers and appears much more stable than the 25 kDa P173 parent or 23 kDa P161 amelogenin, neither of which is present in the deeper enamel layers (Aoba et al., 1987A, B, C; Aoba et al., 1992A, B). The 20 kDa amelogenin accumulates within the tissue during the secretory stage so we can conclude that its breakdown must be fairly slow. Further cleavage occurs between residues 45 (Trp) and 46 (Leu), forming a 5 kDa tyrosine-rich amelogenin peptide (TRAP – residues 1-45) (Fincham et al., 1981; Yamakoshi et al., 1994) and a larger 13 kDa peptide (residues 46-148) (Tanabe 1984; Aoba et al., 1987C). The TRAP sequence is highly conserved and contains an N-acetyl glucosamine binding motif that may be functionally important (Ravindranath et al., 1999). This domain contains 3 tyrosine residues and is also known as the amelogenin tri-tyrosyl motif peptide (ATMP) and will be discussed separately later. An alternative processing route for P148 involves cleavage between residues 62 and 63 which produces an “extended TRAP” (residues 1-62) and an 11 kDa fragment (residues 63-148). Both the 11 and 13 kDa fragments are extremely soluble (in complete contrast to the other amelogenin fragments) and are thought to diffuse out of the developing matrix. Further processing of the TRAP is likely as several peptides with molecular weights lower than TRAP have been discovered in developing bovine enamel (Brookes et al., 1995).

The porcine amelogenin breakdown has been described here as porcine material has been used extensively by researchers in the field of enamel biology due to its relative abundance compared to human and rodent material.

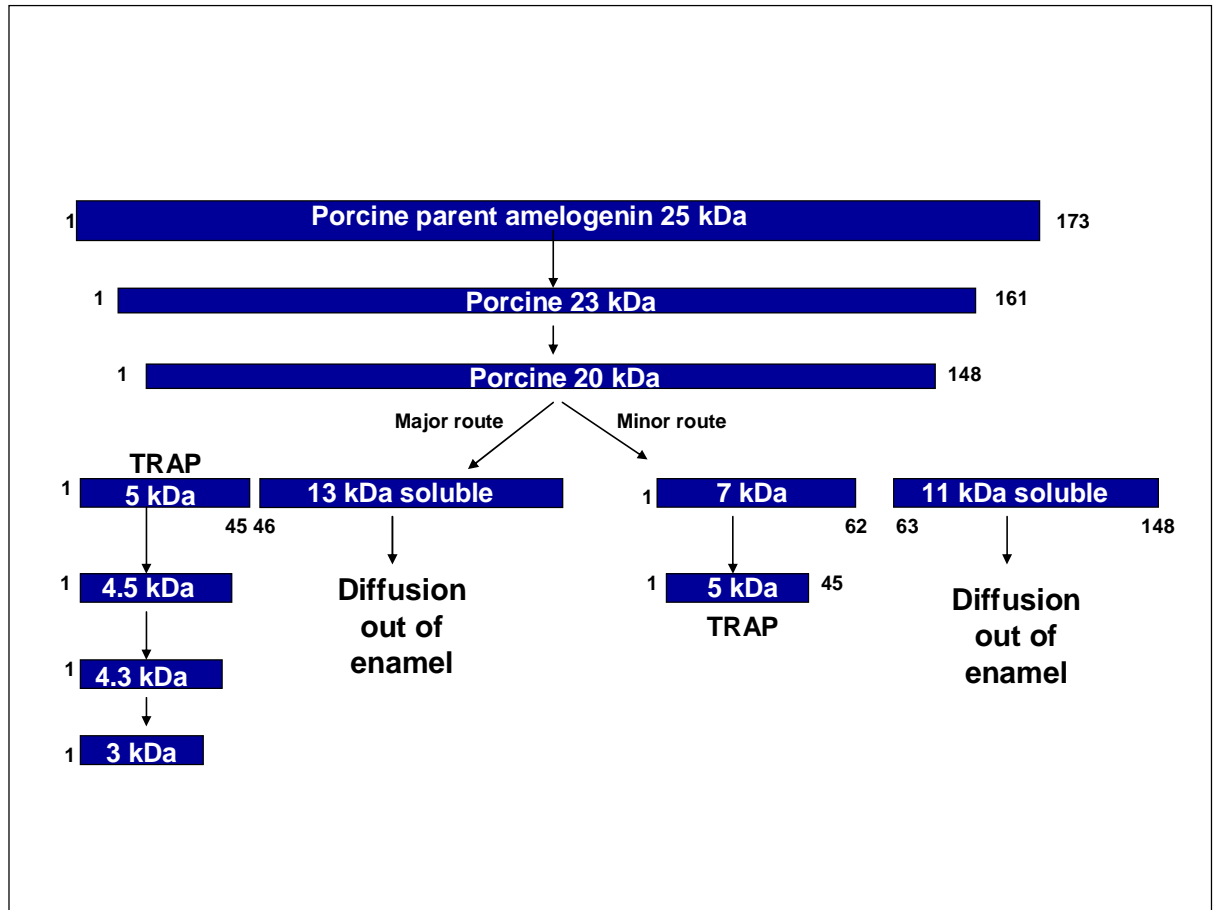


Figure 7. Extracellular processing of porcine 25 kDa amelogenin, showing the breakdown to 23 kDa and 20 kDa daughter proteins, and the further processing via the major and minor routes that generate TRAP and low molecular weight fragments (adapted from Brookes et al., 1995)

1.3.4.1.1 The importance of the amelogenin ATMP domain

The ATMP is found at the C-terminus of the TRAP and comprises of amino acids 33-45 of the full length parent amelogenin. The importance of the highly conserved 13 amino acid ATMP region of amelogenin has been investigated by Ravindranath et al. in a series of studies (1999, 2000, 2001, 2003, and 2004). The sequence consists of the amino acids PYP SYG YEP MGGW. In their initial study, Ravindranath et al. (1999) demonstrated the lectin-like activity of amelogenin by its ability to bind N-acetyl-D-glucosamine (GlcNAc) in a dose dependent fashion. Lectins are proteins that specifically bind (or cross-link) soluble carbohydrates or carbohydrate moieties. Lectins are involved in cell adhesion and have no apparent catalytic activity.

Ravindranath et al. (1999) tested 2 recombinant amelogenins and 6 synthetic peptides. The recombinant murine amelogenins were rM179 full length murine amelogenin and rM166 murine amelogenin lacking the ACP sequence. The

synthetic peptides were TRAP (contains ATMP), LRAP (does not contain ATMP; LRAP is the leucine rich amelogenin peptide, and one of the amelogenin splicing isoforms that lacks the ATMP sequence due to alternative splicing of amelogenin mRNA), ACP, ATMP, T-ATMP (where the third proline of ATMP is mutated to threonine (T)) and F-ATMP (where all three tyrosines of ATMP are mutated to phenylalanine (F)). Ravindranath et al. (1999) showed that rM179, rM166 and TRAP all exhibited lectin-like behaviour but LRAP and ACP did not. This confirmed that the lectin-like activity is located in the ATMP domain. The synthetic ATMP also bound to GlcNAc, but was unable to do so if the third proline was mutated to threonine (T-ATMP) or if all three tyrosines were mutated to phenylalanine. The mutation of the third proline to threonine mimics a point mutation seen in human X-linked AI (Collier et al., 1997) and more importantly for the work presented here, the first of the 3 tyrosines is substituted for histidine in the Y64H amelogenin mutation carried by the mice studied in this thesis.

The hypothesis of this inaugural paper was that amelogenins exhibit lectin-like behaviour and bind to the sugar residues of enamel matrix glycoproteins (EMGs) at the DEJ to facilitate biomineralisation. This could imply a co-chaperone role for the EMG's during amelogenin secretion, or a EMG chaperoning of amelogenin to the site of amelogenesis.

ATMP has 50% sequence homology with the lectin wheat germ agglutination (WGA) i.e.:

ATMP = PYP SYG YEP MGGW

WGA = CCS QYG YCG MGGD

WGA is a lectin that binds tightly to GlcNAc (Peters et al., 1979; Wright, 1984). Intrapeptide tyrosyl residues (Y) in WGA have also been implicated in sugar binding (Wright, 1984). The ATMP region also shows sequence similarity to the GlcNAc binding domain of the lectin UEA-II (Yamamoto et al., 1990). In contrast to WGA and VEA-II which have multiple sugar binding sites, amelogenin only has the single putative binding site (ATMP). In the follow up paper, Ravindranath et al. (2000) hypothesised that amelogenins may interact with peptides that mimic the sugar GlcNAc (GlcNAc mimicking peptides, GMPs). The GlcNAc binding motifs of several lectins recognise and bind to specific GlcNAc mimicking peptides found in cytokeratins (Shikhman et al., 1994). The GMP sequence SFG-SGF-GGY is found in the N-terminal region of cytokeratins 14, 16 and 17. Dosimetric binding of [³H] GMP to amelogenin rM179 and rM166 and TRAP was exhibited when the full length amelogenin was degraded to TRAP the ligand preference of the ATMP

changed from GlcNAc to GMP. The binding of GMP to TRAP was shown to be 20 fold stronger than the binding of GlcNAc, suggesting that GMP is the preferential binding ligand of TRAP. This suggests that proteolytic degradation of amelogenin may modulate its lectin-like GMP binding properties. Cytokeratin 14 (exhibiting a GMP in its N-terminal) is synthesized by ameloblasts prior to amelogenin synthesis and is seen as a marker for ameloblasts in the developing tooth (Tabata et al., 1996). The GMP sequence in cytokeratin 14 has been shown to bind to amelogenin, and could be a possible candidate for interactions with amelogenins during amelogenesis (Ravindranath et al., 2000). However, cytokeratin 14 has not been identified in the extracellular matrix so this or any such role may be related to an intracellular function as amelogenin is synthesised and secreted by ameloblasts.

The idea that cytokeratin 14 functions as an amelogenin binding protein was reinforced by Ravindranath et al. (2001) who suggested a role as a molecular chaperone for cytokeratin 14 during amelogenesis. Confocal laser scanning microscopy (CLSM) showed the co-assembly of amelogenin and cytokeratin 14 in the perinuclear region of ameloblasts in new-born (day 0) mice. Migration of the co-assembly to the apical regions was shown from day 1, peaking at days 3-5. Dissociation occurred at the Tomes' processes by day 9. Could cytokeratin 14 be a molecular chaperone for the secretion of the nascent amelogenin polypeptide? Chaperones are a class of proteins that bind newly synthesised proteins in the endoplasmic reticulum, promote correct folding and prevent abnormal aggregation between hydrophobic domains of the client proteins (Beissinger and Buchner, 1998). Certainly, isolated amelogenin is highly aggregative with low solubility under physiological conditions and it might be expected that nascent amelogenin would require careful chaperoning during its secretion to prevent untimely intracellular aggregation which could lead to endoplasmic reticulum stress; a pathological state potentially leading to cell death (Yoshida 2001).

Cytokeratin 14 has been documented to pair with cytokeratin 5 in basal epithelial cells during cell differentiation (Sun et al., 1984). Cytokeratin 14 is a type I cytokeratin and cytokeratin 5 is a type II cytokeratin. Cytokeratin 5 is also present in ameloblasts (Kasper et al., 1989; Domingues et al., 2000). Cytokeratin 14 and cytokeratin 5 pair via the N-terminal regions of both molecules. Similar to other type II cytokeratins, cytokeratin 5 carries GlcNAc at its N-terminal region (Omary et al, 1998).

Ravindranath et al. (2003) hypothesised that if amelogenin bound to cytokeratin 5 it might define a role for both type I and type II cytokeratins in

amelogenesis. ATMP was shown to bind to cytokeratin 5 but not if the GlcNAc residues were removed. CLSM showed that cytokeratin 5 co-assembled with amelogenin in mouse molar ameloblasts separately from cytokeratin14-amelogenin complexes, and migrated to the apical regions of the ameloblasts on postnatal day 1. Triple signals were noted between postnatal days 3-5, indicating the presence of cytokeratin14-amelogenin, cytokeratin 5-amelogenin and cytokeratin14-cytokeratin 5 complexes. Accumulation of cytokeratin 14-cytokeratin 5 complexes in the Tomes' processes were observed post-natal day 5. Secreted amelogenin was observed in the ECM adjacent to the Tomes' processes, suggesting that following the secretion of amelogenin from the ameloblasts, cytokeratin 14 and cytokeratin 5 formed a co-assembly. The co-assembly was first noted on post-natal day 3 and increased up to postnatal day 7, and disappeared thereafter. This was suggestive of degradation or cell death.

Even though cytokeratin 14 has the GMP motif and has been demonstrated within ameloblasts, it has not been identified in the enamel ECM. Ravindranath et al. (2004) suggested that ameloblastin may in fact be the preferred ECM binding target for ATMP in amelogenin as it has been suggested that the ameloblastin may bind to the amelogenins as well as interacting with the growing hydroxyapatite crystals (Deutsch et al., 1991).

Native ameloblastin is O-glycosylated, but has not been shown to carry a GlcNAc region to potentially interact with amelogenin (Uchida et al., 1997). Recombinant ameloblastin does not contain GlcNAc or NeuAc (since E.coli are unable to make these modifications) but paradoxically it is still bound via the amelogenin ATMP motif (Ravindranath et al., 2004). This is explained by the fact that ameloblastin carries a complete GMP sequence, interrupted by intervening residues. Even though the ameloblastin GMP sequence is fragmented, it might not need to be continuous sequence. The GMP binding sequence of cytokeratin 14 is also fragmented, yet Ravindranath et al. (2000, 2001) showed it to bind ATMP effectively. Folding and coiling of the polypeptide could bring the disparate fragments of the GMP peptide together resulting in the formation of an intact conformational binding site (Wright 1984, 1990; Murphy et al., 2000). Ravindranath et al. (2004) further suggested a role for ameloblastin in amelogenin binding by demonstrating that anti-rM179 amelogenin antibodies detected amelogenin bound to recombinant ameloblastin in both western blots and ELISA experiments, that ATMP binds to recombinant ameloblastin and native amelogenin retrieved from enamel in a dose dependent manner, and that mutations of the third proline in ATMP abolishes binding to both recombinant and native ameloblastin.

In summary, the amelogenin ATMP domain has lectin-like properties in that it binds GlcNAc (a sugar). It also binds amino acid sequences that mimic GlcNAc. These so called GlcNAc mimicking peptide sequences (GMPs) are present in cytokeratins and ameloblastin and it is possible that amelogenin forms complexes with these proteins via the ATMP domain. Significantly single acid mutations in the ATMP domain lead to AI indicating the functional importance of this domain in amelogenesis and the production of functional enamel (see figure 9).

1.3.4.1.2. Amelogenin and its role in mineral crystal formation in tooth enamel

Amelogenins are rich in proline (25-30%), and with high levels of glutamine (13%), leucine (10%) and histidine (8%), making them hydrophobic (Eastoe 1964). This hydrophobic character appears to be responsible for driving the supramolecular assembly of amelogenin monomers into so called “nanospheres” which are assumed to be the functional form of the protein during amelogenesis (Fincham et al., 1995; Du et al., 2005). Amelogenin mutations giving rise to the human X-linked condition amelogenesis imperfecta (AI) have point mutations resulting in altered nanosphere dimensions and assembly kinetics (Lench et al., 1994; Collier et al., 1997). Although amelogenin is hydrophobic, the C-terminal is rich in acidic amino acids resulting in the presence of a hydrophilic “C-terminal teleopeptide.” The teleopeptide enhances amelogenin binding to hydroxyapatite *in vitro* (Aoba et al., 1987C), suggesting that the C-terminal region facilitates initial orientation of amelogenin along the forming enamel crystallites (Kirkham et al., 2000).

Protein function is determined by protein conformation and this in turn is driven by the interactions of the specific amino acid side chains; this gives the necessary stereochemical parameters required for function. Amelogenin has not been crystallised and appears to be devoid of secondary structural features such as beta pleated sheets and alpha-helices. The C terminal of full length amelogenin (teleopeptide) is highly conserved across all species and in contrast to the rest of the molecule is hydrophilic (Fincham et al., 1995; He et al., 2008).

Previous reports based on mechanical molecular modelling have suggested the presence of beta-spiral in bovine amelogenin. A central portion of the amelogenin molecule comprises a hydrophobic core of approximately 100 residues rich in leucine, proline, histidine and glutamine and theoretically in bovine species this core contains a repetitive beta-turn segment and beta-spiral between glutamine 112 and leucine 138; this beta-spiral has been suggested to interact with calcium

ions (Margolis et al., 2006; Palmer et al., 2008). Calcium binding fits well with a role for amelogenin in enamel mineralisation. However, if we examine this critically, the significance of this proposed calcium binding beta spiral in amelogenin function is difficult to accept since amelogenin from non-bovine species lack the repetitive sequence and do not exhibit this beta spiral. On firmer ground, it is well documented that amelogenins self-assemble into nanospheres *in vitro* (Fincham et al., 1994; Moradian-Oldak, 2007). There are indications that similar structural elements exist *in vivo* in the developing enamel (Fincham et al., 1995B; Robinson et al., 1981). The conclusion that the charged C-terminus is exposed on the surface of the nanosphere was derived from the observed MMP-20 cleavage sites and a solid-state NMR study using an alternative slice variant of amelogenin LRAP. Amelogenin self-assembly into nanospheres is driven by inter-molecular hydrophobic which maintains the hydrophobic end away from water, with the hydrophilic end is exposed on the surface. The pH, temperature and protein concentrations all affect the size of the assembled structures. (Beniash et al., 2005; Habelitz et al., 2006; Moradian-Oldak, 2001)., Aichmayer et al. (2005) have provided additional evidence to show that amelogenin nanospheres are composed of a hydrophobic and electron dense core surrounded by a less electron dense and hydrophilic corona of the charged C-termini by using small angle x-ray scattering (SAXS) and dynamic light scattering analyses

Studies have shown that the full length amelogenin nanospheres further connect into chains of connected nanospheres indicating a hierarchical self-assembly into larger structures that could act as a template to drive the growth of hydroxyapatite crystals (Moradian-Oldak et al., 2006; Wiederman-Bidlack et al., 2007) . Using solutions with high protein concentration in a hanging drop over extended periods of time, co-linear arrays of amelogenin nanospheres were observed suggesting that the full length amelogenin could possibly act as scaffold onto which hydroxyapatite crystals grow during enamel maturation (Moradian-Oldak et al., 2006).

For effective enamel development, the cleavage and removal of proteolytic products in a timely manner are essential. The charged C-terminus of amelogenin has significant hydroxyapatite binding affinity with has been proposed to control morphology and organisation of the crystals (Moradian-Oldak et al., 2001; Beniash et al., 2005). It has been hypothesised that the hydrophilic region of amelogenin inhibits crystal growth and nucleation (Aoba et al., 1987B). Several studies have investigated this hypothesis further by removing the C-terminal hydrophilic residue of amelogenin and showing that it does not affect amelogenins ability to inhibit

crystal growth of calcium phosphates (octocalcium phosphate and hydroxyapatite) in directions perpendicular to the C-axis (Beniash et al., 2005; Iijama and Moradian-Oldak, 2005). It was also shown that the crystals that did form in the presence of the hydrophilic C-terminus were organised into parallel arrays, whereas the crystals formed in the absence of the hydrophilic C-terminus were randomly arranged under the same conditions (Beniash et al., 2005).

Hydrophobic protein expression and secretion into extracellular space is commonly seen as a cell-directed activity to provide space for mineral formation (Addadi and Weiner, 1992). Hydrophilic proteins, in contrast, are generally regarded as molecules that have the potential to promote crystal nucleation and growth by defining the position and size of mineral crystallites (Addadi and Weiner, 1992). As described previously, Ravindranath et al. (2007) demonstrated that recombinant mouse amelogenin binds specifically to recombinant ameloblastin via its ATMP tyrosine rich domain (amino acids 33-45). This suggests the possible formation of a heteromolecular assembly. Bouropoulos and Moradian-Oldak (2004) examined the cooperative effects of amelogenin and a 32 kDa enamel fragment on the induction of synthetic apatite crystals precipitated in 10% gelatine gel and proposed that the 32 kDa enamel bound to amelogenin serves as a potential nucleator for apatite crystals. These findings propose the idea of a cooperative role for enamel proteins to control mineral nucleation. Other studies introduced the idea of cooperative mineralisation, with the suggestion that the functional self-assembly of the organic matrix molecules can only occur with enamel crystal growth and alignment in situ and in a collaborative manner (Margolis et al., 2006). It can be confidently hypothesized that the protein components of the developing enamel matrix interact with one another and may function synergistically to produce a suitable template for biomineralisation and the production of highly ordered enamel tissue.

Changes in pH which can induce ionisation of the amine and carboxyl groups as well as the functional side chains can affect protein self-assembly. Intermolecular interactions of macromolecules are often enhanced at their isoelectric point pH, since electrostatic repulsion is minimal and molecules can approach each other closely (Aggeli et al., 2003; Zhao et al., 2003). The calculated isoelectric points (IPs) are close to physiological pH for monomeric 25 kDa amelogenin and the 23 kDa amelogenin being 6.62 and 6.85 respectively. The true IP may vary significantly from these theoretical values for these molecules depending on the protein higher order structure. When the cooperative assembly between two different proteins is required such as amelogenin and enamel, the surface charges of the self-assembled structures become important. Electrostatic

attraction between different proteins may occur when either the dissolved macromolecules or the initially self-assembled nanostructures carry opposite charges, providing an opportunity for close protein to protein interaction that could stimulate a cooperative self-assembling behaviour.

Self-assembly of amelogenin into nanospheres which increase in size with increasing pH was observed by atomic force microscopy (AFM) (Wen et al., 2011). Elongated structures of 100 nm length and 25 nm widths formed over several days for 25 and 23 kDa amelogenins at pH values 6.5 and 7.5, respectively. A mix of both proteins held at pH 7 for 24 hours resulted in self-assembled strings of 200-300 nm length consisting of fused nanospheres. These protein nanostrings formed links and a continuous mesh after 7 days. Electrical conductivity data also showed gradual changes with mixed amelogenins, supporting the idea of elongated structures forming over extended periods. The idea was proposed that due to the difference in isoelectric point, self-assembled nanospheres composed of 23 and 25 kDa amelogenin have opposite ionic charges at pH values around 7 and thus experience ionic attraction that enables cooperative self-assembly (He et al., 2008).

1.3.4.2 Ameloblastin (Amelin/Sheathlin)

As mentioned previously ameloblasts secrete the ECM proteins involved in enamel development; both the amelogenin and the non-amelogenin proteins. Ameloblastin (also known as sheathlin and amelin) (Cerny, 1996) is the most abundant of the non-amelogenins, comprising 5-10% of all proteins present in secretory stage tooth enamel (Simmer et al., 2010) and like amelogenin and enamelin the 65 kDa nascent ameloblastin molecule is subjected to proteolytic processing immediately after secretion, with lower molecular weight fragments being identified by western blot analysis (Brookes et al., 2001). The ameloblastin gene (AMBN) in humans has been localised to chromosome 4q21 and contains 13 exons (Krebsbach et al., 1996; MacDougall et al., 1997). Ameloblastin and amelogenin are sister genes and are believed to have evolved from the *ENAM* gene by gene duplication and neofunctionalisation (Sire et al., 2007).

Ameloblastin is a glycoprotein that is anionic, rich in glycine, leucine and proline. Ameloblastin expression in ameloblast cells is highest during the secretory stage and diminishes in the maturation stage. However, ameloblastin expression is not exclusive to ameloblasts. It is also expressed in odontoblasts (Nagano et al., 2003; Hao et al., 2005), osteoblasts (Tambursten et al., 2011) and cementoblasts

(Nunez et al., 2010). Expression has been noted in dentine and HERS cells (Fong et al., 1996; Bosshardt and Nanci, 1997).

Ameloblastin is secreted from vesicles containing just ameloblastin or more usually a mixture of ameloblastin and amelogenin. The localisation of amelogenin and ameloblastin in the ECM layer is believed to reflect their individual functions. Similar to nascent amelogenin, nascent full length ameloblastin is restricted to the newly secreted enamel matrix immediately adjacent to the ameloblasts where the enamel crystals are undergoing elongation (Nanci et al., 1996A; 1996B).

Ameloblastin is cleaved upon secretion by MMP-20 (Uchida et al., 1997) and is processed in the deeper enamel to generate a range of peptides around 13-17 KDa in size that aggregate (Brookes et al., 2001) and accumulate around the prism peripheries resulting in a 'fishnet'-like or honeycomb patterning following immunohistochemical localisation (Uchida et al., 1991A). The remaining C-terminal fragment is found in the outer superficial layer only and is rapidly degraded (Uchida et al., 1997). The localisation of ameloblastin N-terminal fragments to the prism peripheries led to the suggestion that these molecules play some role in delineating the boundary between prismatic and interprismatic enamel (Iwata et al., 2007).

Ameloblastin contains a number of binding sites for various components. It has been found to contain binding sites for calcium (Yamakoshi et al., 2001), heparin (Sonoda et al., 2009) and fibronectin (Beyeler et al., 2010) which suggests that ameloblastin may have multiple roles.

For example, ameloblastin may act as a linkage between ameloblasts and the enamel ECM (Cerny et al., 1996; Snead et al., 1996). Fukumoto et al., 2004 proposed a role for ameloblastin as a cell adhesion molecule necessary for maintaining the differentiation state of ameloblasts. Ameloblastin null mice initially showed elongation of the dental epithelial cells comparable to wild type mice, but at the secretory stage the cells detached from the ECM and lost polarity. The ameloblasts eventually became smaller and rounder, and then resumed proliferation resulting in the formation of multicellular layers. Expression of amelogenin was also reduced in the ameloblastin null mice. Primary cell culture of dental epithelial cells with recombinant ameloblastin showed preferential binding of ameloblasts to ameloblastin over fibronectin or laminin (Fukumoto et al., 2004). Recombinant amelogenin also inhibited proliferation of ameloblastin null ameloblasts in culture (Fukumoto et al., 2004). These results were not noted with other epithelial cell types, indicating a role for ameloblastin in cell adhesion. Paine et al., 2003 showed that mice over expressing ameloblastin exhibited an

amelogenesis imperfecta like phenotype. These results also indicate a role for ameloblastin in organising ECM proteins to initiate mineral crystal growth. Ameloblastin null mice were also shown to develop tumours with age in the Fukumoto et al., 2004 study. The tumour cells were shown to be expressing enamel ECM proteins implying that the source of the tumours is likely to be the ameloblastin defective ameloblasts. The most common human odontogenic tumour is the ameloblastoma (Kramer et al., 1992) considered to be of dental epithelial origins due to similarities between the tumour and the developing tooth (Snead et al., 1992; Abiko et al., 2007; Yagishita et al., 2001). Perdigo et al., 2004 reported odontogenic tumours resulting from ameloblastin mutations. The tumours are likely to form due to lack of ameloblastin regulation of ameloblast differentiation.

Until recently, no ameloblastin mutations had been identified that give rise to an amelogenesis imperfecta phenotype, although ameloblastin's chromosome location was linked to a local hypoplastic form of AI (MacDougall et al., 1994). However, Poulter et al., 2014B identified a deletion of ameloblastin exon 6 in a family displaying an amelogenin imperfecta phenotype. The teeth from the patients displayed a similar phenotype of a thin dysplastic layer of rough, pitted mineralised tissue lacking any discernible crystal structure comparable to a mouse model lacking ameloblastin exons 5 and 6 (Wazen et al., 2009; Hu et al., 2008).

1.3.4.3 Enamelin

Enamelin falls into the non-amelogenin category along with ameloblastin, previously discussed above. *Enamelin* maps to chromosome 4q21 in humans and contains 9 exons (Hu et al., 2001). It has been suggested that enamel, ameloblastin and amelogenin all arose from a single ancestral gene from which gene duplication generated the amelogenin gene which then translocated to the X and Y chromosomes, while enamel and ameloblastin remained on this original chromosome (Sire et al., 2007). Comprising less than 1% of all proteins present in developing tooth enamel, pig enamel is secreted as a phosphorylated 186 kDa glycoprotein (Fukae et al., 1987). Like amelogenin, enamel undergoes a series of proteolytic cleavages by MMP-20 once secreted (shown in figure 8). Fully mature and intact enamel is present in newly secreted enamel at the mineralisation front perhaps suggesting a role for full length nascent enamel in crystallite elongation (Hu et al., 2005; Kim et al., 2005A). Studies on enamel biochemistry using enamel proteins isolated from developing enamel have focused almost exclusively on the pig model due to the availability of pig developing teeth through

the meat industry and the thickness of the porcine enamel tissue. The major enamelin protein in pig enamel is the 32 kDa processing product generated by proteolytic processing in the deeper enamel (Uchida et al.,1991B) and it is this species that is, without exception, used in biochemical studies relating to enamelin function due to its relative abundance. The 32 kDa enamelin is phosphorylated and glycosylated and has a high affinity for the mineral phase suggesting that its amino acid residues and/or the attached phosphate and sugar groups arrange stereochemically in a way that is complementary to the mineral surface in terms of binding potential. The exact role of enamelin is unclear but the fact that the 32 kDa domain exhibits affinity for mineral surfaces suggests that interaction with mineral is an important function (Al-Hashimi et al., 2009; Bouropoulos and Moradian-Oldak., 2004; Fan et al., 2008; Fan et al., 2009; Fan et al., 2011; Iijama et al., 2010; Uchida et al., 1991; Yamakoshi et al., 1995; Yamakoshi et al., 1998; Yamakoshi 2006) It is possible that this affinity is also directed towards initial clusters of mineral ions which provides sufficient stabilisation for nucleation to occur i.e. the domain acts as a template for mineral nucleation.

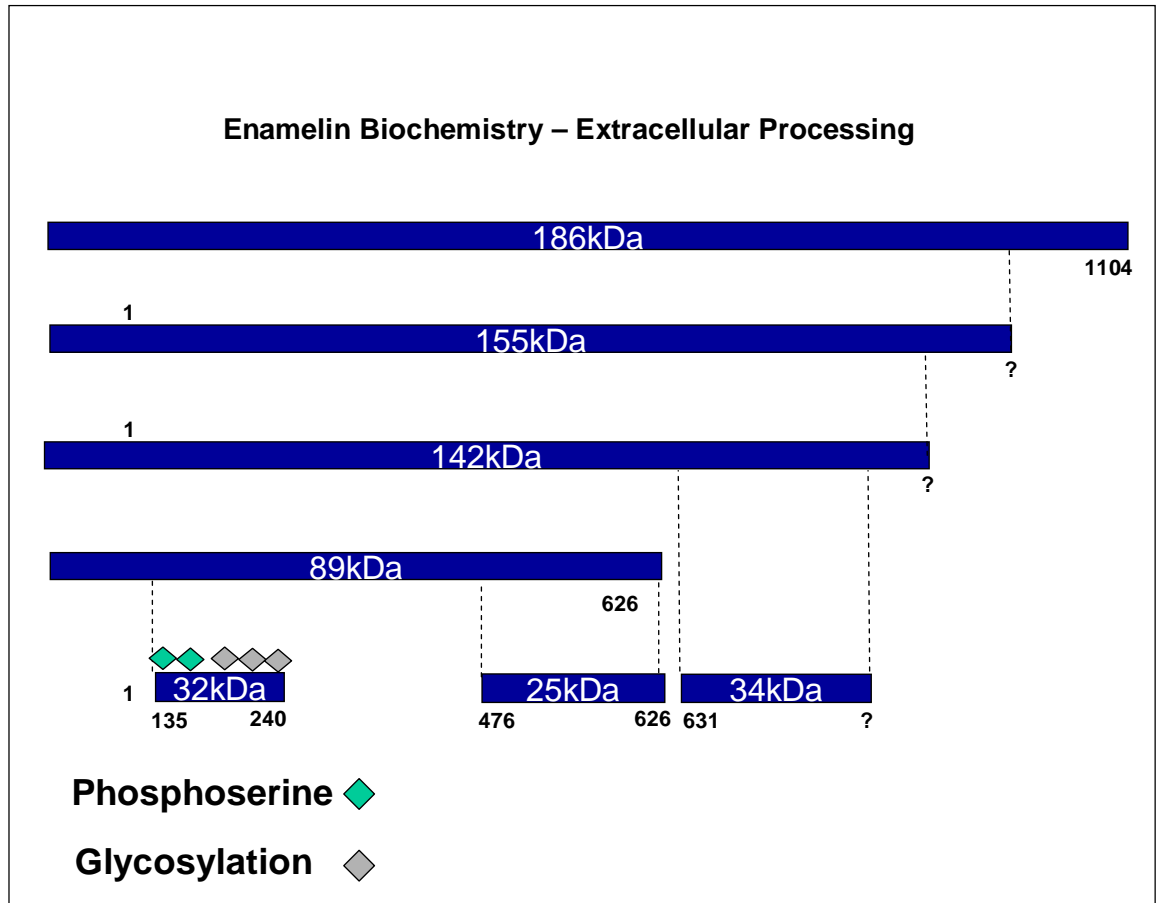


Figure 8. Extracellular processing of porcine enamel protein showing molecular weights of the breakdown products, from the parent 186 kDa protein to the 32 kDa, 25 kDa and 34 kDa fragments. The 32 kDa breakdown product retains the post translational modifications of phosphorylation and glycosylation.

Autosomal dominant hypoplastic amelogenesis imperfecta is linked to mutations in the enamel gene. In humans displaying the AI phenotype linked to enamel mutations, those with single allele mutations had hypoplastic, thin, rough enamel resulting in yellow, temperature sensitive teeth. Those with both allele mutations had teeth with a complete lack of enamel (Ozdemir et al., 2005). A chemically induced mouse model (ENU) (Masuya et al., 2005) a gene targeted mouse model (Hu et al., 2008) and human gene mutations resulting in AI (Rajpar et al., 2001) have all been used to investigate enamel mutations and indicate a fundamental role for enamel in biomineralisation. The resulting thin enamel displaying disorganised mineral crystals seen in human and mouse AI models with *ENAM* null genotypes indicate that enamel is necessary for optimal enamel thickness via crystal formation and prism organisation (Meredith et al., 2009).

A recent study by Hu et al., 2014 describes investigations into the role of enamelin in enamel development. Using mice heterozygous and homozygous for enamelin mutations, the group aimed to characterise any resulting cellular and structural anomalies. They showed that no proper enamel formation occurred as there was no mineralisation along the ameloblasts distal membranes in affected mice. B-galactosidase staining specific for enamelin expression showed expression in the developing tooth organ, and only in the secretory and early maturation stage ameloblasts. Unlike ameloblastin, enamelin expression was not noted in odontoblasts or osteoblasts. In the homozygous *Enam*^{-/-} mice, the ameloblasts were observed to become crowded and to lose contact with the ECM covering the dentine. The ameloblasts continued to secrete amelogenin but displayed enlarged endoplasmic reticulums. The ameloblasts were able to secrete an amelogenin-rich layer onto the dentine despite poorly formed Tomes' process, but mineralisation of this protein layer did not occur and at the secretory stage, no mineral crystal ribbons were noted. In the heterozygous *Enam*^{+/-} mice, the mineral crystals appeared to have the correct conformation but were more loosely packed together.

The above data show, that although enamelin is much less abundant than amelogenin, it is important for the formation and integrity of the enamel ECM and the mature mineralised enamel.

1.3.4.4 Minor Enamel Matrix Proteins

1.3.4.4.1 Kalikrein-4 (KLK-4)

The human *KLK-4* gene has been localised to chromosome 19q13.3-13.4 and consists of 6 exons and 5 introns (DuPont et al., 1999; Hu et al., 2000). It encodes a 254 amino acid protein with a conserved serine protease catalytic triad, and an amino-terminal prepropeptide sequence. In teeth, KLK-4 is secreted by the odontoblasts and by late-secretory and maturation stage ameloblasts. KLK-4 expression correlates with the disappearance of enamel proteins, such as amelogenin, from the enamel ECM. KLK-4 is expressed in its latent proenzyme form. How it is activated has, as yet, not been fully defined (Lu et al., 2008). KLK-4 appears to act upon protein fragments of amelogenin, ameloblastin and enamelin already created from proteolytic degradation by MMP-20. KLK-4 facilitates the removal of these fragments from the enamel layer as part of the maturation stage (Lu et al., 2008). A *KLK-4* mutation has been noted in a family with autosomal recessive hypomaturation amelogenesis imperfecta (Hart et al., 2004) which highlights the importance of proteolytic removal of matrix proteins from the

maturation stage enamel. A *KLK-4* null mouse model shows that the enamel produced is of normal thickness with the correct organisation of prisms and inter-prism substructures seen in normal enamel. However, the maturation and hardening of the enamel is delayed in these animals, with a defect in the mineralisation near the DEJ, causing the enamel to be sheared from the surface of crowns during physical use. The teeth show abnormal wear patterns, with chipped incisor ends (Hu et al., 2009).

The expression of proteolytic enzymes such as *KLK-4* during enamel maturation is necessary for enamel to achieve its high degree of mineralisation. If *KLK-4*, or the other enamel proteinase, *MMP-20*, is absent or functionally defective during enamel secretion, the produced enamel is itself defective or of poor quality (Simmer and Hu., 2002; Hu et al., 2003; Hu et al., 2005). Recent studies have shown that *MMP20* activates *KLK4* by cleaving a propeptide. Hence, a *MMP20* mutation can indirectly compromise *KLK4* function (Yamakoshi et al., 2013).

1.3.4.4.2 Matrix Metalloproteinase-20 (MMP-20)

The human *MMP-20* gene has been localised to chromosome 11q22.3-q23 (Llano et al., 1997) and consists of 10 exons and 9 introns (Caterina et al., 2002). Ameloblasts and odontoblasts of the dental papilla express *MMP-20* (Hu et al., 2002). *MMP-20* is secreted during the secretory phase (Hu et al., 2002). *MMP-20* is expressed in its latent proenzyme form. How it is activated has, as yet, not been fully defined (Ryu et al., 1999). *MMP-20* is secreted into the enamel matrix appearing as a doublet of 41 and 46 kDa on SDS gels following extraction, and *MMP-20* activity accounts for all of the known cleavage sites in amelogenin that occur in the early stages of enamel development (Ryu et al., 1999). *MMP-20* is also responsible for the cleavage of newly synthesised ameloblastin and enamelin (Yamakoshi et al., 2006, Simmer et al., 2009, Simmer et al., 2010). The *Mmp-20* null mouse displays a severely profound tooth phenotype as it is unable to process amelogenin correctly, so may possess an altered enamel matrix and crystal prism pattern, resulting in hypoplastic enamel that delaminates from the dentine (Caterina et al., 2002). The enamel that is present contains little, if any, prism and inter-prism substructure, and is very soft in texture (Bartlett et al., 2003; Bartlett et al., 2004).

1.3.4.4.3 Amelotin

Amelotin is the newest discovered enamel-specific protein and represents a novel component of the maturation stage basal lamina (Dos Santos Neves et al., 2012). The *Amelotin* gene in humans has been localised to chromosome 4q13.3, has 9 exons and 8 introns, and gives rise to a 22 kDa protein. Amelotin displays an N-terminal signal sequence typical of many secreted proteins, but appears to

undergo few, if any, post translational modifications. Investigations are underway to determine this restricted protein expression, and to decipher whether amelotin is indeed a structural protein of the enamel matrix or in fact, a proteolytic enzyme involved in enamel ECM degradation (Iwasaki et al., 2005).

1.3.4.4.4 Biglycan

The biglycan gene in humans has been localised to chromosome Xq28, and contains 8 exons (Fisher et al., 1991). Biglycan is a small cellular or pericellular matrix proteoglycan, and contains 2 glycosaminoglycan (GAG) chains (Iozzo, 1999). Biglycan is expressed by ameloblasts and is present in enamel ECM (Goldberg et al., 2003).

Biglycan expression is not unique to enamel, but it does play a significant role in amelogenesis and enamel biomineralisation due to *biglycan* null mice expressing a larger volume of developing enamel in molar teeth, but not incisors. This resulted from an increase in amelogenin expression. The mature enamel in *biglycan* null mice was morphologically comparable to wild type mouse enamel once fully mineralised. Therefore, biglycan either directly or indirectly acts as a repressor of amelogenin expression during enamel secretion (Goldberg et al., 2002; Goldberg et al., 2005).

1.3.4.4.5 Tuftelin and the tuft proteins

The human tuftelin gene has been localised to chromosome 1q21. Tuftelin is an acidic protein shown to be present in the developing and mature enamel ECM. Tuftelin was originally described and classified as an enamel ECM protein, although it is not unique to ameloblasts or the enamel ECM (Deutsch et al., 1991). Tuftelin is a product of a wide range of cells including cells responsible for mineralising hard tissues (including enamel ECM) as well as cells responsible for non-mineralising tissues. *In vivo* localisation shows a minimal degree of amelogenin and tuftelin colocalisation in the cell cytoplasm (Deutsch et al., 1995). There is lack of evidence to suggest a physiological pathway from the cytoplasm to the ECM, but tuftelin has been repeatedly localised to the ECM, where its presence suggests a role in amelogenesis (Paine et al., 2000). It has been proposed that the tuftelins act to start the mineralisation process of the enamel ECM (Zeichner-David., 2001).

Tuftelin-interacting protein II (TFIP-II) has been immunolocalised to the Tomes' processes and the enamel matrix (Paine et al., 2000), however TFIP-II appears to be a phosphorylated RNA splicing factor and is primarily localised within the cell nucleus (Beausoleil et al., 2004).

Previous studies have shown that cell membrane phospholipids accumulate in the dentine and enamel ECM during biomineralisation (Goldberg et al., 1999). One explanation for this in enamel is that the distal portions of individual Tomes' processes are fragmented during the secretory stages of amelogenesis and the contents become trapped in the ECM. For a structure such as enamel with very specific matrix proteases that target tooth specific proteins, it is conceivable that non-secreted ameloblast-associated proteins can become trapped in the immature or mature enamel. This may explain the localisation of tuftelin and TFIP-II in the enamel matrix (Goldberg et al., 1998; Goldberg et al., 1999).

Tuft protein, a different protein to tuftelin, was revealed during the complete dissolution of mature enamel from human molars. The presence of a considerable amount of insoluble material on the dentine surface was noted, and this material was not soluble even in mineral acids or EDTA (with or without 8M urea or guanidine chaotropic agents) (Hodson et al., 1952), or boiling in SDS or phenol. Analysis showed that this material was proteinaceous with a composition in excess of 80% amino acids (Weatherall et al., 1968; Robinson et al., 1975). Microscopy showed the material associated with the enamel tufts, blades of organic material along the enamel prism boundaries (Beust et al., 1932; Osborn et al., 1969).

Amizuka et al., (1992) showed the presence of 'tuft' proteins in human molars with complex prism structures using electron microscopy. Tuft protein is not related to the other ECM proteins. Keratin has been identified in the tuft protein by immunohistochemistry staining (Robinson et al., 1989), and a fragment of ameloblastin has also been detected (Robinson et al., 2000). It is possible that this tuft protein material is a mixture of different proteins. Antibodies raised against a tuft protein suspension were used to probe sections of rat molar. This showed that the expression of the tuft protein followed the secretory pathway from ameloblasts (Robinson et al., 1989), and therefore was likely to be ameloblastin (Amizuka et al., 1992; Robinson et al 2000). As described above N-terminal ameloblastin degradation products have been shown to be immunologically related to prism boundaries (Uchida et al., 1991B), which fits well with the notion that tuft protein contains ameloblastin as the tuft protein is associated with prism boundaries.

The fact that this tuft protein is very resistant to chemical solubilisation implies chemical cross-linking such as that seen in keratin and collagen. Cross-links such as ϵ - γ -glutamyl-lysine occur between glutamine and a primary amine group such as lysine (Folk and Finlayson, 1977; Lorand and Conrad, 1984) and these have been reported to exist in tuft protein together with transglutamase enzyme responsible for

their formation (Robinson and Hudson, 2011). ECM proteins such as amelogenin, enamelin and ameloblastin all contain large quantities of lysine and glutamine. These cross-links are common in epithelial tissues, with a role in prevention of proteolytic degradation and promoting structural stabilisation. Enamel has epithelial origins, so it is tempting to speculate that these cross-links play a similar role in this tissue. However, enamel matrix proteins are not covalently linked during development (as evidenced by the fact that they can be isolated in their monomeric form) and considering the developing enamel matrix is designed to be proteolytically removed from the tissue, the formation of stabilising cross links at this stage would be counterproductive.

The effects of the proteinase Kallikrein-4 (KLK-4) on tuft protein are not known. Protein degradation such as that elicited by KLK-4 or MMP-20 at the dentine-enamel junction could be ruinous to the developing ECM, therefore the presence of chemical cross-links would provide a protective effect to the tissue and stabilise the interface. This is comparable to the cross-linking of keratin in layers of the skin tissue. Myoung et al (2009) proposed a role for the tuft protein in protecting the tooth under high functional stresses and in self-healing, consistent with cross-linking.

It is likely that tuft protein is a mixture of the degradation products of the enamel ECM proteins, along with a form of degradation resistant cross-linked material from the dentine. This tuft protein product in turn has a protective effect during tooth development, in strengthening and protecting the DEJ, and throughout the life of the tooth in acting as a cushioning layer between the prisms and dentine and enamel layers, to resist the stresses and strains of normal tooth wear.

1.3.4.4.6 Sulphated Proteins

A glycosylated and sulphated 'non-amelogenin' protein of 65 kDa has been identified in the developing enamel of rats by *in vivo* radiolabelling studies using ³⁵S isotopes. The 65 kDa protein is rapidly degraded following secretion. It has been hypothesized that this protein may somehow interact with amelogenin, but this remains to be proven and no specific gene has been identified (Smith et al., 1995; Nanci et al., 1996A; Nanci et al., 1996B). It is possible that this protein is in fact nascent ameloblastin.

1.3.5 Non matrix proteins involved in enamel development

Integral membrane proteins, calcium transport proteins, hard tissue mineralisation proteins and collagen were all identified during screening of a cDNA expression library to find enamel matrix proteins that interacted directly with amelogenin, enamelin or ameloblastin (Wang et al., 2005). These proteins included CD63 (LAMP-3), Annexin A2, α -2-HS-glycoprotein (Ahsg) and types I, II and IV collagen. CD63, LAMP1 and Annexin A2 are products of ameloblast cells (Fukumoto et al., 2004; Tompkins et al., 2006; Wang et al., 2005). LAMP1 has also been identified as a membrane-bound receptor for amelogenin. CD63 and LAMP1 are both found on the membrane of endosomes and lysosomes (Duffield et al., 2003; Goldberg et al., 1990; Mayran et al., 2003). Annexin-2 is involved in the organisation and dynamics of the endosome membrane. These interactions support the existence of signalling pathways through membrane bound receptors to allow the transfer of information from the enamel matrix to the ameloblast to influence gene transcription. Their presence also supports the theory of an anchoring mechanism for orientating the enamel matrix relative to the ameloblast Tomes' processes and for receptor mediated removal of degraded ECM proteins during enamel biomineralisation.

1.3.5.1 LAMP1

Lysosomal associated membrane protein 1 (LAMP1) is a transmembrane protein expressed mainly by late endosomes and lysosomes and is often used as a marker for these organelles (Cook et al., 2004). It is involved in endocytosis, pinocytosis and phagocytosis. LAMP1 is present on the plasma membrane of presecretory, secretory, and post-secretory ameloblasts and is thought to act as a cell surface intermediary that can be shuttled to the lysosome through endocytosis. LAMP1 interacts directly with amelogenin (Tompkins et al., 2006) and has been shown to interact with the LRAP fragment of amelogenin and full length amelogenin on cementoblasts (Zhang et al., 2010).

1.3.5.2 CD63 (LAMP3)

CD63 is a member of the transmembrane 4 glycoprotein superfamily, known as the tetraspanin proteins. The majority of the family members are cell surface proteins, identified by four hydrophobic transmembrane domains. These proteins are involved in the mediation of signal transduction events associated with activation, growth, motility, and the regulation of cell development. CD63 forms complexes with integrins (Yunta and Lazo, 2003). CD63 is found in the cytoplasmic membranes of most cell types, and also in late endosomes, lysosomes and

secretory vesicles, trafficking between these different compartments. CD63 is immunolocalised to the Tomes' processes of ameloblast cells, and is found throughout the cytoplasm of ameloblast cells and neighbouring cells. CD63 is able to interact directly with the secreted enamel proteins, and is perhaps likely to play a role in amelogenesis related to protein-protein interactions at the Tomes' processes. (Zou et al., 2007). It may also play a role in amelogenin degradation by binding to the amelogenin and packaging the protein into vesicles, targeting it for removal from the cell cytoplasm (Xu et al., 2008).

1.3.5.3 Annexin A2

Annexin A2 is a 39 amino acid calcium and phospholipid binding protein. Annexin A2 acts as an autocrine factor to stimulate osteoclast formation and bone resorption and is also a necessary component in endosomal activity. Annexin A2 has been located in the cytosol of ameloblast cells, close to the Tomes' processes, and in the ameloblast secretory vesicles (Goldberg et al., 1990). Annexins are thought play a role in tooth development through exocytosis and endocytosis due to higher levels of Annexin 2 mRNA being identified in pre-and post-secretory ameloblasts, as opposed to secretory ameloblasts (Bartlett et al., 2006).

1.3.5.4. Integrin

Integrins are cell-surface adhesion receptors with roles in cell-cell, cell-matrix and cell-pathogen interactions (Zhang and Chen 2012). Integrins consist of non-covalently linked α and β subunits. ITGB6 binds to integrin- $\alpha 5$ to form integrin- $\alpha v \beta 6$. Integrin- $\alpha v \beta 6$ is epithelial cell specific and binds to the arginine-glycine-aspartic acid (RGD) amino acid motif (Busk et al., 1992). RGD motifs are often found in extracellular matrix proteins such as vitronectin, fibronectin and tenascin-C. The recent discovery of a missense mutation in the I-domain of integrin $\beta 6$ (ITGB) resulting in hypomineralised amelogenesis imperfecta, has indicated a role for integrins in amelogenesis (Poulter et al., 2014A). The P196T mutation identified was in a family of Pakistani origin, presenting with pitted hypomineralised enamel with premature enamel failure. No other diseases were associated with this mutation. The particular point mutation resulted in a phenotype similar to that observed in mice lacking a functional *itgb6* gene. The authors proposed a potential mode of action being that the mutation in ITGB6 failed to allow the binding of the integrin to the latency associated peptide (LAP) of TGF β , which resulted in the inhibition of MMP-20 expression. This would lead to failure to process the ECM in the enamel correctly and hypomineralisation as observed in the human family and mouse model (Poulter et al., 2014B). Enamel hypoplasia and skin blistering in patients with epidermolysis bullosa are also associated with integrin mutations. Six

novel mutations in all 10 genes of ITGB β 4 have been identified with patients with epidermolysis bullosa with pyloric atresia (Pulkkinen et al., 1998).

1.4. Inherited diseases of enamel

1.4.1. Amelogenesis Imperfecta

Amelogenesis imperfecta (AI) is a disease of tooth enamel development where the biomineralisation process has failed. AI can cause teeth to be unusually small, discoloured, pitted or grooved and prone to rapid wear and breakage. The clinical appearance of AI can vary among affected individuals and can affect both primary and permanent teeth. AI is genetic in origin and presents as hypoplastic, hypomineralised and/or hypermineralised enamel. The prevalence of AI varies from 1:700 people in Sweden to 1:14,000 people in the USA (Crawford et al., 2007)

Mutations in the enamel matrix proteins and in cellular proteins affecting ameloblast function underlie many cases of AI. These mutations alter the structure of the proteins or prevent protein secretion. Mutations in the following genes are all known to cause AI: enamelin (*ENAM*; chromosome 4 long arm position 21 – 4q21), amelogenin (*AMELX*; X chromosome short arm position 22.3 to 22.1 – Xp22.3-p22.1), ameloblastin (*AMBN*; 4q21), tuftelin (*TUFT1*; 1q21), amelotin (*AMELOTIN*; 4q13), kallikrein 4 (*KLK4*; 19q13.3-q13.4) and MMP-20 (*MMP20*; 11q22.3-q23).

AI can be X-linked, autosomal dominant or recessive. Four major manifestations of AI are described using the Witkop classification system; hypoplastic (enamel of reduced thickness), hypomaturation (enamel of normal thickness, but softer as mineralisation fails to mature), hypocalcified (enamel of normal thickness, but softer due to reduced mineral content) and hypomaturation-hypoplastic with taurodontism (reduced enamel thickness with reduced mineral content and teeth present with enlarged and elongated pulp chambers (Witkop, 1988). These have been further subclassified into over 14 forms of AI as described in the literature (Aldred and Crawford., 1995). There are also cases of AI that appear to be sporadic, in people with no family history of the disease. Improvements in molecular genetics should help aid identification of further gene mutations.

1.4.1.1 X-linked Amelogenesis Imperfecta

X-linked AI usually manifests as hypoplastic AI. Five percent of AI is caused by mutations in the *amelogenin* (*AMELX*) gene. Males with X-linked AI have more

severe dental abnormalities than females. Males who inherit the AMELX defects have only a very thin layer of enamel, or poorly mineralised, discoloured enamel. Females have 2 X chromosomes, and those who inherit only one altered copy of the AMELX gene are less severely affected as they have a normal copy of the gene on the other X chromosome to produce amelogenin. Their teeth show structural defects such as distinctive patterns of vertical ridges and grooves, or Lyonisation due to alternating bands of normal thickness enamel and reduced thickness enamel (Balmer et al., 2004). Mutations identified include deletions, single base alterations and premature stop codons. Figure 9 shows the amelogenin gene and the locations of known mutations that cause AI in humans. The gene mutation and resulting protein alteration are given. The resulting AI type is also given.

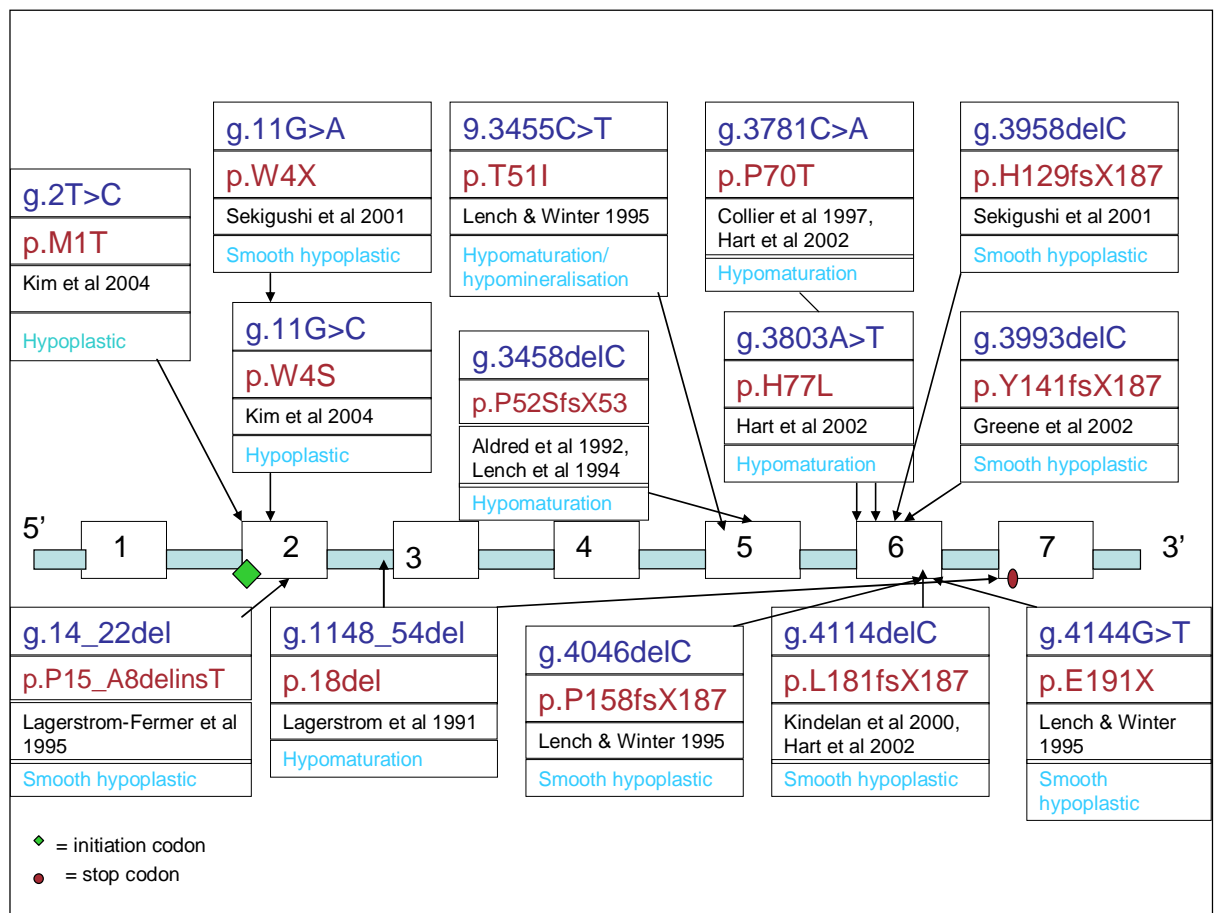


Figure 9. Schematic of the amelogenin gene, showing the genetic location of the identified mutations (g), the resulting protein mutation (p), and the clinical enamel phenotype.

1.4.2 The Y64H amelogenin mutation in mice

1.4.2.1 Wild type and mutant (Y64H) mice teeth

Human *AMELX* mutations include total loss of protein secretion mutations causing loss of the C-terminal of amelogenin (Wright et al., 2003), and mutations

affecting the amelogenin N-terminal region that include a lectin-like tri-tyrosyl domain reported to bind to N-acetyl-D-glucosamine (Ravindranth et al., 1999). Mutations in the amelogenin gene are known to cause amelogenesis imperfecta, a genetic disease resulting in biomineralisation defects of tooth enamel. For example, Collier et al. (1997) showed that a single amino acid mutation in the human amelogenin gene resulted in the substitution of proline at position 70 with threonine and is associated with hypoplastic amelogenesis imperfecta in affected individuals. The mutation lies in the conserved ATMP motif domain (as described previously Chapter 1 Section 1.3.4.1.1) shown below (the proline residue that is substituted by threonine in the mutation is highlighted in red):

Human X	Y	P	S	Y	G	Y	E	P	M	G	G	W	L	H	H	Q
Bovine X	Y	P	S	Y	G	Y	E	P	M	G	G	W	L	H	H	Q
Porcine	Y	T	S	Y	G	Y	E	P	M	G	G	W	L	H	H	Q
Murine	Y	P	S	Y	G	Y	E	P	M	G	G	W	L	H	H	Q
Rat	Y	P	S	Y	G	Y	E	P	M	G	G	W	L	H	H	Q

Studying human amelogenesis is difficult because unerupted teeth are required which invariably means obtaining post mortem material from children (which apart from the ethical issues involved results in tissues affected by post mortem changes unless unerupted wisdom teeth are available). Fortunately, a mouse model phenocopying human hypoplastic amelogenesis imperfecta was available (M100888 mutant from RIKEN Institute) and genetic analysis carried out as part of this research program (by Dr Martin Barron, University of Manchester) showed that the mutation involved the substitution of tyrosine 64 (shown in blue above) with histidine (Y64H substitution) (Barron et al., 2010). Given that the murine mutation is within the same ATMP domain as the proline 70 mutation reported in human amelogenesis imperfect, this mouse model would appear to provide a suitable model for study.

It is difficult to elucidate the underlying molecular mechanisms associated with amelogenesis imperfecta in humans due to the inability to obtain viable, developing (unerupted) teeth. Rodent incisors provide a workable alternative as they continuously erupt throughout the life of the animal and provide access to all stages of enamel development in one tooth. Mice models have been used in gene targeting experiments to define the roles of proteins in enamel development. An N-

ethyl-N-nitrosourea (ENU-) induced mutation in mouse model (M100888 Riken Japan) has an x-linked enamel phenotype suggesting mutations in the *amelogenin* gene (*amelx*; the only ECM protein located on the X-chromosome. This mutation was identified by the Leeds-Manchester group as a single amino acid substitution involving the replacement of tyrosine 64 with histidine (Y64H mutation) (Barron et al., 2010). The Y64H mutation lies in the highly conserved amelogenin ATMP domain (PYPSYGYEPMGGW mutated to PHPSYGYEPMGGW). A P-T mutation of the third proline results in hypomaturation amelogenesis imperfecta in humans (Collier et al., 1997). This mutation has been shown *in vitro* to inhibit normal amelogenin proteolysis and to abrogate the lectin-like binding by the tri-tyrosyl domain (Ravindranath et al., 1999; Li et al., 2001) (see section 1.3.4.1.1). M100888 was identified during a large screen on mutated mice for dominant abnormal phenotypes (Masuya et al., 2005). C57BL/6J male mice (CLEA Japan) were administered with ENU [N-ethyl-N-nitrosourea (C₃H₇N₃O₂)], a highly potent mutagen, at 150-150 mg/kg, and crossed to DBA/2J female mice (CLEA Japan). ENU is an alkylating agent that transfers its ethyl group to the DNA nucleotides, preferentially to thymine (Coghill et al., 2002). ENU can induce one new mutation for every 700 loci, but in too high a concentration can be toxic. It was first extensively used by Bill Russell for designing mouse strains for studies into the effects of toxins and chemicals (Russell et al., 1979). The M100888 ENU mutant was identified during a screen of F1 hybrids for dominant phenotypes at 8 weeks of age (Inoue et al., 2004; Masuya et al., 2005). Six mouse phenotypes were identified that exhibited abnormal incisor surfaces, of which M100888 was one. M100888 was obtained from the RIKEN Institute (<http://www.gsc.riken.jp/mouse/>) and maintained in a DBA/2J genetic background at the University of Manchester in accordance with the Animals (Scientific Procedures) Act, UK, 1986 (Barron et al., 2010). Gross morphology of the affected mice showed uneven, shortened incisors with chalky-white, opaque, rough and pitted surfaces (figure 10 below). Examination of the lower jaw of the affected males shows a large, eroded, discoloured inferior border of the mandible. Dissection of the lower incisors showed that the mineralising enamel distal to the white opaque zone (where removal of the ECM normally occurs) was irregular and discoloured. Genotypic analysis showed that the T to C transition at nucleotide 249 of the *Amelx* coding sequence resulted in a missense mutation Y64H. The Y64H is a mutation of the first tyrosine in the PYP SYG YEP MGGW sequence of amelogenin in the C-terminus of the TRAP domain. The mutation was present in all the affected males (n=72) and all the affected females (n=72) analysed, but was not detected in the wild type littermates (n=160) (Barron

et al., 2010). Affected males and homozygous females displayed a more severe phenotype than heterozygous females.

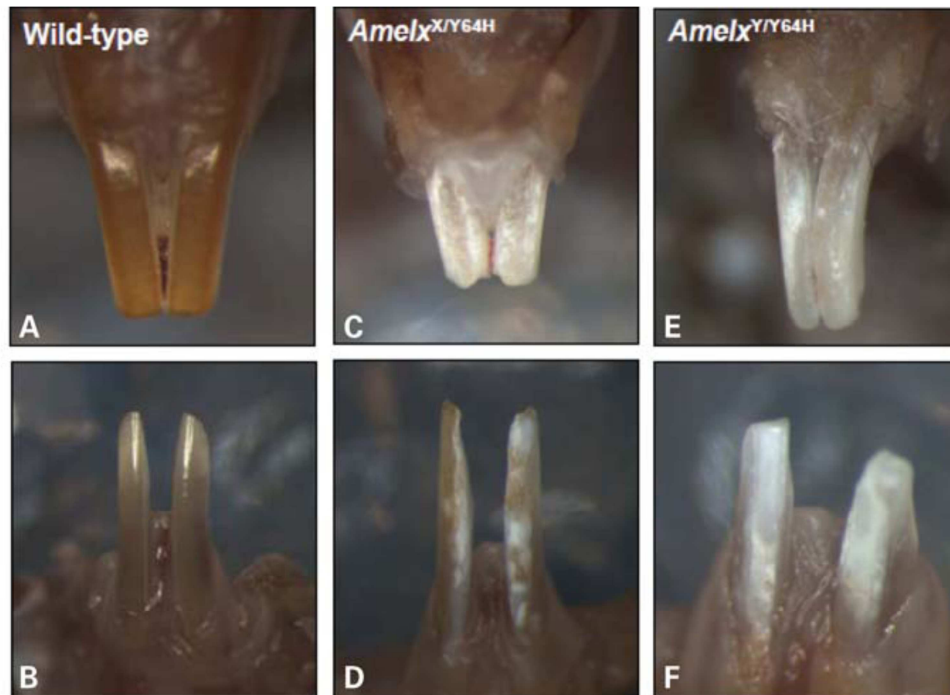


Figure 10. Images showing the wild-type and *Amelx* mice incisors. Wild-type maxillary (panel A) and mandibular (panel B) incisors show smooth enamel, opalescent and orange/brown in colour. Panels C and D show the maxillary (C) and mandibular (D) incisors for heterozygous female mutant mice (*Amelx*^{X/Y64H}), illustrating patches of rough, chalky enamel. Panels E and F show the maxillary (E) and mandibular (F) incisors for hemizygous male mutant mice (*Amelx*^{Y/Y64H}), illustrating the whole of enamel surface as rough, opaque and chalky. The mutant mice teeth also show shortened incisors with irregular edges (C-F). Barron et al., 2010. Reproduced under Creative Commons Attribution License. Modified from figure 3 published in: 'A mutation in the mouse *Amelx* tri-tyrosyl domain results in impaired secretion of amelogenin and phenocopies human X-linked amelogenesis imperfecta' by Barron et al 2010 *Hum. Mol. Genet.* (2010) 19 (7): 1230-1247. Direct link: <http://www.ncbi.nlm.nih.gov/pubmed/20067920>

How does this single amino acid mutation, from tyrosine to histidine at position 64 of amelogenin give rise to the effects seen in amelogenesis imperfecta?

1.4.2.2 Tyrosine and Histidine Biochemistry

Amelogenin is secreted by specialist ameloblast cells prior to the tooth erupting into the mouth, and interacts with other secreted proteins to form an extracellular organic matrix, onto and in to which hydroxyapatite crystals nucleate and grow to form the enamel prisms (Moradian-Oldak, 2001; Hu et al, 2002). The

tertiary structure of amelogenin still remains to be defined. As described previously (section 1.3.4.1.1) the N terminus of amelogenin is a highly conserved region of 45 amino acids, comprising the so called tyrosine rich amelogenin peptide (TRAP) containing 6 tyrosine residues, with the final 3 tyrosine residues lying at the C terminal of TRAP defining the ATMP region.

The tyrosine to histidine change at amino acid 64 (Y64H) clearly has a huge impact on amelogenesis as evidenced by the dramatic clinical phenotype in affected animals (figure 10 above). Tyrosine can act as a receiver of phosphate groups transferred by receptor tyrosine kinases (serine and threonine) during signal transduction (Hanks et al., 1988) but there is no evidence that any tyrosine is phosphorylated in amelogenin. Tyrosine is most often found in beta-pleated sheet structures, as it is hydrophobic and prefers to be buried in hydrophobic protein cores (Farber and Mittermaier, 2008). The aromatic side chain in tyrosine is involved in protein stacking interactions with other aromatic side chains. Tyrosine contains a reactive hydroxyl group that can be involved with interactions with non-carbon atoms. Tyrosine can be substituted by other aromatic amino acids (Betts and Russell, 2003). In contrast, histidine is a polar amino acid that does not substitute well with any other amino acid due to its unique biochemical properties. Histidine is highly hydrophilic and is most commonly found in alpha helical structures. The imidazole ring of the histidine side chain has a pKa near to physiological pH which means that subtle shifts in pH will change its net charge. This makes histidine the ideal amino acid for charge relay systems such as catalytic triads and cysteine and serine proteases (Wolfe et al., 2001). That the imidazole side chain changes from neutral to positive depending on pH, means that histidine may be hidden in a protein core or be exposed (Betts and Russell, 2003). In effect, histidine can act as a variable charge centre whose charge is controlled by pH and intuitively the insertion of such a disruptive residue into a protein is likely to affect both structure and function.

In support of this contention, tyrosine to histidine mutations has been noted in several proteins. Tang et al., 1999 showed that a tyrosine to histidine mutation at position B5 of insulin changes the structure from an extended conformation (T state) to a stable alpha helix (R state). This R state is stabilised by non-polar interactions between the phenolic molecules and the B5 histidine. Pegg et al., 1999, showed that an alteration in the conserved tyrosine residue at position 158 to histidine in human O⁶ – alkylguanine-DNA alkyltransferase renders it insensitive to the inhibitor O⁶- benzylguanine. The presence of the charged residue in the active site pocket discourages the binding of hydrophobic residues. The charged residue

influences the steric effect, increasing resistance. Bobola et al., 2001, showed that a naturally occurring tyrosine to histidine replacement at residue 33 of human thymidylate synthase confers a 4 fold increase in resistance to 5-fluoro-2-deoxy uridine in mammalian and bacterial cells.

A tyrosine to histidine mutation has also been shown to play a role in several diseases.

Age related macular degeneration (AMD) has been shown to be caused by a tyrosine to histidine mutation at position 402 located on C1q exon 9, and is located in the complement factor H (CFH) protein (SCR7) and contains overlapping binding sites for C-reactive protein, heparin and M protein (Giannakis et al., 2003). The T402H mutation causes increased inflammation in the outer retina. Subjects heterozygous for the mutation have a 2.5 to 4.6 fold increase in AMD. Subjects homozygous for the mutation have a 5.6 to 7.4 fold increase in AMD (Klein et al., 2005).

Von Hippel Lindau syndrome results in benign tumours of blood vessels, central nervous system, eyes, adrenal glands and renal cell carcinoma. Tyrosine to histidine substitutions (Y112H and Y98H in von Hippel-Lindau tumour suppressor protein (VHL)) prevent the binding between VHL and the hypoxia inducible transcription factor (HIF), resulting in overexpression of angiogenic growth factors and local proliferation of blood vessels (Zbar et al., 1996; Ohh et al., 2000).

It is clear that substitution of tyrosine with histidine can have great effects on the biochemistry and stereochemistry of proteins. In some substitutions, the stereochemical properties of the substituent may be sufficiently similar that protein function is maintained and not every point mutation leads to a noticeable phenotypic effect. However, due to its rather unique acid-base properties described above, histidine does not substitute particularly well for other amino acids (Betts and Russell, 2003). Not every site in a protein is equally vulnerable to mutations. Some areas of a protein will remain functional even with multiple sequence changes, while other areas cannot be altered at all without serious consequences. Active centres of enzymes and residues involved in protein stability are functionally important and evolutionary conserved and are especially vulnerable to the effects of any mutation (Steward et al., 2003). Although not an enzyme active centre, the amelogenin ATMP domain is believed to be functionally important (see section 1.3.4.1.1) and substitution of tyrosine 64 (in blue below) with histidine adds a third histidine to the domain which could dramatically alter amelogenin structure and function as observed in Y64H mutant mice.

.....Y P S Y G Y E P M G G W L H H Q.....

The discussion sections 4.2 and 4.4 will discuss the results showing the impact of the Y64H mutation on the potential of amelogenin (with and without 32 kDa enamelin) to nucleate mineral *in vitro*.

The mutation in amelogenin investigated in the murine model occurs at amino acid 64, the third tyrosine in the amelogenin trityrosyl amelogenin peptide (ATMP) motif. This third tyrosine is mutated to a histidine amino acid. Figure 11 compares the structures of the two amino acids.

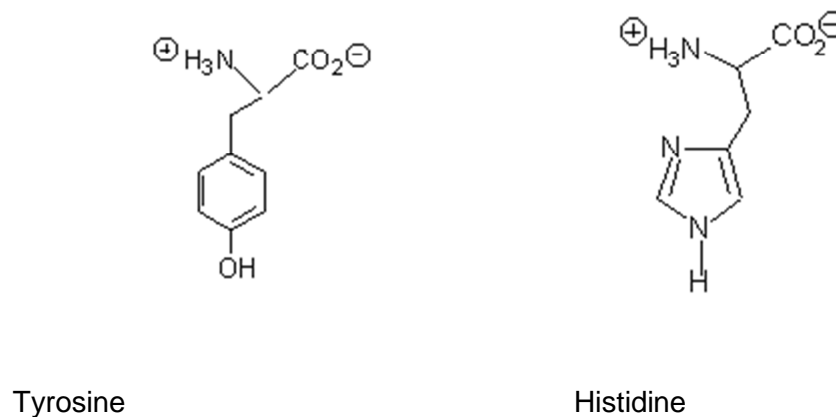


Figure 11. The structures of tyrosine and histidine amino acids at physiological pH.

Tyrosine is partially hydrophobic so prefers to be buried in protein hydrophobic cores (Betts and Russell, 2003). Although essentially hydrophobic, the presence of the hydroxyl group allows tyrosine to participate in hydrogen bonding with other amino acids or ligands. This allows tyrosine to behave like a polar amino acid, such as arginine or lysine. However, tyrosine is overall less polar due to the presence of the non-polar C-C and C-H bonds in the phenolic side chain. This side chain allows tyrosine to be water soluble, even though it is partially hydrophobic. The aromatic side chain means tyrosine is involved in stacking interactions with other aromatic side chains. Tyrosine has a reactive hydroxyl group making it likely to be involved in interactions with non-carbon atoms. A common role for tyrosine (and serine and threonine) within intracellular proteins is phosphorylation. Protein

kinases frequently attach phosphates to these 3 residues as part of signal transduction pathways.

Histidine is in fact an amino acid with an ionisable imidazole side chain having a pKa of 6.5. Histidine is generally polar, but due to its chemical properties, it does not substitute particularly well with any other amino acid. Because its side chain pKa is near to physiological pH histidine is switched between the uncharged protonated and the charged un-protonated form on relatively small fluctuations in environmental pH. This flexibility has two effects; 1) ambiguity about whether it prefers to be buried in the protein core or exposed to solvent, and 2) histidine is the ideal residue to serve as a charge relay centre in a range of enzymes as the side chain can accept or donate protons.

For example. in catalytic triads, the basic nitrogen of histidine is used to subtract a proton from serine, threonine or cysteine to activate it as a nucleophile.

The imidazole ring is aromatic at all pH values. It contains 6 pi electrons; four from 2 double bonds and 2 from a nitrogen lone pair. It can form pi stacking interactions but is complicated by the potential positive charge incurred when the side chain nitrogen is protonated.

Tyrosine and histidine, along with phenylalanine and tryptophan, are aromatic amino acids in that they have aromatic side chains. Aromatic residues are proposed to participate in 'stacking' interactions (Hunter et al., 2001). Here numerous aromatic rings stack on top of one another such that their PI electron clouds are aligned. They can also play a role in binding to specific amino acids, such as proline. SH3 and WW domains use these residues to bind their polyproline-containing interaction partners (Weisner et al., 2002).

Looking at the genetic codes for tyrosine and histidine reveals that this amino acid mutation can actually be pin-pointed to a single base pair change. The mutation is a uracil to cysteine change in the first position of the RNA codon. Uracil and cysteine are both pyrimidines, containing one small aromatic ring.

1.4.3 Autosomal dominant amelogenesis imperfecta (ADAI)

Autosomal dominant forms of AI map to chromosome 4q11-q21. ENAM, AMBN and albumin all map to this same region (Hu et al., 2000; Dong et al. 2000). Autosomal dominant inheritance describes the route by which the mutation occurs. Two copies of the gene occur on the chromosomes, in this case chromosome 4, but autosomal dominant inheritance means that only one copy of the gene needs to be

altered for the associated phenotypic disease to manifest i.e. the mutated gene is dominant to the wild type gene.

Eight mutations have been identified in the *ENAM* gene which give rise to ADAI. These have a variety of phenotypic effects on the enamel. Some mutations decrease the amount of enamelin produced (Kida et al., 2002; Hart et al., 2003; Kim et al., 2005A) . Others result in a shortened or altered enamelin which results in shallow pits and horizontal grooves in the tooth enamel. Kida et al. (2002) identified a Japanese family with a single G deletion with a series of 7 G residues at exon 9 – intron 9 boundary of the enamelin gene. *ENAM* mutations result in hypoplastic enamel; thin enamel with spaced apart teeth. Figure 12 shows the human manifestation of this hypoplastic enamel.



Figure 12. Hypoplastic enamel due to a mutation in the enamelin gene (photograph courtesy of Roger Shore).

Figure 13 shows the enamelin gene and the locations of known mutations that cause AI in humans. The gene mutation and resulting protein alteration are given. The resulting AI type is also shown. Exon 2 is not found in humans, but is found in the rodent enamelin.

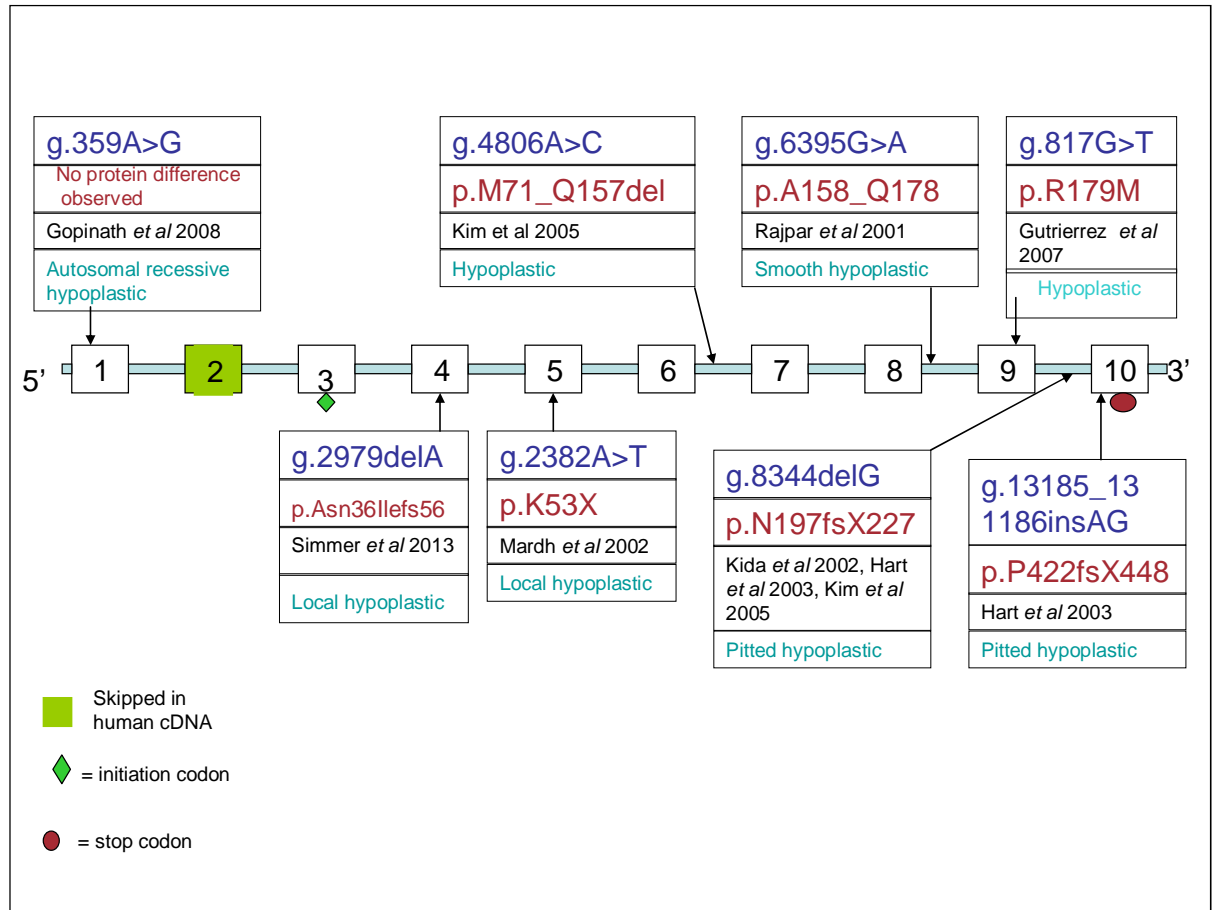


Figure 13. Schematic diagram of the enamelin gene showing the genetic location of the identified mutations (g), the resulting protein mutation (p), and the clinical enamel phenotype. and the resulting enamel phenotype.

1.4.4 Autosomal recessive amelogenesis imperfecta (ARAI)

Kallikrein-4 maps to 19q13.4 and a mutation in the gene has been identified as causing autosomal recessive hypomaturation AI (Hart et al., 2004). Autosomal recessive inheritance means that both copies of the gene need to be altered for the disease to manifest i.e. the wild type gene is dominant to the mutant gene. Three mutations have been identified in the MMP-20 gene that results in autosomal recessive AI (ARAI). All three are single point mutations that prevent the secretion of functional MMP-20 protein (Kim et al., 2005B; Ozdemir et al., 2005; Kim et al., 2006). This results in other organic matrix proteins not being cleaved properly during amelogenesis, and results in soft enamel with abnormal crystal structure (hypomaturation AI). This causes teeth to be rough, discoloured and prone to breakage (Hart et al., 2004; Hu et al., 2005).

The fact that these mutations in the genes for the enamel matrix proteins and proteases leads to defects in enamel formation underpins the importance of these

proteins in the biomineralisation process in tooth enamel development. Mutations in both the proteins and the proteases involved in amelogenesis lead to enamel defects, indicating that both the proteins and proteases are as important as one another in this finely orchestrated process.

1.4.5 Other genes implicated in amelogenesis imperfecta

Mutations in the 'family with sequence similarity 20, member A' gene (FAM20A) map to chromosome 17q24.2. FAM20 consists of 3 members. FAM20B is a kinase involved in phosphorylation and is expressed during the maturation stage of amelogenesis (Koike et al., 2009; O'Sullivan et al., 2011). FAM20C is essential for bone development (Hao et al., 2007). FAM20A is expressed in the enamel organ and gingiva (O'Sullivan et al., 2011). Mutations in the FAM20A gene are associated with hypoplastic AI and gingival overgrowth, resulting in the retention of primary dentition and delayed eruption of the permanent dentition (O'Sullivan et al., 2011).

Mutations in the family with sequence similarity 83, member H gene (FAM83H) map to chromosome 8 (8q24.3) and code a protein associated with intracellular vesicles and trans Golgi organelles (Ding et al., 2009). FAM83H is expressed in developing teeth but is not limited to teeth and is expressed in other tissues of the body (Kweon et al., 2013). Mutations in FAM83H result in autosomal dominant hypocalcified AI (Lee et al., 2011). So far, 16 mutations have been identified that are non-sense or frameshift mutations in exon 5, causing premature translation termination between Serine 287 and Glutamine 674 (Lee et al., 2011) and resulting in a truncated protein (Kim et al., 2008; Lee et al., 2008; Hart et al., 2009; Wright et al., 2009; El-Sayed et al., 2010; Lee et al., 2011).

The WD repeat containing protein 72 gene (WDR72) encodes for an intracellular protein involved in protein-protein interactions. A point mutation in exon 15 (c.2358C>G) results in a premature stop codon manifesting as autosomal dominant recessive AI (El-Sayed et al., 2009, 2011). El-Sayed et al., 2011 hypothesised that the late stage of enamel maturation is affected by this mutation due to ultrastructural analysis of deciduous teeth revealing a reduction in mineral density in erupted teeth and a difference in electron density compared to normal enamel.

Distal-less homeobox 3 gene (encoding DLX3) maps to chromosome 17 (q21-q22). DLX3 is a homeodomain transcription factor expressed in dental epithelium and mesenchyme, as well as the neural crest, hair follicles, placenta and epidermal cells (Beanan and Sargent, 2000). A two base-pair deletion results in a premature

stop codon, causing an 88 amino acid truncated protein, manifesting as a unique syndromic AI known as amelogenesis imperfecta hypomaturation-hypoplastic type with taurodontism (AIHHT) displaying teeth with thin, hard enamel and enlarged pulp chambers (Dong et al., 2005).

As more families present with amelogenesis imperfecta phenotypes, it is likely that more gene candidates for AI will be discovered. This will all assist with expanding the existing knowledge about amelogenesis and the complex blueprint for biomineralisation in enamel.

1.4.6 Syndromic and non-syndromic disease of enamel

Even though the enamel defects noted with AI are more often than not seen in isolation, some forms do have associated anomalies within the oral cavity or other regions of the body (Cobourne and Sharpe 2013). Hart et al 2013 noted that autosomal recessive AI due to an ENAM mutation is associated with open bite of the jaws. Dong et al 2005 noted a DLX3 mutation that resulted in autosomal dominant AI also resulted in taurodontism. MacGibbon syndrome is an autosomal recessive form of AI, manifesting as hypoplastic, thin or absent enamel and nephrocalcinosis (deposition of calcium in the kidneys) (MacGibbon 1972).

A number of conditions also result in enamel defects as one of the phenotypic presentations.

Syndromes

Kohlschutter-Tonz syndrome presents as AI, yellow teeth, spasticity and developmental delays (Kohlschutter et al., 1974). Tuberous sclerosis results in enamel hypoplasia and multiple organ hamatomas (benign tumours) (van Slegtenhorst et al., 1997). Focal dermal hypoplasia manifests as enamel hypoplasia, skin atrophy and pigmentation, fat herniation, papillomas and anomalies of the digits (Grzeschik et al. 2007). Smith Magenis syndrome present as enamel dysplasia, facial anomalies, hearing loss and delay in speech (Slager et al., 2003). Vitamin D-dependent rickets type 1 manifests as enamel hypoplasia with yellow-brown discolouration, hypocalcemia, hypophosphatemia, and impaired bone formation (Kitanaka et al., 1998). Automimmune polyendocrinopathy is a syndrome that results in enamel hypoplasia, chronic mucocutaneous candidiasis and multiple autoimmune endocrinopathies (Perinola et al., 1998).

Tricho-dento-osseus (TDO) syndrome has hypoplastic and hypomature enamel, taurodontism and defects of bone, nails and hair (Price et al., 1998; Wright et al., 2008). Jalili syndrome is a rare autosomal recessive disease caused by

mutation in the conserved domain protein 4 gene (CNNM4) that presents with hypoplastic and hypomineralised enamel, and conerod dystrophy of the retina (Parry et al., 2009; Polok et al., 2009). Morquio syndrome, also known as mucopolysaccharidosis type IV A, is an autosomal recessive lysosomal storage disease (Kirirons and Nelson, 1990). It is caused by the accumulation of GAGs, such as keratin sulphate and chondroitin-6-sulphate, intracellularly, due to a mutation in galactosamine-6-sulphate sulphatase (GALNS) (Fukuda et al., 1992). Patients present with dental anomalies akin to hypoplastic AI and widely spaced, flared maxillary incisors and pointed posterior teeth, skeletal dysplasia and opacity of the corneas (Barker and Welbury, 2000; Levin et al., 1975). Type III Dentinogenesis Imperfecta was first identified in a population in Brandywine, Maryland, US. Teeth are opalescent with marked attrition. The pulps of developing teeth are larger than normal, but become almost completely obliterated. Scanning electron microscopy shows a significant reduction in the number of dentin tubules on fractured dentin surfaces. Enamel pitting is also noted in patients with type III DI (Levin et al., 1983).

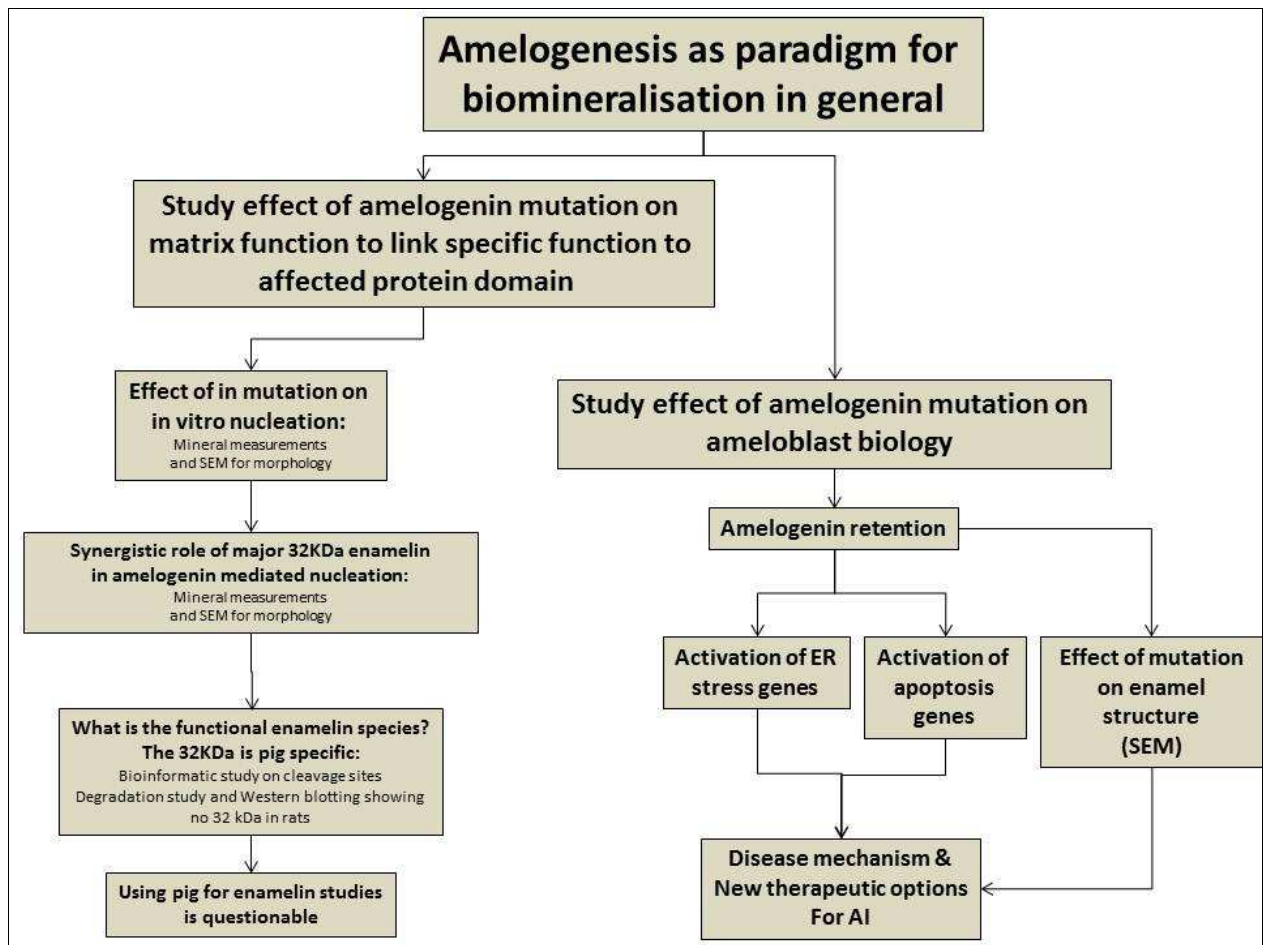
Aims and Objectives

The research carried out in this project complements a larger programme of work funded by the Wellcome Trust. This work uses tooth formation as a paradigm to study biomineralisation - specifically the role of the extracellular organic matrix in this process.

The specific objectives for this doctoral thesis were to investigate the *in vitro* hydroxyapatite nucleating potential of enamel proteins (amelogenin and enamelin) and how these proteins subsequently regulate crystal growth. Recombinant proteins were generated for use in these studies so as to compare the effects of a specific mutation in mouse amelogenin (Y to H substitution at position 64) identified by the group. The mineral produced during these *in vitro* studies was characterised chemically and by electron microscopy so that the relationship between the nature of the matrix protein components and resulting mineral chemistry and morphology could be explored.

The main focus is on a Y64H mutation in mouse amelogenin that has similarities to a human amelogenin mutation, known to cause amelogenesis imperfecta. This mouse mutation was used to investigate whether amelogenesis imperfecta is caused by the secreted protein behaving differently to wild type amelogenin during nanosphere formation and mineralisation, or whether the mutation causes non-secretion of the protein. The latter possibility was explored using quantitative real time PCR to determine amelogenin biology at the transcriptomic level.

Below is an outline of the thesis and the areas investigated.



A number of hypotheses will be explored as part of this thesis.

Hypothesis 1: Is the 32 kDa enamelin breakdown product is conserved across all species? The majority of studies to date have used the porcine 32kDa enamelin product due to its ready availability. To investigate this hypothesis, western blot analysis of porcine and rat enamelin will be used, as will a bioinformatic exploration of enamelin sequences across many species.

Hypothesis 2: The AI phenotype generated as a result of the Y64H amelogenin mutation in mice is a result of the mutated protein behaving differently upon secretion. To investigate this hypothesis, *in vitro* nucleation studies will be performed to explore the effect of the mutation on the ability of amelogenin, and amelogenin in conjunction with enamelin, to nucleate hydroxyapatite mineral. *In vitro* binding studies will also be performed using the wild type and Y64H mutant amelogenin to investigate the effect of the mutation on protein-protein interactions.

Hypothesis 3: The AI phenotype generated as a result of the Y64H amelogenin mutation in mice is a result of the mutated protein being retained in the ameloblast and not being secreted correctly. Similar mutations in other proteins have resulted

in endoplasmic stress in cells, resulting in transcription and translation downregulation and ultimately apoptosis of the secretory cells. Quantitative PCR and SEM analysis of wild type and Y64H mutant mice incisors will be performed to probe whether ER stress and the unfolded protein response could be responsible for the AI phenotype in Y64H mutant mice.

Chapter 2

General materials and methods

This chapter describes the techniques and materials used throughout the research including the production and purification of recombinant proteins, gel electrophoresis, staining and antibody blotting, production of labelled proteins, and culture of cells *in vitro*. Specific experimental detail relating directly to the experiments conducted will be explained in detail in this chapter.

All chemicals and reagents were from Sigma-Aldrich, Poole, Dorset, UK unless otherwise stated.

2.1 Recombinant protein production

2.1.1 Production of recombinant 32 kDa enamel protein

The sequence for the human 32 kDa enamel protein (figure 14 below) was inserted into a pCepPU vector. This contains a BM-40 signal which allows the protein to be secreted. The vector was inserted into human embryonic kidney cells (293-EBNA) which were then cultured in serum free medium (Rock et al., 2004; Marson et al., 2005). The use of eukaryotic cells maintains the post translational modifications of the proteins. Following intracellular transcription and translation, the protein was secreted into, and recovered from, the serum free media. The recovered protein was confirmed by mass spectrometry and western blot analysis. Protein production was performed by Dr J. Maycock at Manchester University.

PWP IPQRPPTAF GRPKFSNEEG NPYYAFFGYH GFGGRPYYSE
EMFEDEYEKPK EKPPKPEDP PPDDPPPEAS TNTVPDANA TQSOPEGGND
TSPIGNTGPG PNAG

Figure 14: The amino acid sequence for the 32 kDa recombinant mouse enamel protein. The amino acids in red and underlined are the sites of the post-translational modifications.

2.1.2 Production of recombinant wild type and Y64H mutant amelogenin protein

An overview for the production process for wild type and Y64H mutant amelogenin recombinant proteins is shown in figure 15.

In brief, in Step 1 full length wild type and mutant Y64H mouse amelogenins were expressed using a pET28 expression vector (Novagen, Merck KGaA, Darmstadt, Germany) modified with a HRV 3C protease site and HIS tag in Rosetta DE3 *E.coli* cells (Novagen, Merck KGaA, Darmstadt, Germany). In Step 2, the cells were harvested by centrifugation and lysed using 6M guanidine-HCl. Step 3, the proteins were purified using nickel affinity chromatography (His Trap Nickel column, GE Biosciences, Little Chalfont, Bucks, UK) in the presence of 8M urea. In Step 4 the histidine tag was removed by incubating the protein with HRV 3C protease (A.G. Scientific, Inc., San Diego, California) overnight in 50 mM tris buffer (pH 8.0) at a concentration of 25µg/mL. Step 5 was the further purification of the cleaved and uncleaved recombinant amelogenin proteins by preparative SDS-PAGE (Bio-Rad Model 491 Prepcell, Bio-Rad, Hemel Hempstead, UK) using an 8 cm 12% polyacrylamide gel run at a constant power of 1 Watt. Fractions were collected over 300 minutes at a flow rate of 70 µL/min and fractions containing the cleaved purified recombinant amelogenin protein were identified by standard SDS PAGE. This was step 6. In Step 7 the relevant fractions where the cleaved and uncleaved recombinant proteins were located were desalted against 125 mM formic acid using a Hi Prep 26/10 desalting column (GE Biosciences, Little Chalfont, Bucks, UK). This resulted in step 8; purified, cleaved and uncleaved recombinant amelogenin protein. The uncleaved protein was returned to step 4 for further cleavage. The cleaved protein was freeze-dried and protein identity confirmed by mass spectrometry and western blotting (step 9).

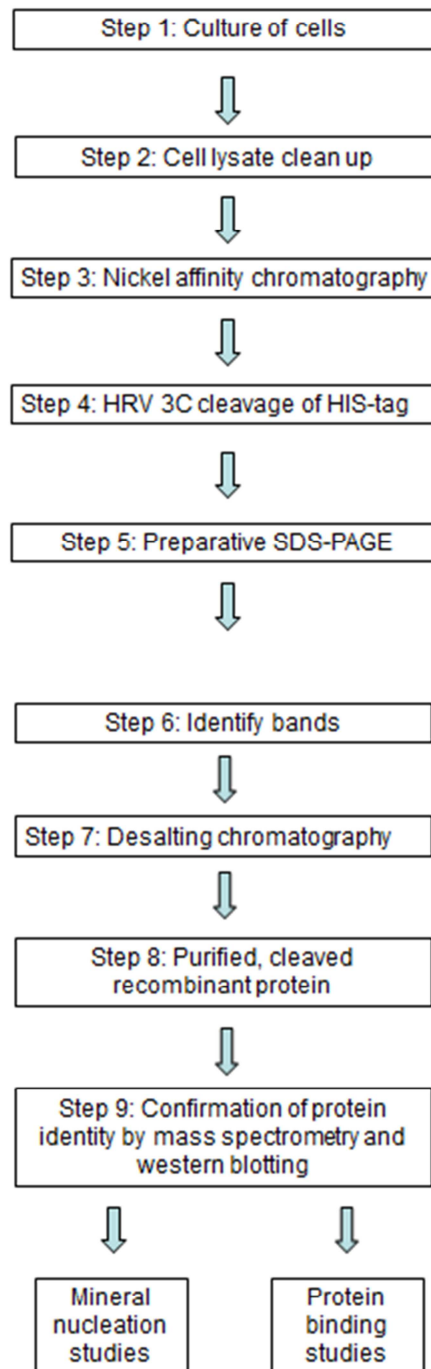


Figure 15: Sequence for recombinant amelogenin protein purification. The same procedural steps were used for recombinant wild type and recombinant Y64H mutant amelogenin production.

Step 1: The sequences for wild type and mutant amelogenin were inserted into a PET28 expression vector with a HRV 3C protease site (Leu-Glu-Val-Leu-Phe-Gln-Gly-Pro), and transfected into Rosetta DE3 *E.coli* cells. This was spread onto an agar plate and incubated overnight at 37°C. Resulting colonies were picked

with an inoculation loop and incubated in 10 mL tryptone soya broth for 7 hours at 37°C with shaking (200-300 rpm). This resulting inoculant was used as a starter culture or for creating glycerol stocks for future use. Glycerol stocks were created by mixing 0.5 mL starter culture with 0.5 mL 50% glycerol in a cryovial. These were stored at -80°C until needed.

Cells were cultured in 5 x 50 mL culture medium in 2 L conical flasks. The medium consisted of 2.5 g yeast extract and 13.5 g tryptone soya broth in 450 mL distilled water. This was autoclaved before use and supplemented with 2.5% 1 M Na₂HPO₄, 2.5% 1 M KH₂PO₂, 5% 1 M NH₄Cl, 0.5% 1 M Na₂SO₄, 0.4% 1 M MgSO₄, 0.1% CaCl₂, 0.5% Glycerol, 0.2% Lactose, 0.25% 1 M Glucose, 500 µL of 30 mg/mL kanamycin and 500 µL 34 mg/mL chloramphenicol. All supplements were sterilised before use. One 10 mL starter culture was added to each flask, and the flask was incubated overnight at 37°C with shaking.

Step 2: The following morning, the cultures were centrifuged at 10,000 rpm for 10 minutes. The supernatant was discarded and the cell pellet lysed in 6 M guanidine hydrochloride-HCl buffer pH8.0 (15 mL of 10 x stock buffer (68.995 g NaH₂PO₄ and 6.0 g tris volumised to 500 mL with distilled water) plus 85.95 g guanidine hydrochloride, volumised to 150 mL with distilled water), containing 3 protease inhibitor tablets per 150 mL buffer (Roche, Welwyn, Herts UK). The pellets were vortexed to smash open the cells. The slurry was then centrifuged for 1 hour at 20,000 rpm. After centrifugation, the supernatant was filtered using a disposable filter (Nalgene, Thermo Fisher Scientific, Loughborough, UK).

Step 3: Following centrifugation and filtration as described above, the filtrate was loaded onto a 5 mL Hi-Trap chelating column (GE Biosciences, Little Chalfont, Bucks., UK) primed with nickel sulphate. The protein attached to the column via the HIS tag, a series of 6 histidines. The protein was eluted with 8M urea buffer containing 0.4% imidazole (10 ml 10 x tris buffer (30.28 g tris plus 116.8 g sodium chloride, volumised to 500 mL with distilled water) plus 2.72 g imidazole and 48.08 g urea, volumised to 1000 mL with distilled water and the pH adjusted to 8. The eluent was then run on the Hi-Prep 26/10 desalting column on the AKTA explorer FPLC (GE Biosciences, Little Chalfont, Bucks., UK), using degassed 125 mM formic acid as the buffer.

Step 4: The protein fractions obtained from FPLC were freeze dried using a Christ freeze dryer (SciQuip, Shrewsbury, UK). To cleave the HIS Tag, the lyophilised protein was resuspended at 2 mg/mL in 50 mM tris-HCl pH 8. Cleavage occurred with the addition of HRV 3C protease (human rhinovirus 3C protease, a

cysteine protease that cleaves between Gln and Gly) (A.G. Scientific, San Diego, California) followed by overnight incubation at 4°C. Confirmation of cleavage was performed by running a small fraction of the cleaved protein on a SDS-PAGE mini-gel and staining with Coomassie Blue stain (Instant Blue ready to use Coomassie stain, Expedeon, Cambridge)(see below).

Step 5: The cleaved protein was then run down the PrepCell 491 (Bio-Rad, Hemel Hempstead, UK) to separate cleaved and uncleaved protein. In order to prepare purified fractions from cleaved amelogenin, preparative SDS-polyacrylamide gel electrophoresis was used (discontinuous buffer system analytical SDS-PAGE). Separation of individual protein components was carried out on the basis of molecular size using SDS-PAGE according to the method of Laemmli (1970). The resolving gel (15% acrylamide containing 3% bisacrylamide in 1.5 M Tris-HCl buffer, pH 8.8, 0.1% SDS) was cast in a 37 mm diameter tube using the model 491 Prep Cell (Bio-Rad, Hemel Hempstead, UK) according to the manufacturer's instructions (total volume of gel used = 50 mL). The resolving gel contained 20% glycerol, allowing the stacking gel layer to be overlaid immediately. The stacking gel comprised of 10 mL 4% acrylamide (3% bisacrylamide in 0.5 M Tris-HCl, pH 6.8, 0.1% SDS) and was overlaid with water-saturated butan-2-ol. The gel was left to polymerise overnight at room temperature. Maintenance of the gel at room temperature during polymerisation of the gel was achieved by circulating water between a reservoir and the cooling core within the gel tube using a recirculation pump. This prevented excessive heat build up and assisted in the formation of uniform gels. The water-saturated butan-2-ol was removed and the top of the gel washed with SDS running buffer. Each 2 mL of HRV-3C treated recombinant amelogenin was mixed with 500 µL of 4 x SDS sample buffer (containing bromophenol blue) (see recipe below) and loaded onto the top of the gel. Electrophoresis was performed at 12 watts constant power at room temperature with running buffer circulating through the cooling core. Once the bromophenol blue dye front of the protein loading reached the bottom of the gel (approximately 6 hours) the elution pump was turned on and set to elute at 0.75 mL/min with the fraction collector collecting samples every 10 minutes. A total of 80 fractions were collected. After collection, every third fraction was re-electrophoresed by diluting 15 µL of the fraction with 5 µL of 4x SDS sample loading buffer (0.625M Tris-HCl, 10% glycerol, 2% SDS, 0.00125M bromophenol blue) and running on 12% SDS-PAGE mini-gels. This allowed the specific fraction location of proteins of interest to be identified. Fractions with similar protein molecular weight size content were pooled together. These were then desalted using an AKTA explorer FPLC

system (GE Biosciences Little Chalfont, Bucks., UK) and a Hi-prep™ 26/10 desalting column and 0.125 M formic acid. The desalted protein was then freeze-dried and used for further experiments.

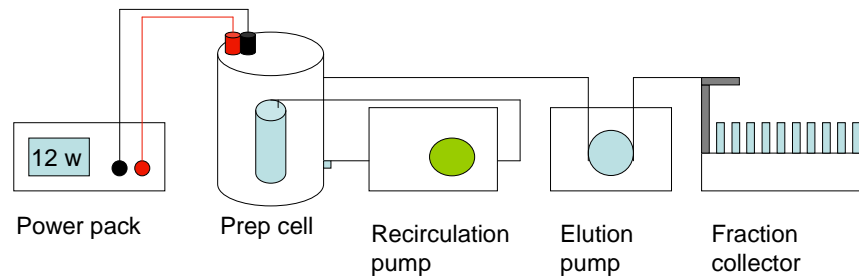


Figure 16. Schematic diagram of the Bio-Rad PrepCell 491 in action.

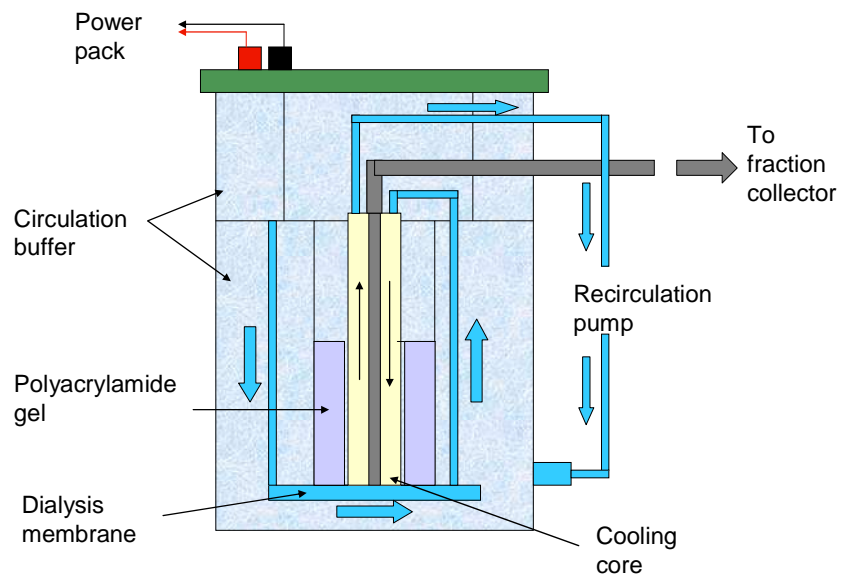


Figure 17. Schematic diagram of the flow inside the Bio-Rad PrepCell 491.

Step 6: SDS-PAGE gels of the fractions were run and silver stained to visualise the proteins. Separation of proteins was carried out on the basis of molecular size using SDS-PAGE based on the procedure described by Laemmli

(1970). Gels were cast in Protean Tetra mini gel rigs (Bio-Rad, Hemel Hempstead, UK) according to the manufacturer's instructions. The resolving gel consisted of 12% total monomer (acrylamide and N'N'-bis-methylene-acrylamide (bisacrylamide) of which 3% was bisacrylamide) in gel buffer (1.5M Tris-HCl, pH 8.8, 0.1% SDS) with a stacking gel of 4% total monomer (3% bisacrylamide) in gel buffer (0.5M Tris-HCl, pH 6.8, 0.1% SDS). Once polymerisation was complete, the gel surface was washed well with 1 x SDS running buffer (25 mM Tris, 0.192 M glycine, 0.1% SDS, pH 8.3). Recombinant amelogenin proteins were dissolved in SDS sample buffer (160 mM Tris-HCl, pH 6.8, 2% SDS, 26% glycerol, 0.1% bromophenol blue) to a concentration of 1 µg/µl and heated at 90°C for 2 minutes prior to loading. Molecular weight markers covering the range 2 to 250 kDa (Precision protein standards, Bio-Rad) were loaded at 5 µL per lane. Gels were run at room temperature using 1 x SDS running buffer at 200 V constant voltage until the blue dye front reached the bottom of the gel (approximately 45 minutes). After removal from the glass plates, the gels were either stained in Coomassie blue R250 (Instant Blue Stain, Expedeon Ltd, Babraham Hall, Cambs., UK) or silver stained. Coomassie blue is a triphenylmethane dye that was first used to visual proteins in polyacrylamide gels by Meyer and Lamberts (1965). The Coomassie blue dye binds to proteins in the gels by a combination of van der Waals bonds and electrostatic bonds to form strong non-covalent complexes. The formation of this dye-protein complex allows the blue colour to be visualised due to stabilisation of the negatively charged anionic form of the dye. The number of dye molecules binding to the proteins in the gel is semi-quantitative as the Coomassie blue dye binds more strongly to basic amino acids than acidic amino acids. InstantBlue Coomassie stain was provided ready to use. The gel was briefly washed with distilled water prior to placing into Coomassie stain, sufficient to cover the gel. The gel was incubated in Coomassie stain at room temperature with shaking for a minimum of one hour (overnight if applicable). Following incubation in Coomassie stain, the stain was decanted and the gel briefly washed in distilled water to remove any excess stain prior to scanning. For silver staining, the gel was placed into a solution of DL-Dithiothreitol (DTT) (4 µL 1M DTT in 100 mL distilled water) for 20 minutes. The DTT solution was removed and the gel briefly washed in distilled water, before staining in a 0.2% solution of silver nitrate for 20 minutes. The silver nitrate solution was removed and the gel briefly washed in distilled water. A small amount of developer solution (3% sodium carbonate, 0.5% formaldehyde (37%)) was added to the gel and discarded when the solution turned black. Further developer was added until the bands became visible. The gel was stored in 10% acetic acid.

Step 7: The cleaved and uncleaved fractions were pooled separately and run down the desalting column. The resulting fractions were pooled and freeze dried. The uncleaved samples can be cleaved again with HRV 3C protease (back to step 4).

Step 8: The purified, cleaved recombinant wild type and Y64H mutant amelogenin proteins were then used in three ways. For confirmation of identity, samples of the recombinant amelogenin proteins were subjected to mass spectrometry and western blotting (step 9 below). Once the correct identity was confirmed, the recombinant amelogenin proteins were used in *in vitro* mineral nucleation studies (section 2.2) and *in vitro* protein- protein binding studies (section 2.3).

Step 9: The identification of the recombinant amelogenin proteins was confirmed by mass spectrometry and western blotting.

2.1.2.1 Mass spectrometry

The molecular weights of the recombinant proteins were identified by time of flight mass spectrometry. A small sample of purified lyophilised protein was sent to the mass spectrometry service within the University of Leeds. Dr James McNult ran the fractions on Q-TOF MS/MS – tandem electrospray time of flight mass spectrometry- to give an accurate molecular weight for the proteins.

2.1.2.2 Western blotting

Western blotting uses antibodies raised against specific proteins to permit a more specific protein identification following separation on SDS-PAGE. Recombinant amelogenin proteins were loaded and run on SDS-PAGE as described in step 6 above and transferred onto nitrocellulose membrane (Geneflow, Fradley, UK) using a transblot module (Bio-Rad) using Towbin's transfer buffer (0.025M Tris, 0.192M glycine, 10% methanol, pH 8.6) (Towbin et al., 1979). Transfer occurred at 100 volts for 1 hour. The nitrocellulose membrane was then placed into 3% non-fat milk powder (Bio-Rad, Hemel Hempstead, UK) in tris buffered saline (TBS), and incubated overnight at room temperature. This blocks non-specific background proteins from reacting with the antibodies. The block was removed and the membrane thoroughly washed in TBS containing 0.05% Tween-20 (TBS-T). Primary antibody (rabbit anti-amelogenin teleopeptide (Eurogentec)) was applied at 1:1000-1:3000 dilution in 1% non-fat milk in TBS, and incubated for 1 hour at room temperature with shaking. The primary antibody was removed and the membrane thoroughly washed in TBS-T. The secondary antibody was applied at 1:3000 dilution in 1% non-fat milk in TBS. The secondary antibody was selected

on the basis of it being species specific to the primary antibody, e.g. goat-anti-rabbit secondary antibody. All secondary antibodies used in this thesis were conjugated to horse radish peroxidase (HRP) to permit visualisation following reaction with a chromogenic substrate. The membrane was incubated for 1 hour at room temperature with shaking in the secondary antibody. The membrane was then thoroughly washed before applying the colour developer. One ml of 25 times concentrated alkaline phosphatase developer concentrate was mixed with 24 mL ddH₂O and 0.25 mL reagent A (NBT – nitroblue tetrazolium) and 0.25 mL BCIP (5'-bromo-4-chloro-3-indoyl phosphate). Cross reacting protein bands stained purple.

2.2 *In vitro* mineral nucleation studies using recombinant amelogenin and enamelin proteins

In order to determine the ability of the recombinant amelogenin proteins (wild type and Y64H mutant amelogenin) and recombinant 32 kDa enamelin protein to nucleate hydroxyapatite mineral, an *in vitro* steady state agarose gel system was used. The system used in this thesis was based on the system used by Hunter and Goldberg (1993), although several different methods have been used by researchers worldwide to investigate the mineral nucleating properties of recombinant ECM proteins (see discussion section 4.2 and appendix 1). The *in vitro* steady state agarose system was used by Hunter and Goldberg to investigate the mineral nucleating properties of bone extracellular matrix proteins. In this particular steady state system, the recombinant protein(s) of interest was immobilised in an agarose gel plug in a central chamber. Either end of the gel was capped with a piece of dialysis membrane. Reservoir chambers were placed on either end of the central chamber and the whole block screwed tightly together to prevent leakage of buffer. Into one reservoir chamber, buffer containing a supersaturation level of phosphate was pumped at a constant rate, and into the opposite reservoir chamber buffer containing a supersaturation level of calcium was pumped. The calcium and phosphate ions diffused across the agarose gel and where they encountered protein, the potential for mineral nucleation occurred. If the recombinant protein was able to nucleate mineralisation, a white deposit was visible in the agarose gel. The identity of this mineral deposit was interrogated using quantification of phosphate, and energy dispersive X-ray spectroscopy (EDX), and the structure of the mineral crystals examined by scanning electron microscopy and transmission electron microscopy.

2.2.1 Steady state agarose gel system

Modified dialysis cells were used based on the system of Hunter and Goldberg (1993). The devices were constructed out of 1cm thick Perspex. The two reservoir chambers had in/out ports for buffer flow and a 1 mL capacity reservoir. The central chamber piece had a hole drilled all the way through it, with a 1.0 cm diameter and 0.95 mL capacity. All three pieces were held together with galvanised screws and wing nuts (figure 18). Each modified dialysis cell contained either a negative control (gel and buffer only), positive control (gel, buffer and PGA) or recombinant protein (gel, buffer and recombinant protein at certain concentrations). Triplicates of the negative controls, positive controls, and recombinant proteins (each concentration) were connected together to form the steady state agarose gel system. Each steady state system set up was incubated for 7 days at 37°C with a constant rate of calcium buffer pumping through one side of the dialysis cells, and a constant rate of phosphate buffer pumping through the opposite side of the dialysis cells.

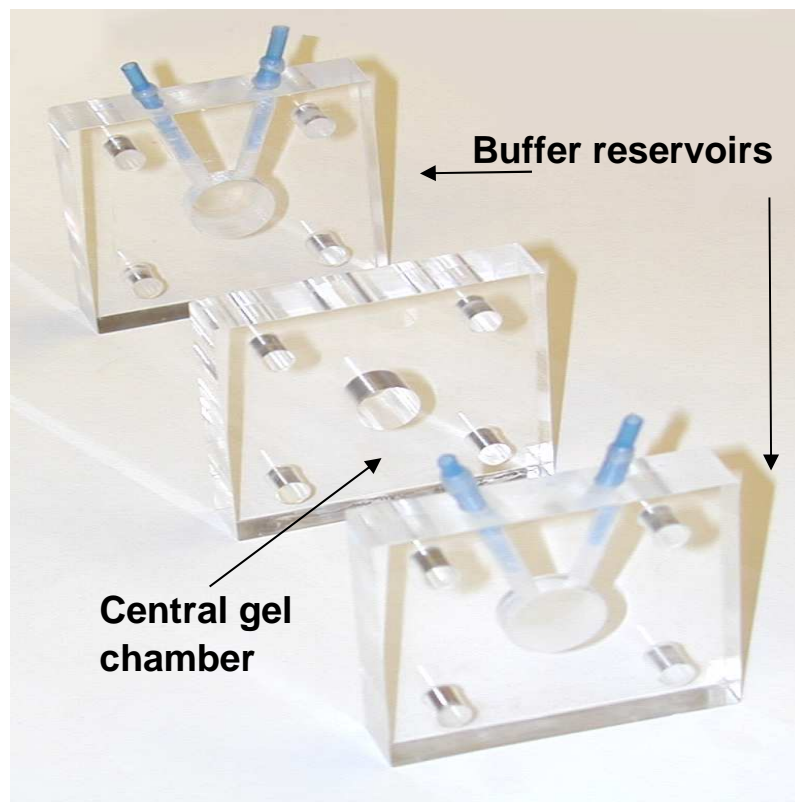


Figure 18. Exploded view of the modified dialysis cell used for the steady state agarose gel system. The end buffer reservoir chambers show the in/out ports in blue. A buffer reservoir is visible in each end piece. The central gel chamber piece shows the hole through the middle into which agarose gel is poured.

The system uses metastable, supersaturated (with respect to hydroxyapatite) conditions and is very sensitive to concentration changes. Prior to use, all Perspex components and glassware were washed in Decon 90 (Decon Laboratories, Hove, UK), rinsed with distilled water, acid washed (0.1 M HCl overnight) and further rinsed twice with distilled water. The central gel chambers were silinised by dipping in dichlorodimethylsilane (DCMS) for a few seconds in a fume hood. They were allowed to air dry and rinsed in distilled water. They were then wiped down with lint-free tissue. Any dust or particles can cause nucleation, giving false positive results.

The reservoir of one buffer reservoir end piece was covered by a piece of 1,000 Dalton molecular weight cut off dialysis membrane (Spectrapor 7 membrane, VWR 132105, VWR, Lutterworth, Leics., UK). The central gel chamber was placed over this and held in place with 2 screws/nuts. Low melting point sea plaque agarose (Bio-Rad, Hemel Hempstead, UK) was dissolved at 2% in distilled water, by microwaving, then cooled and maintained at 50-55°C. It was important to maintain the temperature below 60°C or the recombinant proteins and PGA positive control would be denatured when added to the agarose gel. The 2% agarose solution was mixed with an equal volume of double concentrated steady state buffer (40 mM HEPES, 300 mM NaCl, pH 7.4), vortexed and maintained at 50-55°C. This was the negative control. The positive control was prepared in the same way as the negative control but contained 10 µg/mL Poly-L-glutamic acid (PGA – Sigma P4886). The test samples (recombinant 32 kDa enamel in at 10 µg/mL, 5 µg/mL, 2.5 µg/mL and 1 µg/mL) were prepared as per the PGA positive control. Bradford assay analysis (Bio-Rad, Hemel Hempstead, UK) allowed the recombinant 32 kDa enamel in to be diluted to a stock solution of 100 µg/mL with distilled water. The recombinant 32 kDa enamel in was further diluted to the concentration described above with steady state buffer (20 mM HEPES, 150 mM NaCl, pH 7.4). For a description of the Bradford assay, see section 2.3.3 in the protein-protein binding assay section.

All samples were carefully sonicated to remove any air bubbles. Once prepared, 0.95ml of each sample was pipetted in triplicate into the central gel chambers, so that the solution was slightly higher than the height of the cavity (to allow for contraction when cooled). Once cool, another piece of dialysis membrane was placed over the central piece and the other end piece placed over. The devices were assembled with 4 screws/nuts per device and connected in series with 180 PVC tubing (Saint-Gobain Performance Plastics, Bristol, UK). A calcium buffer (20

mM HEPES, 150 mM NaCl, 6.5 mM Ca (NO₃)₂·4H₂O, pH7.4) was pumped through the devices on one side, and a phosphate buffer (20 mM HEPES, 150mM NaCl, 3.9mM Na₂HPO₄·2H₂O, pH7.4) was pumped through the devices on the other side counter currently. A peristaltic pump was used at a flow rate of 10 mL/hour (1 mL/hour/cell). The entire apparatus was incubated at 37°C for 7 days. A schematic showing one of the modified dialysis cells is shown in figure 19.

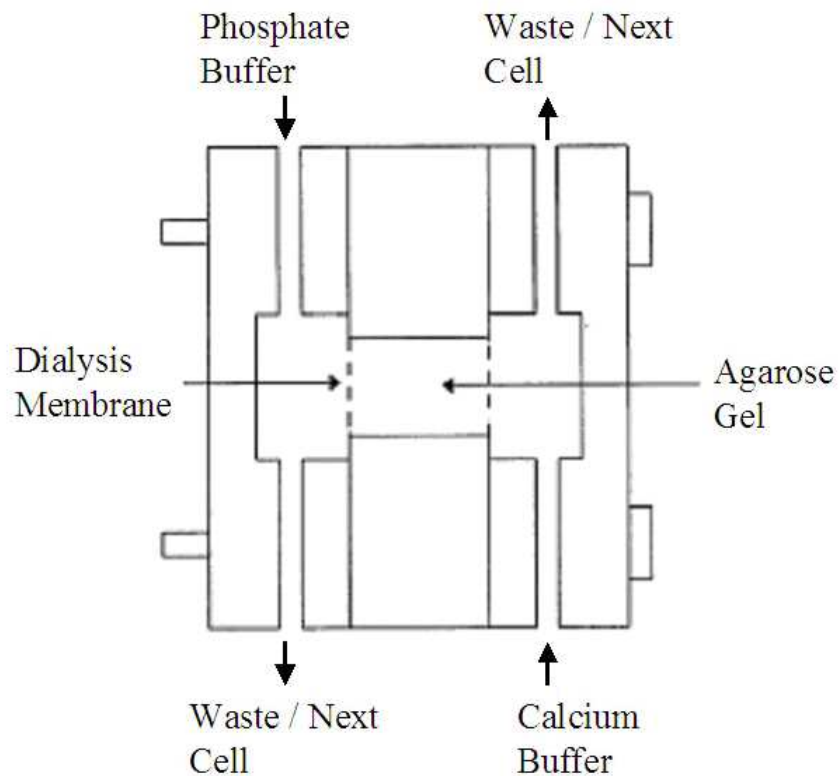


Figure 19. Diagram of a single steady state cell looking down onto the top of the cell. Buffers containing calcium and phosphate are circulated counter currently. The agarose gel in the central gel chamber is separated from the buffer reservoir chambers by dialysis membrane. Agarose gel is present in the centre portion only. Diagram provided by Ashley Firth, Department of Oral Biology.

2.2.2 Phosphate assay

The phosphomolybdate method is a common technique for the analysis of inorganic phosphate (Pi or PO₄³⁻). The assay is based upon the reaction of Pi with an excess of molybdic acid (generated by combining sulphuric acid with ammonium molybdate) which produces the colourless phosphomolybdous acid complex. The colour generated is quite stable and follows Beer's law (the absorbance measured is proportional to the concentration of the inorganic

phosphate). This method is restricted to measurement of inorganic phosphates. Organophosphates do not react with molybdic acid and do not produce colour in the assay (Smith and Ames, 1966).

The degree of mineral deposition in the gels was determined by phosphate analysis. After incubation, the steady state system apparatus was dismantled and the agarose gels centres removed from the central chamber and photographed. Any presence of mineralisation (a milky white precipitate) was noted. One of each triplicate gel sample (positive control, negative control or recombinant protein) was used for SEM/TEM studies and two ashed for phosphate analysis. For ashing, the individual agarose gels were placed into separate small conical flasks, 5 mL of concentrated nitric acid was added and the agarose gel in acid boiled gently until less than 1 mL remained. This was then made up to 10 mL with distilled water and stored at 4°C in air tight containers until needed.

Phosphate standards of 0-100 μM were prepared from a stock solution of BDH phosphate standard (10 mM). Three hundred μL of blank/standard/sample was mixed with 0.7 mL of the colour developer (10% ascorbic acid mixed with 6 parts of 0.42% ammonium molybdate.4H₂O in 0.5M H₂O) and incubated at 37°C for 2 hours. Two hundred μL aliquots, in triplicate, were placed into the wells of a 96-well plate and absorbance (minus blanks reading) read at 820 nm (Dynex plate reader, Dynex Technologies, Worthing, UK).

The standards were used to construct a linear calibration curve from which phosphate content of the samples was determined.

Figures 20 and 21 show the white mineral deposit *in situ* within the apparatus, after incubation of the steady state agarose gel system for 7 days at 37°C.



Figure 20. Picture of a dialysis cell fully assembled, post steady state run. Gel is present in the centre and white mineral precipitate is visible.

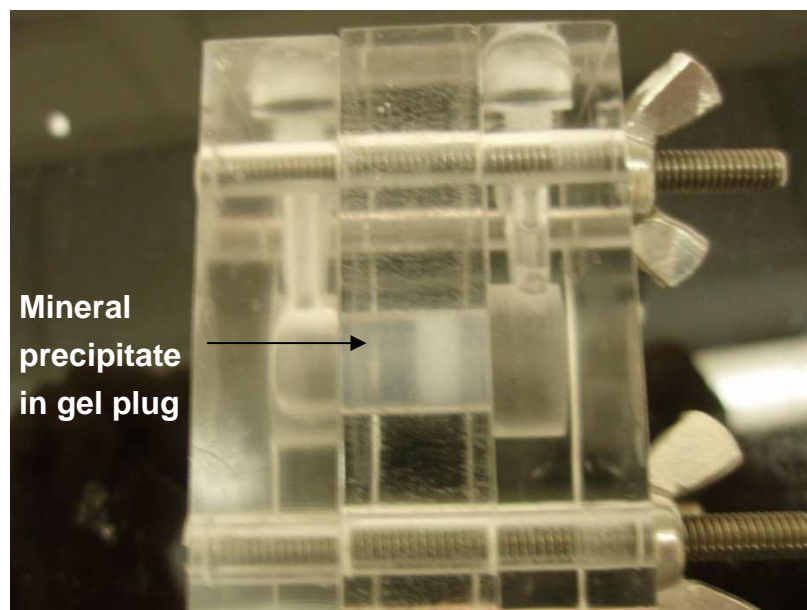


Figure 21. Side view of the fully assembled dialysis cell after a steady state run. A band of white mineral precipitate is clearly visible in the centre gel.

2.2.3 Scanning electron microscopy (SEM)

To investigate the morphology of the mineral crystals nucleated in the presence or absence of recombinant proteins, electron microscopy (both scanning and transmission) was used. The areas of the agarose gels containing the visible mineral precipitation were excised using a razor blade, and was then cut in half. One piece of agarose gel containing the mineral deposit was prepared for SEM by

washing with water taken to pH 10 with ammonium hydroxide. The agarose gel piece was then incubated in 6% sodium hypochlorite overnight or until the gel disappeared. The released mineral crystals were pelleted by centrifugation and washed again with water at pH 10. The crystals were finally resuspended in absolute ethanol. A 50 μ L aliquot was placed onto a SEM stub and allowed to air dry before vacuum drying overnight. Samples were sputter coated with 5 nm of gold for SEM using a JEOL JSM35 Genie Scanning Electron Microscope (SEM), or 5 nm of platinum for SEM using a Leo 1530 field emission gun scanning electron microscope (FEGSEM – GEMINI, Oxford Instruments).

2.2.4 Energy dispersive X-ray (EDX) spectroscopy

The chemical composition of the recovered mineral crystals was analysed using energy dispersive X-ray (EDX) spectroscopy using the JEOL JSM35 Genie Scanning Electron Microscope.

2.2.5 Transmission electron microscopy (TEM)

To corroborate the morphologies of the mineral crystals nucleated by recombinant proteins seen by SEM analysis, TEM was also used. The second half of the agarose gel containing the mineral deposits excised as described in section 2.2.3 was washed with water at pH 10 and fixed in 2% glutaraldehyde (buffered at pH 7.3 by 0.1M sodium cacodylate) for 2 hours at ambient temperature. The fixed agarose gel pieces containing mineral deposits were then rinsed four times in 0.1M sodium cacodylate buffer (pH 7.3). The fixed agarose gel pieces containing mineral deposits were then washed twice with pH 10 water, and dehydrated through a series of ethanol solutions; 30 minutes in each of 30%, 50%, and 70% ethanol, two times for 30 minutes in 90% ethanol, and three times for 30 minutes in 100% ethanol. The fixed agarose gel pieces containing mineral deposits were then embedded in LR white resin in beam capsules.

Ultra-thin sections of 50-70 nm were cut using an ultra-microtome and mounted onto 300-mesh carbon/formavar coated copper EM grids. The sections were viewed using a Philips E-400 transmission electron microscope at varying magnifications.

2.3 Protein- protein binding assays

To investigate whether the Y64H mutation in amelogenin was a loss of function mutation, impacting on the ability of the protein to form the ECM for mineralisation, *in vitro* binding assays were used. The recombinant wild type and Y64H mutant amelogenin proteins were used in a modified ligand-binding platform (based on a FITC-FITC alternative system to ELISA, Harmer and Samuel., 1989) to determine the ability of the recombinant protein to bind to itself and other ECM proteins

2.3.1 Production and labelling of recombinant proteins

Amelogenin wild type and Y64H mutant recombinant proteins were produced as previously described (see general materials and methods section 2.1.2). Correct molecular weight was confirmed by mass spectrometry, and the nature of the protein was confirmed by western blot analysis.

Fluorescein isothiocyanate (FITC) labelling was performed on the recombinant proteins, as described in section 2.3.2 below. Analysis of fluorescence was performed by SDS-PAGE analysis.

Unlabelled and FITC labelled proteins were freeze-dried before use. Lyophilised proteins were stored at -20°C prior to use.

2.3.2 Fluorescein labelling of recombinant amelogenin proteins

Fluorescein isothiocyanate (FITC) (Sigma, Poole, Dorset, UK) was used to add a fluorescent tag to recombinant amelogenin proteins for use in protein binding experiments. Protein was dissolved in 0.1M sodium carbonate buffer (pH 9) to give a final concentration of 4 mg/mL of protein. FITC was dissolved in anhydrous dimethyl sulphoxide (DMSO) to give a final concentration of 1 mg/mL. The FITC solution was prepared fresh for every reaction. For every 1 mL of protein solution, 50 µL of FITC was added slowly in 5 µL increments, while continuously stirring. The mixture was then incubated in the dark at 4°C, stirring continuously. After 6 hours incubation, ammonium chloride was added to give a final concentration of 50 mM. Incubation continued for a further 2 hours. The FITC-labelled protein was then dialysed against PBS for 72 hours at 2-8°C, changing the buffer every 24 hours. Slide-a-lyser™ cassettes were used for dialysis (Pierce, Thermo Fisher Scientific, Loughborough, UK). A 5 µL sample of labelled protein was run on an SDS-PAGE mini-gel, and viewed under dark light (dark light reader – Merck KGaA, Darmstadt,

Germany) to confirm fluorescence. The labelled protein was then freeze-dried prior to further use.

2.3.3 Bradford assay to determine protein concentration

The Bradford assay is a quick and sensitive method for determining microgram quantities of protein in a solution. It utilises the principle of protein dye binding by measuring the colour change of Coomassie Brilliant Blue G-250 dye in response to varying concentrations of protein. The dye binds primarily to basic (especially arginine) and aromatic amino acids in the protein sequence. The greater the concentration of protein, the more intense blue colour is seen in the reaction (Bradford, 1976).

The Bio-Rad Quick Start Bradford assay (Bio-Rad, Hemel Hempstead, UK) was used to confirm the recombinant protein concentrations prior to use in further experiments using a 96-well plate format. Seven concentrations of bovine serum albumin (BSA) were used as standards. Concentrations of 0.125, 0.25, 0.5, 0.75, 1.0, 1.5 and 2.0 mg/mL BSA were used to produce a standard curve. These, and the unknown concentrations of recombinant protein, were mixed 50:50 with the Quick Start Bradford reagent. This was incubated for 5 minutes before aliquoting in triplicate into the wells of a clear 96-well plate. The plate was read at 595 nm on the plate reader (Dynex Technologies, Worthing, UK) and the protein concentrations determined by interpolating the absorbance values for the unknown protein concentrations against the BSA standard curve values.

2.3.4 Binding assays

Several combinations and concentrations of proteins were used to investigate recombinant amelogenin protein binding to recombinant amelogenin protein. The experimental procedure remained the same for all. Wild type or Y64H mutant recombinant amelogenin was dissolved in 0.1M sodium carbonate buffer (pH 9). One hundred microlitres of unlabelled protein was placed into the wells of the specialized plate in triplicate. Microfluor 2 (7205 – Thermo Fisher Scientific, Loughborough, UK) polystyrene plates were used for all of the binding assay studies. These were a black plate to reduce background signal to noise, to improve assay sensitivity, to minimize crosstalk and prevent light piping between the wells. The plates have a slightly hydrophilic surface for increased binding of biomolecules

with a hydrophilic/hydrophobic character, such as proteins. The plates have a 96-well format.

The plates were incubated overnight at 4°C. The unbound, unlabelled protein was removed and the plate was washed three times with TBS-T (tris buffered saline containing 0.05% Tween-20). The potential for non-specific binding was then blocked by applying 100 µL 1% BSA in TBS for 1 hour at room temperature. The blocking solution was removed and the plate washed three times with TBS-T. FITC-labelled wild type or Y64H mutant amelogenin was dissolved in 0.1M sodium phosphate buffer (pH7). One hundred microlitres of the FITC-labelled protein was applied to the wells of the plate, and the plate was incubated for 2 hours at room temperature. The plate was read on an Ascent Fluoroskan plate reader (Thermo Fisher Scientific, Loughborough, UK) after washing three times with TBS-T to remove any unbound, FITC-labelled protein. After washing, 100 µl distilled water was placed into the wells prior to reading. Excitation of fluorescence was achieved at 488 nm and emission at 538nm. Ascent software was used to analyse the data. The system has sensitivity of 0.01 RFU (relative fluorescence units).

2.4 Enamelin breakdown studies

The majority of studies into enamel use the 32 kDa enamel breakdown product. As described in the introduction (section 1.3.4.3) the major enamel processing product is the 32 kDa enamel, and due to the ready availability from the meat industry, the porcine 32 kDa enamel is the most commonly used enamel for enamel ECM studies. To investigate whether the 32 kDa enamel processing product is the major enamel product across species, the enamel organs from pig and rat teeth were extracted and the molecular weights of the breakdown products over time investigated by SDS-PAGE and western blotting.

2.4.1 Extraction of the enamel organ from rat incisors

Male Wistar rats of approximately 150 g were euthanized by CO₂ inhalation and the lower incisors dissected from the lower mandibles. The enamel organ was gently wiped with damp tissue and left to air dry for one minute to expose the white opaque zone. This white opaque zone layer represents the start of the maturation stage in amelogenesis resulting from the hugely hydrated porous tissue drying out on exposure to air (Hillier et al., 1975). The developing enamel was carefully dissected with a scalpel in to the early secretory (S1), secretory (S2), transition (T) (all 1.5-2 mm sections apical to the white opaque zone), the white opaque zone (early maturation –M1), mid-maturation (M2) and late maturation (M3). All enamel sections were stored at ≤-65°C until needed.

2.4.2 Extraction of the enamel organ from pig molars

Pigs of approximately 6-months old were euthanized by anaesthetic overdose by the University of Leeds animal house. The lower mandibles were removed and the molar teeth removed from the lower mandibles. The enamel organ and pulp tissues were removed, and the tooth enamel wiped with damp tissue. The soft secretory stage enamel was scraped from the tooth with a scalpel, and stored at ≤-65°C until needed.

2.4.3 Preparation of enamel samples for enamel breakdown studies

The series of enamel samples from the rat incisor were extracted by grinding the samples with a glass rod in 500 µL of 10% acetic acid. The resulting extracts

were then centrifuged at 13,000 rpm for 5 minutes and the supernatants removed. The remaining pellet was then resuspended in a further 15 µL 10% acetic acid. The extract and supernatant were mixed and then centrifuged at 13,000 rpm for 5 minutes in a centrifugal filter (Millipore Centricon) to concentrate. The filter was washed with 10% acetic acid, inverted into a clean tube and re-centrifuged at 13,000 rpm for 5 minutes to remove the concentrated protein extracts. This double extraction technique solubilised all the ECM proteins effectively as all material was solubilised, being equivalent to protein extraction based upon acid demineralisation of the tissue. The proteins extracted were then mixed 1 to 1 (volume for volume) with 15 µL of doubly concentrated SDS-PAGE sample loading buffer (pH 6.8) (described in step 6 section 2.1.2). Porcine secretory stage enamel was prepared in a similar way, using 500 µL of 10% acetic acid and double concentrated SDS-PAGE sample loading buffer per mg of enamel.

All samples were denatured by heating at 90°C for 2 minutes, and 10 µL per sample loaded per lane on to a 1 mm thick 12% resolving mini-gel (Mini-protean IV, Bio-Rad, Hemel Hempstead, UK). Gels were electrophoresed at 200 V until the blue dye front reached the bottom of the gel. Gels were stained with Coomassie blue G250 (Instant Blue, Expedeon, Cambridge, UK). Duplicate gels were trans-blotted onto nitrocellulose membrane (Mini-trans blot, Bio-Rad, Hemel Hempstead, UK) at 100v for one hour. The membranes were blocked overnight in 5% non-fat milk powder in tris-buffered saline (TBS) pH 7. Electrophoresis was performed as described in step 6 in section 2.1.2 and western blotting as described in 2.1.2.2 with the exceptions noted below.

2.4.4 Western blotting of enamel proteins

Antibodies to the synthetic peptide EEMFEQDFEKPKEEDPPK, which corresponds to the sequence at the centre of the putative rat 32 kDa enamelin, were raised in rabbits (Eurogentec, Southampton, UK). There is sequence homology between the rat and pig enamelins so that the antibody should recognise enamelins from both species.

The blocked membranes were washed and incubated for one hour at room temperature with shaking with 1:1000 anti-enamelin antibody in TBS containing 0.05% TWEEN-20 (TBST). The blots were washed for 3x5mins TBST and then incubated in anti-rabbit IgG peroxidase conjugate (Sigma-Aldrich, Poole, Dorset, UK), diluted 1:750 for one hour with shaking at room temperature. The blot was

washed 3x5mins in TBST and developed using metal enhanced DAB substrate (Sigma-Aldrich, Poole, Dorset, UK) resulting in brown-black staining of the proteins.

2.4.5 Comparison of rat and pig enamelin protein breakdown

As described in the introduction section 1.3.4.3 and figure 8, the major breakdown product of enamelin is the 32 kDa fragment. Most of the studies performed on enamelin using the 32 kDa breakdown product focused on the porcine product due to its ready availability. To investigate whether the 32 kDa enamelin breakdown product was produced in the rat secretory enamel with time, a proteolytic breakdown study was performed.

A 150g male Wistar rat was euthanized by schedule 1 killing (CO₂ inhalation) and the lower incisors removed from the mandible. The secretory zone of the enamel was removed from both incisors and placed into a sterile micro-tube containing 200 µL Dulbecco's Phosphate Buffered Salt solution (DPBS – Lonza, Slough, UK) containing 130 mg/L calcium chloride. The enamel pieces in DPBS were immediately frozen at $\leq -65^{\circ}\text{C}$. The next day, the enamel was thawed, crushed and sonicated to form a slurry. A further 200 µL of calcium enhanced DPBS was added to form a more diluted slurry. This was divided into six 50 µL aliquots in sterile micro- tubes. One tube was placed immediately into the freezer at $\leq -65^{\circ}\text{C}$, and the remaining tubes were placed into a 37°C incubator. One tube was removed from the incubator and placed into the freezer at 4 hours, 8 hours, 16 hours, and 32 hour time points. The samples were then run on 15% SDS-PAGE mini gels, and analysis performed by Coomassie staining and western blot. Non-specific binding was blocked by incubation with non-fat milk solution, followed by incubation with rat-specific anti-enamelin antibody (polyclonal antibody raised in rabbits – Eurogentec, Southampton, UK). Goat anti-rabbit secondary antibody was used, followed by incubation with streptavidin/biotin. The blot was then incubated in colour developer until bands appeared (Bio-Rad, Hemel Hempstead, UK).

Two mg of secretory enamel from a pig molar (euthanized and extracted as previously described in section 2.4.2) was crushed into 400 µL of DPBS with calcium, and sonicated to form a slurry. The slurry was divided into six 50 µL aliquots and incubations and subsequent analysis performed as for the rat enamel samples described above.

2.5 Quantitative PCR studies to compare the gene profiles of mice teeth containing the wild type or Y64H *Amelx* gene

To investigate whether the morphological changes expressed in mice with the Y64H amelogenin mutation were due to down-regulation of the amelogenin gene, non-secretion of the amelogenin protein or apoptosis of the ameloblasts, q-RT-PCR investigations of the gene expression profiles for mice expressing wild type amelogenin and mice with the Y64H amelogenin mutation were compared.

2.5.1 Collection of mice teeth

Mice containing the wild type amelogenin or mutant (Y64H) amelogenin genes were created by the RIKEN institute. The mice were bred, husbanded and phenotyped by our collaborators on the Wellcome Programme at Manchester University. Phenotyping was performed on ear samples from the mice by Dr Martin Barron at Manchester. Mice were culled and their lower incisors immediately extracted and placed into *RNALater*[™] solution (Applied Biosystems, Warrington, UK). *RNALater*[™] stabilises and protects the RNA in fresh specimens by rapidly permeating the tissue. It eliminates the need to immediately process or freeze samples. Tissue samples can be stored for extended periods in *RNALater*[™] solution where normally RNA degradation would occur – 1 week at room temperature. Samples can be stored indefinitely in *RNALater*[™] at -20°C or below. *RNALater*[™] is fully compatible with the TRI-reagent used in the RNA extraction process. Samples were frozen in *RNALater*[™] solution in Manchester, and transferred to Leeds using a cryocase (Starlabs, Milton Keynes, Bucks., UK) and stored at ≤-65°C prior to processing.

2.5.2 RNA extraction

RNA was extracted from whole mouse lower incisors or sections of mouse lower incisor, using the Ambion RiboPure RNA extraction kit (Applied Biosystems, Warrington, UK). Samples were homogenised in TRI reagent, a monophasic solution containing phenol and guanidine thiocyanate, which rapidly lyses cells and inactivates nucleases. Bromochloropropane (BCP - Sigma) was added, which caused the separation of the homogenate into aqueous and organic phases. RNA partitioned into the aqueous phase, while DNA and protein remained in the interphase and organic phase. The RNA was isolated from the aqueous phase by binding it to a glass fibre filter. The filter was washed twice to remove contaminants,

and the RNA was eluted from the filter with low salt buffer. The eluted RNA was stored at $\leq -65^{\circ}\text{C}$.

RNA concentrations were determined using the 260/280 absorption method using a Shimadzu spectrophotometer (Shimadzu, Milton Keynes, UK). To determine the RNA concentration, 5 μL RNA was added to 495 μL distilled water. This was read on the spectrophotometer at 260 nm. To determine the RNA concentration in $\mu\text{g}/\text{mL}$, the following calculation was used:-

$$\begin{aligned} & \text{A260 reading} \times \text{dilution factor} \times \text{extinction coefficient} \\ & = \text{A260 reading} \times 10 \times 40 = \text{RNA } \mu\text{g}/\text{mL} \end{aligned}$$

Genomic DNA contamination was removed using the Invitrogen Turbo DNase kit (Invitrogen, Paisley, UK). To 10 μg of RNA, 1 μL of Turbo DNase and 1 μL of Turbo buffer were added. The reaction mix was incubated at 37°C for 30 minutes. After incubation, 2 μL of DNase inactivation reagent was added, and the reaction mixture incubated for 2 minutes at ambient temperature, with gentle tapping of the tube to mix. The tubes containing the reaction mixture were then centrifuged at 10,000 rpm for one minute and the supernatant removed to a clean, sterile microtube.

2.5.3 Confirmation of RNA purity

RNA purity was also confirmed by running RNA samples on an agarose gel. One g of agarose was dissolved in 72 mL water to which 10 mL of 10x MOPS running buffer (40mM 3-(N-morpholino) propanesulfonic acid, 2mM sodium acetate, 1mM EDTA, pH7) and 18 mL 37% formaldehyde were added. This was poured into gel caster trays cleaned with RNase Away. Three μg samples of RNA were mixed with RNA loading dye (Sigma R4268) and denatured at 65°C for 15 minutes. Samples were loaded on the gel and run with 1 x MOPS buffer at 100 V for 1 hour. RNA marker 0.28-6.6 KB (Sigma R7644) was also loaded. Gels were imaged on a UV light box (GelDoc, Geneflow, Fradley, UK).

2.5.4 Transcription of RNA to cDNA

cDNA was produced from the treated RNA using the Ambion High Capacity RNA-to-cDNA kit (Applied Biosystems, Warrington, UK). The kit contents were removed from -20°C storage and thawed on ice. A mastermix of the reagents was

prepared by mixing 200 µL of the RT buffer with 20 µL of 20 times enzyme mix and 140 µL of nuclease free water. To 2 µL of the DNase treated RNA from section 2.5.2, 18 µL of the mastermix was added. Each preparation was then incubated for 60 minutes at 37⁰C. At the end of the incubation, the preparations were heated to 95⁰C for 5 minutes. The preparation tubes were then centrifuged at 13,000 rpm for 1 minute and placed on ice.

2.5.5 Confirmation of cDNA purity

cDNA purity was determined by performing conventional reverse transcription (RT) PCR using the Phire hot start PCR kit (New England Biolabs, Hitchin, Herts., UK) This is a hot start DNA polymerase, providing increased sensitivity, specificity and yield, and allow assembly of the PCR reactions at room temperature, as activation of the polymerase does not occur until the reaction has been heated at 94⁰C. For the Phire hot start kit, 10 µL of 5x reaction buffer was mixed with 1 µL of 10 mM dNTP's, 1µL of primer A (forward primer for gene of interest), 1 µL of primer B (reverse primer for gene of interest), 1 µL of Phire polymerase, 5 µL of cDNA (produced in section 2.5.4) and 31 µL of nuclease free water. These reaction mixes were placed into 0.2 mL sterile PCR tubes. The tubes were placed into a Techne MJ 100 thermocycler and the following protocol applied:

Step 1: 98⁰C for 30 seconds

Step 2: 98⁰C for 5 seconds

Step 3: 65⁰C for 5 seconds

Step 4: 72⁰C for 20 seconds

Step 5: Repeat steps 2, 3 and 4 30 times

Step 6: 72⁰C for 1 minute

Step 7: 4⁰C hold

A positive control cDNA and primers were provided with the Phire kit.

Forward primer – 3' ATG CCC CTA CCA CCT CAT C 5'

Reverse primer – 3' ACT TCT TCC CGC TTG GTC TT 5'

These primers generated a product of 536 base pairs.

PCR products were run on a 2% agarose gel. One g of agarose was mixed with 1 x gel-red buffer (Biotium, VWR, Lutterworth, Leics. UK) and heated to dissolve. The molten agarose was poured into horizontal gel trays and allowed to set. The samples were mixed with gel-red loading buffer and loaded onto the gel. A 100 base pair (bp) ladder was also loaded to aid identification of bands (Sigma P1473). The gel was run at 100v for 1 hour, and imaged on a UV light box (GelDoc, GeneFlow, Fradley, UK). The gel-red system uses a fluorescent nucleic acid stain for visualization of DNA bands within the gel without the need for ethidium bromide, thereby providing a safe, non-toxic alternative to traditional DNA imaging.

2.5.6 Quantitative real time polymerase chain reaction (Q-RT-PCR)

Conventional PCR detects the amplified DNA product by end point analysis, usually by running an agarose gel of the DNA products. Real-time PCR allows detection of the amplified product to be detected and measured as it occurs. The main advantage of real time over conventional PCR is the ability to accurately determine the starting template copy number with high sensitivity. Real time PCR can be evaluated without gel electrophoresis, allowing quicker reaction time and increased output (Bio-Rad Q-RT-PCR handbook).

Q-RT-PCR was performed on a Roche Lightcycler 480 (Roche, Burgess Hill, West Sussex, UK) using Taqman gene assays and Taqman master mix (Applied Biosystems, Warrington, UK catalogue number 4251372). Each reaction sample was prepared as follows: 27 μ L of cDNA (prepared as section 2.5.4) mixed with 30 μ L Taqman mastermix and 3 μ L Taqman probe (specific for each gene, catalogue code given below). All gene assays were set up in triplicate, with a blank (negative) control, where water replaces the cDNA in the assay. The assay assembly was performed on ice and assembly was performed in 0.2 mL sterile PCR tubes. The tubes were briefly centrifuged (1000 rpm for approximately 10 seconds) before transferring 20 μ L in triplicate into the wells of a sterile 96-well PCR plate (StarLabs). The plate was covered with a plate seal to prevent evaporation and loaded into the Lightcycler instrument. The following cycling conditions were used:

Step 1: 95°C hold for 10 minutes (4.4°C per second ramp rate)

Step 2: 95°C for 10 seconds (4.4°C per second ramp rate)

Step 3: 60°C for 30 seconds (2.2°C per second ramp rate)

Step 4: 72°C for 1 second (4.4°C per second ramp rate)

Step 5: Repeat steps 2, 3 and 4 44 more times

Step 6: 40°C for 30 seconds (4.4°C ramp rate)

Step 7: 4°C hold

Gapdh was used as the endogenous control. Amelogenin (*Amelx*), Grp-94 (HSP-90), *Bip* (HSP-5), *Chop* and *Xbp-1* expression levels were all evaluated. The result was a value for the crossing threshold (CT).

The gene product from the Q-RT-PCR assays resulted in an amplicon of a specific number of base pairs. This amplicon was run on agarose gel electrophoresis to confirm the expected size. This was performed as described in section 2.5.5 as for cDNA PCR product analysis.

Amelx – Mm01166221_m1 = 74 amplicons

Grp94 – Mm00441927_m1 = 72 amplicons

Bip – Mm00517691_m1 = 75 amplicons

Chop – Mm00492097_m1 = 82 amplicons

Xbp1 – Mm01187751_m1 = 79 amplicons

Gapdh – Mm99999915_g1 = 105 amplicons

The perfect optimised Q-RT-PCR reaction would have a linear standard curve ($R^2 > 0.98$), high amplification efficiency (90-105%) and consistency between replicates. To determine if a Q-RT-PCR assay is optimised, it is good practice to run serial dilutions of template DNA and use the results to generate a standard curve. This is constructed by plotting the log of the starting quantity of template or dilution factor against CT values. The equation of the linear regression line, along with Pearson's correlation coefficient (r) or the coefficient of determination (R^2) can then be used to evaluate assay optimisation.

Standard curves were performed for each gene assay and endogenous control for each cDNA sample. The standard curve was performed using a 1:10 serial dilution of the cDNA. A 1 in 5 dilution of the 'stock' cDNA was performed to

give a starting concentration of 20 ng/μL cDNA. This was diluted further 1 in 10 to give 2 ng/μL cDNA. This was diluted further 1 in 10 to give 0.2 ng/μL. A further 1 in 10 dilution was performed to give 0.02 ng/μL. This was diluted further 1 in 10 to give 0.002 ng/μL. Each dilution was used in the q-RT-PCR assay as described above. The result should be a linear increase in the CP (crossing point) values for the log of each dilution. All standard curves should be parallel to one another. Standard curves gave the efficiency of the gene expression (should be 2).

Relative quantification was employed to compare changes in multiple samples. It compared the levels of two target sequences in a single sample, and expresses the final result as a ratio of gene levels. This number is only meaningful when compared between samples.

$$\text{Relative ratio} = \frac{\text{Concentration target gene}}{\text{Concentration reference gene}}$$

The reference gene is usually a constitutively expressed gene or housekeeping gene. This is also known as an endogenous control and provides the basis for normalising sample-to-sample differences. Different experimental conditions should not affect the expression levels of housekeeping genes. For the Q-RT-PCR experiments in this thesis, two housekeeping genes were used; *Gapdh* and Actin B. *Gapdh* expression remained invariable with all experimental conditions, but Actin B expression varied. Due to this, *Gapdh* was selected as the housekeeping gene to normalise the data to.

The Livak method ($2^{-\Delta\Delta CT}$) is a widely used and easy to perform method for relative gene expression analysis (Livak and Schmittgen, 2001). Firstly, the CT value of the target gene is normalised to the CT value of the reference (housekeeping) gene, for both the calibrator (wild type) and test (mutant) samples.

$$\Delta CT (\text{test/mutant}) = CT (\text{test gene}) - CT (\text{reference gene} / \textit{Gapdh})$$

$$\Delta CT (\text{calibrator/wild type}) = CT (\text{test gene}) - CT (\text{reference gene}/\textit{Gapdh})$$

Secondly, the ΔCT of the test/mutant is normalised to the calibrator/ wild type ΔCT .

$$\Delta\Delta\text{CT} = \Delta\text{CT test (mutant)} - \Delta\text{CT calibrator (wild type)}$$

Finally, the expression ratio is calculated:-

$$2^{-\Delta\Delta\text{CT}} = \text{normalised expression ratio}$$

This is the fold increase or decrease of the test gene in the test (mutant) sample relative to the calibrator (wild type) sample. Normalising the expression of the test gene to a housekeeping gene compensated for any difference in the amount of sample tissue. The Livak method assumes a reaction efficiency of 2 for the equation $2^{-\Delta\Delta\text{CT}}$

For the Q-RT-PCR analysis performed in this thesis, ΔCT was calculated by subtracting the CT value from the endogenous control away from the CT value of the gene of interest.

$$\text{e.g. } \Delta\text{CT} = \text{CT } Amelx - \text{CT } Gapdh$$

$\Delta\Delta\text{CT}$ was calculated by subtracting the ΔCT value of the wild type (calibrator) away from the ΔCT value of the mutant (test) for the gene of interest

$$\text{E.g. } \Delta\Delta\text{CT } Amelx = \Delta\text{CT mutant } Amelx - \Delta\text{CT wild type } Amelx$$

Changes in gene expression were calculated using the Livak method ($2^{-\Delta\Delta\text{CP}}$).

$$\text{e.g. up or down regulation of } Amelx = 2^{-\Delta\Delta\text{CP } Amelx}$$

This was normalised relative expression.

2.6 Scanning electron microscopy (SEM) of mice incisors

Mandibular incisor teeth from wild type female, female mice heterozygous for the Y64H *amelogenin* mutation and male mice homozygous for the Y64H *amelogenin* mutation were dissected from the mandible following cervical dislocation. The enamel organ was removed using a lint-free tissue. The incisors were placed into polypropylene tubes to allow easier mounting onto SEM stubs. The incisors were ground with fine carborundum paper to obtain transverse sections through the incisor approximately 2 mm from the tip. The teeth were etched with 30% phosphoric acid for 20 seconds to remove any smear layer. The phosphoric acid was removed by thorough washing with distilled water and dried overnight under vacuum. The incisors were sputter coated with gold and imaged using a Hitachi S-3400N scanning electron microscope operate at an accelerating voltage of 20 kV and an emission current of 94 μ A. The images were taken under backscatter conditions at 450 and 1600 times magnification.

Chapter 3

Results

3.1 Recombinant protein production

Amelogenin and enamelin are both present in the developing enamel matrix and presumably may interact functionally. To investigate whether the Y64H mutation of amelogenin affects the interaction of the protein with enamelin, microplate based protein binding assays were used. To investigate whether the Y64H mutation of amelogenin affects the proteins ability to nucleate mineralisation, steady-state agarose gel assays were used. Recombinant human 32 kDa enamelin was provided courtesy of Dr J. Maycock and data arising from its production are not presented here. However, wild-type and Y64H mutant amelogenin were both produced for this thesis; the results of which are presented in the following sections.

3.1.1 Recombinant amelogenin protein production

Wild-type and mutant (Y64H) amelogenin were produced using a prokaryotic system using *E.coli* (section 2.1.1). These recombinant proteins contained a HIS tag (a sequence of 6 histidines) to aid their purification from the bacterial proteins using a nickel affinity column in conjunction with FPLC (proteins with the His tag bind preferentially to the nickel column). Figure 22 shows how the recombinant amelogenin was purified from the crude *E. coli* lysate using nickel column purification and the removal of the HIS tag by HRV 3C protease enzyme. Cleavage of the HIS tag was not 100% efficient and preparative SDS-PAGE was carried out to separate the cleaved protein from uncleaved protein and the liberated HIS tag. Figure 23 shows the results of the preparative SDS-PAGE and isolation of the cleaved amelogenin from the uncleaved amelogenin still carrying the HIS tag. The fractions containing the cleaved amelogenin were subsequently pooled and desalted ready for use. See section 2.1.2. and figure 15 for a schematic of the production and purification process.

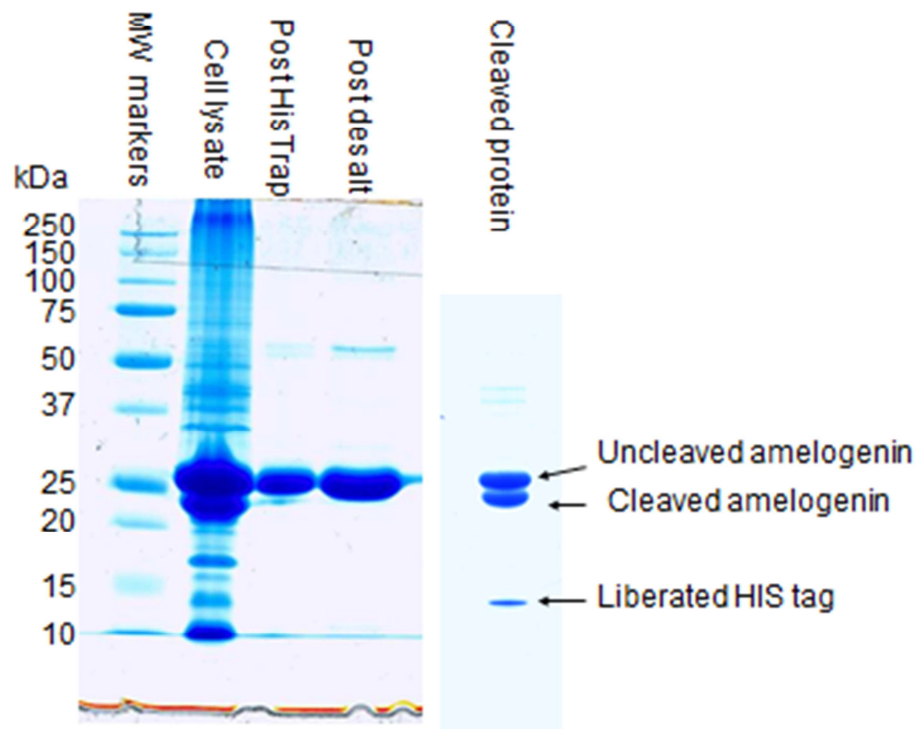


Figure 22. Coomassie stained SDS-PAGE gel of various fractions of recombinant amelogenin protein obtained throughout the protein purification process. Molecular weight markers are displayed in the left hand lane. The cell lysate contained all the proteins recovered from the E.coli. The post His Trap column shows the protein recovered from the nickel chromatography His Trap column. "Post desalt" shows the protein recovered from the desalting column." Cleaved protein" shows the protein after it had been cleaved overnight at 4°C with HRV 3C. Note that cleavage was not 100% efficient with much of the protein remaining uncleaved.

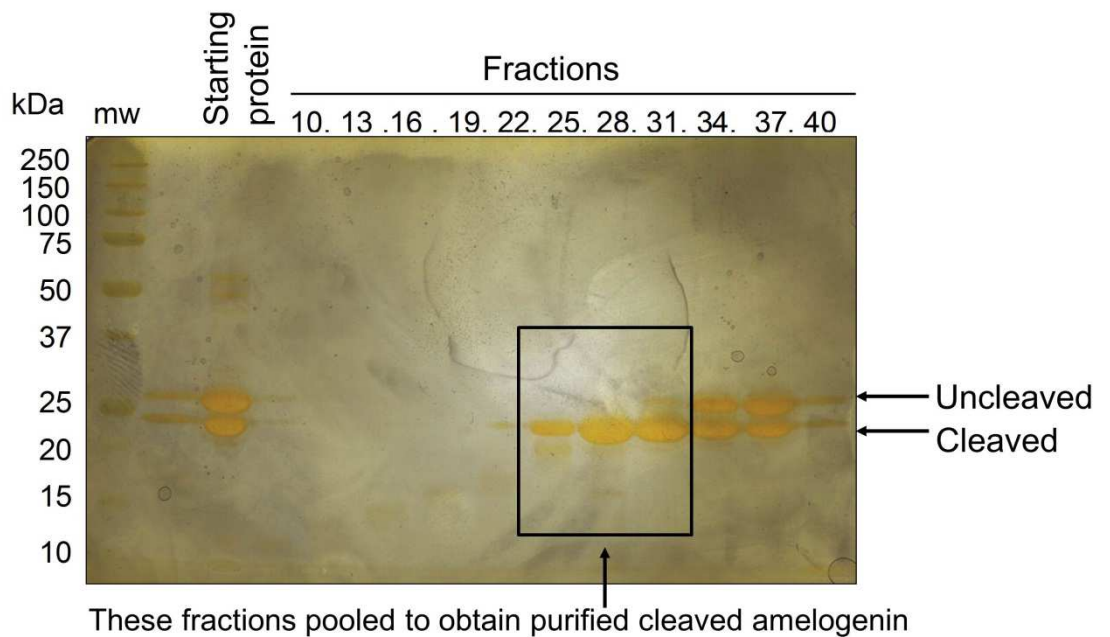


Figure 23. Silver-stained SDS-PAGE gel showing fractions of cleaved recombinant amelogenin obtained by preparative SDS-PAGE. MW is the molecular weight ladder and starting protein is the partially cleaved sample. Every third fraction obtained from the prep-cell was run on the gel allowing the fractions containing cleaved protein only to be identified and pooled. Similar gels were obtained for the wild type and mutant amelogenin.

Pooled fractions were desalted and freeze dried. A sample was provided for mass spectrometry analysis to confirm the removal of the HIS tag and the correct molecular weight. Figure 24 shows the mass spectrometry profile for wild-type amelogenin, with a molecular weight of 20590 Da (predicted molecular weight 20590.65 Da), and figure 25 shows the mass spectrometry profile for Y64H mutant amelogenin, with a molecular weight of 20564 (predicted molecular weight 20564.62 Da).

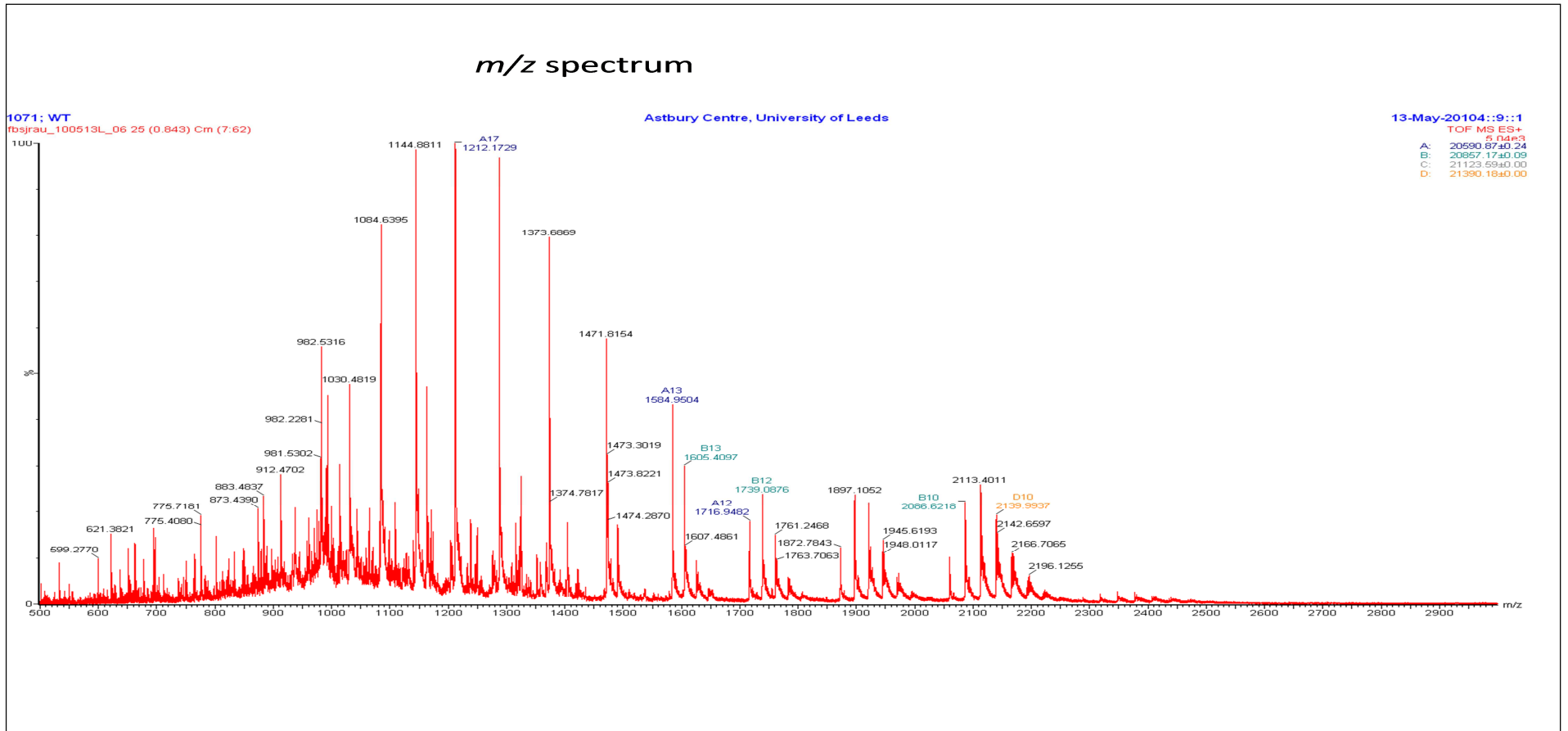


Figure 24. Mass spectrometry profile for recombinant wild type amelogenin showing a molecular weight of 20590 Daltons.

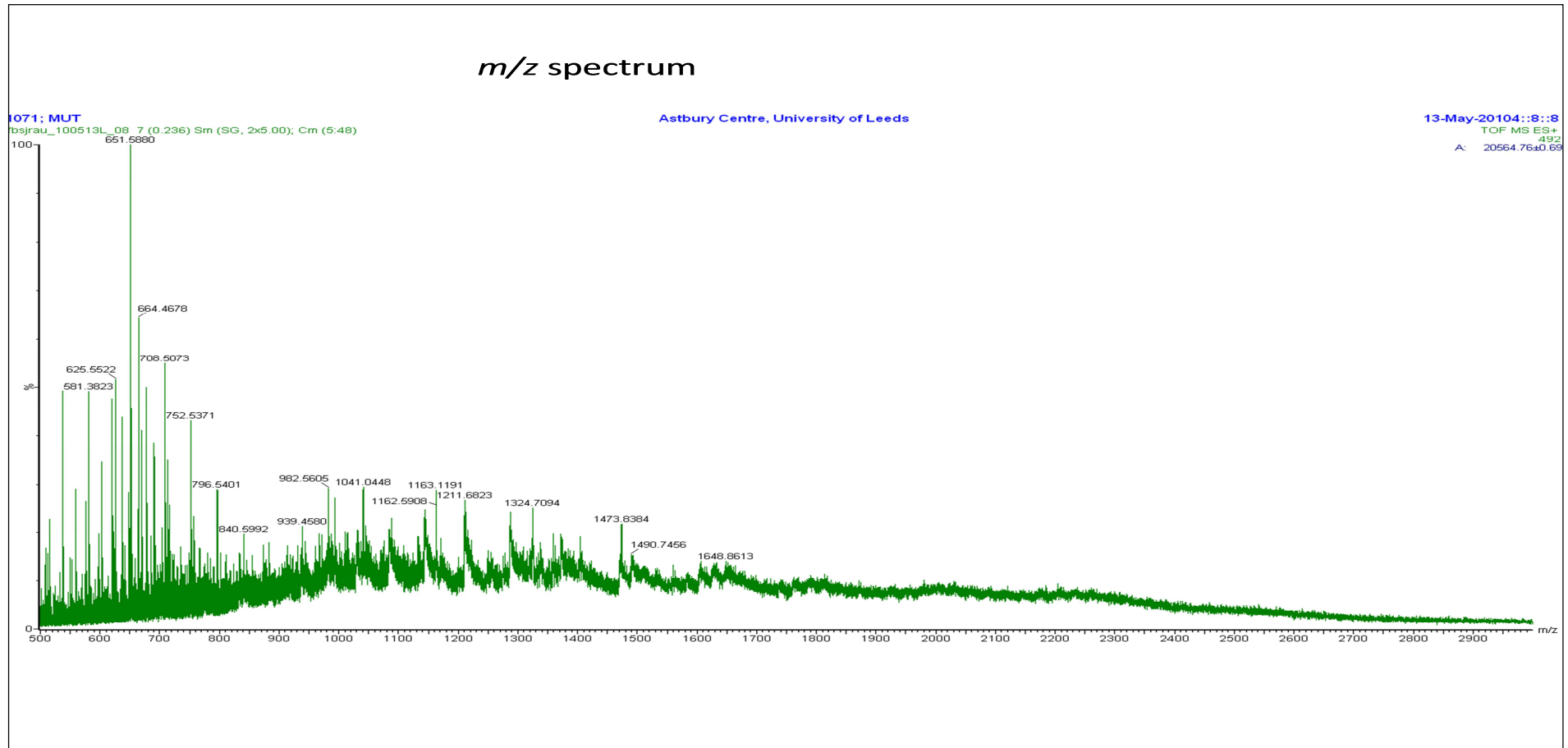


Figure 25. Mass spectrometry profile of recombinant Y64H mutant amelogenin showing a molecular weight of 20564 Daltons.

3.2 The ability of recombinant amelogenin and recombinant 32 kDa enamelin to nucleate mineral *in vitro* using a steady-state agarose gel system

The mineral nucleating properties of extracellular matrix proteins have already been demonstrated by Hunter and Goldberg using a modified dialysis cell system (Hunter and Goldberg, 1993; Hunter and Goldberg, 1994; Hunter et al., 1996). This system was used here to investigate the hydroxyapatite nucleating potential of recombinant human 32 kDa enamelin and recombinant mouse amelogenins (wild type and mutant), independently and in combination, given that they are both present in the developing enamel. Using both the recombinant wild type and Y64H mutant recombinant amelogenin proteins separately and in combination with the 32 kDa recombinant enamelin protein in the steady-state agarose gel system allowed the effects of the Y64H mutation in amelogenin on mineral nucleation to be investigated.

3.2.1 Visual characterisation of nucleated mineral deposits at the gross level

After 7 days incubation at 37°C, gel plugs retrieved from the steady-state cells containing PGA or recombinant protein typically contained white bands of mineral precipitate. Figure 26 panels A, B and C shows three representative images of bands obtained when using 10 µg/mL recombinant 32 kDa enamelin as a potential nucleator. Panel A shows an instance where mineral seemed to have precipitated around the periphery of the gel. Panel B demonstrated the variability in band thickness seen within triplicates in the same experiment. Panel C shows a further instance where variability was less marked. Each panel consists of triplicate gel plugs for an experiment, with each panel representing an experiment performed on separate assay occasions.

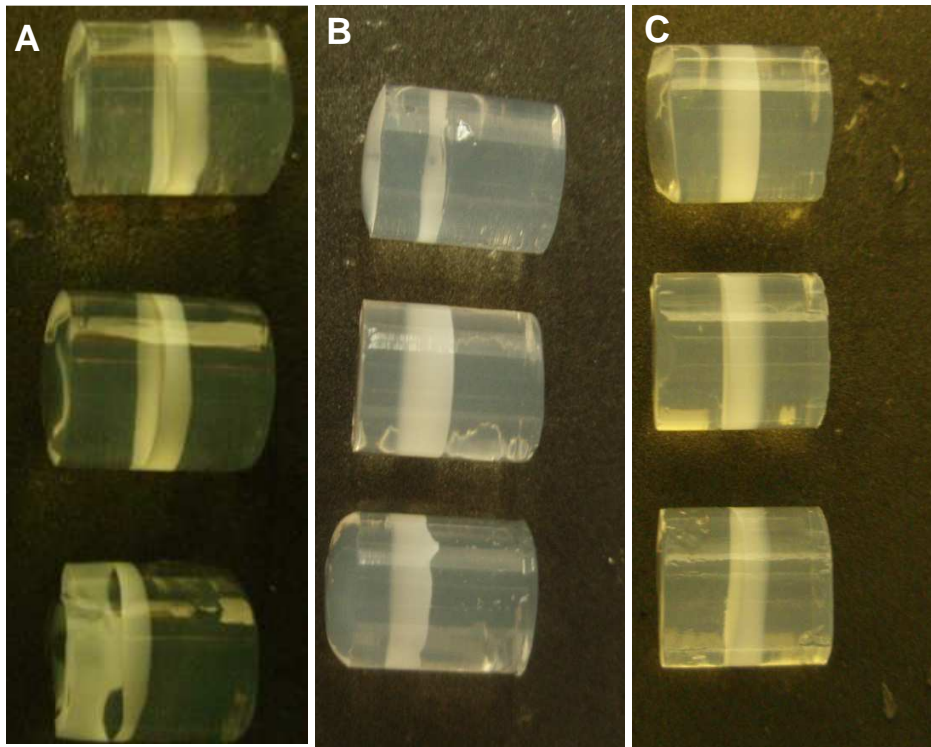


Figure 26. Panels A, B and C. Typical images of recovered agarose gel plugs showing recombinant 32 kDa enamelin nucleated mineral precipitation. Note the variability of mineral patterns obtained. Each panel represents the triplicates from a different steady-state assay run.

Any variations in colour in the photographs are due to different settings being used on the digital camera, and are not due to colour variations in the gels. It would have been preferable to standardise the digital photography but these photographs are for illustrative purposes only and are not presented as quantitative data.

Variability was also seen when using 10 $\mu\text{g/mL}$ PGA (positive control) as the potential nucleator. Figure 26 shows representative images for gel plugs recovered after 7 days incubation at 37°C in the steady state agarose gel system when 10 $\mu\text{g/mL}$ PGA positive control was used as the mineral nucleator. Panel A shows very broad, somewhat diffuse bands of mineral. Panel B shows 2 separate bands of mineral and panel C shows bands that only extend partially across the gel plugs.

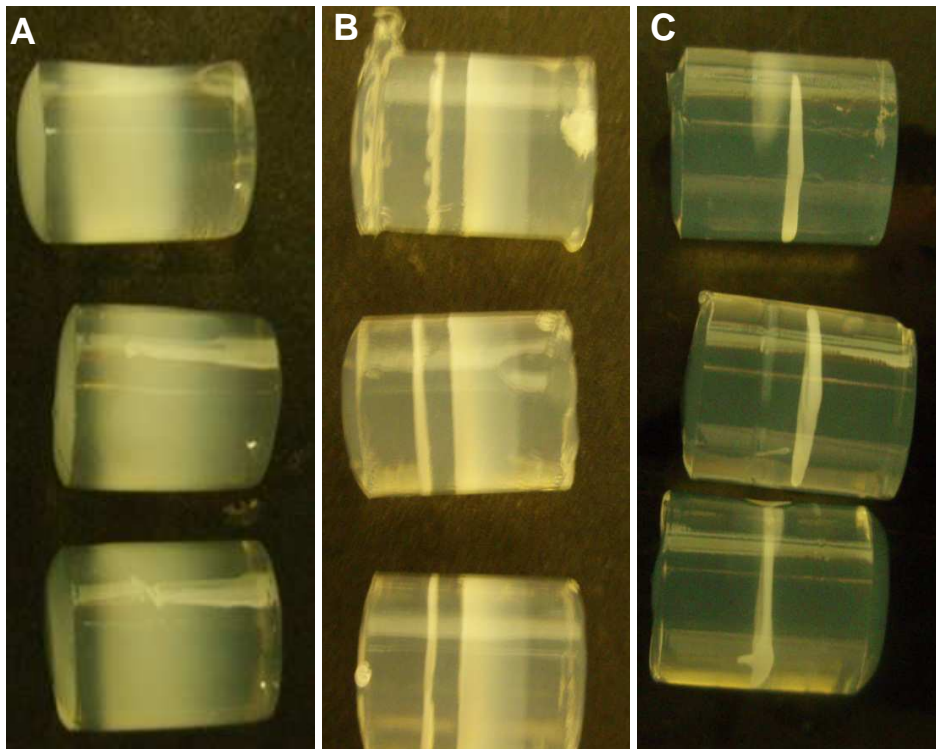


Figure 27. Panels A, B and C. Images for bands of mineral precipitation obtained when using 10 $\mu\text{g/mL}$ PGA positive control as the nucleating agent. Variation in band thickness and patterns are evident. Each panel represents the triplicates from a different steady-state assay run.

Liesegang rings are precipitation geometries (Stern, 1954) that were previously seen when PGA was used in a gel-diffusion system (Hunter and Goldberg (1994). Likewise, Liesegang rings were periodically observed in the gel plugs recovered when 10 $\mu\text{g}/\text{mL}$ PGA positive control was used as the mineral nucleator in this study (figure 28). Though in contrast, the mineral precipitates formed in the presence of recombinant 32 kDa enamel, or in negative controls, did not exhibit Liesegang rings.



Figure 28. Images for agarose gels containing 10 $\mu\text{g}/\text{mL}$ PGA positive control as the mineral nucleator. Liesegang rings are evident.

Figure 29 shows that mineral precipitation occurred to some degree even in the negative controls. Each panel shows the triplicate plugs from a single experimental run. The steady-state agarose gel system is a very delicately balanced system and any very slight changes in the buffer concentrations and ratios, or the presence of any heterogeneous nucleator such as lint or dust, can trigger spontaneous precipitation of mineral, as seen in the negative controls exemplified in figure 29. In the recovered gel plugs containing PGA or recombinant 32 kDa enamel protein nucleated samples, however, the amount of mineral precipitation was visibly greater than the negative controls.

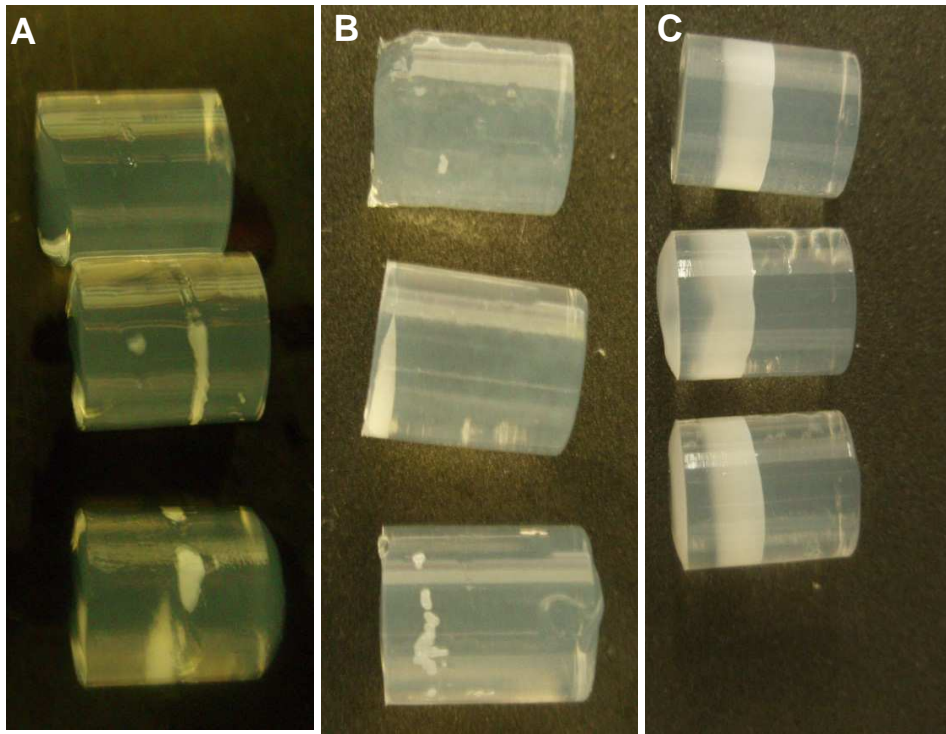


Figure 29. Panels A, B and C. Images obtained for negative control agarose gel plugs. It is clear that spontaneous nucleation occurred even in the absence of a nucleating agent.

3.2.2 Quantification of mineral deposition in agarose gels containing recombinant 32 kDa enamelin

The amount of mineral precipitation in the presence of various concentrations of recombinant 32 kDa enamelin was determined by measuring the phosphate content of the recovered agarose gel plugs following ashing (section 2.2.2). The phosphate content was calculated against standard curves prepared using known concentrations of phosphate that were run with each assay. Linear regression was then used to allow the back-calculation of phosphate concentration in the experimental samples. Figure 30 shows a typical standard curve obtained with the phosphate assay.

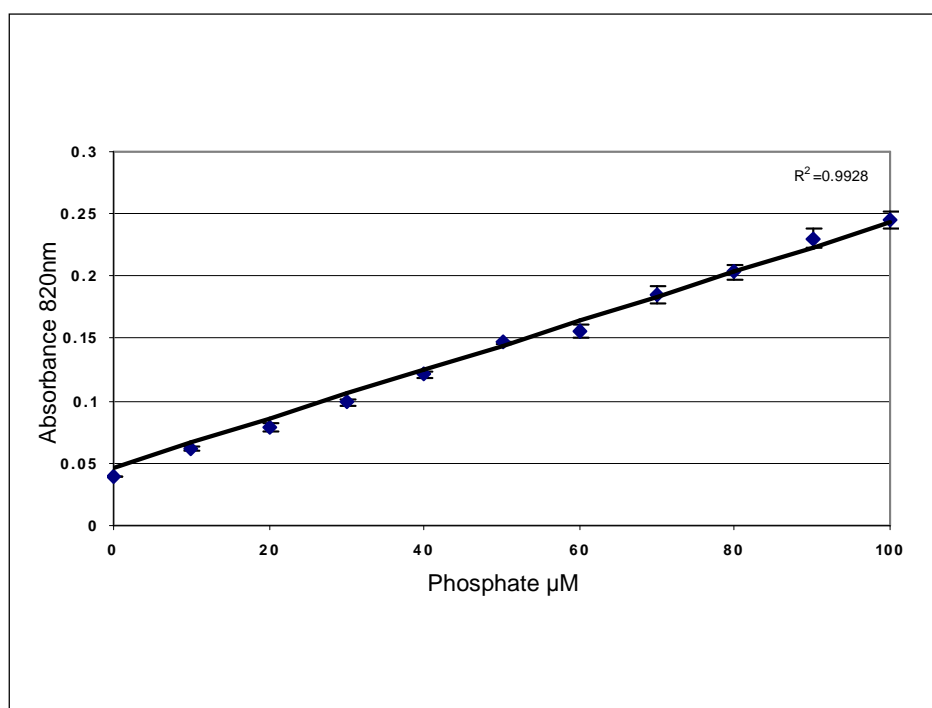


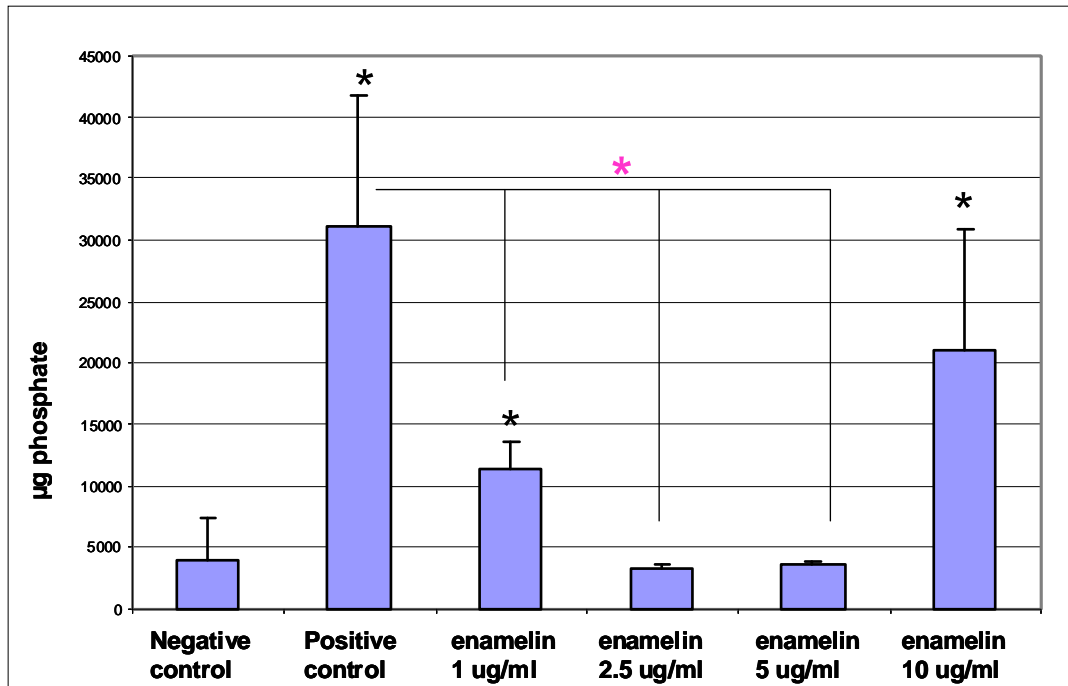
Figure 30. Typical standard curve data generated for phosphate analysis assay. Concentrations from 0 to 100 µM phosphate were used for the standard curve.

The steady-state agarose gel system to assess the nucleating potential of 10 µg/mL recombinant 32 kDa enamelin was performed on five separate occasions. The steady-state mineralisation assay to investigate the nucleating potential of recombinant 32 kDa enamelin at concentrations of 5.0 µg/mL, 2.5 µg/mL and 1.0 µg/mL was

performed on three separate occasions. All assay occasions included duplicates of positive and negative controls. Results shown in figure 31 are for mean values. A students two-tailed T-test was performed on the data to test for statistical significance ($p < 0.05$).

Figure 31 shows the degree of mineral precipitation in the gel plugs in terms of the phosphate present. The positive control (10 $\mu\text{g/mL}$ PGA), recombinant 32 kDa enamelin at 1 $\mu\text{g/mL}$ and recombinant 32 kDa enamelin at 10 $\mu\text{g/mL}$ were statistically significantly different to the negative control i.e. PGA and recombinant 32 kDa enamelin at 1.0 and 10 $\mu\text{g/mL}$ nucleate mineral. Recombinant 32 kDa enamelin at 2.5 $\mu\text{g/mL}$ and 5.0 $\mu\text{g/mL}$ were not significantly different to the negative control i.e. recombinant 32 kDa enamelin at 2.5 and 5 $\mu\text{g/mL}$ did not nucleate more mineral above the borderline level of the negative control.

The phosphate content of the mineral deposits recovered from the gel plugs using recombinant 32 kDa enamelin at 1.0 $\mu\text{g/mL}$, 2.5 $\mu\text{g/mL}$ and 5.0 $\mu\text{g/mL}$ as the mineral nucleating agent were all statistically significantly lower than the phosphate content of the gel plugs using 10 $\mu\text{g/mL}$ PGA as the positive control. The phosphate content of gel plugs containing recombinant 32 kDa enamelin at 10 $\mu\text{g/mL}$ was not statistically significantly different to the phosphate content of the gel plugs containing 10 $\mu\text{g/mL}$ PGA as the positive control.



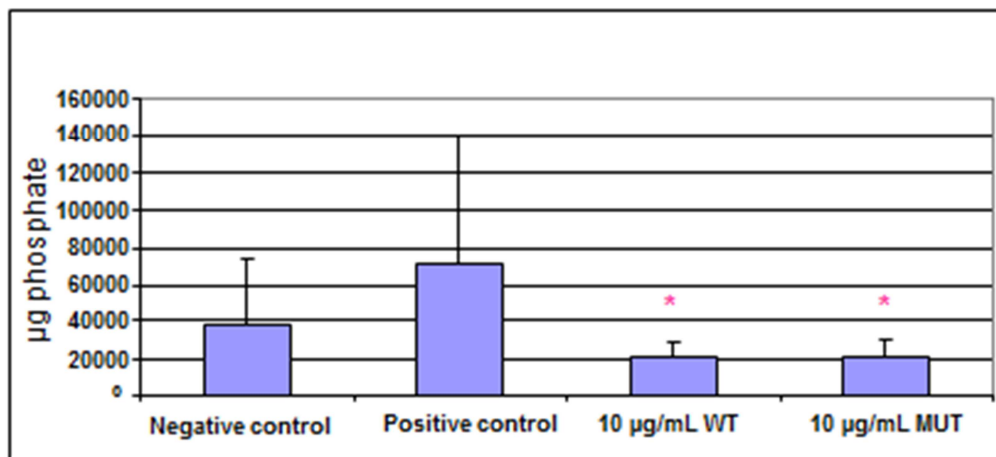
* Statistically significantly different to positive control

* Statistically significantly different to negative control

Figure 31. Graph showing mean levels of phosphate precipitation for negative control, positive control and recombinant 32 kDa enamelin at various concentrations in the steady state agarose gel nucleation assay. Negative control (no nucleating agent) and positive control (10 µg/mL PGA) n=28, 1 µg/ml, 2.5 µg/ml and 5 µg/ml recombinant 32 kDa enamelin n=6, 10 µg/ml recombinant 32 kDa enamelin n=10. Statistical significance = $p < 0.05$. Error bars for the standard deviations are also shown.

3.2.3 Quantification of mineral deposition in agarose gels containing wild type of Y64H recombinant amelogenin

Figure 32 shows the data obtained from the steady-state agarose gel system when 10 µg/mL recombinant wild-type amelogenin or 10 µg/mL recombinant mutant amelogenin was included in the agarose gels. Negative controls of agarose gel alone and positive controls of 10 µg/mL PGA were also included. Three separate experimental runs each including triplicates of each sample and controls were run. Duplicate gels were ashed to obtain phosphate assay data.



* Statistically significantly different to positive and negative control

Figure 32. Graph showing the phosphate content of gels containing no added nucleating agent (negative control), 10 µg/mL PGA (positive control), 10 µg/mL recombinant wild type amelogenin or recombinant Y64H mutant amelogenin. Statistical significance = $p < 0.05$. $n = 6$. Error bars for the standard deviations are shown.

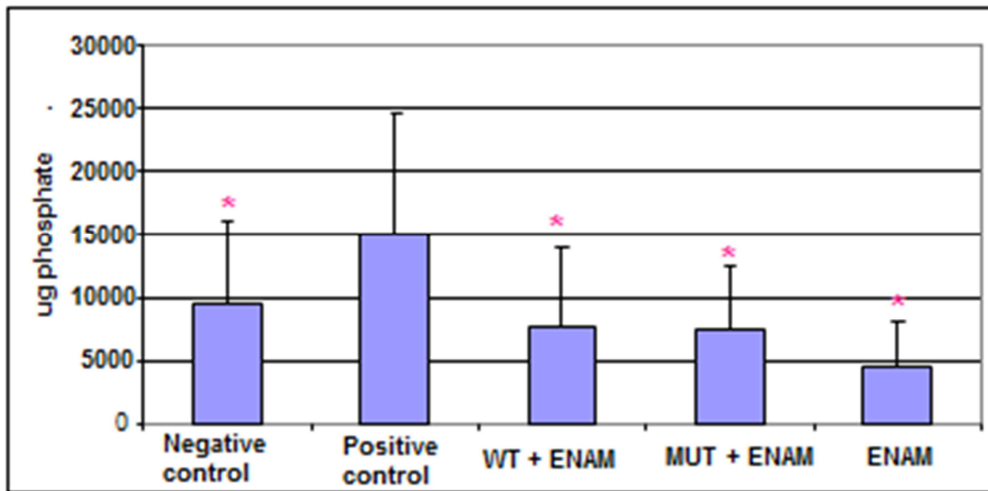
This data showed that both 10 µg/mL recombinant wild type and Y64H mutant amelogenin were unable to nucleate hydroxyapatite crystal formation *in vitro*. The fact that the levels of phosphate detected were lower than the negative control containing no protein ($p < 0.05$), suggested that amelogenin may in fact have suppressed nucleation.

3.2.4 Quantification of nucleating potential of either wild type or Y64H recombinant amelogenin in combination with recombinant 32 kDa enamelin

As amelogenin and enamelin do not occur independently in the ECM, the steady-state agarose gel experiment was performed using samples comprising of a combination of recombinant amelogenin and recombinant 32 kDa enamelin together in the agarose gel. Ten $\mu\text{g/mL}$ of recombinant wild type amelogenin or recombinant Y64H mutant amelogenin were mixed with 5 $\mu\text{g/mL}$ recombinant 32 kDa enamelin and run in triplicate in the steady-state system. Controls of 5 $\mu\text{g/mL}$ recombinant 32 kDa enamelin, 10 $\mu\text{g/mL}$ PGA and negative controls of blank agarose gels were also run in triplicate. The experiment was performed on three separate occasions.

Figure 33 shows the amount of phosphate recovered from mineral deposits recovered from the agarose gels in the presence or absence of amelogenin/recombinant 32 kDa enamelin combinations for the three experimental runs. The results suggest that the presence of recombinant 32 kDa enamelin with either recombinant wild type amelogenin or recombinant Y64H mutant amelogenin reduced the apparent inhibition of nucleation shown by wild type or mutant amelogenin alone (figure 32). No significant differences were seen in the amount of phosphate recovered between recombinant wild type amelogenin in combination with recombinant 32 kDa enamelin or recombinant Y64H mutant amelogenin in combination with recombinant 32 kDa enamelin compared with the negative control. No significant difference was seen in the amount of phosphate recovered from the mineral deposits between the recombinant wild type amelogenin and recombinant Y64H mutant amelogenin, in the presence of recombinant 32 kDa enamelin.

Together with the data presented in figure 32 (the effect of recombinant wild type amelogenin and recombinant Y64H mutant amelogenin alone on nucleation) the data implies that the Y64H mutation in the amelogenin protein does not affect the nucleation potential of amelogenin.



* Statistically significantly different to positive control

Figure 33. Graph showing phosphate precipitated in negative control gels (no nucleating agent), positive control gels (10 $\mu\text{g}/\text{mL}$ PGA), gels containing 10 $\mu\text{g}/\text{mL}$ recombinant wild type amelogenin + 5 $\mu\text{g}/\text{mL}$ recombinant 32 kDa enamelin, 10 $\mu\text{g}/\text{mL}$ recombinant Y64H mutant amelogenin + 5 $\mu\text{g}/\text{mL}$ recombinant 32 kDa enamelin, and 5 $\mu\text{g}/\text{mL}$ recombinant 32 kDa enamelin. N=6. Statistical significance = $p < 0.05$. Standard deviations are shown.

3.2.5 Characterisation of nucleated mineral deposits using scanning electron microscopy (SEM)

SEM was performed on the mineral nucleated in the agarose plugs to investigate the morphology of the mineral crystals formed by recombinant 32 kDa enamelin alone and in conjunction with recombinant wild-type and recombinant Y64H mutant amelogenin. The following section presents representative images obtained using SEM.

The top panel in figure 34 shows crystals nucleated in the presence of 10 µg/mL recombinant 32 kDa enamelin imaged at 24750 times magnification. This shows that the crystals exhibited a flat, planar morphology measured in the micron range, at approximately 6 µm in length. The bottom panel shows crystals nucleated in the presence of 10 µg/mL recombinant 32 kDa enamelin imaged at 66740 times magnification. The flat crystal plates are clearly visible.

The top panel in figure 35 shows crystals nucleated in the presence of 5 µg/mL recombinant 32 kDa enamelin imaged at 12950 times magnification. This shows that the crystals exhibited an oblate morphology measured in the micron range, at approximately 6 µm in length. The bottom panel shows crystals nucleated with 5 µg/mL recombinant 32 kDa enamelin imaged at 50000 times magnification. The flat crystal plates are clearly visible.

Figures 34 and 35 for the SEM data for the crystals nucleated in the presence of 10 µg/mL and 5 µg/ml recombinant 32 kDa enamelin display very similar morphology of the crystals, with large plates of mineral crystal of approximately 6 microns in length. This was in spite of the fact that when the agarose gels recovered from the steady state agarose gel system were analysed by the phosphomolybdate phosphate assay, the amount of mineralisation recovered for the 5 µg/mL enamelin gel plugs was not statistically significantly different to the negative controls. Therefore, although the levels of mineral nucleated were different for the agarose gel plugs containing either 10 µg/mL or 5 µg/mL recombinant 32 kDa enamelin protein, the crystal morphologies were comparable.

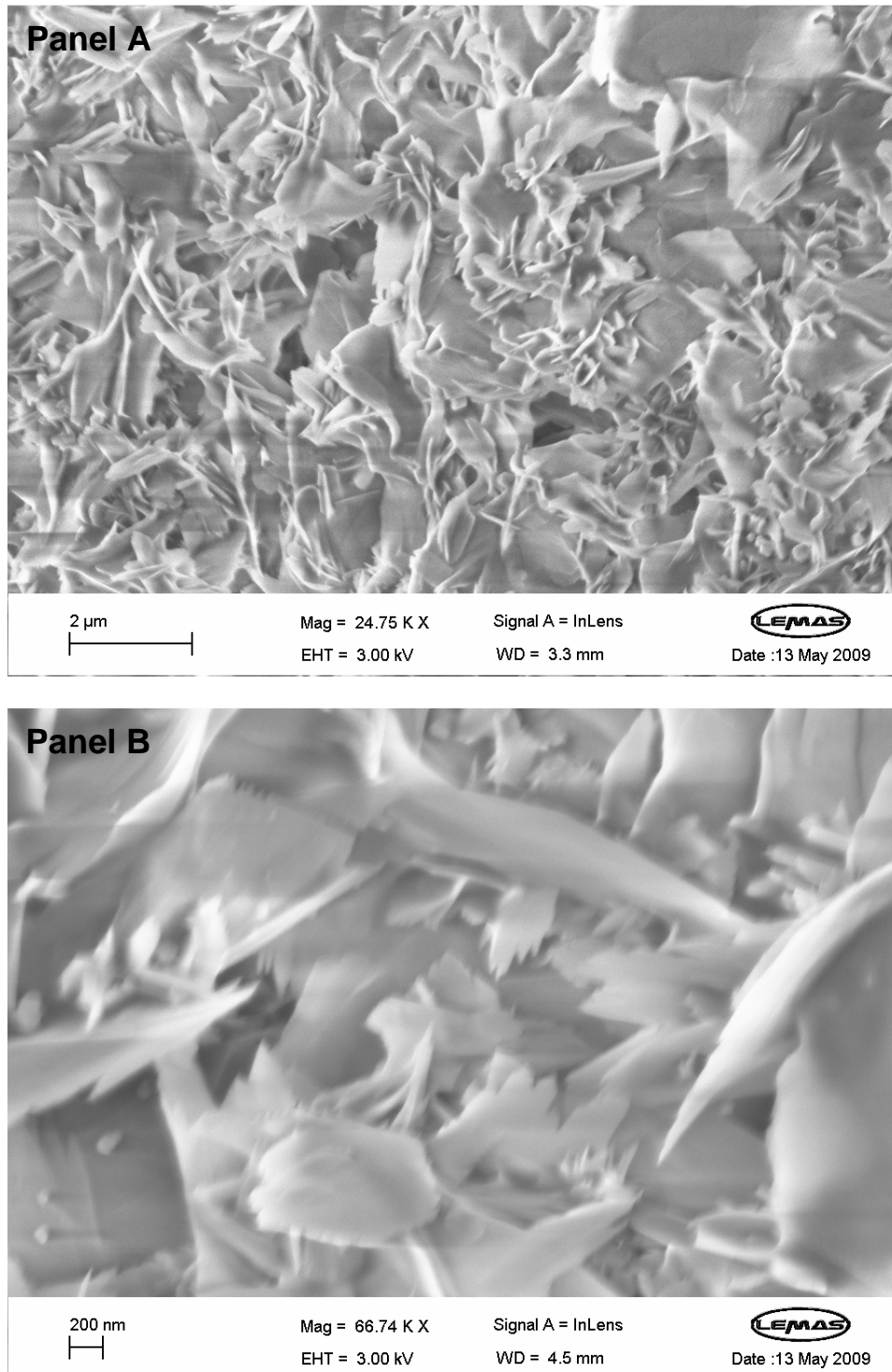


Figure 34. SEM data for crystals nucleated in the presence of 10 μ g/mL recombinant 32 kDa enamelin. Panel A shows the crystal morphology imaged at 24750 times magnification. Panel B shows the crystal morphology imaged at 66740 times magnification.

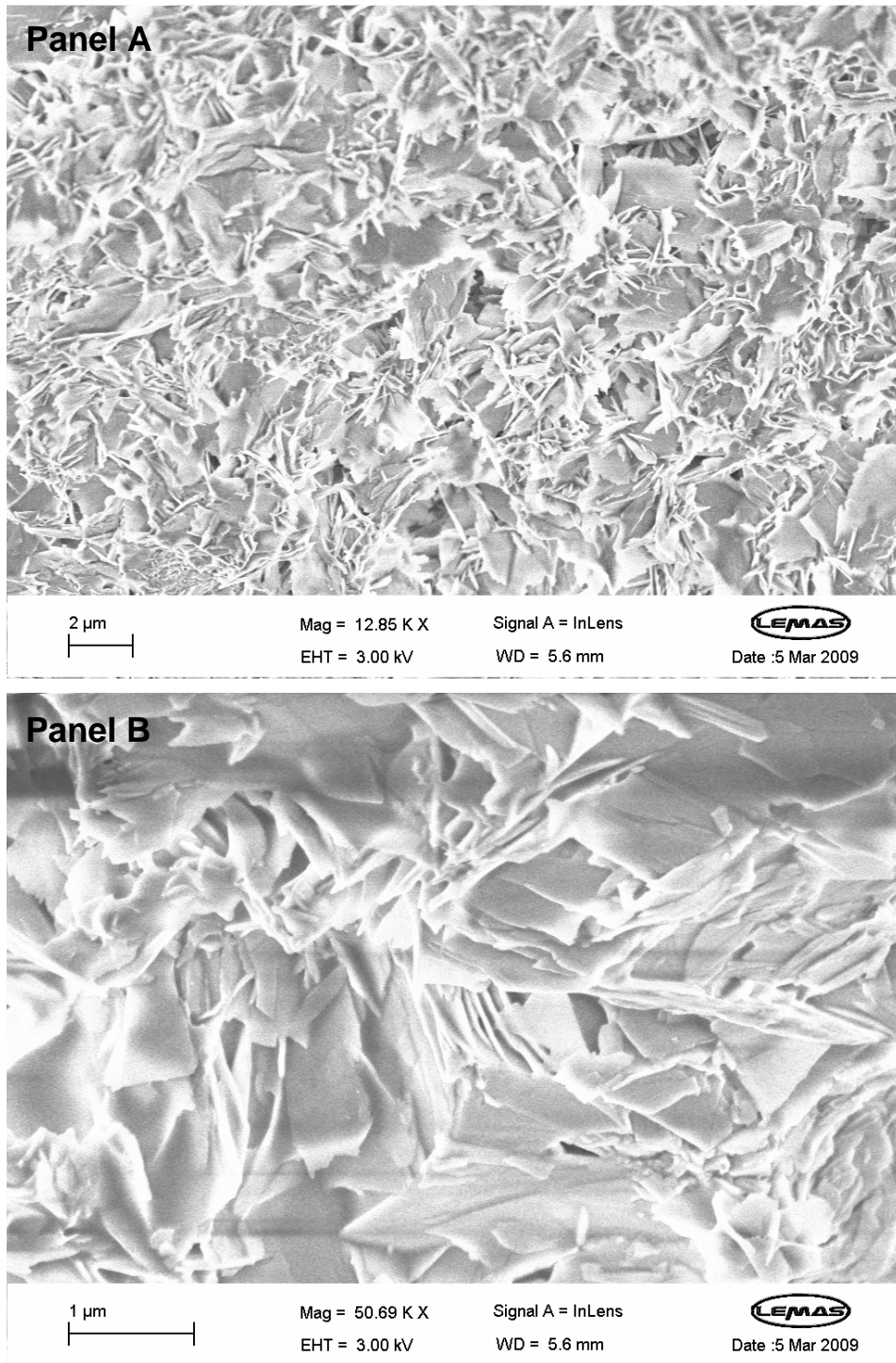


Figure 35. SEM data for crystals nucleated in the presence of 5 μ g/mL recombinant 32 kDa enamelin. Panel A shows the crystal morphology imaged at 12850 times magnification. Panel B shows the crystal morphology imaged at 50690 times magnification.

Although recombinant 32 kDa enamelin at 2.5 µg/mL did not nucleate mineral deposition in the steady state agarose gel system any better than negative controls (when analysed by the phosphomolybdate phosphate assay), the mineral crystals that were recovered are shown in figure 36. Mineral nucleated in the presence of recombinant 32 kDa enamelin at 2.5 µg/mL exhibited two distinct morphologies; both of them different to the flat crystals nucleated in the presence of 10 µg/mL or 5 µg/mL recombinant 32 kDa enamelin (as shown in figure 36). The upper two images (panels A and B) show the presence of small spherical clusters (approximately 10 nm in length). These are very similar in appearance to globular clusters of calcium phosphate seen by Wada *et al* (1996) during their investigations into *in vitro* mineralisation nucleated by dentine ECM proteins. In contrast, smaller, needle like crystals were also observed as shown in the bottom two images (panels C and D).

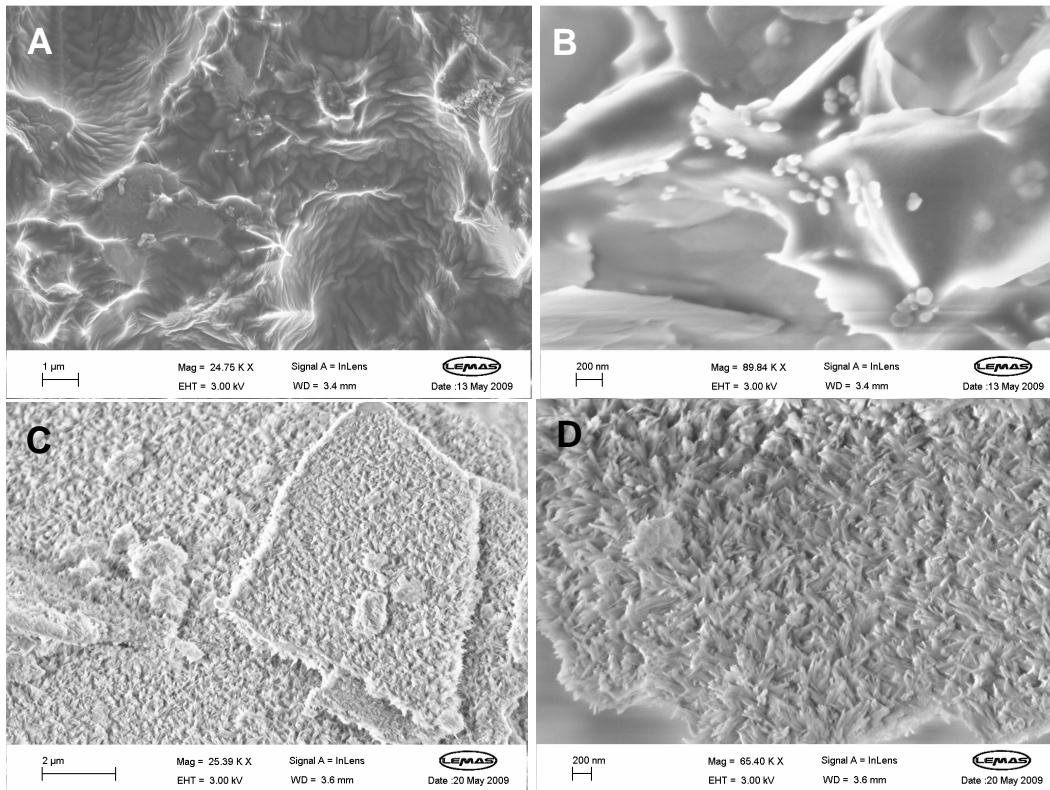


Figure 36. SEM data for mineral crystals from the steady state agarose gel system nucleated in the presence of 2.5 µg/ml recombinant 32 kDa enamelin. Panel A shows the crystal morphology imaged at 24750 times magnification. Panel B shows the crystal morphology imaged at 89840 times magnification. Panel C shows the crystal morphology imaged at 25390 times magnification. Panel D shows the crystal morphology imaged at 65400 times magnification. Note the presence of clusters of small spheres in panels A and B. Panels C and D show smaller crystals exhibiting a different morphology.

Figure 37 shows crystals nucleated in the presence of 1 µg/mL recombinant 32 kDa enamelin. Again the large plate like crystals of approximately 6 microns are visible that are more akin to the crystals nucleated with 10 µg/mL and 5 µg/mL recombinant 32 kDa enamelin. When the gel plugs containing the mineral nucleated in the presence of 1 µg/mL recombinant 32 kDa enamelin was analysed by the phosphomolybdate phosphate assay, these showed the mineral content to be statistically significantly increased compared to the negative controls. This was also true for the 10 µg/mL recombinant 32 kDa enamelin gel plugs and resulting mineral.

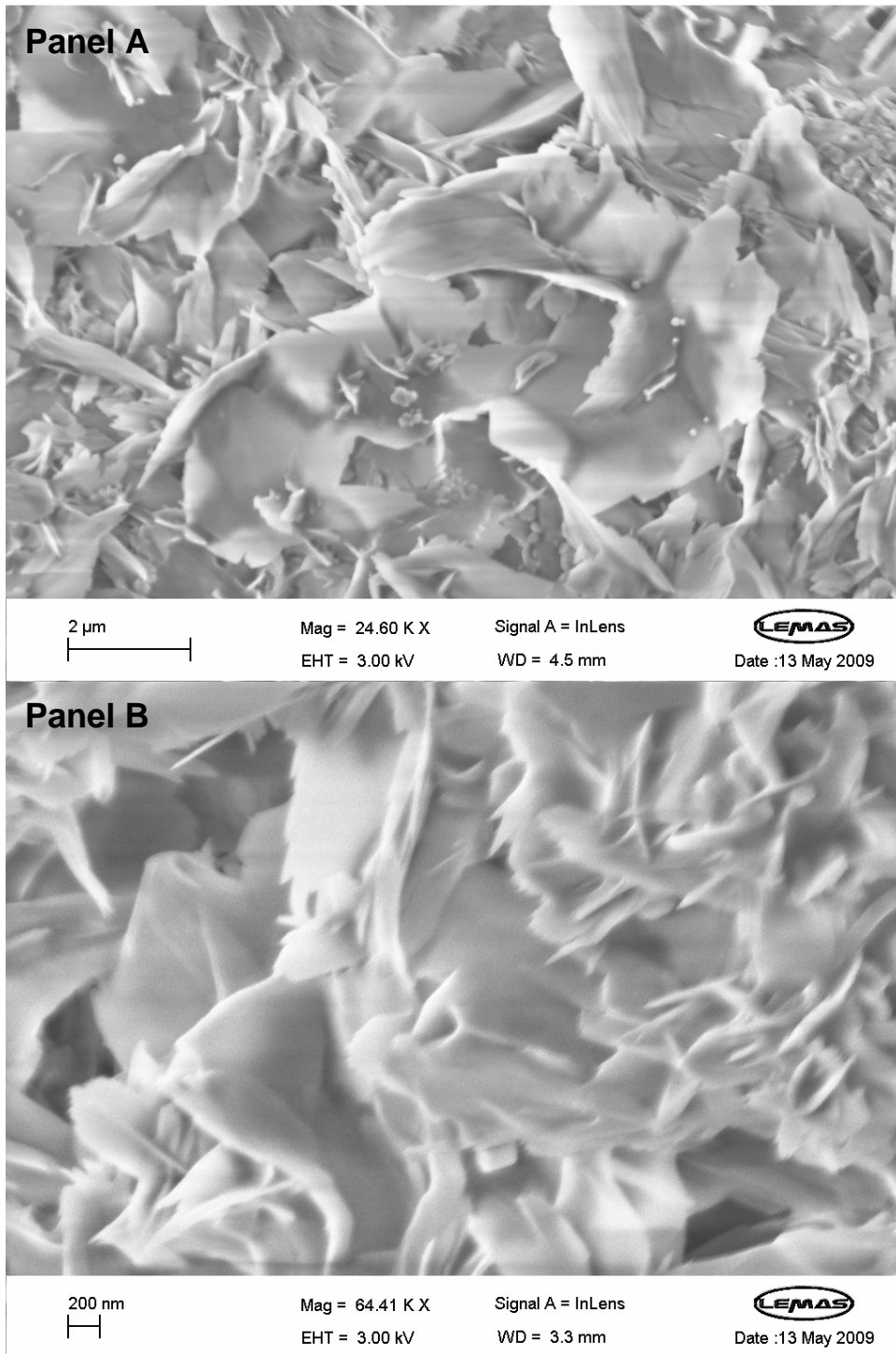


Figure 37. SEM data for crystals nucleated in the presence of 1 µg/mL recombinant 32 kDa enamelin. Panel A shows the morphology of the crystals imaged at 24600 times magnification. Panel B shows the morphology of the crystals imaged at 64410 times magnification.

Figure 38 shows SEM images of commercially available hydroxyapatite, not exposed to the steady state agarose gel system, for comparison of morphology. These mineral deposits were not obtained from the steady state agarose gel system. Commercial hydroxyapatite was mounted onto a SEM stub and sputter-coated with gold as for the mineral deposits obtained in the steady state agarose gel system (section 2.2.3). Large plates-like crystals of approximately 18 μm in length are visible in the top image (panel A), but the surfaces of these large plates are covered in much smaller, needle like crystals. The bottom image (panel B), taken at higher magnification, shows these smaller crystals more clearly. These crystals are much smaller, approximately 0.3 μm in length, than those obtained from the steady state agarose gel system and nucleated in the presence of recombinant 32 kDa enamelin, or indeed PGA.

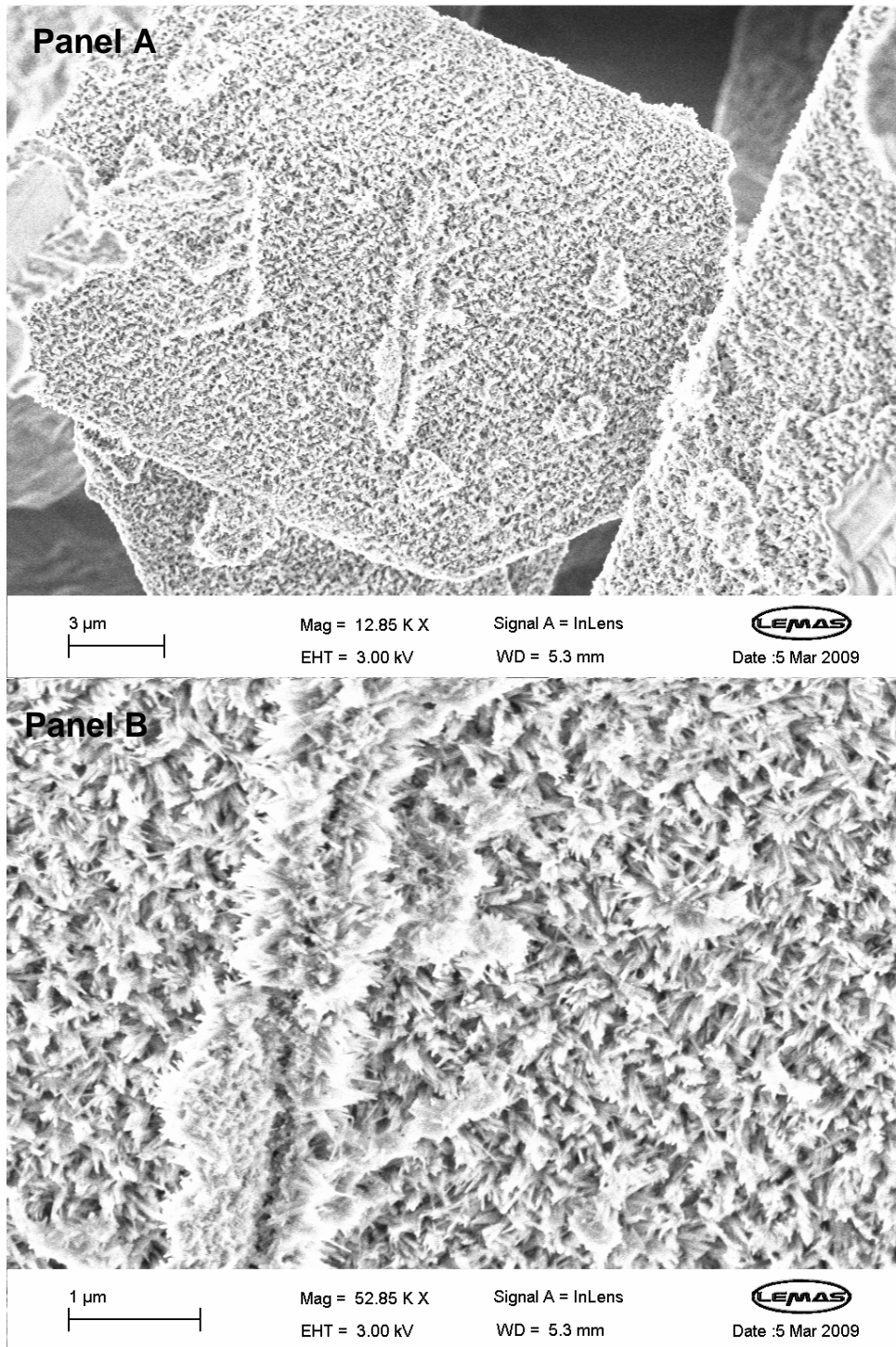


Figure 38. SEM images for commercially available hydroxyapatite not exposed to the steady state agarose gel system. Panel A shows the commercially available hydroxyapatite imaged at 12850 times magnification. Panel B shows the commercially available hydroxyapatite imaged at 52850 times magnification.

Figure 39 shows crystals nucleated in the presence of the positive control (10 $\mu\text{g/mL}$) PGA. The crystals had a pointed appearance and appeared to radiate out of central areas. They were stellate in appearance. The bottom two images (panels C and D) of the figure show large plate like structures, similar to those nucleated in the presence of recombinant 32 kDa enamelin. These were approximately 1200 μm in length.

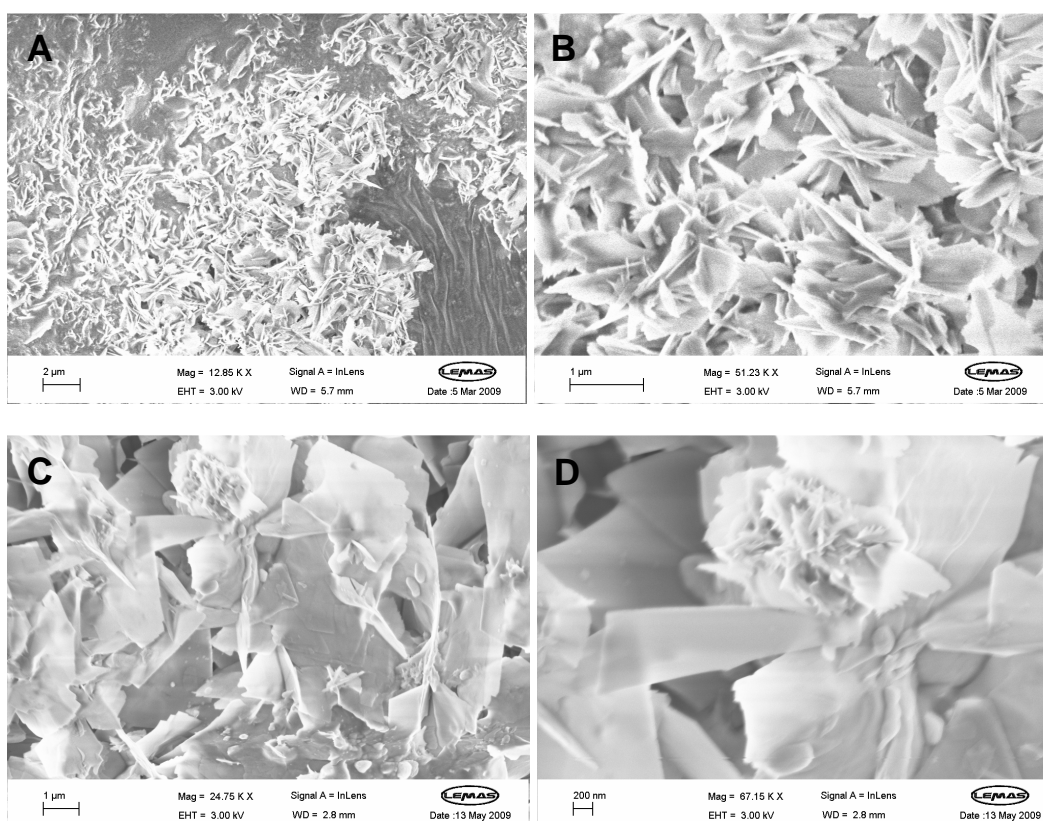


Figure 39. SEM data for the morphology of the mineral crystals nucleated in the presence of 10 $\mu\text{g/ml}$ PGA recovered after 7 days exposure to the steady state agarose gel system. Panel A shows the crystals imaged at 12850 times magnification. Panel B shows the mineral crystals imaged at 51250 times magnification. Panel C shows the mineral crystals imaged at 24750 times magnification. Panel D shows the mineral crystals imaged at 67150 times magnification.

Figure 40 shows the images of crystals obtained for the negative controls, agarose gel without any additional nucleator. A much smoother, bubbly appearance was seen without any distinct crystal morphology.

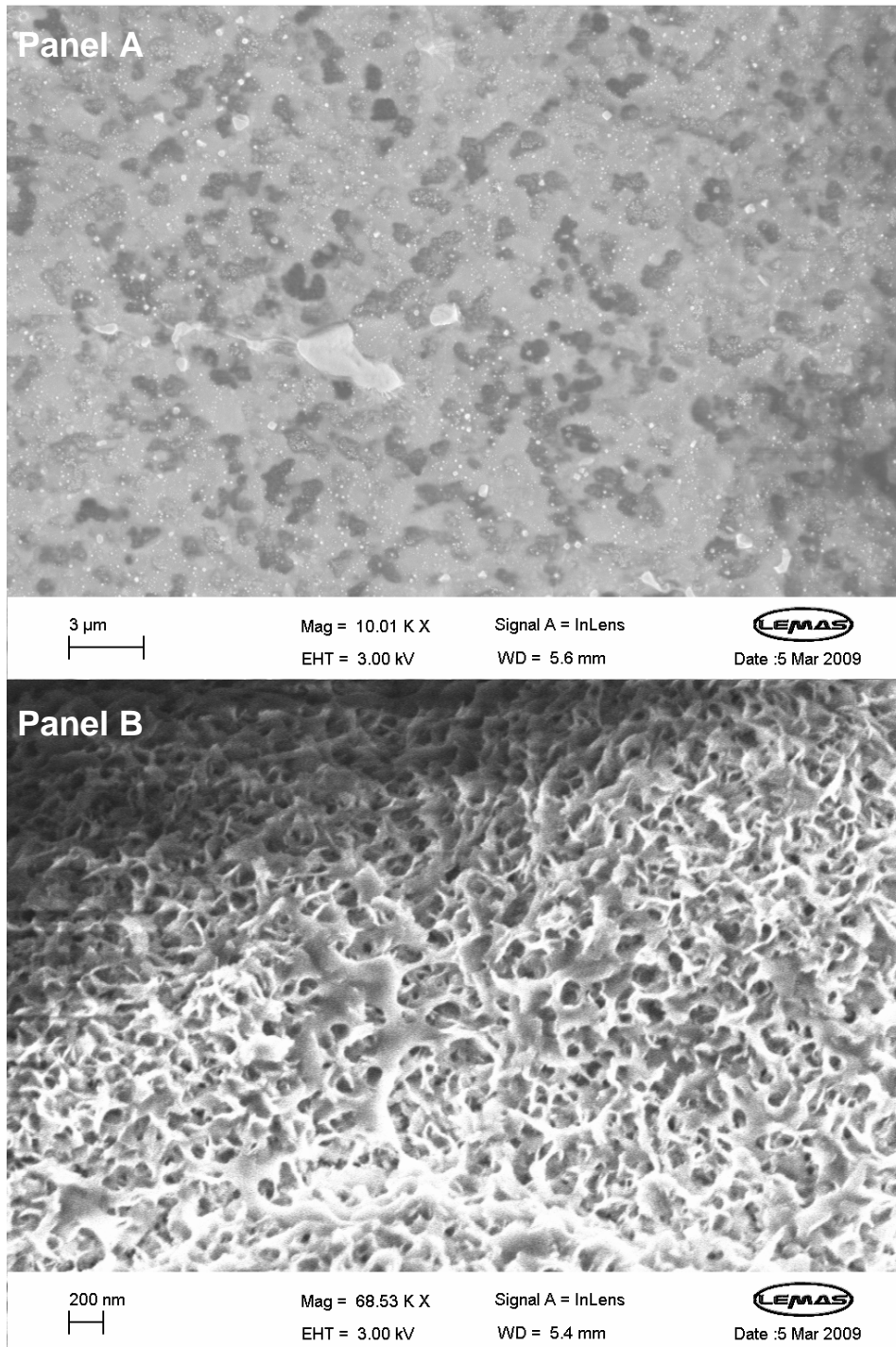


Figure 40. SEM data for mineral crystals recovered from the negative control agarose gels. These were agarose gel plugs without the addition of any recombinant protein or PGA, but that had been exposed to the mineralisation solutions in the steady state agarose gel system. Panel A shows the mineral crystals imaged at 10010 times magnification. Panel B shows the mineral crystals imaged at 68530 times magnification.

3.2.6 Characterisation of nucleated mineral deposits by energy dispersive X-ray spectroscopy (EDX)

EDX was used to determine the elemental composition of the nucleated mineral in the agarose gel plugs following their retrieval after the steady state run. Figures 41-44 show the EDX results for commercially available hydroxyapatite; the agarose gel blank (agarose gel not exposed to mineralising solutions); the negative controls (agarose only, no nucleator added); PGA positive controls and samples containing recombinant 32 kDa enamel in at 10 $\mu\text{g}/\text{mL}$ respectively.

The calcium to phosphate (Ca:P) ratios for material nucleated in the presence of PGA (figure 44) and recombinant 32 kDa enamel in (figure 45) were very similar to the EDX data obtained for commercial hydroxyapatite (figure 41) – all exhibiting a Ca:P molar ratio typical of hydroxyapatite (1.66). The Ca:P ratio of 1.05 ± 0.32 obtained following EDX analysis of negative controls (figure 43) indicated that the bulk of any crystalline material deposited was unlikely to be hydroxyapatite. The Ca:P ratio of 0.60 ± 0.12 obtained for the blank samples (figure 42) shows very little similarity to hydroxyapatite. This was expected as the blank was not exposed to mineralising solution and these figures represent the background ratio of calcium and phosphorus in the agarose gel.

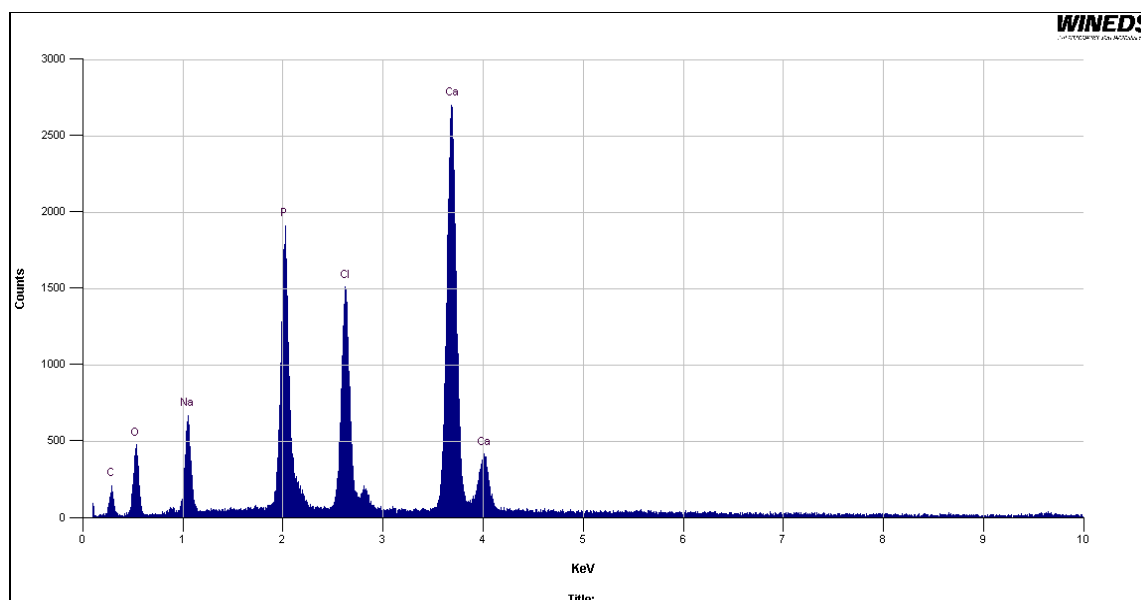


Figure 41. EDX data for commercially available hydroxyapatite (not exposed to the steady state agarose gel system). A Ca:P ratio of 1.52 was observed (within 10% of the theoretical value of 1.66 for pure hydroxyapatite).

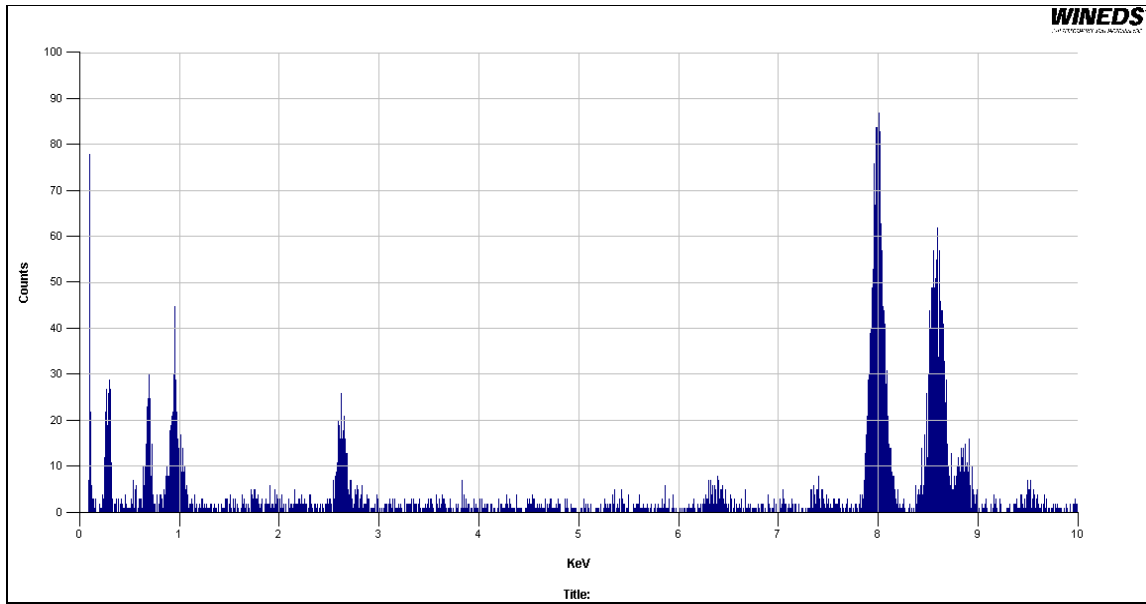


Figure 42. EDX data for agarose blank (agarose gel not exposed to mineralising solutions). Mean Ca:P from 5 steady state agarose gel runs = 0.60 ± 0.12 .

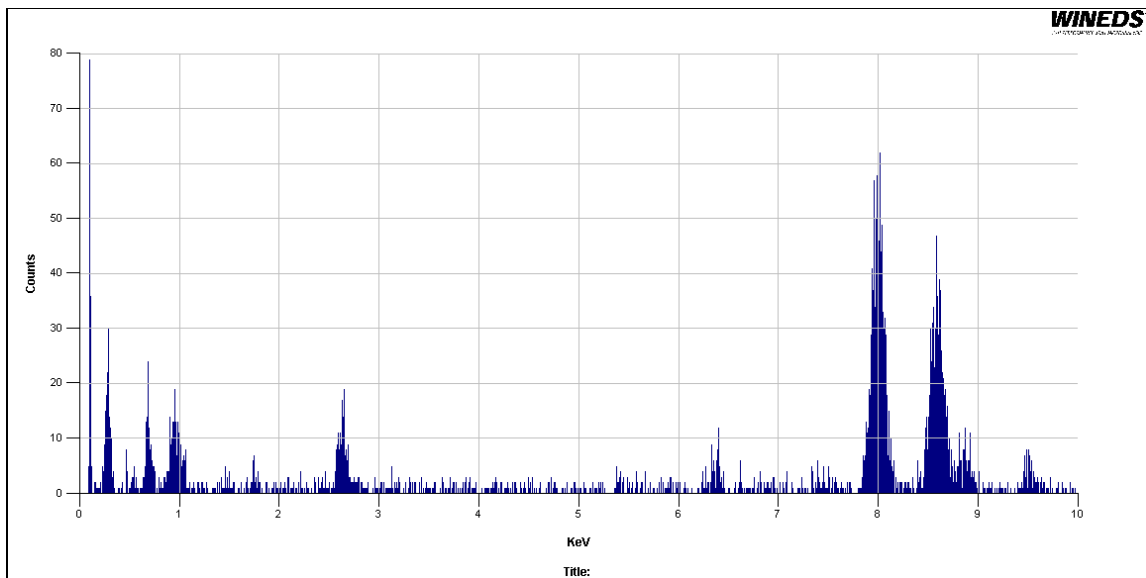


Figure 43. EDX data for negative control agarose gels (gels exposed to mineralising solutions). Mean Ca:P from 5 steady state agarose gel runs = 1.05 ± 0.32 .

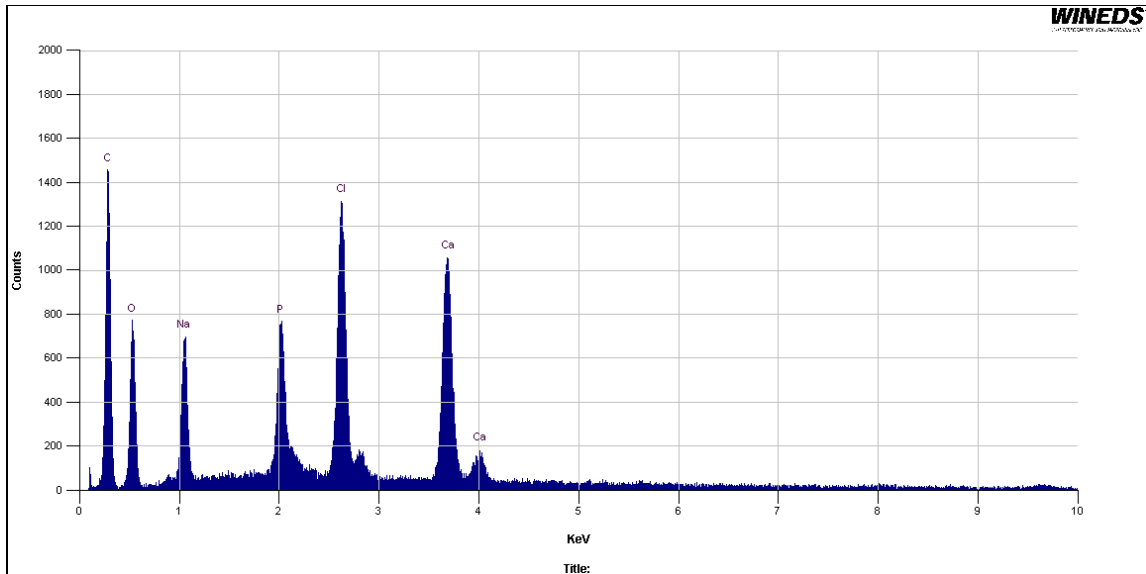


Figure 44. EDX data for the mineralised crystals nucleated in the presence of 10 µg/mL PGA positive control for 7 days at 37°C under steady state conditions. Mean Ca:P from 5 steady state agarose gel assay runs = 1.73 ± 0.12 (within 10% of theoretical value for hydroxyapatite).

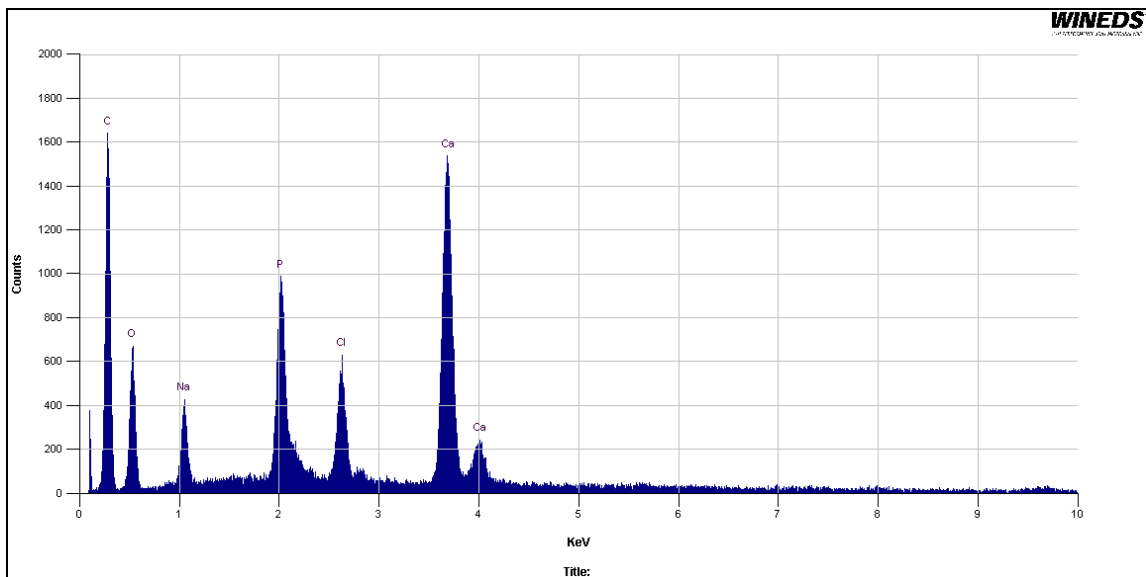


Figure 45. EDX data for the mineralised crystals nucleated in the presence of 10 µg/mL recombinant 32 kDa enamelin protein for 7 days at 37°C under steady state conditions. Mean Ca:P from 5 steady state agarose gel assay 5 runs = 1.61 ± 0.03 (within 10% of theoretical value for hydroxyapatite).

3.2.7 Characterisation of nucleated mineral deposits by transmission electron microscopy (TEM)

Transmission electron microscopy was used to investigate the morphology at high resolution of individual mineral crystals isolated from the agarose gel plugs containing recombinant protein or PGA positive control following incubation in the steady-state agarose gel system.

Figures 46 and 47 below show TEM images of mineral crystals nucleated in the presence of 5.0 $\mu\text{g/mL}$ recombinant 32 kDa enamelin protein. These crystals had a flat, planar appearance with a jagged edge. This crystal appearance is very similar to what was seen in SEM; that the crystals nucleated by recombinant 32 kDa enamelin have a flat, oblate morphology.

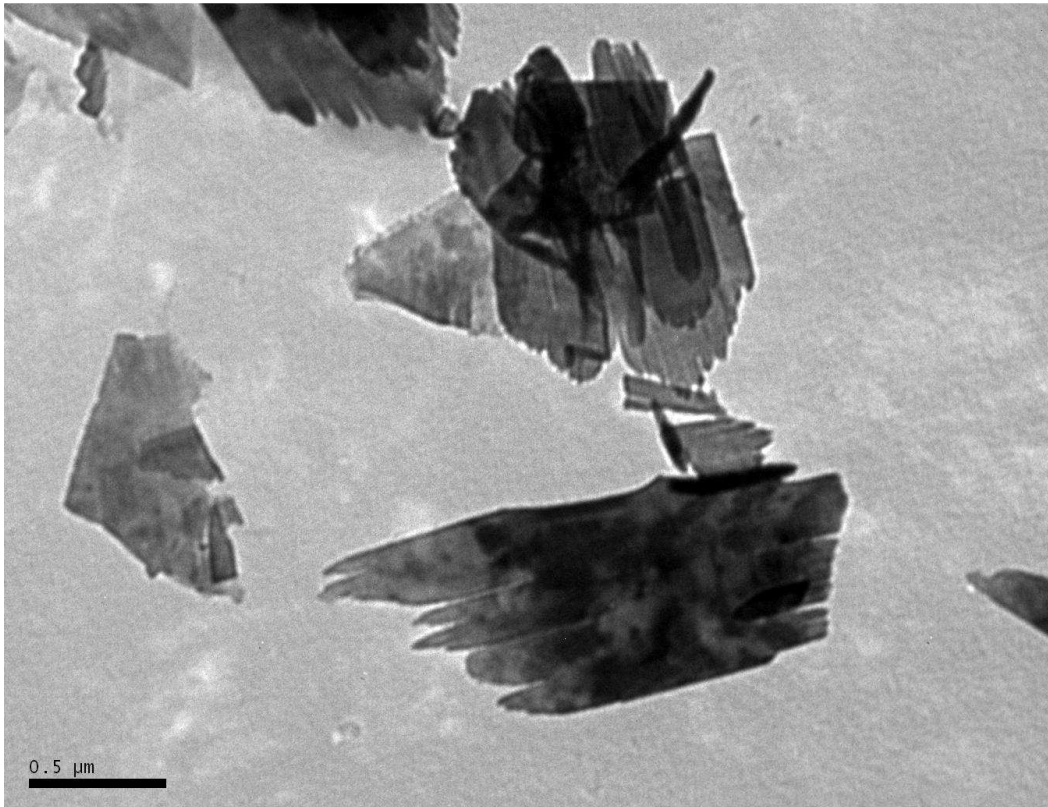


Figure 46. TEM image of crystals nucleated in the presence of recombinant 32 kDa (5 $\mu\text{g/mL}$). Note the large, flat planar appearance of the crystals. The crystal at the bottom of the screen measures approximately 4 μm by 0.7 μm . Image taken at 28,000 times magnification.

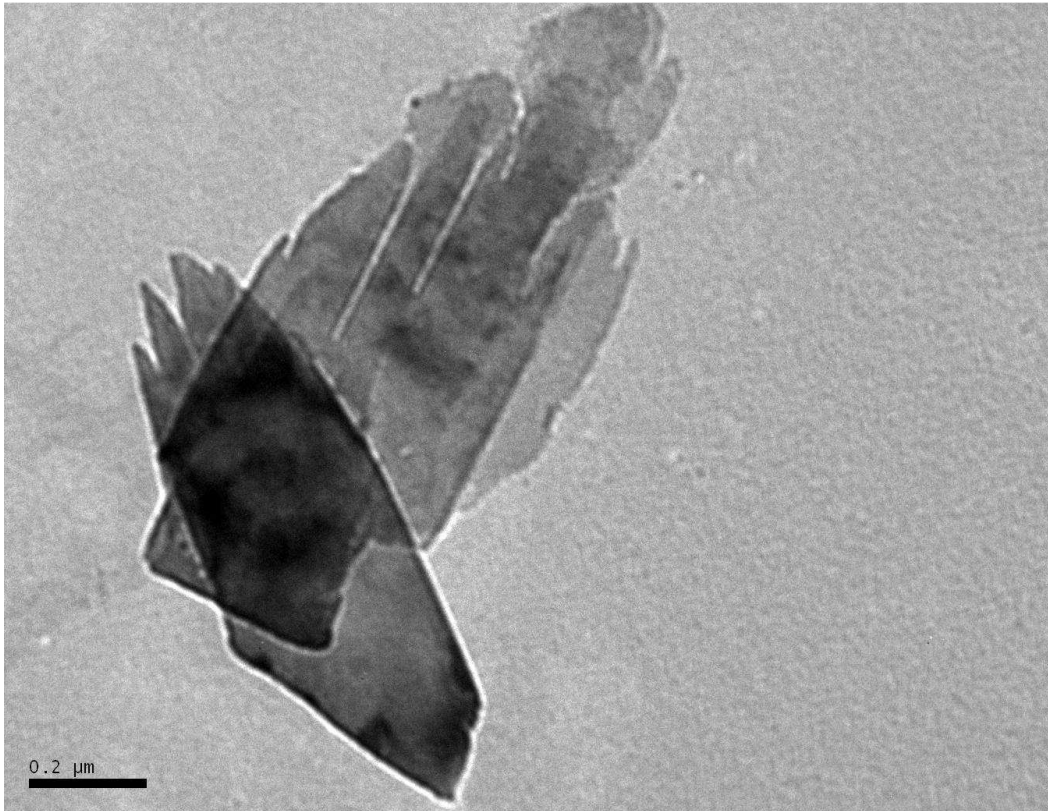


Figure 47. TEM image of 2 overlapping crystals nucleated in the presence of recombinant 32 kDa enamelin (5 μg/mL). The smaller crystal measures approximately 0.4 μm by 1.3 μm and the larger crystal 0.7 μm by 1.6 μm. Image taken at 60,000 times magnification.

In comparison, the crystals nucleated in the presence of the 10 μg/mL PGA positive controls exhibited a much more 'rosette' like appearance. This can be seen in figures 48 and 49. The crystals appeared smaller (1 micron radius), more feather-like and to radiate around a central core. This also confirmed the SEM appearance of these crystals.

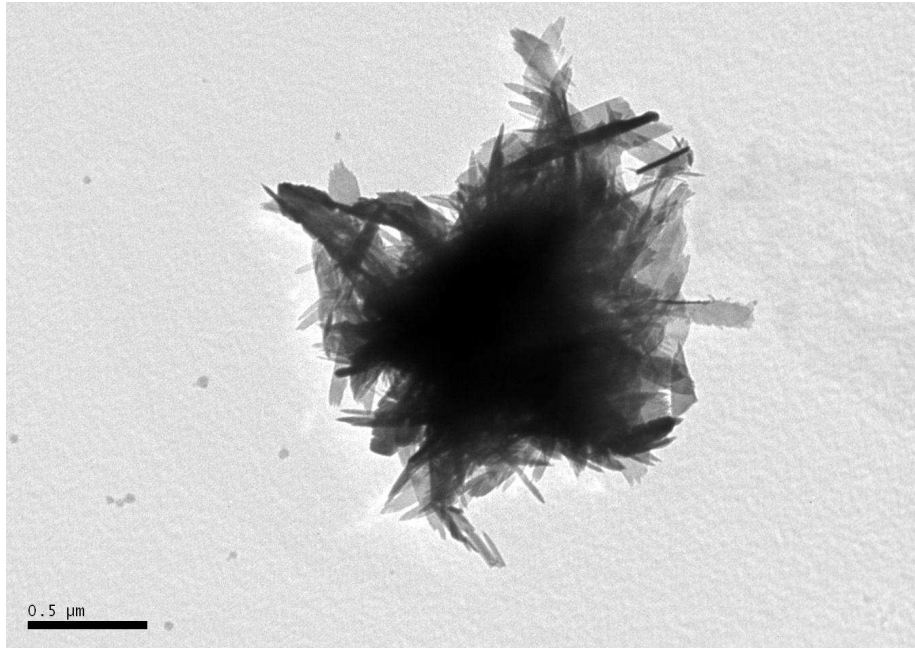


Figure 48. TEM image of crystals nucleated in the presence of PGA (10 $\mu\text{g}/\text{mL}$) following incubation in the steady state agarose gel system. The crystal rosette has a diameter of approximately 2 μm . Image taken at 28,000 times magnification.

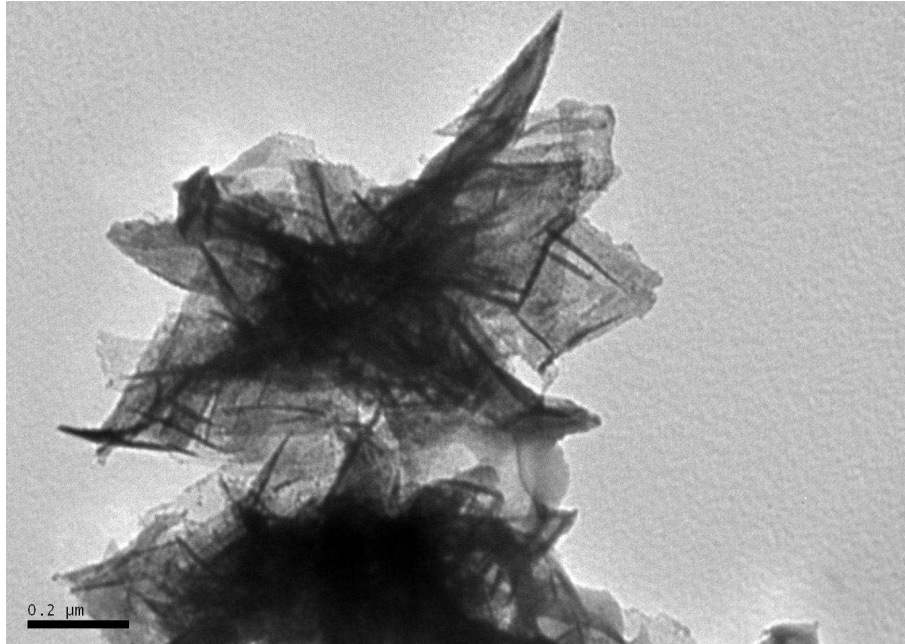


Figure 49. TEM image of crystals nucleated in the presence of PGA (10 $\mu\text{g}/\text{ml}$) positive control recovered following incubation in the steady state agarose gel system. The top crystal has a maximum diameter of 3.5 μm . Image taken at 60,000 times magnification.

Figure 50 shows a TEM image of commercially available hydroxyapatite crystals. These were not obtained from the steady state agarose system. Rather a solution of commercial hydroxyapatite was dried onto a TEM grid. These were far smaller than the crystals nucleated by recombinant 32 kDa enamelin or PGA, and had a much more needle-like appearance.

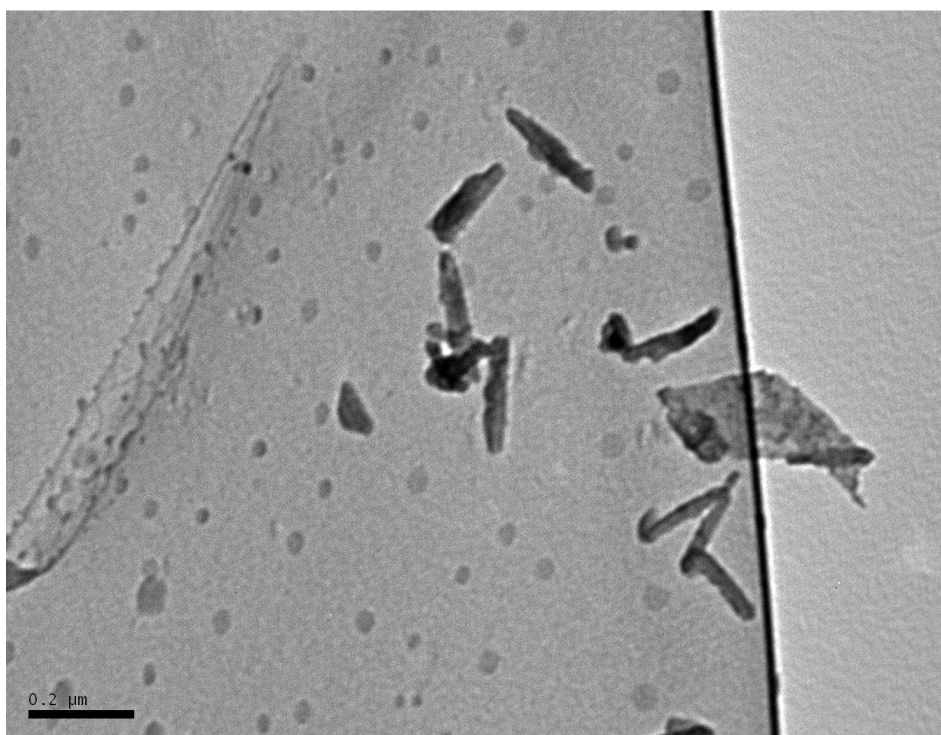


Figure 50. Image of commercially available hydroxyapatite crystals. The crystals are more rod like with a length of approximately 0.2 μm . Image taken at 60,000 times magnification.

These nucleation studies showed that recombinant 32 kDa enamelin is capable of nucleating and supporting hydroxyapatite crystal growth at concentrations of 1 $\mu\text{g/mL}$ and 10 $\mu\text{g/mL}$. The degree of nucleation of hydroxyapatite was highly variable between experimental runs using the steady state agarose gel system, even in the positive control (PGA). EDX analysis confirmed that the crystals nucleated by PGA and 10 $\mu\text{g/mL}$ recombinant 32 kDa enamelin had a similar Ca:P ratio to that of commercially available hydroxyapatite and near to the theoretical value for the molar ratio of this mineral. SEM analysis showed that both crystals nucleated in the presence of PGA and commercially available hydroxyapatite crystals have a similar rosette-like appearance with needle like

crystals radiating from a central core. SEM analysis showed that the crystals nucleated in the presence of recombinant 32 kDa recombinant 32 kDa enamelin were much larger with a flat, layered appearance. TEM analysis confirmed the crystal appearance seen in SEM.

Recombinant wild-type and recombinant Y64H mutant amelogenin were both apparently unable to nucleate hydroxyapatite *in vitro*. No significant difference was seen in the phosphate levels obtained for wild type or mutant amelogenin, alone or with 5 µg/mL recombinant 32 kDa enamelin, suggesting that the Y64H mutation in the amelogenin protein does not affect the protein's role in hydroxyapatite nucleation.

3.3 Studies of 32 kDa enamelin biochemistry in the developing enamel matrix

To date, most studies of enamelin biochemistry and function have used the 32 kDa porcine enamelin processing product due to the ready availability of pig developing enamel and the relatively high concentration of the 32 kDa species in the enamel matrix. There is a tacit assumption that the 32 kDa enamelin is the functional enamelin subunit. It is unclear how applicable this data is to other species since enamelin biochemistry is poorly described in non-porcine species. To investigate the hypothesis that the 32 kDa fragment of enamelin is the functional enamelin subunit in all species, the enamelin proteome in developing rat enamel was compared to the porcine enamelin proteome using SDS-PAGE and western blotting assays (see materials and methods section 2.4). Rat incisors were extracted from male Wistar rats as described in section 2.4.1. Pig teeth were extracted from juvenile pigs as described in section 2.4.2. Developing enamel was removed and sectioned into secretory and maturation stage samples for SDS and Western blot analysis. In addition, a bioinformatics analysis was carried out to investigate the cross-species conservation of the proteolytic cleavage sites present in pig enamelin that are responsible for the generation of the 32 kDa enamelin cleavage product in pigs.

3.3.1 Characterisation of the enamelin proteome in secretory and maturation stage rat and pig enamel

Rat incisor enamel samples from secretion (S1, S2) through to the maturation stage (M1, M2, M3 – early, mid and late maturation stage respectively) were subjected to SDS PAGE and analysed for enamelin content by western blot probing with an anti-enamelin antibody. Pig secretory stage enamel was analysed in the same way for comparison. The resulting gels and blots are shown in figure 51. Protein bands (stained blue on the gels) migrating below 25 kDa correspond to the amelogenins, confirmed by the western blot analysis. In the case of the rat samples, the loss of the amelogenins from maturation stage samples was evident. Enamelin was present in the developing enamel matrix at very low concentrations and was only detectable on the blots; it was not detectable by Coomassie staining on the gels. In rat, the enamelin antibody cross reacted predominantly with a range of high molecular weight proteins centred around 70 kDa. Critically, there was little staining in the 32 kDa region. In rat maturation stage enamel samples there was a shift in cross reactivity to a slightly lower molecular weight (approximately 50 kDa) as enamelin shares the fate of amelogenin and is degraded and removed from the tissue but even here, no obvious 32 kDa processing product was present. In complete contrast, the predominant enamelin molecule present on the blot of pig secretory stage enamel was at the lower molecular weight of 32 kDa (marked by * in figure 51, pig blot) generated, as described widely in the literature, by proteolytic processing of a larger precursor enamelin.

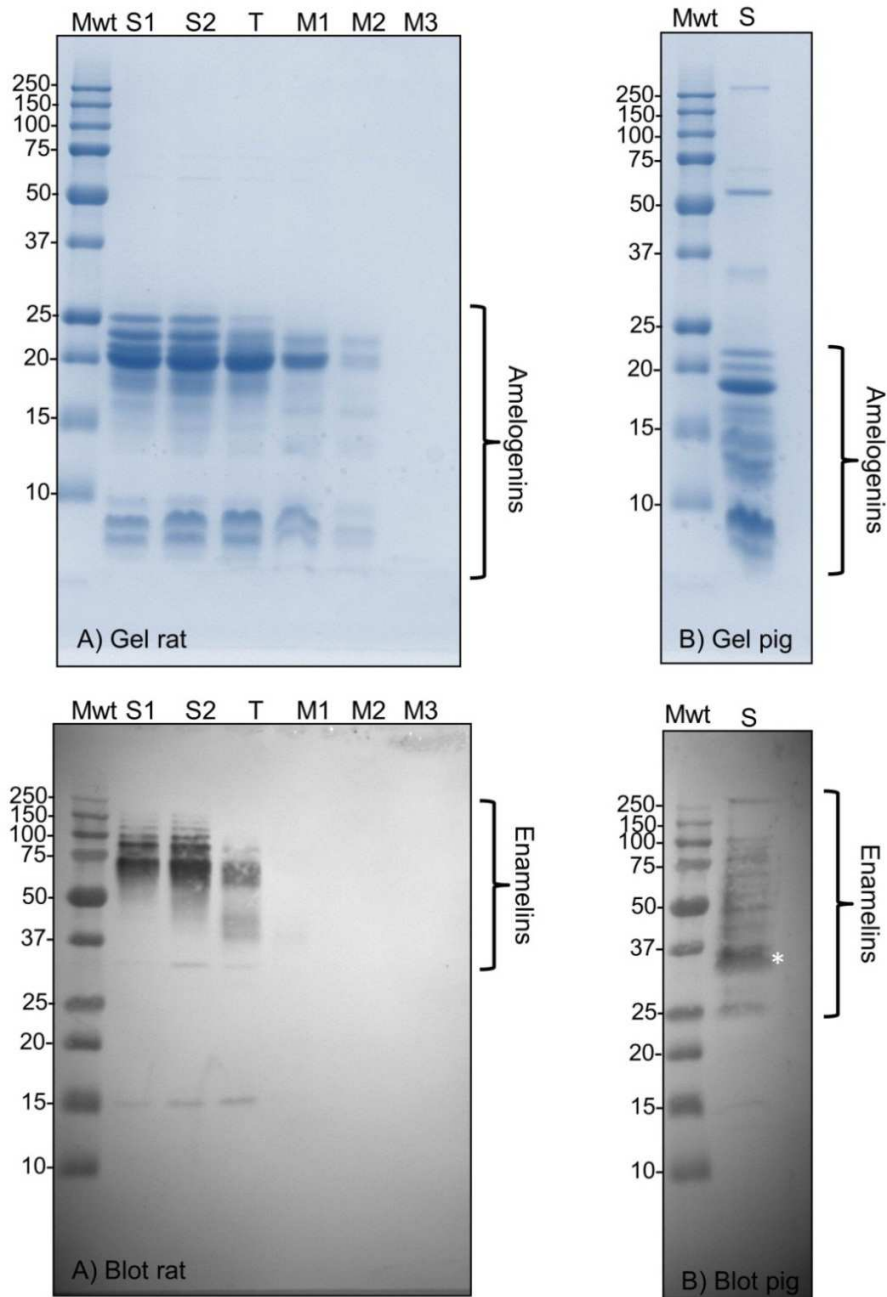


Figure 51 Shows SDS-PAGE (top panels) of rat enamel from secretory through to the maturation stage and pig secretory enamel. The blue stained bands migrating below 25KDa are attributable to amelogenins. The corresponding western blots (bottom panels), probed with anti-enamelin antibody show higher molecular weight enamel bands in the rat enamel samples. These bands migrate at around 70 kDa. In contrast, the pig secretory enamel contains a prominent enamel band migrating at 32 kDa (marked *). The results indicate that rat amelogenesis does not involve the generation of a predominant 32 KDa enamel molecule.

3.3.2 The effect of continued proteolytic processing on the enamelin proteome in secretory stage rat enamel

The results described above indicated that rat amelogenesis proceeds in the absence of a discrete 32 kDa processing product. To investigate whether the rat enamel matrix proteolytic enzymes could cleave rat enamelin with time to generate a 32 kDa enamelin homologue, rat secretory stage enamel was incubated *in vitro* for varying lengths of time. Secretory stage enamel from a rat incisor was removed and crushed in 10% acetic acid. An aliquot was taken at time = 0, and the remaining enamel placed into a 37°C incubator. Further aliquots were taken at 4, 8, 16 and 32 hours to investigate the proteolytic breakdown of the enamelin protein over time by the endogenous proteases in the enamel matrix. Figure 52 shows a Coomassie stained gel of these aliquots. The predominant bands are below 25 kDa, corresponding to the amelogenins as shown by the corresponding western blot. There was an obvious loss of full length parent amelogenin as it is degraded with time to lower molecular weight processing products.

A corresponding western blot probed with anti-enamelin antibody showed that the enamelin proteins shifted to a slightly lower molecular weight with time consistent with limited proteolytic processing but again no 32 kDa enamelin was generated.

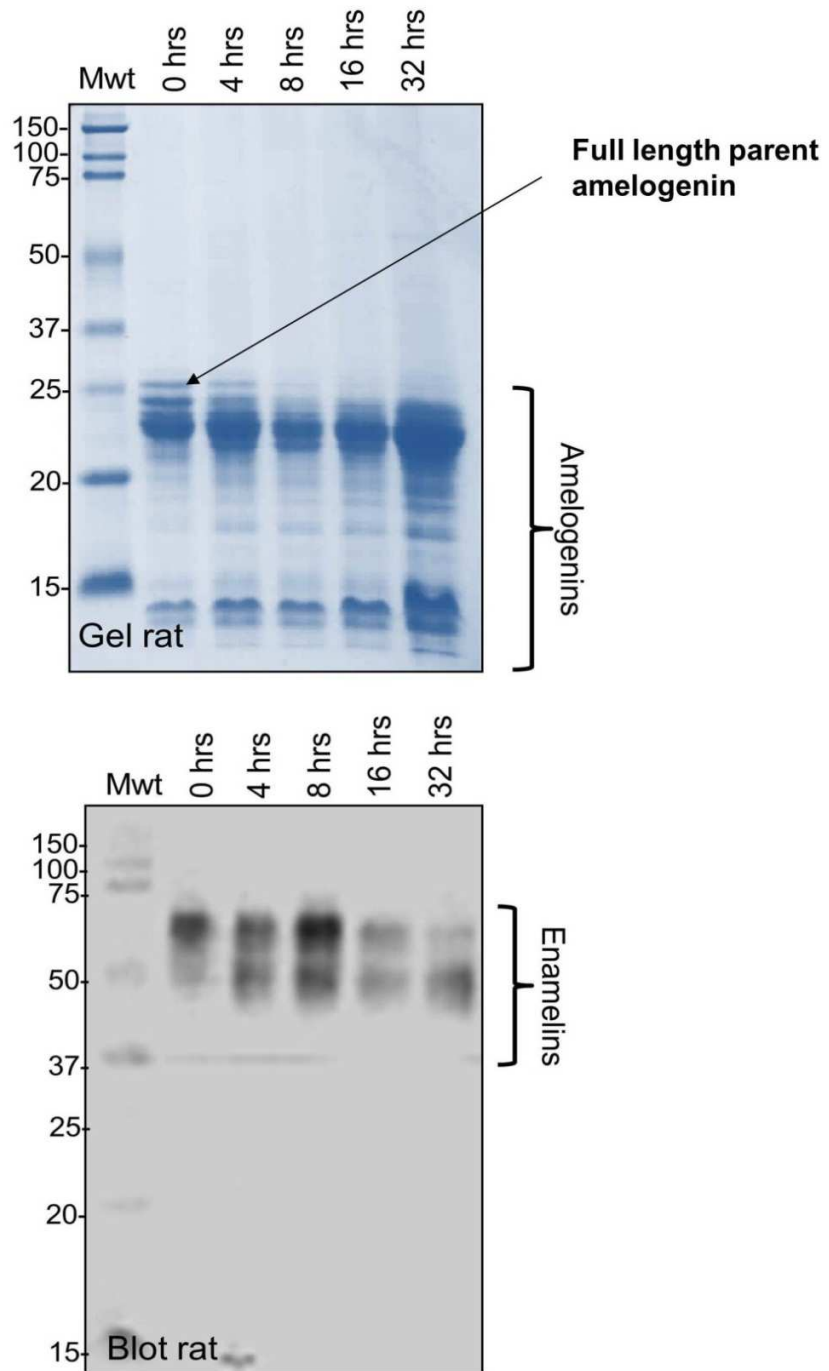


Figure 52. SDS PAGE and enamel Western blot using anti-enamelin antibodies of rat secretory stage enamel matrix allowed to degrade over a period of 32 hours. Enamelin components shift to a lower molecular weight but no obvious 32 kDa species is generated.

3.3.3 Bioinformatics analysis of enamelin protein sequences across multiple species

The data presented above strongly suggested that rat amelogenesis, unlike pig amelogenesis, does not involve the generation of a 32 kDa enamelin molecule. To investigate possible reasons for this, bioinformatics databases were scrutinised and the homology of the cleavage sites responsible for generating the pig 32 kDa enamelin component were identified and compared to the homologous site in other species.

Figures 53 and 54 show the N-terminus cleavage site and C-terminus cleavage site responsible for generating the 32 kDa enamelin in pig (Yamakoshi et al., 2006). In descending order, the homologous sequences for human, mouse, rat, chimpanzee, dog and guinea pig are shown. A full comparison of the enamelin sequences for 295 species is shown in Appendix 2 but this limited data below set illustrates the point that the combination of both cleavage sites responsible for generating the N and C-terminals of the 32 KDa enamelin in pig (as indicated by the blue line cutting between the amino acids P-L and R-S respectively) are absent in all other species. It appears therefore that the generation of the 32 KDa enamelin in pig amelogenesis may be unique as other species do not exhibit the specific cleavage sites present in pig that are responsible for the generation of the 32 KDa enamelin.

154	TQTPQAFPPFGNGLFPYQQP	LWHVPHRIP-PGYGRPPTSNEEGNPNYFGFFGYHGFGGRP	212	PIG
153	AQPPQAFPPFGNGLFPYQQP	PWQIPQRLPPPGRPPISNEEGNPNYFGYFGYHGFGGRP	212	HUMAN
158	AQPPQFPFPFGNGLYPYQP	PWPQPGRPPTAFGRPKFSNEE-GNPYYAFFGYHGFGGRP	216	MOUSE
228	AQPPQFPFPFGNGLYPYQQP	PWPQPQTGPPTGFGRPKFSNEE-GNPYYAYFGYHGFGGRP	286	RAT
153	AQPPQAFPPFGNGLFPYQQP	PWQIPQRLPPPGRPPMSNEEGNPNYFGYFGYHGFGGRP	212	CHIMP
155	GQPPQAFPPFGNGLFLYQQP	PWQVPHRVP-PGYGRPPASNEEGNPNYFGYFGYQGFGRP	213	DOG
155	AQPPQFPFPFNGLFPYQQP	PWPQPGRMPPPGYGRPPLSNEDGNPNYFGFFGYPGFGGRP	214	GUINEA PIG

Figure 53. Bioinformatics analysis of the amino acid sequences around the cleavage sites for generating the N terminus sequence cleavage site of enamelin (shown by blue line).

264	NDTSPGTGTSQGPNPR	SNPTGQNGP----AVNVSGQGVPRSQSPWGRQTIHENYPNPN	319	PIG
265	NDTSPGTGNSTPGLNTG	NNPPAQNGIGPLPAVNASGQGGPGSQIPWRPSQPNIRENHPYPN	324	HUMAN
269	NDTSPIGNTGPGPNAG	NNPTVQNGVFPPPKVNVSGQGVPKSQIPWRPSQPNIYENYPYPN	328	MOUSE
342	NDS SPVGN TGPGPNAG	NNPTVLNGVFPLPKVNVSGQGVPKNQIPWRPSQPNIYENYPYPN	401	RAT
265	NDTSPGTGNSTPGLNTG	NNPPAQNGIGPLPAVNASGQGGPGSQIPWRPSQPNIRENHPYPN	324	CHIMP
266	NDTSPGTGNSGPGPNTV	SNPTAQNGVISPATVNVISGQGVPRSQISWGPNQPNIHENYPNPN	325	DOG
262	NDTGPTLNSIPGLNTG	NNPTVQNGIFPLPTVNFSGQVIPGSQIPWKPQPNIIYGSYPKPN	321	GUINEA PIG

Figure 54. Bioinformatics analysis of the amino acid sequences around the cleavage sites responsible for generating the N C terminals of the 32 kDa enamelin in pig. The relevant cleavage sites in pig appear to be unique and are not shared by other species.

3.4 Recombinant wild type and Y64H mutant amelogenin protein binding/aggregation studies

In *vitro* experiments were performed to determine whether the Y64H mutation in recombinant amelogenin affected its aggregative properties (the basis of nanosphere formation). Wild type and Y64H mutant recombinant amelogenin proteins were used to coat 96-well microtitre plates and act as a 'bait' to capture wild type or Y64H mutant recombinant amelogenin proteins, labelled with the fluorescent tag fluorescein (FITC). BSA bait protein was used as a control to examine non-specific amelogenin binding. The level of binding interaction (i.e. aggregation) was assessed by reading the fluorescence.

3.4.1 Adsorption and blocking of recombinant amelogenin proteins to microtitre plates

Binding experiments were performed by adsorbing a bait protein of interest (unlabelled amelogenin or BSA) onto microtitre plate wells. Any remaining exposed well surface was blocked with a blocking protein and then the binding partner (labelled amelogenin) added (section 2.3). Blocking was essential to prevent the labelled amelogenin simply adsorbing to the wells and giving a false positive result. It was equally important that the binding partner did not bind to the blocking protein. Several different blocking solutions were initially investigated with 1% BSA in TBS proving to be the most suitable (data not shown).

3.4.2 FITC-labelled protein binding

Following bait protein adsorption, the wells were aspirated, washed and blocked. FITC labelled binding partner (either labelled wild type or labelled Y64H mutant recombinant amelogenin) was then added and allowed to bind to the bait protein. The wells were aspirated and washed to remove unbound FITC labelled protein and the degree of binding determined by reading the fluorescence on a fluorimeter.

The results are shown in figure 55. Reading left to right the first column shows the fluorescence associated with FITC labelled wild type recombinant amelogenin binding with unlabelled wild type recombinant amelogenin bait initially bound to the well (WT-WT). The second column shows the fluorescence associated with FITC labelled Y64H mutant recombinant amelogenin binding with unlabelled wild type recombinant amelogenin bait initially bound to the well (WT-MUT). From this data it was clear that the Y64H mutant recombinant amelogenin apparently showed a greater binding affinity (approximately 3 times greater) to wild type recombinant amelogenin than wild type recombinant amelogenin did to itself. The next two columns show the fluorescence associated with FITC labelled wild type recombinant amelogenin binding with unlabelled Y64H mutant recombinant amelogenin bait initially bound to the well (MUT-WT) and the fluorescence associated with FITC labelled Y64H mutant recombinant amelogenin binding with unlabelled Y64H mutant recombinant amelogenin bait initially bound to the well (MUT-MUT). From this data it was clear that the Y64H mutant recombinant amelogenin apparently showed a greater binding affinity (approximately 3 times greater) to Y64H mutant recombinant amelogenin than wild type recombinant amelogenin does. Binding of either FITC labelled wild type or Y64H mutant recombinant amelogenin to the BSA bait showed no fluorescence, indicating that binding of either amelogenin type to BSA did not occur; this indicated that specific amelogenin-amelogenin interactions were being detected. Interestingly, the interaction shown in column 3 (between FITC-Y64H mutant recombinant amelogenin to unlabelled wild type recombinant amelogenin bait (MUT-WT)) was much less than FITC-wild type recombinant amelogenin to unlabelled Y64H mutant recombinant amelogenin (WT-MUT shown in column 2). Both columns represent interactions between wild type and mutant proteins; the difference being in which protein (wild type or Y64H mutant) that was initially bound to the well to act as bait protein. When Y64H mutant amelogenin acted as bait, the resulting binding was reduced compared to the results obtained when wild type amelogenin acted as the bait.

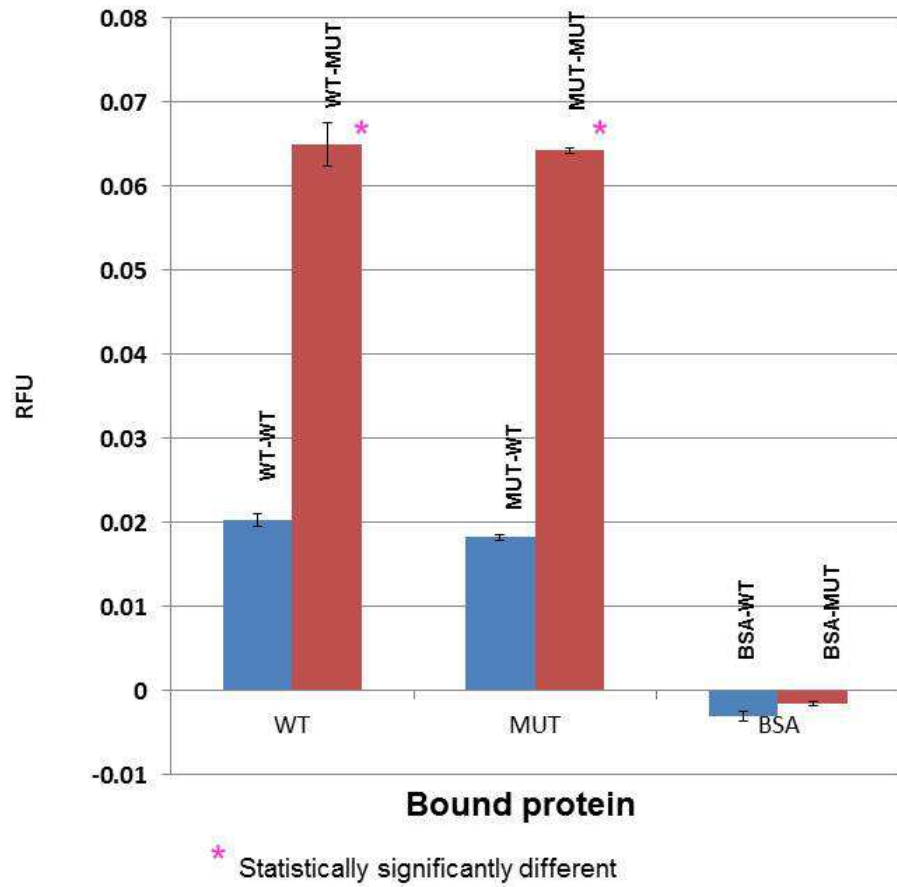


Figure 55. Results of FITC binding experiments showing 100 µg/mL of unlabelled wild type amelogenin, Y64H mutant amelogenin or BSA bound to a 96-well microtitre plate and interrogated with 100 µg/mL of either wild type or mutant FITC-labelled amelogenin. N = 6. Standard deviation error bars are shown

3.5 Q-RT-PCR of ER stress genes and amelogenin in wild type and Y64H mutant mice incisors

3.5.1 Comparison of the expression of ER stress genes in enamel organs of wild type and Y64H mutant amelogenin mice.

Immunocytochemical investigation of ameloblasts expressing the Y64H mutant amelogenin (carried out by Dr Martin Barron, University of Manchester) revealed the presence of abnormal vesicles packed with amelogenin protein. Figure 71 (Discussion section 4.7) shows a typical TEM image of affected ameloblasts including following probing with anti-amelogenin antibodies. This abnormal retention of protein in the ER can lead to the phenomenon of ER stress which raised the possibility that the mechanism underpinning amelogenesis imperfecta in the Y64H mutant mice was based on cellular ER stress rather than functional failure of mutant amelogenin in the extracellular enamel matrix. To investigate this radical hypothesis further q-RT-PCR was used to determine levels of amelogenin and proteins known to be expressed by cells attempting to combat ER stress in wild type and Y64H mutant mouse incisor enamel organs.

3.5.2 RNA extraction from mice enamel organs

Mice expressing the Y64H amelogenin mutation were bred by our Wellcome Trust collaborators at the University of Manchester (Materials and Methods Section 2.5). The mandibular incisors from five male animals carrying the Y64H amelogenin mutation and four male animals carrying wild type amelogenin were extracted. Each tooth was treated as a separate entity. The enamel organ was dissected from the incisors and the RNA extracted as described in Section 2.5.2.

Figure 56 shows an image of an agarose gel of the RNA extracted from two wild-type and two mutant mice incisors. The 28S and 18S subunits were visible indicating successful RNA extraction.

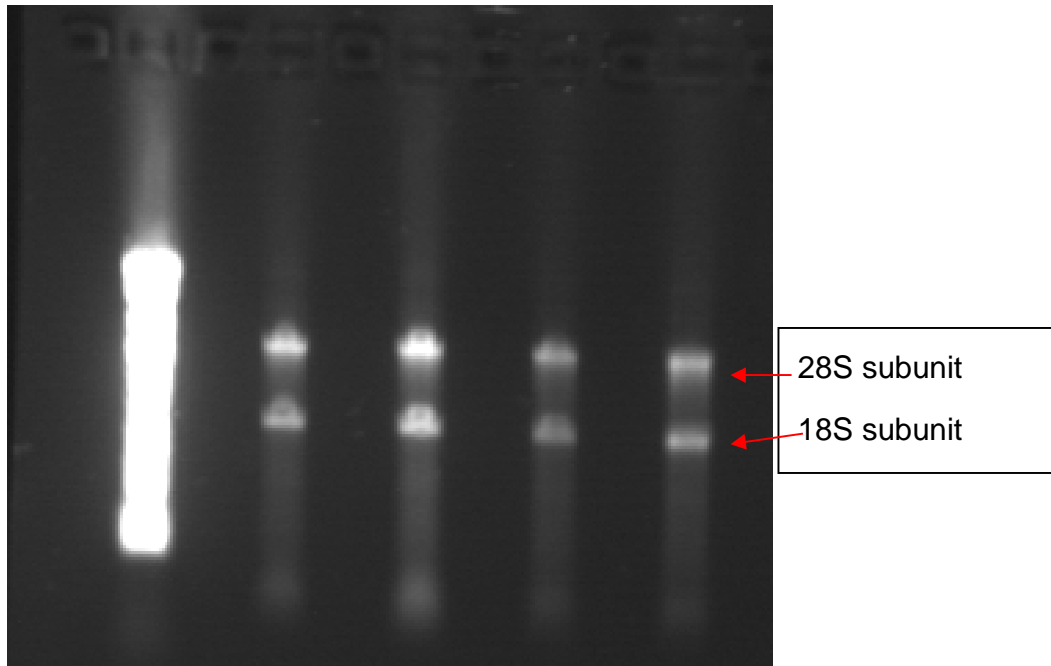


Figure 56. Image of an agarose gel of the extracted mouse tooth RNA. RNA markers are shown on the left, then the RNA for two wild-type mouse incisor enamel organs and then the RNA for two mutant mouse incisors.

This RNA was treated to remove any genomic DNA contamination and transcribed into cDNA using a commercially available kit as per Section 2.5.4. Figure 57 shows an image of an agarose gel for the cDNA created using the extracted RNA using reverse transcription PCR (RT-PCR) for two wild type and two Y64H mutant extracted enamel organs.

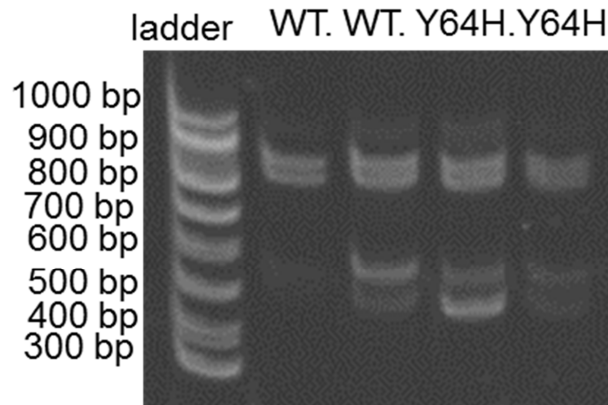


Figure 57. Image of an agarose gel showing the cDNA PCR product achieved after performing RT-PCR on the RNA extracted from mice enamel organs using the Phire Hot-Start PCR kit from New England Biotech. Full-length amelogenin product at 540bp can be seen for both the wild type and Y64H mutant amelogenin cDNA.

3.5.3 Quantitative real time PCR of the transcribed cDNA

cDNA obtained as described above was used as the template for quantitative real time PCR (q-RT-PCR) analysis. Primers for the amelogenin gene (*Amelx*), marker genes for ER stress proteins (*Bip*, *Grp94*, *chop*, *Xbp1*) and a housekeeping gene (*Gapdh*) were used determine the effects of the Y64H mutation on gene expression of amelogenin and proteins associated with ER stress. Following DNA amplification, each gene was expected to produce DNA of a particular size, known as an amplicon. This is shown in figures 57 and 58 after horizontal agarose gel electrophoresis of the q-RT-PCR products (amplicons) and the differences in molecular weights (base pairs). Figure 58 is a representative gel for a wild-type mouse enamel organ and figure 59 is a representative gel for a Y64H mutant mouse enamel organ. Figure 60 shows the amplicons for *Amelx* across all the mice enamel organs, both mutant and wild type, investigated.

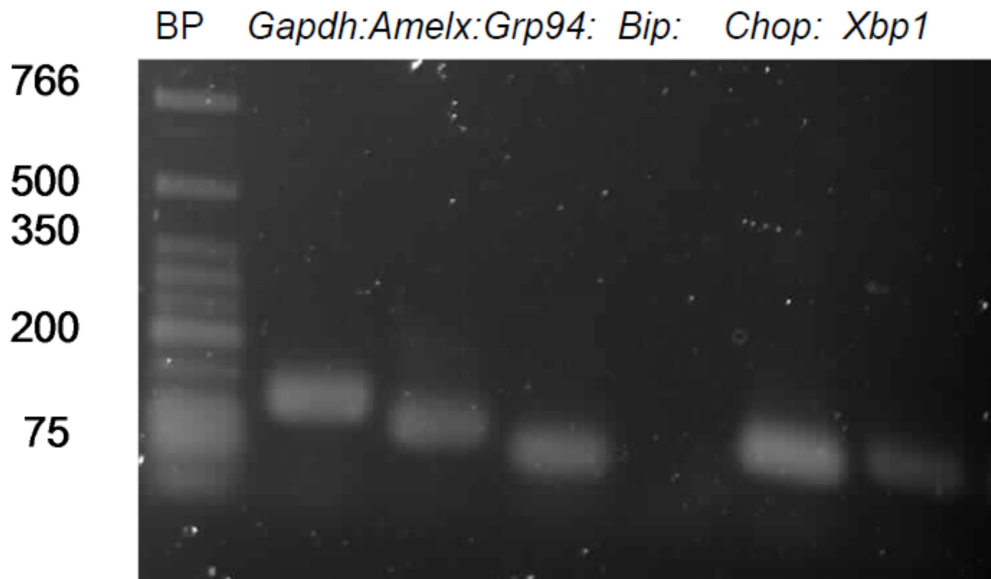


Figure 58. Horizontal gel electrophoresis of q-RT-PCR amplicons from Wild-type amelogenin mice incisors enamel organs. BP= base pairs for the New England Biolabs low molecular weight DNA ladder.

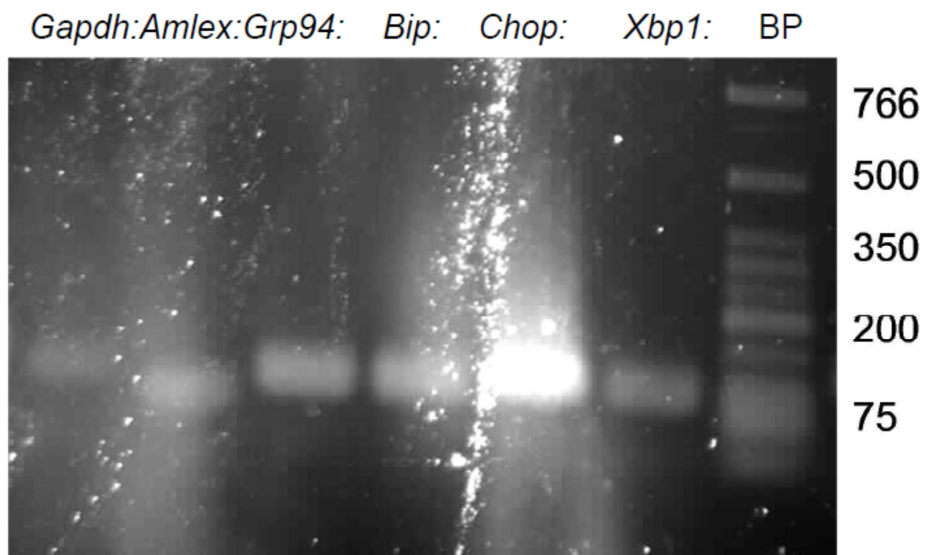


Figure 59. Horizontal gel electrophoresis of q-RT-PCR amplicons from Y64H amelogenin mice incisors enamel organs. BP= base pairs for the New England Biolabs low molecular weight DNA ladder.

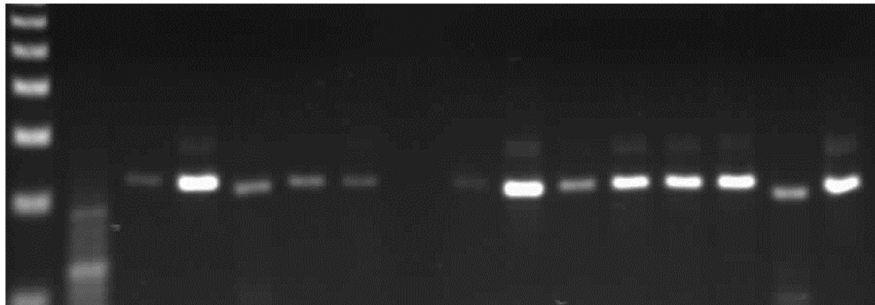


Figure 60. Agarose gel stained with Biotium Gel-red stain and viewed under UV light on GelDoc, showing RT-PCR product for extracted RNA with amelogenin forward and reverse primers.

Standard curves were performed for each gene using a dilution series of cDNA. A linear response is required to show efficiency of amplification. Figure 61 shows a standard curve for GAPDH housekeeping control gene, as generated by the Lightcycler 4800.

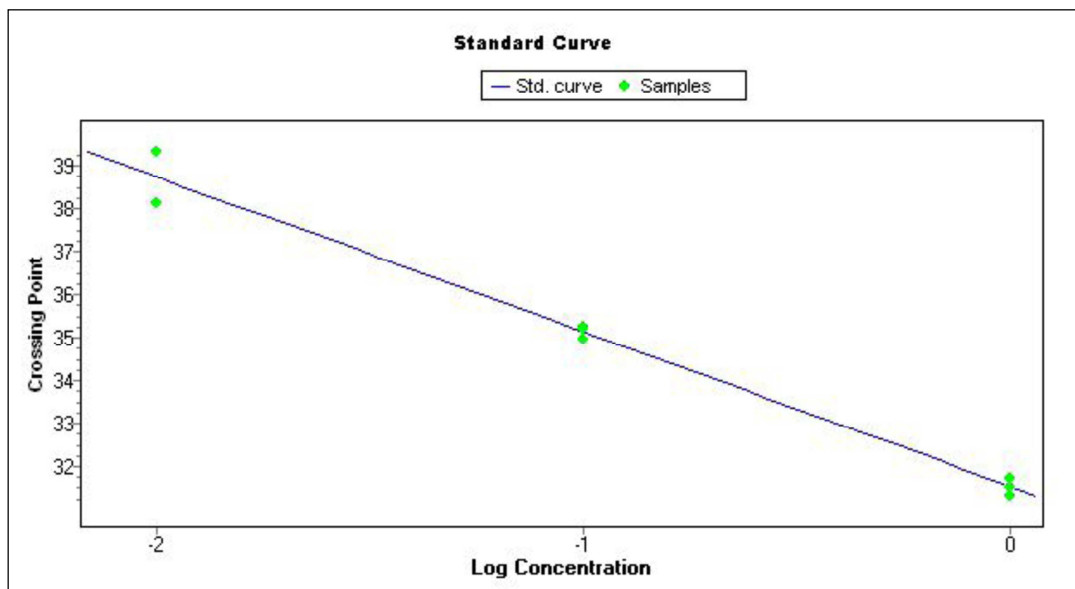


Figure 61. Standard curve for *Gapdh* control. This curve is typical of the data obtained from the Light Cycler 4800 (see appendix for an example of the data obtained). The curve has an efficiency of 1.892 (expected value is approximately 2), a slope of -3.610, a Y Intercept of 31.52, with an error of 0.0203.

Standard curves were run for each gene of interest and with each cDNA sample, using a 1 in 10 dilution range. Plotting the log of concentration against the CP values resulted in a linear fit comparable to the Gapdh control in figure 61.

Figure 62 shows the amplification curves for *Gapdh* extracted from mice enamel organs containing wild type *Amelx*. This is a typical example of the amplification curves obtained throughout the study. The cycle number at which the amplification increases is known as the crossing point or CP. This is the point at which the levels rise above background/threshold. The graph show that the negative controls (concentration 0) stay at threshold. A representative q-RT-PCR report from the Lightcycler is shown in Appendix 3.

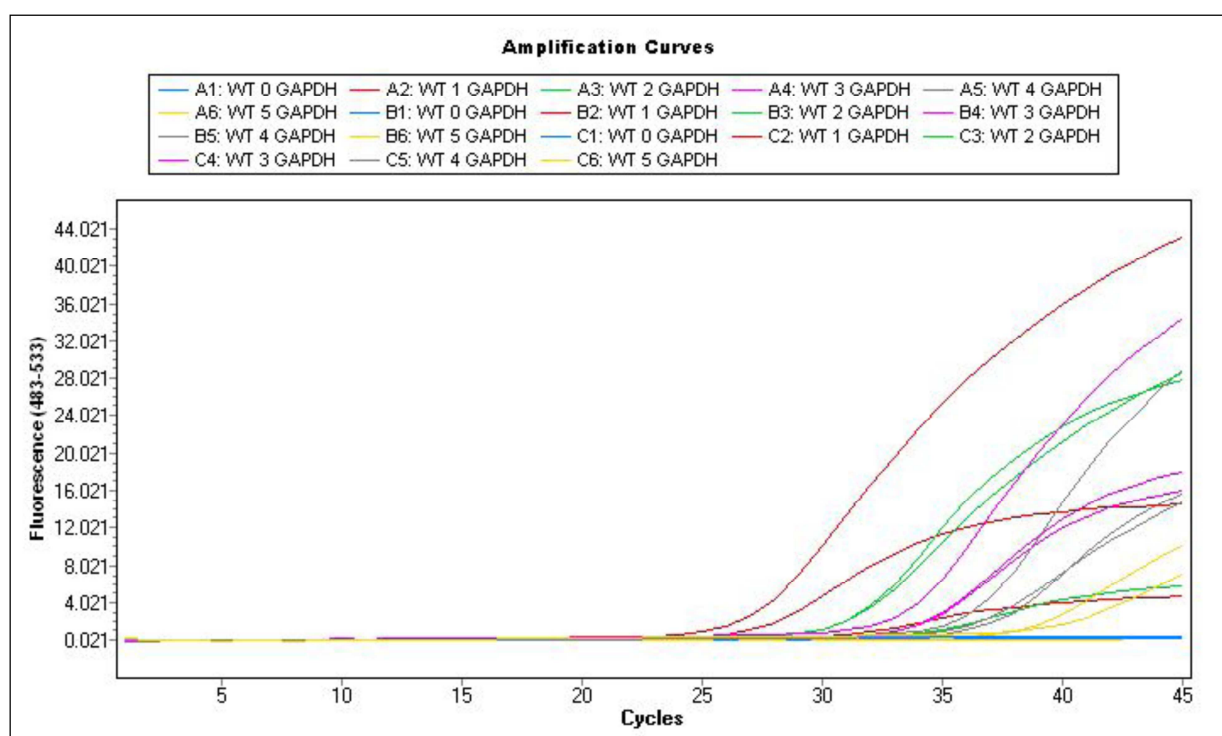


Figure 62. Typical graph generated by the LightCycler 4800 to show the CP values and amplification of samples. In this case, cDNA transcribed from mice carrying wild type *Amelx* is amplified for *Gapdh*.

Table 1 Shows the CT values for all 11 Y64H amelogenin mutant mice enamel organs and the 6 genes investigated. Where no data is shown, no data was generated. Figures 62 shows representative fold changes in gene expression for each individual Y64H mutant amelogenin mouse enamel organs for each of the 6 genes.

Table 1. CT values for all Mutant (M) and wild-type (WT) AMELX mice incisors for 6 genes. N/D = not detected.

	<i>Gapdh</i>	<i>Amelx</i>	<i>Grp94</i>	<i>Bip</i>	<i>Chop</i>	<i>Xbp1</i>
1A M	35.16	29.31	33.86	34.37	40.00	34.77
1B M	34.20	27.72	33.50	33.53	40.00	35.19
2A M	33.59	27.48	34.49	34.93	40.00	35.19
2B M	32.75	25.84	31.06	32.71	25.88	33.62
3A M	34.07	28.87	33.83	35.75	40.00	39.20
4B M	33.14	28.63	33.38	34.25	40.00	35.25
5A WT	35.81	29.49	35.35	36.88	40.00	39.78
5B WT	31.81	23.29	30.93	32.73	40.00	32.63
6A WT	34.62	28.59	34.01	35.34	N/D	36.01
6B WT	31.78	24.22	31.75	32.94	39.51	33.20
7A M	33.93	27.16	33.97	34.53	40.00	33.69
7B M	32.87	24.56	33.68	33.40	40.00	35.65
8A WT	32.17	25.00	31.65	33.74	40.00	33.39
8B WT	38.59	30.46	36.05	37.58	40.00	35.49
33A WT	34.48	26.81	32.60	34.19	40.00	35.93
33B WT	32.38	24.92	33.19	33.04	40.00	34.90
34A M	36.39	30.35	31.07	35.87	40.00	39.68
34B M	34.73	28.05	36.00	36.22	39.27	32.13

Figure 63 shows a graph representing the crossing point data for all the mice incisor enamel organs examined with the panel of 6 genes, represented as a fold difference compared to *Gapdh* housekeeping control. Each gene is the mean of 11 replicates. From this data it is clear to see that *Amelx* is statistically significantly down-regulated in Y64H mutant mice enamel organs, while *Chop* is statistically significantly up-regulated.

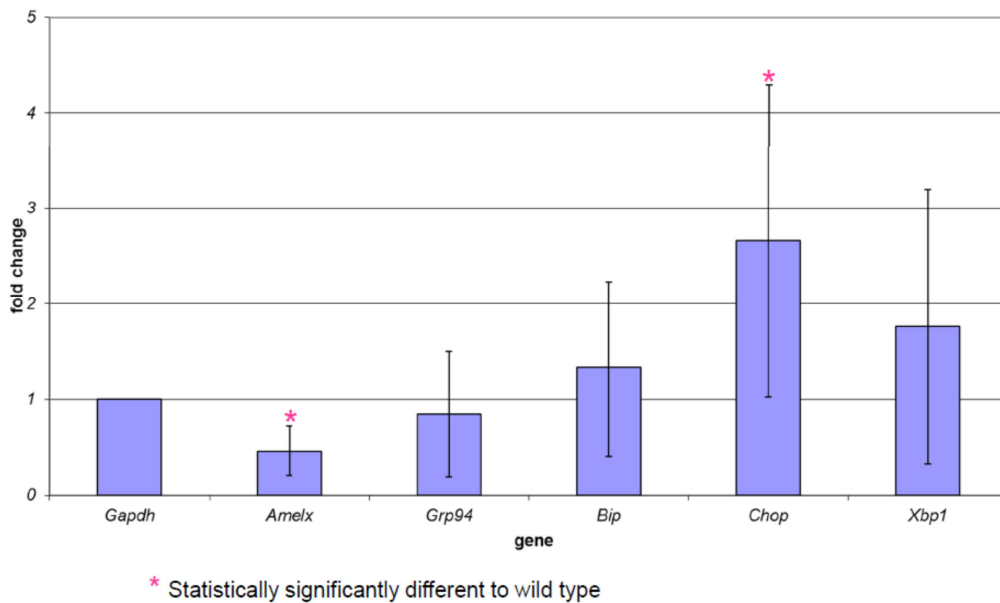


Figure 63. Overall fold change ($\Delta\Delta CT$) for Y64H mutant amelogenin enamel organs compared to wild type amelogenin enamel organs (n=10) Grubbs outlier test applied. Student's two-tailed T test applied to determine upregulation and down-regulation to *gapdh* housekeeping control.

Several statistical methods were employed to investigate any upregulation or downregulation of the CT levels of the genes of interest, comparing gene expression in the enamel organs of wild type mice and mice carrying the Y64H amelogenin mutation. Non-parametric analysis was performed using SPSS (IBM) software. The student 2-tailed T test performed on the $\Delta\Delta CT$ values (Y64H amelogenin mutant compared to wild type) showed that *Amelx* was statistically significantly down-regulated in the Y64H amelogenin mutant enamel organs and *Chop* statistically significantly up-regulated in the Y64 amelogenin mutant enamel organs ($p < 0.05$ in both cases). However, the *Chop* data should be viewed with caution as the difference observed is accounted for by the results obtained from a particular sample which skewed the mean values (sample 2BM, table 1). In general *Chop* was at very low levels in most samples as evidenced by the CT value of 40 obtained.

In summary, the q-RT-PCR data showed that amelogenin expression was significantly down regulated in Y64H mutant amelogenin ameloblasts. Down regulation of general protein synthesis is a classical UPR survival response. *Chop* (a marker for

apoptosis) was also significantly upregulated although the reliability of this data is questionable as this result is based on a single sample exhibiting a high expression of *chop*.

3.6 SEM analysis of Y64H mutant amelogenin mouse incisors

In an attempt to better understand the mechanism by which the Y64H mutation affects amelogenesis, the micro-ultrastructure of the resulting affected mature enamel was investigated using SEM.

Wild type female mouse incisors, Y64H mutant amelogenin heterozygous female mouse incisors and male Y64H mutant amelogenin homozygous mouse incisors were prepared as described in Chapter 2 section 2.6 and imaged using a Hitachi S3400N scanning electron microscope using backscatter mode.

Figure 64 shows a typical wild type female mouse incisor in transverse section. The characteristic decussating interlocking weave pattern of the enamel prisms emanating from the dentine layer is clear. Figure 65 shows a higher magnification of the enamel layer, displaying the ordered disposition of the enamel prisms.

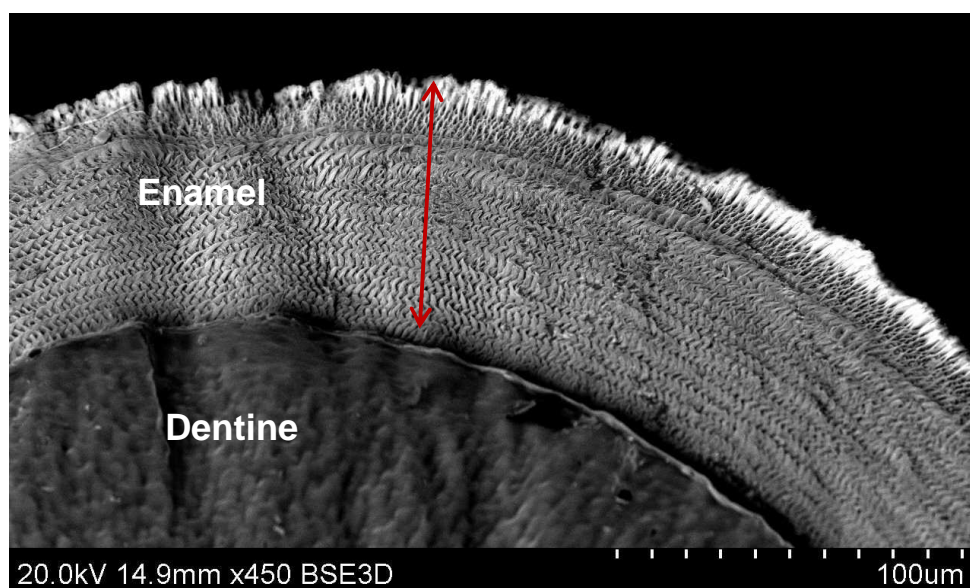


Figure 64. SEM image of a female wild type mouse incisor imaged at 450 times magnification. The decussating interlocking weave pattern of the enamel prisms emanating from the dentine layer is clear. The enamel layer is even in thickness at approximately 75 microns (shown with red arrow).

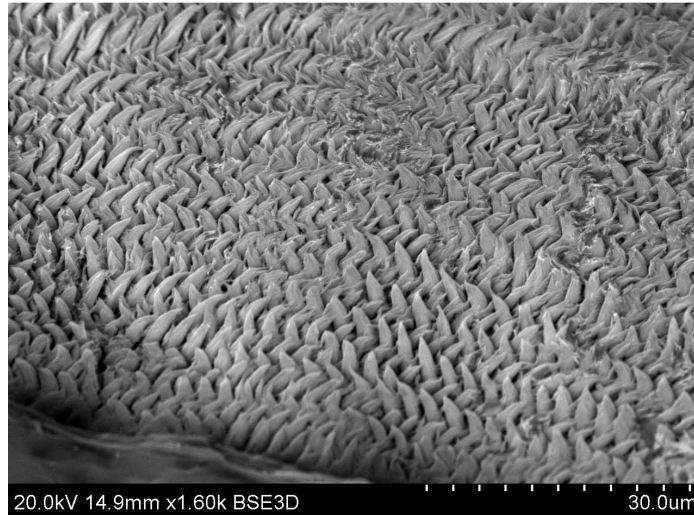


Figure 65. Higher magnification SEM image of the wild type female mouse incisor enamel layer shown in figure 63. The decussating interlocking weave pattern of the enamel prisms emanating from the dentine layer is clear.

Figure 66 shows a typical SEM image of a female mouse incisor that is heterozygous for the Y64H amelogenin mutation in transverse section. The characteristic decussating interlocking weave pattern of the prisms is evident in the inner enamel adjacent the dentine. However, in contrast to wild type enamel, the ordered enamel structure is disturbed in the mature outer enamel tissue layer.

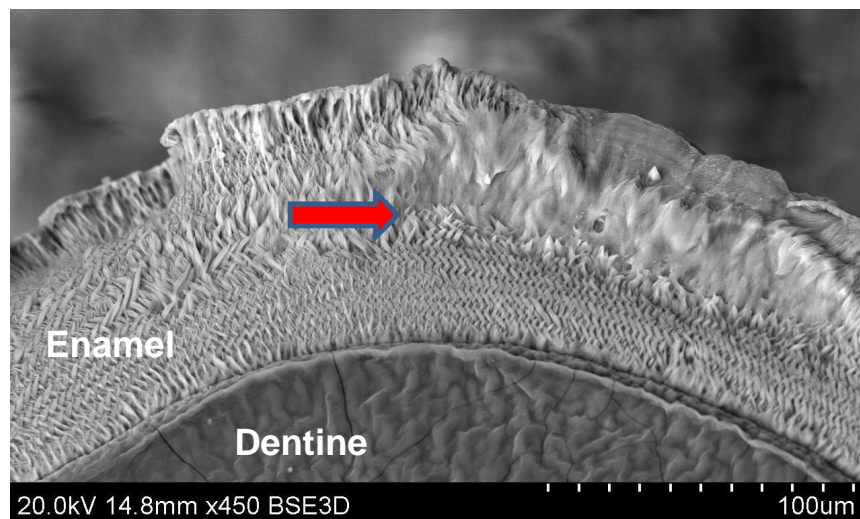


Figure 66. SEM image of a section through an erupted mouse incisor of a female animal heterozygous for the Y64H amelogenin mutation. Imaged at 450 times magnification. The decussating interlocking weave pattern of the enamel prisms emanating from the dentine layer is clear in the inner enamel, but is lost in the outer enamel layer, shown by the red arrow.

Figure 67 shows a higher magnification of enamel layer of the section through the incisor from the female mouse heterozygous for the Y64H amelogenin mutation with the loss of enamel structure clearly visible at the interface between the normal inner enamel and structurally abnormal outer enamel layer.

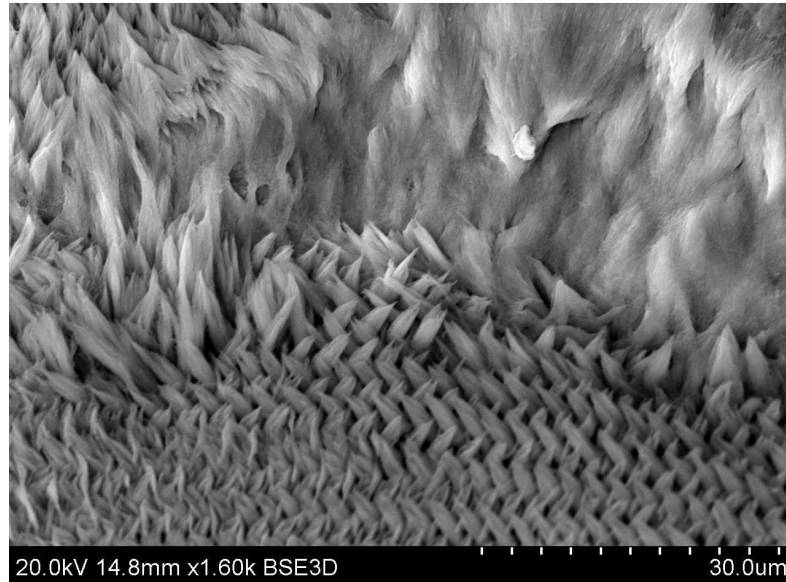


Figure 67. Higher magnification SEM image of the section through the incisor from the Y64H mutant amelogenin heterozygous female mouse incisor enamel layer shown in figure 65. Note the interface between the normal decussating interlocking weave pattern of the enamel prisms and the abnormal outer enamel layer.

Figure 68 shows the outer edge of the enamel layer of the section through the mouse incisor from a female mouse heterozygous for the Y64H mutant amelogenin where pieces of enamel at the outer edge are absent suggesting that the outer abnormal enamel is mechanically inferior to the underlying enamel and has sheared off in the mouth has retained a normal structure. However, it is also possible that the enamel was missing prior to eruption i.e. the enamel was never present to begin with.

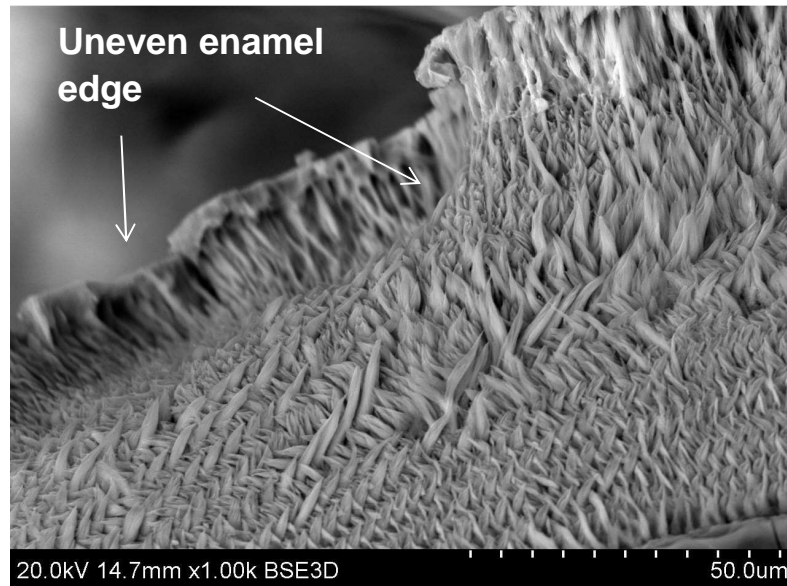


Figure 68. SEM image of a section through an incisor from a Y64H mutant amelogenin heterozygous female mouse. This image shows the pieces of the outer enamel structure have broken away leaving an uneven edge (shown with white arrows) suggesting the abnormal enamel is mechanically compromised during mastication.

Figure 69 shows a SEM image of a section through an incisor from a male mouse homozygous with respect to the Y64H amelogenin mutation, imaged at 450 times magnification. The mature enamel layer is thin, at approximately 30 microns or less, and lacks the characteristic decussating prism structure. Figure 70 shows a higher magnification of the enamel layer, clearly showing that the normal prism structure is missing.

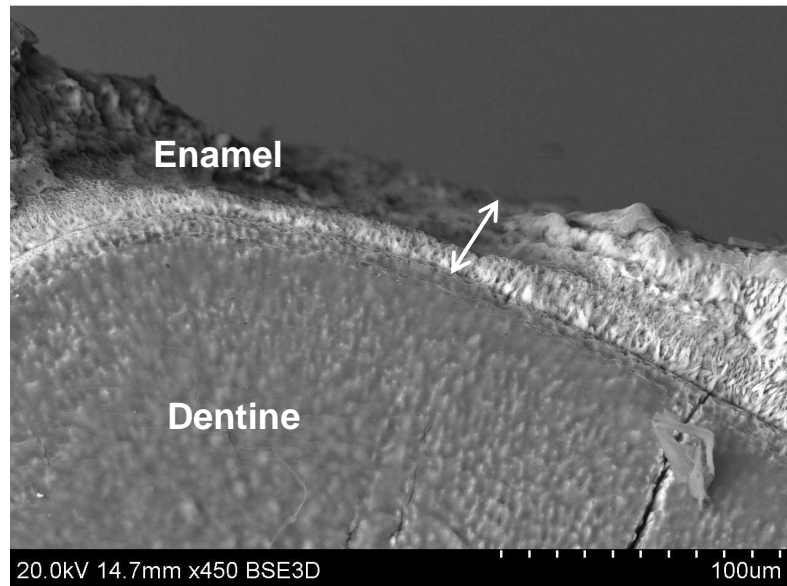


Figure 69. SEM image of a section through an incisor from a Y64H mutant amelogenin homozygous male mouse imaged at 450 times magnification. The enamel layer (thickness shown with white arrows) is shown above the darker dentine layer, but the characteristic prism structure is not visible.

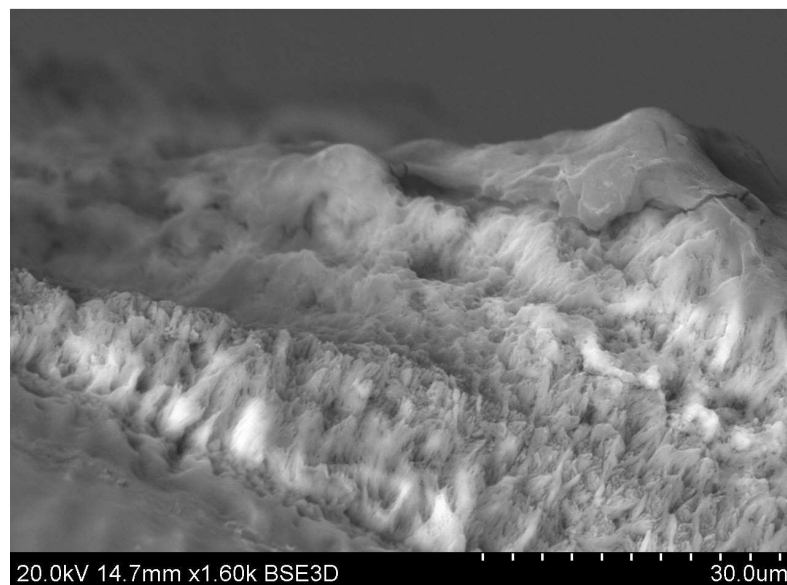


Figure 70. SEM image (times 1600 magnification) of the enamel layer for the male homozygous Y64H amelogenin mutant mouse incisor. The characteristic prism structure is not visible.

In summary, the SEM analysis revealed that heterozygous female mice carrying the Y64H mutation appeared to secrete an initial enamel layer that was normal in appearance. However, with time, the ability of the ameloblasts to secrete a visually normal enamel layer was lost and the final outer enamel layer secreted was structurally abnormal. In contrast, the ameloblasts in affected male mice were only able to secrete a thin enamel layer that was devoid of normal structure.

Chapter 4

General discussion

This chapter will discuss the results presented in the previous chapter, and how these results fit with and expand our current understanding of the processes involved in amelogenesis.

The research presented in this thesis was undertaken as part of a larger multicentre research program and the discussion will explain how the research presented here contributed to the overall project outcomes. It is difficult to discuss the results presented here without reference to the work of other members of the research group and particular attention will be paid to acknowledging the work of others where it is included in order to better contextualise the results presented in this thesis.

The overall aim of the larger research project was to use amelogenesis as a paradigm for biomineralisation. A major focus of the research was to understand the role of amelogenin in amelogenesis by studying the effects of an amelogenin mutation in mice that resulted in an obvious biomineralisation defect. Initially, the hypothesis was that any amelogenin mutation would disrupt amelogenin function in terms of mineral nucleation/crystal growth including how any protein-protein interactions may be affected, potentially allowing the affected amelogenin domain to be linked to a specific function. To this end, the effect of the Y64H mutation on the ability of amelogenin to nucleate mineral *de novo* and *in vitro* was investigated using recombinant wild type and mutated amelogenin in isolation or in combination with the 32 kDa enamelin (previously reported to cooperatively enhance the nucleation potential of amelogenin (Bouropoulos and Moradian-Oldak, 2004)). An unexpected outcome of this work was the realisation that the 32 kDa enamelin used almost exclusively for enamelin biochemical and functional studies worldwide may be unique to pig amelogenesis and not play as large a role in amelogenesis in other species as previously thought. During the course of the research it became clear that the Y64H amelogenin was actually blocking the intracellular secretory pathway in ameloblasts and that ER stress driven ameloblast apoptosis was a major factor in the disease mechanism operating in affected mice. This section discusses the existing literature and how the present results relate to these previous studies and also develops hypothesis to be tested in future studies. The thesis map in

the aims and objectives section provides a summary to the content and structure of the Discussion.

4.1 Effect of the Y64H mutation on the nucleating potential of amelogenin

This effect of the Y64H mutation on the nucleation potential of amelogenin in the presence and absence of 32 kDa enamel was investigated using a steady-state agarose gel based *in vitro* nucleation system. The interpretation of data in this area is difficult to appraise due to the fact that the same protein can exhibit opposite behaviors (i.e. promote nucleation or inhibit nucleation) depending on the experimental conditions used. The situation was best summed by Hunter et al 1996 who in their Discussion section admitted that:

“...the diversity of experimental systems used [to study promotion/inhibition of nucleation] makes any overall conclusions very difficult to find.”

That aside, it is clear that certain biochemical features are associated with proteins thought to control skeletal biomineralisation. The steady-state agarose gel system was first used by Hunter and Goldberg in 1993 to investigate the nucleation of hydroxyapatite by bone sialoprotein (BSP) and later extended to other proteins which at least allows comparisons to be made against a fixed experimental baseline.

BSP is a major phosphorylated protein in mammalian bone and has been proposed to have a role in mineral initialisation (Hunter and Goldberg, 1993). Mature BSP is a 33 kDa protein and is predominantly made up of glutamic acid and glycine residues (32% of all residues). The glutamic acid residues occur in clusters of up to 10 consecutive repeats. BSP is highly acidic (pKa approximately 3.9) and contains no α helices or β sheet, or structural domains. BSP has extensive post-translational modifications amounting to approximately 50% of the native protein. Tye et al., (2003) used the steady state agarose gel system to identify which regions of BSP are required for hydroxyapatite nucleation. The conformation of the wild type and mutant proteins were studied by circular dichroism and X-ray scattering which revealed that a sequence of at least 8 contiguous glutamic acid residues are required for the nucleation of hydroxyapatite by BSP. Hunter and Goldberg drew the conclusion that polycarboxylate

sequences (i.e. glutamate and aspartate) represent a general site for growth modulating interactions between proteins and biological crystals. The carboxyl groups that terminate the side chains of both glutamate and aspartate are negatively charged (see figure 71 below) at physiological pH and when linked by peptide bonds into long chains (as they appear in BSP) can provide a negatively charged array that could potentially bind calcium ions through ionic interactions in a suitable stereochemical arrangement to trigger mineral nucleation.

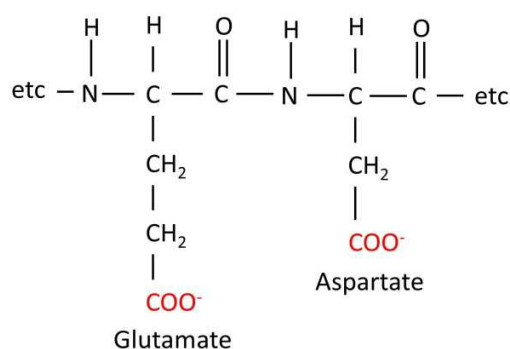


Figure 71. Structure of glutamate and aspartate polycarboxylate sequence

Like BSP, dentine phosphoprotein was found to promote nucleation in the agarose gel system (though less potently) (Hunter et al 1996). Dentine phosphoprotein is extremely acidic due to its very high content of polyaspartic acid residues (Richie and Wang, 1996), again supporting the notion that polycarboxylic acids are a feature of nucleating proteins.

However, it is clear that the presence of polycarboxylic acids *per se* is not enough to give a protein nucleating potential. The acidic phosphorylated bone protein osteopontin is a phosphorylated sialoprotein similar to BSP but in contrast exhibits domains of polyaspartic acid rather than polyglutamic acid. Although these amino acids are structurally and chemically similar, osteopontin proved to be a potent inhibitor of mineral nucleation in the agarose gel system (Hunter et al 1996). Desphosphorylation and chemical modification of osteopontin showed that the ability of osteopontin to inhibit nucleation required phosphate and carboxylic acid groups, and possibly the conserved sequence of contiguous aspartic acid sequences (Hunter and Goldberg 1994).

Another acidic bone protein, osteocalcin, contains three gamma carboxyglutamic acid residues that participate in the binding of calcium ions. On calcium binding a major conformational change occurs that greatly increases the α helical content of the protein (Hauschka 1986). Using the steady-state agarose gel system osteocalcin was found to delay nucleation (Hunter et al 1996).

It is clear that predicting the mineral nucleating behaviour of a protein from its amino acid sequence is difficult. It is clear that polycarboxylic acids and phosphorylation are common features associated with bone and dentine biomineralisation; regardless of whether the protein in question promotes or inhibits nucleation. The potency of polyglutamic acid sequences as a nucleator is evidenced by the now common use of long chains of glutamic acid synthesised chemically for use as a positive control in mineral nucleation experiments. PGA at 10 $\mu\text{g}/\text{mL}$ was used as the positive control for assessment of mineral nucleation in the steady state agarose gel system used in this thesis.

How do enamel proteins compare in terms of phosphorylation and polycarboxylic acid content? Enamelin contains 2 phosphorylated serine residues and 3 glycosylated asparagine residues which are located in the domain that forms the 32 kDa fragment in pig enamel following cleavage of the full length protein. Like the mineralised tissue proteins described above, the 32 kDa enamel is acidic (isoelectric point of 5.27) but contains only two examples of diglutamic acid units (Hu and Yamakoshi, 2003). The 32 kDa enamel protein used in the experiments presented in this thesis was produced in a eukaryotic system and the resulting protein should have all the appropriate post-translational modifications such as phosphorylation and glycosylation (Hu and Yamakoshi, 2003). Given these modifications, the 32 kDa enamel has the potential capacity to interact with mineral and influence growth (Robinson et al., 1998; Bouropoulos and Moradian-Oldak, 2004; Fan et al., 2008; Fan et al., 2009B; Al-Hashimi et al., 2009).

Table 2 shows a comparison of the key features of extracellular matrix proteins that have been used to investigate hydroxyapatite nucleation potential.

Table 2. Table to show comparison of common features of proteins that have been examined for hydroxyapatite nucleating potential. Note that the frequency of aspartic acid and glutamic acid invertebrate proteins is on average around 6% (Mann, 2001)

Protein (Porcine)	PKa	MW kDa	PTM	Tertiary Structure	Aspartic Acid	Glutamic Acid	Shown to nucleate HAP?
Bone sialoprotein 2 ¹	3.9 ¹	33 ¹	50% ¹	No ¹	5.4% ¹	19% ¹	Yes ²
Phosphoryn ³	Acidic	33	yes	Yes with Ca ²⁺	20%	5%	Yes
Osteocalcin ³	5.5	6	Yes	Yes	4%	8%	No
Osteopontin (Bone sialoprotein 1) ²	Acidic	32.6	Yes	Yes	15%	9%	No
Osteonectin ³	5.9	44	Yes	Yes ⁸	8%	11%	No
32 kDa Enamelin	5.3	32 ⁵	Yes ⁵	No (Mainly α helices) ⁶	3% ⁴	9.4% ⁴	No
Amelogenin	6.5 ⁷	25	Yes	B sheet (bovine)	1.5%	2.5%	No

¹ Oldberg et al., 1988; ² Hunter and Goldberg, 1993; ³ Hunter et al., 1996;

⁴ Hu and Yamakoshi 2003; ⁵ Yamakoshi, 1995; ⁶ Fan et al, 2008;

⁷ He et al., 2008; ⁸ Fujisawa et al., 1996

In contrast to enamel, which exhibits at least some similarities with the mineralised tissue proteins discussed above; amelogenin is not particularly acidic (isoelectric point 6.5) and has a low glutamic and aspartic acid content. Indeed, Hunter et al (1999) reported that recombinant mouse amelogenin in agarose gels failed to induce or inhibit *in vitro* nucleation at protein concentrations ranging from 1-300 μ g/mL.

However, Tarasevich *et al.* (2007) tested recombinant mouse amelogenin, rM179 *in vitro* and found that the protein nucleated mineral up to a protein concentration of 6.5 µg/mL in free solution. At higher concentrations the nucleating potential decreased until at 130 µg/mL nucleating potential was essentially zero. However, higher concentrations of amelogenin are not necessarily inhibitory because on close examination of the Tarasevich's 2007 publication it is apparent that the mineralising solutions remained metastable and did not nucleate mineral in the absence of protein; in other words this experimental system was not suitable for determining whether higher concentrations of amelogenin are able to inhibit nucleation simply because even in the absence of amelogenin, nucleation does not occur. To show if these higher concentrations of amelogenin are able to inhibit nucleation they would need to be added to a system that is able to induce nucleation in the absence of the added amelogenin. Previous studies have shown that proteins may inhibit mineralisation by the sequestering of mineral ions. The binding of calcium ions to proteins and proteoglycans lowered the concentration of calcium in solution and inhibited nucleation (Hunter and Szigety, 1985; Hunter *et al.*, 1994). Protein concentration *in vitro* being able to influence mineralisation suggests that amelogenin's function *in vivo* may be dependent on concentration, with roles such as nucleator being promoted at low concentration and other roles such as growth modifier occurring at high concentration. The concentration of recombinant amelogenin protein used in the steady-state agarose gel system in this thesis was 10 µg/mL, above the limit of 6.5 µg/mL amelogenin shown by Tarasevich *et al.*, (2007) where amelogenin switches from a nucleator to an inhibitor. The experiments in section 2.2 agree with this theory, with 10 µg/mL recombinant amelogenin eliciting an inhibitory effect on mineral nucleation in the steady state agarose gel system.

Bouropoulos and Moradian-Oldak (2004) showed that crude amelogenin extracts (comprising nascent amelogenin and its processing products) added to gelatine gels in amounts far exceeding 6.5 µg/ml (i.e. 0.75 or 1.5% (w/w)= 7.5-15 mg/mL) had an inhibitory effect on *in vitro* hydroxyapatite nucleation. They also tested the nucleation potential of the 32 kDa enamelin at 18 µg/mL in the same system and reported that it too inhibited nucleation. However, when amelogenin at 1.5% (w/w) was used in conjunction with 32 kDa enamelin, nucleation was accelerated. This striking result suggested a synergistic role for amelogenin and the 32 kDa enamelin in terms of hydroxyapatite nucleation.

Based on this, the nucleating potential of wild type and Y64H mutant recombinant amelogenin was tested in the absence and presence of recombinant 32 kDa enamelin.

When deciding on relevant amelogenin concentrations to use in the present work several things needed to be considered:

1) *How the concentrations used in the in vitro system compare to those in vivo:*

Secretory stage enamel is approximately comprised of equal volumes of protein (mostly amelogenin), water and mineral meaning that *in vivo* amelogenin concentration approaches 100% (v/v) or 1350 mg/mL (assuming an average density of 1.35g/cm³ for protein (Fischer et al 2004)). Researchers studying amelogenin have been frustrated by the low solubility of amelogenin at physiological pH which is around 200 µg/mL in calcium-phosphate solution (Tan et al 1998). This explains why Tarasevich *et al.* (2007) used amelogenin concentrations of only up to 130 µg/mL in calcium-phosphate solution. Bouropoulos and Moradian-Oldak (2004) used amelogenin at much higher concentrations of 7.5 and 15 mg/mL but here amelogenin was added to gelatine gels and presumably the amelogenin was only partially solubilised in these gels and as such closer to the situation found *in vivo* where the amelogenin must exist as a hydrated protein gel. In general, amelogenin experiments are conducted using solutions that are orders of magnitude more dilute than *in vivo* concentrations but dispersing the amelogenin in gelatine or agarose (as is the case in this thesis) may be a better approximation to *in vivo* conditions compared to experiments conducted with amelogenin free in solution.

2) *The availability of amelogenin to use in in vitro mineralisation experiments:*

In vitro mineralising experiments, including the system described in this thesis, have to be designed with the knowledge that amounts of recombinant protein available are likely to be a limiting factor. Scaling down the experimental mineralising system helps to some extent, but this is countered by an increase in measuring error as volumes decrease. Using amelogenin at *in vivo*-like concentrations was simply not practical due to limited availability of protein and the solubility issues described above. An amelogenin concentration of 10 µg/mL dispersed in agarose gel was used in this study as this was the maximum amount that could be sustained in terms of recombinant protein production that also aligned with concentrations used previously in the literature, enabling the results to be interpreted with reference to what has gone before.

4.2 Nucleation potential of wild type and Y64H mutant recombinant amelogenin

At 10µg/mL both wild type and Y64H mutant recombinant amelogenin significantly inhibited nucleation of hydroxyapatite mineral *in vitro* compared with a PGA positive control with no significant difference in levels of inhibitory activity between the two amelogenin forms. Under these experimental conditions at least, Y64H mutation did not alter the nucleating potential of amelogenin in the agarose gel based system used here; both proteins significantly inhibit nucleation relative to the negative control by approximately 50%. This inhibitory effect was consistent with previous reports for wild type amelogenin studied in a gel based experimental system (Bouropoulos and Moradian-Oldak 2004 - see above) but conflicts with Hunter et al (1999) who as described above examined the nucleating potential of recombinant amelogenin and found it neither nucleated nor inhibited in their agarose gel based system (similar to the system used in this thesis).

Bouropoulos and Moradian-Oldak (2004) also reported that wild type amelogenin and 32 kDa enamelin at 18 µg/mL inhibited nucleation in isolation. However, together they synergistically promoted nucleation. To test if the Y64H mutation disturbed this synergistic relationship, the nucleating potential of the 32 kDa enamelin alone and in combination with either WT or Y64H amelogenin was determined.

4.3 Nucleation potential of recombinant 32 kDa enamelin

Initially, the nucleating potential of 32k Da enamelin alone was determined in the present study. Recombinant 32 kDa enamelin was available in limited amounts due to the relatively inefficient expression system used. For that reason its nucleating ability was tested at concentrations between 1-10 µg/mL. In contrast to Bouropoulos and Moradian-Oldak (2004), the 32 kDa enamelin used here induced significant nucleation at 1 and 10 µg/mL compared to the negative control whereas 32 kDa enamelin at 2.5 and 5 µg/mL was not significantly different to the negative control (figure 30 Section 3.3.2). This apparently conflicting phenomenon, where protein concentration can reverse nucleation behaviour is well known. For example dentine phosphoprotein at 100 µg/mL inhibited mineral formation but promoted it at <1 µg/mL (Boskey *et al.*, 1990).

Increasing the protein concentration could conceivably reduce nucleation due to calcium binding by the protein causing a drop in supersaturation levels but it is difficult to reconcile this with the parabolic-like response exhibited by the 32 kDa enamel in this thesis. Furthermore, the steady state agarose gel apparatus used is designed to provide constant composition conditions and any enamel calcium binding sites would be saturated and levels of supersaturation would remain fixed at the predetermined level. One possible explanation for this parabolic response is that any quaternary structure existing between two or more 32 kDa enamel monomers varies with concentration which in turn affects the conformation of the 32 kDa enamel and its ability to nucleate. However, there is no evidence to date that supports this hypothesis.

The Ca:P molar ratio of enamel nucleated mineral was 1.61 ± 0.03 (see figure 43 Section 3.2.6); close to the theoretical value for hydroxyapatite (1.66). Polyglutamate, the positive control nucleated mineral with a Ca:P of 1.73 ± 0.12 ; again close to the theoretical value for hydroxyapatite of 1.66. In complete contrast any mineral deposits formed in the absence of protein (agarose only) had a non-apatitic ratio of 1.05 ± 0.32 which clearly shows the potential of both 32k Da enamel (at permissive concentrations of 1 and 10 $\mu\text{g}/\text{mL}$) and polyglutamate to nucleate apatitic mineral. Brushite has a Ca:P of 1.0 though this information alone does not allow this phase to be identified as brushite unequivocally. Brushite is dicalcium phosphate dehydrate ($\text{CaHPO}_4 \cdot 2\text{H}_2\text{O}$) is a phase of calcium phosphate that is relatively soluble in simulated physiological solutions (Kumar et al., 1999). However, brushite in solution is only stable in acidic solutions less than pH 6.5 (Cheng and Pritzker, 1983). Below pH 4.3, brushite is more stable than hydroxyapatite. In theory, brushite should form at pH 7.4 at 37°C when the concentrations of the total calcium and phosphate ions exceeds 5 mM (Koutsoukos et al., 1980), such as the conditions used in the steady state agarose gel system in this thesis.

It is clear from the SEMs that the crystal morphology of mineral nucleated is affected by the recombinant 32 kDa enamel. As described in section 3.2.5, the morphology of the crystals was affected but the concentration of the recombinant 32 kDa enamel in the agarose gel plugs. Recombinant enamel at 1 $\mu\text{g}/\text{mL}$, 5 $\mu\text{g}/\text{mL}$ and 10 $\mu\text{g}/\text{mL}$ nucleated mineral crystals with a large plate like appearance of approximately 6 microns. Mineral crystals nucleated in the presence of recombinant enamel at 2.5 $\mu\text{g}/\text{mL}$ exhibited two morphologies, both different to those seen for the crystals nucleated

in the presence of recombinant 32 kDa enamelin at 1 µg/mL, 5 µg/mL or 10 µg/mL. These two morphologies were small spherical clusters of approximately 10 nm in length or needle like crystals. TEM images of the mineral nucleated in the presence of 5 µg/mL recombinant 32 kDa enamelin showed the crystals to be large (approximately 4 microns in length) and flat. Mineral crystals nucleated in the presence of PGA (10 µg/mL) were shown by both TEM and SEM analysis to be rosette like in appearance, radiating from a central area. Individual crystals were smaller, approximately 1 micron in radius, than those nucleated in the presence of recombinant 32 kDa enamelin.

4.4 Nucleation potential of 32 kDa enamelin in combination with either wild type or Y64H mutant recombinant amelogenin

When recombinant 32 kDa enamelin at 5 µg/mL was combined with either wild type or Y64H mutant amelogenin the inhibitory effects previously observed for all the amelogenin proteins observed in isolation (relative to precipitation in the negative control) were lost. This result does not support the results obtained by Bouropoulos and Moradian-Oldak (2004) where 18 µg/mL enamelin + 15 mg/mL amelogenin accelerated nucleation but at least the trend was the same in that 32 kDa enamelin combined with either WT or Y64H synergistically reduced inhibition of nucleation in the system used here. In explaining the difference in results obtained by Bouropoulos and Moradian-Oldak (2004) attention can be drawn to the fact that they used higher concentrations of 32 kDa enamelin (18 µg/mL compared to 1-10 µg/mL used here) and the amelogenin was a crude guanidine-HCl extract containing several amelogenin processing products and probably other non-amelogenin contaminants such as ameloblastin that would have been co-extracted with the amelogenins.

In summary, the crucial finding here is that the results obtained with 32 kDa enamelin combined with either WT or Y64H amelogenin were not significantly different i.e. within the limits dictated by the *in vitro* nucleation system used to be able to discern any effect of the Y64H mutation on the nucleating behaviour of amelogenin (in the presence or absence of 32 kDa enamelin).

The overall conclusion to be drawn from these *in vitro* nucleation experiments is that the amelogenin imperfecta phenotype observed in mice carrying the Y64H amelogenin mutation is not due to the Y64H amelogenin behaving differently from the

wild type molecule in terms of its behaviour with respect to mineral nucleation (in the presence or absence of 32 kDa enamelin).

4.5 The assumed role of the 32 kDa enamelin in amelogenesis

The calcium binding constant of amelogenin is estimated to be significantly lower than other enamel ECM proteins ($K_a = <4.5 \times 10^2 \text{ M}^{-1}$ versus $K_a = 1.0 \times 10^4 \text{ M}^{-1}$) (Yamakoshi *et al.*, 2001). This suggests that an interaction between amelogenin and the non-amelogenins such as enamelin may be necessary for enamel mineralisation

Historically enamelin has been regarded as the non-amelogenin most likely to play a role in mineral nucleation (Robinson *et al.*, 1998; Bouropoulos and Moradian-Oldak, 2004) and as such is a candidate molecule that may act in tandem with amelogenin to promote nucleation; a contention supported by the results obtained by Bouropoulos and Moradian-Oldak, (2004) using 32 kDa enamelin in combination with amelogenin as described above. Enamelin is a phosphorylated glycoprotein, specific to enamel. It constitutes only 1-5% of the ECM, but plays a key role in enamel formation, evidenced by enamelin mutations resulting in amelogenesis imperfecta (Rajpar *et al.*, 2001; Mardh *et al.*, 2002; Kida *et al.*, 2002; Hart *et al.*, 2003; Kim *et al.*, 2005A; Gutierrez *et al.*, 2007; Gopinath *et al.*, 2008; Simmer *et al.*, 2013). The gene sequences for many species including mouse (Hu *et al.*, 1998), pig (Hu *et al.* 1997) and human (Hu *et al.*, 1998) enamelin are known (Al-Hashimi *et al.* 2009). However, studies at the protein levels have focused almost exclusively on porcine enamelin owing to the ready availability of porcine developing enamel from the meat industry. Upon secretion, the porcine 186 kDa enamelin protein is subjected to extensive proteolytic cleavage. Enamelins with molecular weights of 155, 142, 89, 45, 32, and 25 kDa have been isolated from developing porcine enamel (Fukae *et al.*, 1996). The 32 kDa fragment extends from Leu¹⁷⁴ to Arg²⁷⁹ of the full length enamelin molecule, and its carbohydrate moieties have been elucidated (Fukae *et al.*, 1996; Dohi *et al.*, 1998; Yamakoshi, 1995). The 32 kDa enamelin is hydrophilic, has an acidic PI of 5.3 is rich in proline, glycine, threonine and glutamic acid (Hu and Yamakoshi, 2003), has 2 phosphorylated serines (Ser¹⁹¹ and Ser²¹⁶) and 3 glycosylated asparagines (Asn²⁴⁵, Asn²⁵² and Asn²⁶⁴) (Yamakoshi, 1995). This is the most abundant enamelin product found in the developing tissue and the most stable, accumulating in the deeper, older layers of the developing porcine enamel.

Immunohistochemistry studies have shown that the porcine 32 kDa enamelin accumulates in the inner layer of crystallite-containing prism and interprismatic areas of the enamel matrix (Uchida et al., 1991B). The 32 kDa enamelin also caused elongation of hydroxyapatite crystals *in vitro* in agarose gels, indicating a role in controlling crystal nucleation and/or growth (Hu et al., 2008). Crucially, Bouropoulos and Moradian-Oldak (2004) showed that the combination of the 32 kDa enamelin with amelogenins promoted the nucleation of hydroxyapatite crystals. Fan et al. (2008) applied circular dichroism (CD) and Fourier transform infrared (FTIR) spectroscopy to study secondary structural preferences of the porcine 32 kDa enamelin in the presence and absence of calcium ions. In the absence of calcium, 32 kDa enamelin showed a high content of α -helix (81.5%). Although the 32 kDa enamelin had a calcium association constant of $1.55 (\pm 0.13) \times 10^3 \text{ M}^{-1}$ (which is a relatively low affinity) CD showed that with increasing calcium ion concentration, the enamelin undergoes a conformational change to β -sheet. This may allow a preferable interaction of the 32 kDa enamelin with hydroxyapatite crystal surfaces.

Fan et al. 2009A used the extracted 32 kDa enamelin fragment from developing porcine enamel, along with a recombinant amelogenin (rP172 – analogous to full-length porcine amelogenin, only lacking the first methionine and a phosphate on Ser¹⁶) to elucidate the role of protein interactions *in vivo*. Dynamic light scattering showed that the 32 kDa enamelin caused partial dissociation of amelogenin nanospheres in a dose-dependent manner at pH 8.0. If this data is examined critically, attention should be drawn to the fact that the full length amelogenin is only present in newly secreted surface enamel while 32 kDa enamelin is generated with time in the deeper enamel by proteolysis of larger precursor proteins (Uchida et al. 1991B). In other words the full length amelogenins are unlikely to interact with the 32 kDa enamelin *in vivo* because they are temporally and spatially separated in the developing tissue. However, Fan et al later repeated their work using the 20 kDa amelogenin processing product (P148) which does co-localise with the 32 kDa enamelin. In this case they reported that the 32 kDa enamelin increased the size of amelogenin nanospheres indicating a conformation change that may influence interactions with the mineral interface (Fan et al., 2011).

These data emphasise the volume of research already conducted using the 32 kDa enamelin molecule and the 32 kDa enamelin continues to be the enamelin of choice in experiments designed to study the role of enamelin in amelogenesis.

However, one unexpected finding arising from this thesis forces us to completely reevaluate the role, if any, of the 32 kDa enamelin as a discrete entity in amelogenesis. This controversial finding is discussed in detail next section.

4.6 Is the 32 kDa enamelin required in amelogenesis?

One of the aims of this study was to see whether enamel matrix proteins (enamelin and amelogenin) nucleate crystal growth *in vitro* and how mutations in amelogenin might affect any nucleating potential exhibited. In the case of enamelin, several nucleation and protein–protein interaction studies have been carried out using the 32 kDa enamelin processing product purified from developing pig enamel (Uchida et al., 1991A and B; Dohi et al., 1998; Bouropoulos and Moradian-Oldak, 2004; Habelitz et al., 2006; Fan et al., 2008; Hu et al., 2008; Iijima et al., 2010). The 32 kDa enamelin is the most abundant enamelin-derived protein in pig secretory stage enamel and although still present as a tiny fraction of the total protein is the obvious target for purifying enamelin protein for use in *in vitro* studies. The focus on the 32 kDa enamelin is also linked to widespread belief that the 32 kDa moiety is functionally important. This perception was most emphatically stated by Al-Hashimi et al in their 2009 publication:

“Evolutionary analysis of mammalian enamelin, the largest enamel protein, supports a crucial role for the 32-kDa peptide and reveals selective adaptation in rodents and primates.”

They noted that the amino acid sequence comprising the 32 kDa enamelin peptide was highly conserved across 36 species especially in terms of its phosphorylation, glycosylation and “proteolytic sites”. On this basis a recombinant peptide corresponding to the human 32 kDa enamelin sequence was constructed and used in the nucleation studies described in this thesis. However, during the course of these studies it became apparent that there is a crucial difference between the amino acid sequences of pig enamelin and enamelin in other species. Although cleavage sites *within* the 32 kDa sequence are well conserved between species, the cleavage sites that are cleaved to release the 32 kDa fragment from its larger precursor are not well conserved at all. Critically, Al-Hashimi focused their attention on internal cleavage sites that are hydrolysed during the degradation of pig 32 kDa enamelin but neglected the fact that the cleavage sites required to release the 32 kDa enamelin (i.e. cleavage between proline and leucine to generate the new N terminus, and arginine and serine for generating the

terminals of the 32 kDa enamelin) are absent from non-porcine species. The sequence alignment of 290 enamelin sequences shown in Appendix 3 shows that the residues comprising the cleavage sites responsible for generating the N and C terminals of the pig 32 kDa enamelin are only present in the pig. It is believed that MMP20 is responsible for liberating the 32 kDa moiety in porcine enamel (Yamakoshi et al., 2006). MMP20 does not cleave all peptide bonds as evidenced by the fact that it generates a spectrum of discrete processing fragments from amelogenin and enamelin and it is unclear how flexible MMP20 might be in terms of releasing the 32 kDa enamelin fragment from enamelins that do not exhibit the specific cleavage sites used to liberate the porcine 32 kDa enamelin. The amino acids corresponding to the pig 32 kDa cleavage sites (proline/leucine and arginine / serine) are proline / proline and glycine / asparagine in rat. Assuming narrow specificity for the protease that releases the pig 32 kDa enamelin, it is reasonable to assume that rat amelogenesis does not involve the participation of a discrete 32 kDa enamelin since the specific cleavage sites responsible for its generation are absent. To test this, developing rat enamel matrix was compared to developing pig enamel matrix by SDS PAGE and western blot probing with a rabbit anti-enamelin antibody recognising a region within the 32 kDa enamelin sequence.

The anti-enamelin probed Western blots of rat and porcine developing enamel (Chapter 3 Section 3.3.1 figure 51) showed that rat amelogenesis does not involve the generation of a 32 kDa enamelin molecule. This supports the hypothesis outlined above, that based on sequence analysis, only the pig enamelin molecule contains the specific cleavage sites required to generate the 32 kDa enamelin.

The different kinetics of enamel production in the rat and the pig may cause this difference in the predominant enamelin species produced. Rat enamel takes approximately one week to progress through the secretory stage, at which point the matrix is removed at the maturation stage. It could be possible that the proteases present at the secretory stage are not active enough to process the rat enamelin to the 32 kDa level. As the enamel is much thicker in pig teeth, and remains in the secretory stage for much longer, the proteases have longer to interact with, and breakdown the enamelin. To test this, rat enamel matrix proteins were homogenised and incubated for various time periods to encourage enamelin proteolysis. However, no 32 kDa enamelin molecules were generated.

The data strongly indicates that rat amelogenesis occurs *without* the generation of a discrete 32 kDa enamelin processing product. The sites of porcine 32 kDa enamelin

post translational modifications (N-linked glycosylation and phosphorylation) are well conserved among all species (including pig, mouse, rat and human) indicating a functional role for these modifications (Al-Hashimi et al., 2009). The larger enamelin of non-porcine species will of course contain the 32 kDa sequence domain, and these post translational modifications, and the biochemical activity associated with these modifications may be critical in terms of the function of enamelin larger than 32 kDa. However, the functional behaviour of the phosphorylated/glycosylated 32 kDa domain may be quite different when it is within larger enamelin due to the influence of the additional sequences flanking the 32 kDa domain.

Given that the generation of the 32 kDa enamelin processing product is not essential for amelogenesis in rat, and that its production in pig appears to be an anomaly, the use of discrete 32 kDa moieties in enamelin functional studies should be viewed with caution and results interpreted with the caveat that the 32 kDa enamelin processing product is not common to amelogenesis in non-porcine species. In fact, the anomalous production of the 32 kDa enamelin in pig amelogenesis may explain why pig enamel only attains a mineral content of ~60% by volume which is significantly lower than other species (Kirkham et al., 1988). The pig 32 kDa enamelin has the highest affinity for hydroxyapatite of all enamel proteins and is a potent inhibitor of hydroxyapatite crystal growth following its adsorption (Tanabe et al., 1990). Pig amelogenesis may therefore be compromised to some degree due to the release and accumulation of 32 kDa enamelin from its larger enamelin precursor. Pig enamel remains perfectly functional even though it exhibits a reduced mineral density compared to other species and therefore there is little evolutionary pressure to eradicate the production of the 32 kDa enamelin during pig amelogenesis.

The above discussion questions the validity of using 32 kDa enamelin (either purified from pig tissues or produced as a recombinant protein as in this thesis) in studies designed to explore the function of enamelin. An obvious criticism of the work examining the effect of recombinant 32 kDa enamelin in the nucleation assays reported in Chapter 3 section 3.2 is that the 32 kDa enamelin may not be relevant in amelogenesis in general and the enamelin function is associated with enamelin(s) with molecular weights greater than 32 kDa. Isolating sufficient amounts of full length enamelin from developing enamel is not practical due to its very low concentration in the matrix and as yet no one has managed to produce a recombinant full length enamelin presumably due to the technical issues related to producing large recombinant DNA molecules. Given these limitations, studying the functionality of discrete enamelin

domains such as the 32 kDa sequence may be the only option at present but clearly the caveat must be made that the behaviour of this domain may be different when it is a component part of larger enamelinins.

4.7 Intracellular effect(s) of the Y64H amelogenin mutation on the ameloblast secretory pathway

The *in vitro* nucleation data presented in Chapter 3 section 3.2 and discussed above would indicate that the wild type and Y64H mutant amelogenins behave in a similar fashion in terms of mineral nucleation/inhibition. During the course of the wider research program it became clear that it was the ameloblasts themselves that were affected by the mutation; i.e. the disease mechanism underpinning amelogenesis imperfecta in Y64H mutant mice appeared to be related to a deleterious effect of amelogenin on ameloblast cell biology rather than the dysfunctional behaviour of mutated protein in the enamel matrix. SDS PAGE and western blotting data obtained within the research group showed that the enamel matrix of male Y64H mutant mice exhibited a paucity of full length amelogenin (Barron et al., 2010). The obvious conclusions from this data are that full length amelogenin was not expressed or the normal secretory pathway was stalled in ameloblasts carrying the Y64H amelogenin mutation, resulting in a failure to secrete amelogenin. In the present study, the question was posed as to whether or not failure to detect Y64H full length amelogenin in the developing enamel matrix of affected teeth was due to a failure in protein trafficking out of the cell or a failure in gene transcription. Quantitative RT PCR was therefore carried out to determine levels of amelogenin transcript in affected animals. The PCR data presented in figure 64 section 3.5.3 suggested that amelogenin is expressed (albeit at lower levels) in Y64H mutant mice leaving the possibility that Y64H amelogenin is not secreted correctly. Figure 72 shows an electron transmission micrograph of Y64H mutant mouse ameloblasts labelled immunochemically for amelogenin (courtesy of Dr Martin Barron Manchester) of displaying abnormally engorged vesicles packed with amelogenin which suggested that that amelogenin is accumulating in cells; i.e. the secretory pathway is indeed blocked.

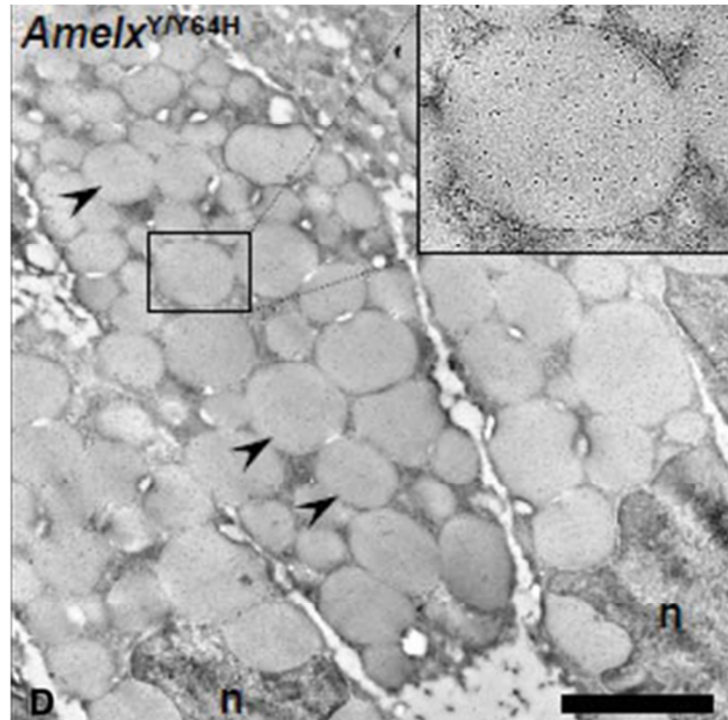


Figure 72. This figure shows the secretory ameloblast cells of a male Y64H mouse as seen by immunoelectron microscopy. The cytoplasm is abnormally engorged with vacuoles strongly immunoreactive for amelogenin (see black dots in the top right insert). The scale bar is 2 μm ; N = nuclei. (Barron et al., 2010). Reproduced under Creative Commons Attribution License. Modified from figure 3 published in: 'A mutation in the mouse *Amelx* tri-tyrosyl domain results in impaired secretion of amelogenin and phenocopies human X-linked amelogenesis imperfecta' by Barron et al 2010 *Hum. Mol. Genet.* (2010)19 (7): 1230-1247. Direct link: <http://www.ncbi.nlm.nih.gov/pubmed/20067920>

It is well known that mutated proteins can misfold and undergo abnormal aggregation as they transit the endoplasmic reticulum (ER) in a range of cell types (Steward et al., 2003). The ER is an organelle where newly synthesised proteins begin their journey on the secretory pathway out of the cell. During ER trafficking, proteins are modified as any post translational modifications are carried out and proteins fold (assisted by chaperone proteins) to attain the correct conformation. The abnormal retention of proteins in the ER results in ER stress which triggers the so called unfolded protein response (UPR) (Ron and Walter. 2007). The UPR attempts to restore

proteostasis, but if unsuccessful, will eventually direct the cells towards apoptosis and ultimately cell death. Mutant proteins can therefore lead to disease due to reduced secretion of protein or in extreme cases, death of cells and tissues. ER stress and the UPR is associated with diseases such as Huntington's disease, Alzheimer's, diabetes (type 2), cystic fibrosis, atherosclerosis, connective tissue disease and cancer (reviewed by Schroder and Kaufmann 2005). Given the evidence presented in this thesis together with that of the wider group, it appeared that ameloblast ER stress, due to retention of Y64H mutant amelogenin, could also be the driver for amelogenesis imperfecta in the affected mice. One possible reason for retention of Y64H amelogenin in the ER might be that amelogenin carrying the mutation is more highly aggregative than its wild type counterpart.

To explore this possibility, the interaction of Y64H amelogenin with other Y64H amelogenin molecules and with wild type amelogenin molecules was investigated. This would indicate if Y64H amelogenin is more prone to aggregation.

4.8 Effect of the Y64H mutation on amelogenin-amelogenin interactions

The amelogenin binding studies reported in Chapter 3 section 3.4 shows the binding of solubilised FITC labelled wild type and FITC labelled Y64H mutant amelogenin to unlabelled wild type and Y64H mutant amelogenin and BSA (control) immobilised to cell culture plates. To aid discussion of these results the data is reproduced here along with an additional cartoon figure that represents the results pictorially (figure 73).

The first thing to note was that neither labelled mutant or WT amelogenin bound to immobilised BSA which was included as a control protein to test if amelogenin bound other proteins non-specifically under these experimental conditions (figure 55 section 3.4.2). In contrast, labelled mutant amelogenin and labelled WT bound to immobilised Y64H and WT amelogenins (columns A & B in figure 55 section 3.4.2). This immediately indicated that both of these amelogenins have the ability to interact specifically and we are not just observing a general protein binding phenomenon. FITC- labelled Y64H mutant amelogenin appeared to bind to both immobilised WT and Y64H amelogenin to a greater extent than free labelled WT (with fluorescence readings being approximately 2-

3 times higher in all cases). Interestingly, labelled WT amelogenin did not show any increase in binding to Y64H mutant amelogenin immobilised on the plate whereas in the reciprocal case, solubilised labelled Y64H amelogenin showed increased binding to immobilised WT amelogenin. The reasons for this are unclear but may be related to the higher affinity that the mutant protein appears to have for itself. The data can be explained if we assume that bait (immobilised) proteins are adsorbed to the wells as monolayers. Adsorption is carried out at pH 9.6 which favours binding of protein to the plastic well but inhibits protein-protein interactions. This is illustrated in figure 73 below where the adsorbed unlabelled WT and unlabelled Y64H mutant bait proteins are depicted as monolayers bound to the wells. In well 1, labelled WT amelogenin from solution is binding unlabelled bait (bound) WT but the affinity is such that a relatively small amount binds; illustrated here pictorially as a monolayer. In well 2 we have the same bait binding to labelled mutant amelogenin. The greater binding affinity of the mutant amelogenin to itself means that labelled mutant proteins build up by mutant-mutant interaction; illustrated pictorially as a thicker layer which would give rise to a greater fluorescence signal. In well 3, we have the same binding partners as in well 2 but here the mutant is the bait protein and the binding partner is the labelled WT amelogenin in solution. The fluorescent signal is about 3 times less than well 2 and comparable with well 1. This is simply explained by the lower affinity that WT amelogenin has for itself. An initial layer of labelled WT amelogenin binds the mutant bait amelogenin but no more labelled WT binds to this initial partnership. Finally, in well 4 in which unlabelled mutant bait protein is binding labelled mutant protein a large fluorescent signal is returned (comparable to well 2). Again this is explained by the high affinity of the mutant for itself. An initial layer of the labelled mutant binds the bait followed by further growth of the layer as more labelled mutant protein binds the initially bound material.

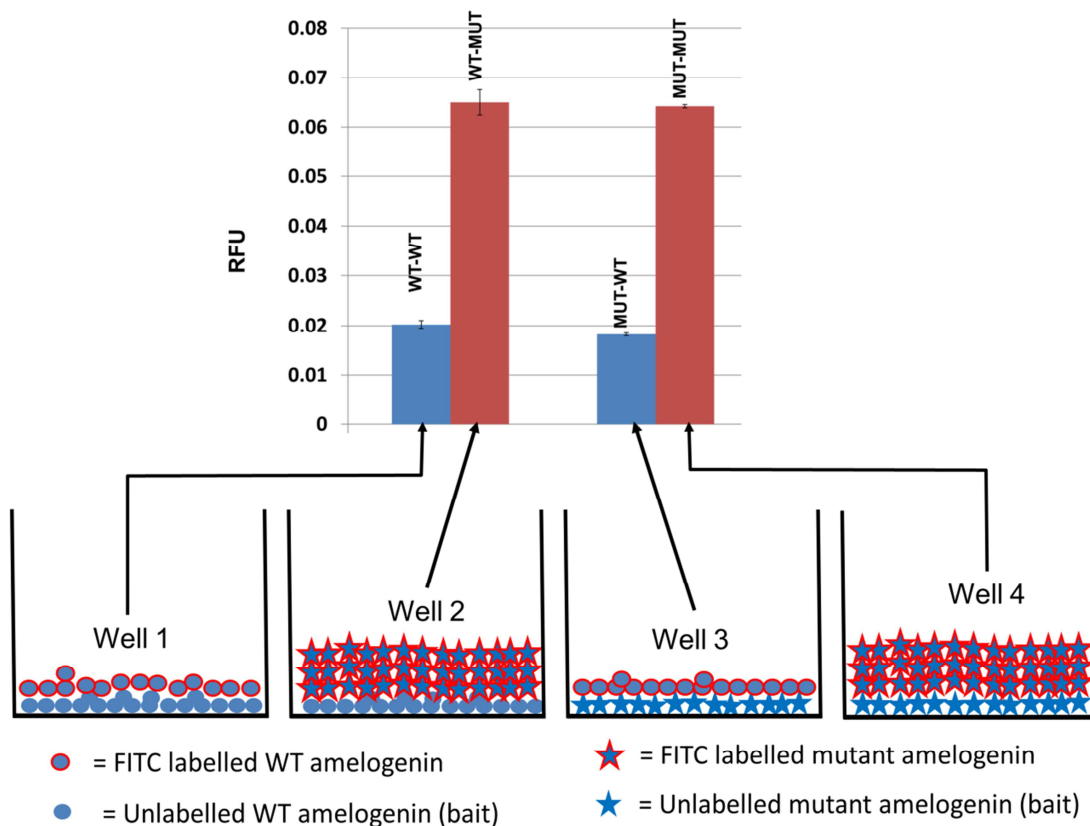


Figure 73. Results of FITC binding experiments showing 100 µg/mL of unlabelled wild type amelogenin or Y64H mutant amelogenin bound to a 96-well microtitre plate and interrogated with 100 µg/mL of either wild type or mutant FITC-labelled amelogenin. N =6. Standard deviation error bars are shown. The cartoon below the graph depicts the hypothesis of the protein-protein interactions.

That the Y64H amelogenin mutation increases amelogenin-amelogenin binding may be important in terms of pathogenic mechanisms. Previous studies have indicated that wild type amelogenins interact prior to secretion and form complexes containing up to 6 monomers (Brookes et al 2006). Following secretion, amelogenins assemble (i.e. aggregate) further to generate nanospheres comprising 100 or more amelogenin nanospheres (Fincham et al 1998), which represent the normal extracellular habit for amelogenin as described in the Introduction (section 1.3.4.1.2). In Y64H amelogenin mutant mice, the mutant amelogenin accumulates in the ER and the ameloblasts become engorged with vesicles packed with amelogenin. Given that Y64H amelogenin

appears to exhibit a greater propensity to interact with other Y64H amelogenin molecules, the obvious hypothesis is that Y64H amelogenin molecules interact inappropriately during their passage through the ER, by aggregating and blocking the secretory pathway, triggering the UPR and thus exposing the ameloblasts to the possibility of apoptosis.

4.9 ER stress, UPR and apoptosis in Y64H ameloblasts

Genetic information required to generate proteins from the 20 amino acids is stored in the chromosomes in the nucleus of the cell as DNA. This information is transcribed into messenger RNA (mRNA) which carries the information to the ribosomes which translate the mRNA into a protein containing the specified amino acids in the specified order. Ribosomes synthesising proteins destined for import into intracellular organelles (e.g. mitochondria) or proteins destined for secretion into the extracellular medium associate with the outer membrane of the endoplasmic reticulum (ER) and as the protein chain is synthesised it is translocated into the ER where, as it is trafficked through the ER lumen, it undergoes further modification (e.g. glycosylation, phosphorylation etc.) and 'quality control' checks (Ellgaard and Helenius., 2003). Once proteins are ready to exit the ER they are packaged into vesicles known as transition vesicles, which bud off from the ER and travel to the Golgi apparatus. The vesicles fuse with the Golgi and proteins are sorted and packaged into new vesicles which bud off and carry the cargo to the correct destination (Pfeffer and Rothman, 1987). In the case of secretory proteins such as amelogenin, vesicles migrate to the cell membrane and release the protein to the outside of the cell (figure 74).

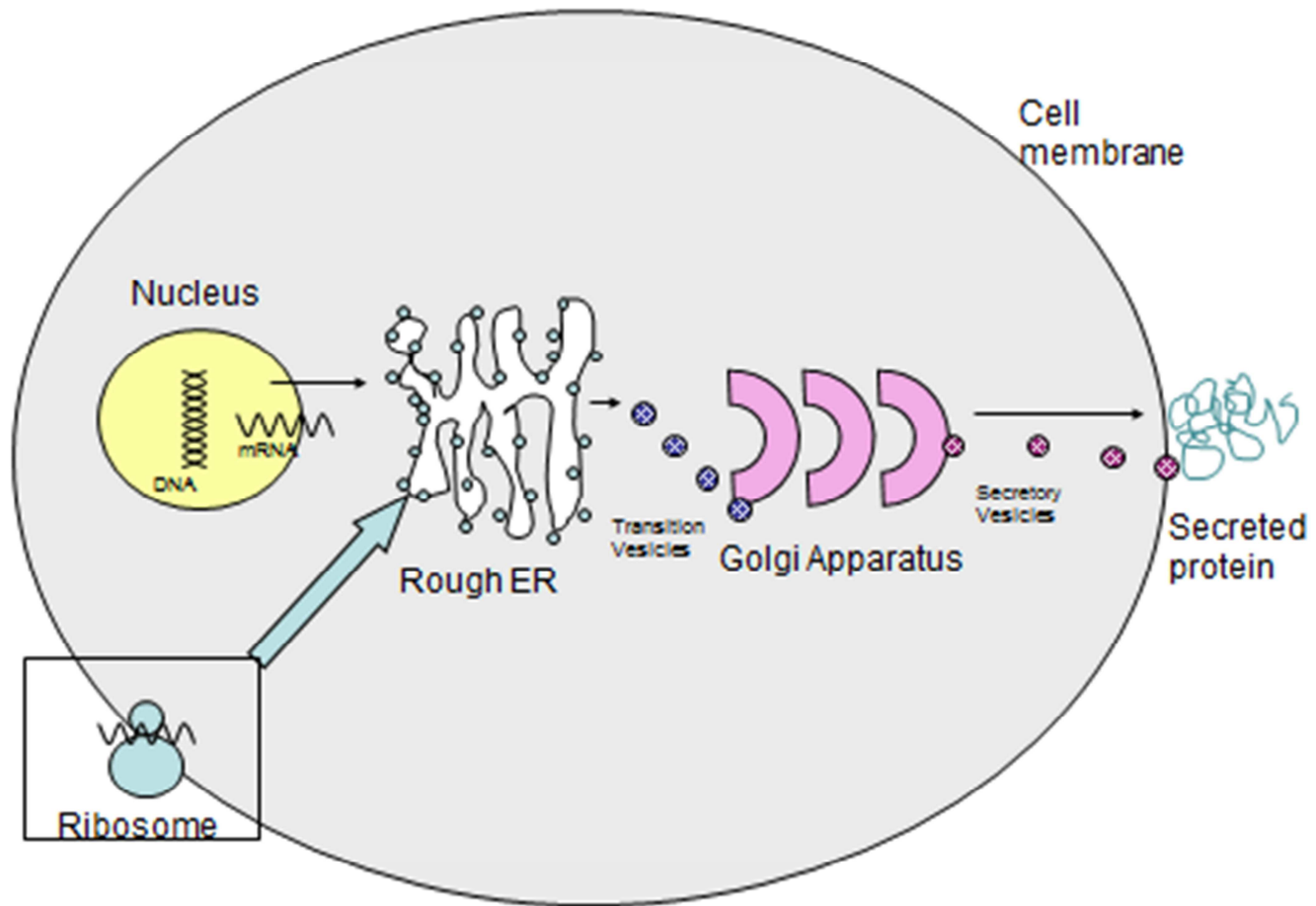


Figure 74. Schematic diagram of protein synthesis, intracellular trafficking and secretion.

Newly synthesised proteins entering the ER undergo a series of post-translational modifications such as N-linked glycosylation, signal peptide cleavage, and di-sulphide bond formation (Bateman et al., 2009). These modifications dictate how the proteins fold and direct the protein to attain the correct secondary and tertiary structures.

Protein folding is assisted by chaperones, co-chaperones, foldases and oxidoreductases. These assistant proteins prevent misfolded proteins from aggregating via exposed hydrophobic sequences and provide an environment conducive to correct protein folding. Enzymes such as protein disulphide isomerases (PDI) catalyse disulphide bond formation and exchange. Other ancillary proteins are involved in securing and delivering the energy requirement for protein folding and in maintaining the correct redox state to permit the reversible formation of disulphide bonds in the ER lumen (Boot-Handsford and Briggs, 2010).

The ER quality control mechanisms ensure that misfolded proteins do not accumulate or progress along the secretory pathway. Instead they are kept in the ER and targeted for degradation (Anelli and Sitia, 2008). This occurs by two mechanisms. Firstly, the protein can be returned to the cytoplasm where it is ubiquitinated which targets it for degradation by proteasomes during ER-associated degradation (ERAD) (Brodsky, 2007). Alternatively, portions of the ER become engorged with misfolded protein and are budded off to become an autophagosome. This fuses with a lysosome and the contents are degraded. This usually occurs with proteins that have aggregated or become multimers, and are unable to undergo ERAD (Bernales et al., 2007). This quality control system is operative in all cells at all times as up to 30% of proteins fail to attain their correct conformation (Shubert et al 2000) and must be disposed of by the systems described above.

Proteins abnormally accumulating in the ER trigger so called ER stress; a condition also caused by many different stimuli including heat shock, energy deprivation, hypoxia, metabolic dysfunction and drugs such as tunicamycin, which inhibits N-linked glycosylation, and thapsigargin which disrupts ER calcium ion balance. When ER stress is due to accumulating unfolded or misfolded protein within the ER, ER stress goes on to trigger the so called unfolded protein response (UPR) in an attempt to restore protein folding homeostasis (Boot-Handsford and Briggs, 2010). The UPR is a conserved cellular mechanism that protects cells against accumulation and aggregation of misfolded proteins during synthesis. It achieves this by stopping protein translation and

upregulating the expression of chaperones that drive protein folding (Hetz, 2012). When the aggregation of misfolded or damaged protein exceeds the capacity of the UPR, it can no longer protect the ER from stress and activation of apoptosis is triggered (Gardner et al., 2013).

The level of ER stress experienced by a cell is related to the amounts of protein passing through the cell's ER. Professional secretory cells such as hepatocytes, insulin producing beta cells of the pancreas, and antibody-producing lymphocytes are particularly susceptible to ER stress, as are other strongly secretory cells such as chondrocytes, osteoblasts, and fibroblasts (Rutkowski and Kaufman, 2007). It is logical therefore, to assume that ameloblasts, the specialised ECM secreting cells in tooth enamel development, are also highly susceptible to ER and in fact secretory ameloblasts in wild type mice have been shown to ubiquitously express genes characteristic of an activated UPR (Tsuchiya et al., 2008). The UPR triggers a number of cell responses with the aim of relieving ER stress and restoring proteostasis; typical responses include; increasing the volume of the ER, increasing chaperone synthesis and damping down transcription of client proteins transiting the ER (Ron and Walter, 2007). Under persistent exposure to ER stress, the cells may reduce the stress to acceptable levels via the UPR, though this is not without consequence. In fact, if the levels of ER stress become unacceptable a signalling cascade is triggered by IRE-1 mediated JNK phosphorylation and through the activity of Chop, and may result in the cell undergoing apoptosis, which may have pathogenic consequences. This can occur in metabolic diseases such as type II diabetes, where ER stress is crucial in insulin resistance. This increases demand on the insulin-producing beta cells of the pancreas. The increased insulin load causes elevated and persistent ER stress which can result in beta cell apoptosis and the subsequent need for insulin therapy (Lin et al., 2008; Zhang and Kaufman, 2008).

The unfolded protein response (UPR) has developed to counteract any stresses that occur in the ER due to the misfolding of proteins. The UPR is a complex homeostatic mechanism that has developed in mammalian cells to maintain the protein folding equilibrium within the ER (Boot-Handford and Briggs, 2010).

In order to overcome the problems associated with ER stress, a four-pronged response pathway has developed. This is discussed below with reference to the data presented in this thesis and obtained elsewhere in the research program.

1) Transcriptional and Translational attenuation

The first response to ER stress is to reduce the general secretory load by transcriptional (Wu and Kaufman, 2006) and translational attenuation (Scheuner et al., 2001). The synthesis of new protein is decreased to prevent further accumulation of unfolded protein in the ER. Interestingly, the data present in section 3.5.3 suggests that amelogenin transcription is significantly attenuated in Y64H mice which appears to be an attempt to reduce the secretory load. However, as evidenced by the intracellular accumulation of Y64H amelogenin in affected ameloblasts, this strategy is not sufficient to relieve the ER stress. The issue may be that amelogenin is synthesised in huge amounts (it is the major secretory product of ameloblasts) and though transcription is reduced the amount of protein translated is still evidently enough to overcome this initial line of defence against ER stress.

2) Upregulation of ER chaperone proteins

The second response to ER stress is the upregulation of ER chaperone protein genes such as binding immunoglobulin protein (BiP) (also known as 78 kDa glucose-regulated protein (GRP-78) or heat shock 70 kDa protein 5 (HSPA5)) and enzymes (e.g. protein disulphide isomerase, sarco/endoplasmic reticulum calcium ATPase) to increase the protein folding capability of the ER (Harding et al., 2003).

BiP is multifunctional; it is a classic chaperone molecule whose expression is increased when proteins misfold. BiP binds exposed hydrophobic regions on the misfolded proteins in an attempt to direct them towards the normal folding pathway by reducing the potential for aggregation driven by interactions between exposed hydrophobic regions on the misfolding proteins (Bertlotti et al., 2001). In respect of this thesis, the question asked was: is BiP expression upregulated in ameloblasts affected by Y64H amelogenin mutation, as the UPR attempts to relieve ER stress? To answer this, BiP mRNA expression levels from wild type and Y64H affected ameloblasts were compared by quantitative RT-PCR. The results shown in figure 62 show that BiP expression was elevated but this did not reach statistical significance in this set of experiments. However, the qualitative detection of BiP mRNA on sections of early secretory stage ameloblasts from wild type females and female Y64H mice heterozygous for the mutation (using *in situ* hybridisation) showed very obvious increased levels of BiP mRNA in Y64H ameloblasts. This work was carried during the

research program by Dr Martin Barron and is reproduced in figure 75 to emphasise the result.

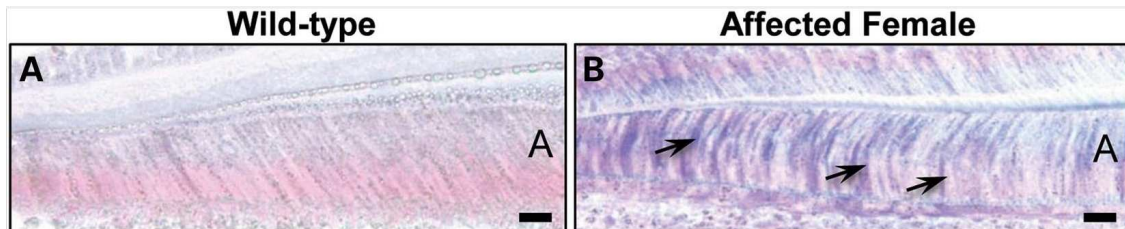


Figure 75. In situ hybridisation: BiP protein in early secretory stage ameloblasts from wild type and Y64H affected female mice. The darker blue staining, indicates clear upregulated BiP expression in affected ameloblasts (arrowed). Reproduced under Creative Commons Attribution License. Modified from figure 3 published in: “Endoplasmic reticulum stress in amelogenesis imperfecta and phenotypic rescue using 4-phenylbutyrate”; by Brookes et al 2014 Hum. Mol. Genet. (2014) 23 (9): 2468-2480. Direct link: <http://www.ncbi.nlm.nih.gov/pmc/articles/PMC3976337/>)

The *in situ* hybridisation results in figure 75 suggested that BiP expression was indeed increased in ameloblasts affected by the Y64H amelogenin mutation indicating that affected ameloblasts were upregulating chaperone production in an attempt to increase the probability of correct protein folding in the ER. An obvious question here is: why is the increase in BiP mRNA levels so much more convincing using *in situ* hybridisation compared to quantitative RT PCR? The likely answer is due to the fact that quantitative RT PCR is carried out on dissected tissue samples; i.e. the secretory stage mouse incisor enamel organs, measuring a few millimetres in length and a couple of hundred microns in thickness. The levels of BiP mRNA were measured relative to the *Gapdh* gene, a so called “housekeeping” gene we assume is expressed at constant levels in all cells. The ameloblasts are a single monolayer of cells within the enamel organ and are therefore a minority of the total cell population. Hence, any increase in *Bip* expression occurring in affected ameloblasts is lost to some extent (i.e. diluted/averaged out) against the lower levels of *Bip* expression in the non-ameloblast cells of the enamel organ. This demonstrates a potential pit fall when using quantitative RT PCR to measure gene expression in a sub population of cells within a larger tissue or organ and emphasises why it is important to support the PCR data by using a technique such as *in situ* hybridisation which is more sensitive to changes in gene expression within single cells.

It is worth noting that not all ameloblasts in the Y64H amelogenin affected female mouse shown in figure 75 are stained heavily for BiP (this further reinforces the point made above how quantitative RT-PCR can only provide ensemble gene expression data that are averaged over all cells present in the sample). This staining pattern is to be expected since as described in the Introduction (section 1.3.4.1); the amelogenin gene is present on the sex chromosomes. Thus females heterozygous for the Y64H mutation have 2 copies of the amelogenin gene; one on each chromosome. During early embryogenesis one of the X-chromosomes is randomly inactivated so that 50% of the ameloblasts present in an affected heterozygous female are totally normal (expressing wild type amelogenin) while the remaining 50% are affected as they express Y64H mutated amelogenin. This is a very important point and will be referred to later.

Later in the UPR there is an increase in the transcription of ERAD components to increase the ability of the cell to eliminate misfolded proteins via the ubiquitin-proteasome pathway (Zhang and Kaufman, 2008). However, this was not investigated in the Y64H amelogenin mutant mice.

From the above discussion it is clear that the UPR attempts to relieve stress by reducing general protein synthesis, increased the cell's ability to dispose of misfolded protein and has increased the ability of the ER to direct proteins away from misfolding via hydrophobic interactions towards the correct folding pathway via the increased production of chaperones. If these measures fail to relieve stress the UPR switches from a pro-survival mode and directs the cell towards death via apoptosis (Fribley et al 2009).

3) NF κ B activation

The third response is NF κ B activation for the mediation of immune and anti-apoptotic responses (Baeuerle and Baltimore; 1996). This is known as the ER overload response (EOR) as it is triggered by accumulation of membrane proteins in the ER. NF κ B activation was not investigated as part of this thesis with regards to the Y64H amelogenin mutation, as amelogenin is not a membrane protein. NF κ B activation is a highly complex situation with differing and opposing effects dependent on the cell type.

4) Apoptosis

If the UPR cannot relieve ER stress, it goes on to drive cells towards apoptosis which protects the organism by removing damaged cells that are expressing the problem mutation (Ron and Walter; 2007). Naturally, if the stressed cells comprise a significant

bulk of the tissue or organ then the effects can be catastrophic. Apoptosis is important in tissue homeostasis maintenance (Zhang et al, 2002). Dysregulation of apoptosis has been implicated in many diseases such as increased apoptosis in neurodegenerative disease, diabetes and AIDS, and altered apoptosis in cancer and autoimmune disease (Boot-Handsford and Briggs, 2010; Tsai and Weissman, 2010).

There are 3 molecular signalling pathways known to be involved in modulating the various UPR responses described above and these will now be discussed with reference to data presented in this thesis and obtained elsewhere in the research program.

4.9.1 Modulation of the UPR

The ER responds to increases in misfolded protein levels via three pathways activated respectively by the transmembrane ER-stress inducing proteins inositol requiring enzyme-1 (IRE1), pancreatic ER eukaryotic initiation factor (elf)-2a kinase (PERK), and activating transcription factor - 6 (ATF-6). These three proteins are all associated with the luminal side of the ER inner membrane and continually monitor the status of the ER cargo as it transits the ER (Boot-Handsford and Briggs, 2010). Figure 76 is a schematic for the proteins involved in the unfolded protein response in their unstressed state. The multifunctional nature of the folding chaperone BiP is exemplified again because BiP also plays a key role in detecting misfolded proteins in the ER. Under normal conditions with basal levels of misfolded proteins entering the ER, BiP is found associated with the 3 transmembrane receptors IRE1, PERK and ATF-6. While BiP remains bound to these receptors they are dormant and the UPR is not active. However, as levels of misfolded protein increase BiP binds to the exposed hydrophobic domains of the misfolded protein and the transmembrane receptors are activated (Bertolotti et al., 2009). The consequences of activating these receptors are described next.

Figure 77 shows a schematic for the proteins involved in the UPR in the stressed state, when the UPR is activated. BiP is removed from the cell surface receptors to act as a chaperone for the unfolded protein. The results from Q-RT-PCR analysis of wild-type and Y64H mutant amelogenin mice incisors showed an increase in *Chop* and a decrease in *Amelx* expression. This suggests that the PERK pathway has been activated,

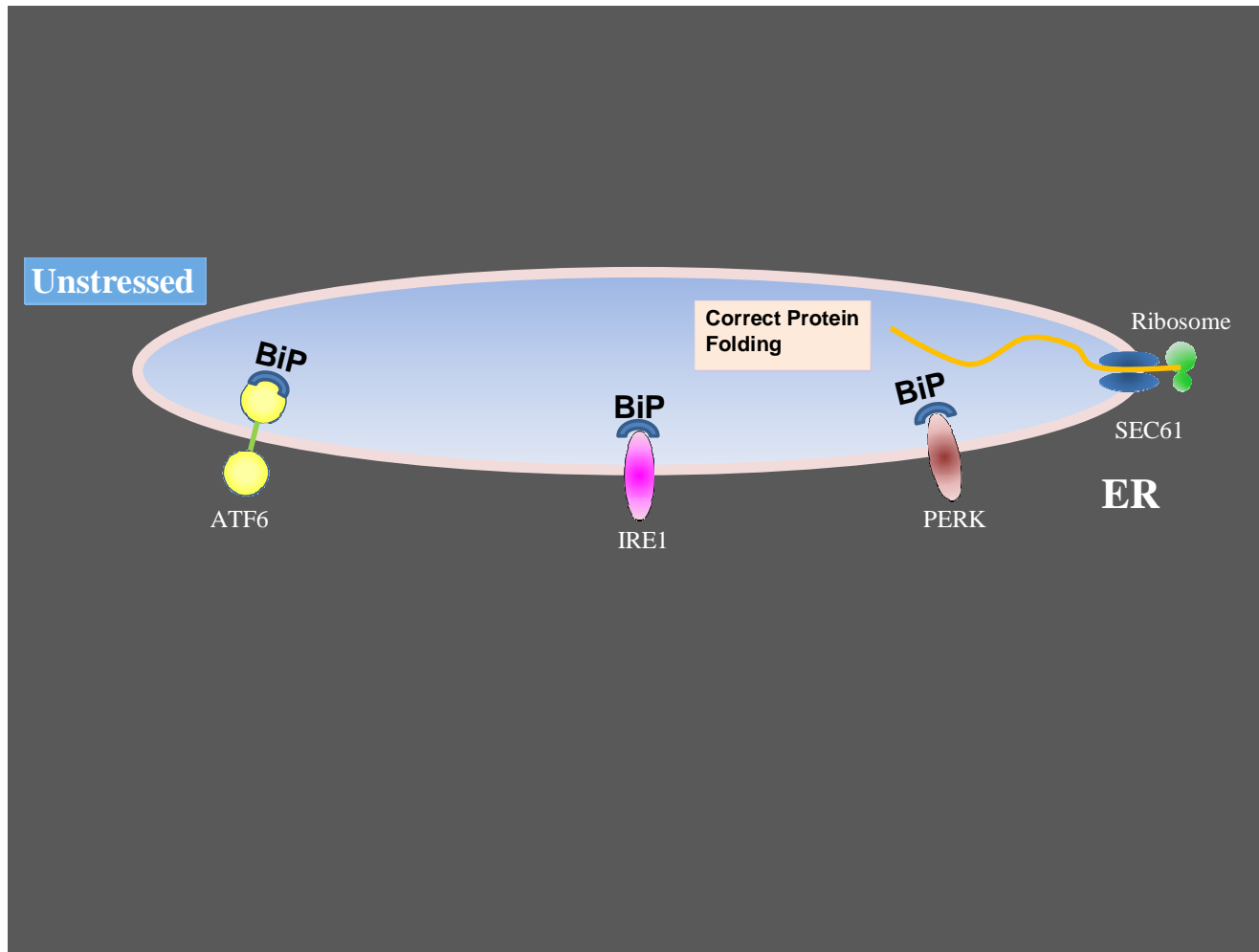


Figure 76. Diagram to show the protein receptors of the unfolded protein response (UPR) when the cell is in an unstressed state – UPR not activated.

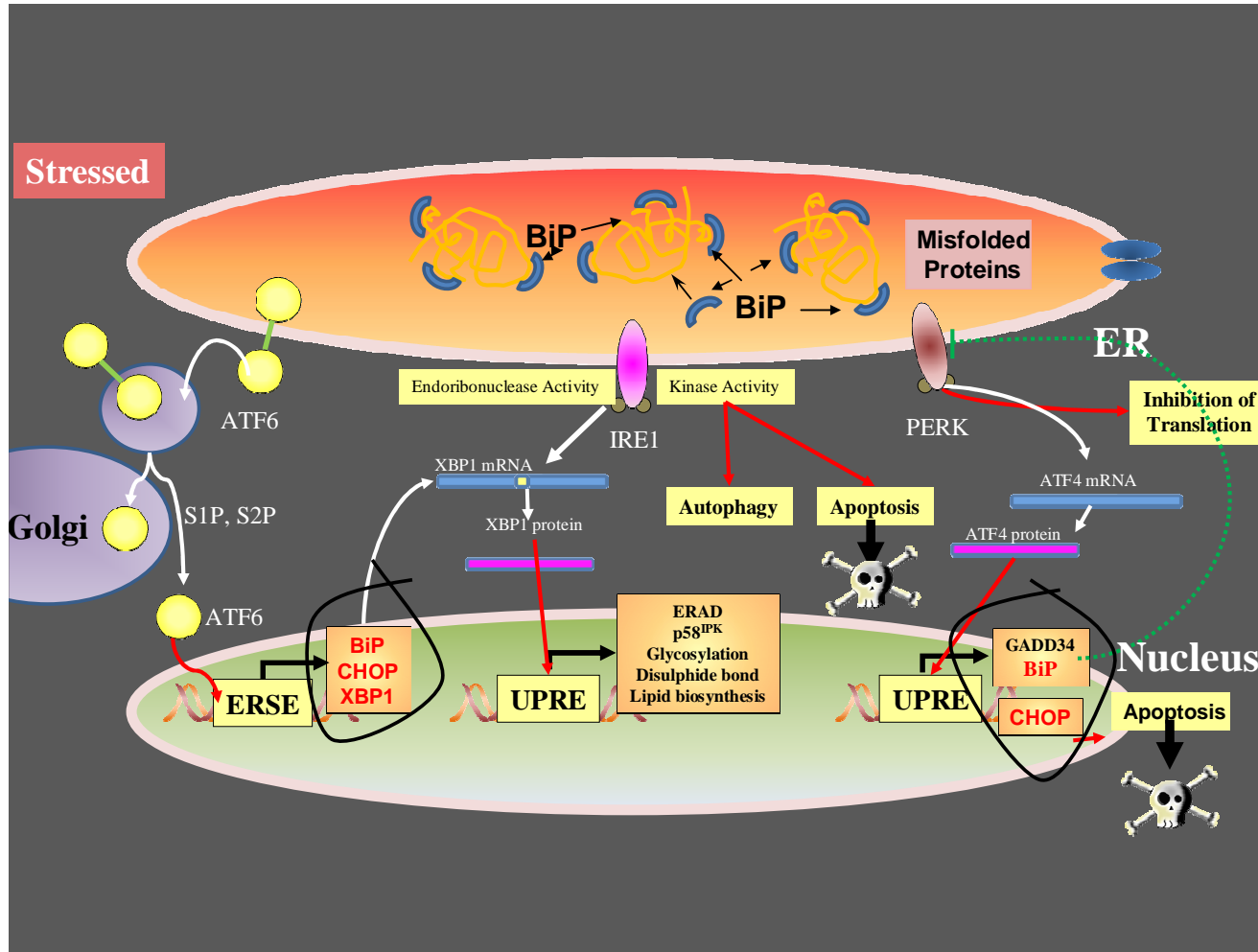


Figure 77. Diagram to show the activation of the protein receptors in the unfolded protein response when the cell is in a stressed state – UPR activated.

4.9.1.1 The IRE1 Pathway

Dissociation of BiP (HSPA5/GRP78), the resident HSP70 orthologue in the ER, from IRE1 (figure 77) due to detection of unfolded or misfolded protein initiates the splicing of XBP1. Spliced XBP1 is a potent transcriptional activator that increases expression of a subset of UPR genes involved in the efficient protein folding, maturation and degradation in the ER (Lee et al., 2003; Schroder and Kaufman., 2005). This is described in more detail below, but the main outcome from this pathway is to switch off translation of protein in the ER lumen and reduce ER stress.

Once the binding equilibrium between BiP and IRE1 is disturbed by the presence of misfolded protein in the ER, IRE1 oligomerises in the plane of the ER membrane, triggering autocatalytic phosphorylation of the cytoplasmic domain and activation of its ribonuclease activity. IRE1 is an endoribonuclease that catalyses the unconventional splicing of mRNA coding for x-box binding protein 1 (XBP1). Spliced XBP1 upregulates the transcription of several genes involved in the initial UPR responses described above, i.e. up regulation of chaperones and proteins involved in ERAD (Todd et al., 2008). IRE1 also catalyses cleavage and destruction of a subset of mRNA's linked to the rough ER, reducing the entry of new proteins into the ER lumen. The activated, phosphorylated form of IRE1 also interacts with tumour necrosis factor receptor associated factor 2 (TRAF2), activating JUN N-terminal kinase (JNK), which has downstream involvement in apoptosis and autophagy (Ogata et al., 2006; Szegezdi et al., 2006; Oh and Lim, 2009).

GRP94 is the only HSP90-like protein resident in the ER. GRP94 is a ubiquitously expressed chaperone protein with increased expression in the secretory tissues. The most important role for GRP94 is in directing the folding and/or assembly of secreted and membrane proteins. GRP94 is more selective than other ER chaperones. Its clients include integrins, immunoglobulins, IGF and TLR. The only common feature between them all is the presence of disulphide bonds. *In vitro* As the ER workload increases, the level of GRP94 transcription is co-regulated with other chaperones to increase the protein folding efficiency and to decrease the chance of misfolded proteins leaving the ER.

BiP and GRP94 are the most abundant ER proteins, and not just when the ER is undergoing stress. GRP94 follows BiP in folding immunoglobulins and thyroglobulins. IGF interacts with GRP94 and not BiP. Different proteins may have different chaperone requirements. GRP94 cooperation with BiP is not an inherent property of GRP94's mode of action. GRP94 has not been shown to act with lectin chaperones. Mammalian cells show a compensatory relationship between

chaperones. BiP knockout, BiP cleavage by subtilase, or BiP mutations cause expression of GRP94, PDI, calreticulin and Ep57. Silencing of calreticulin increases the expression of GRP94 and PDI, and calreticulin null embryonic fibroblast show increased levels of GRP94 and other ER proteins. However, GRP94 null cells do not demonstrate increased expression of other chaperones. BiP +/- mice show an adaptive transcriptional response with induction of chaperones including GRP94. GRP94 +/- mice do not show increased levels of BiP, calnexin or calreticulin. GRP94 has roles in protein folding, calcium binding and targeting proteins to the ERAD.

The results shown in this thesis (section 3.5.3) show that XBP1 and GRP94 were indeed upregulated in Y64H mice. Although statistical significance was not reached in the data reported here, later analyses using increased numbers of animals and carried out by Dr Martin Barron University of Manchester (Brookes et al., 2014) showed that the upregulation was significant. Amelogenin transcription was found to be statistically down regulated in this thesis (figure 62). The reason for the difference between the data reported here and the data obtained in Manchester (in terms of reaching mathematical significance) is unclear. However, the work presented here was carried out early in the research program and it may be as simple as the dissection technique improved with practice and the diluting effect of non-ameloblast cells (see section 2.5.2) was less of an issue. Regardless, these data strongly suggest activation of the IRE1 branch of the UPR is present in Y64H mice. It would appear that the UPR is attempting to relieve the ER stress caused by Y64H amelogenin retention in the ER by reducing the transcription of new amelogenin in the ameloblasts.

4.9.1.2 The PERK pathway

Dissociation of BiP from PERK aims to reduce protein load in the ER by switching off protein synthesis through phosphorylation of the α -subunit of eukaryotic translation-initiation factor 2 α (eIF2 α) which in turn increases translation of activating transcription factor 4 (ATF4) mRNA (Harding et al., 1999). ATF4 activates the expression of several UPR target genes involved in antioxidant responses, such as the transcription factor Nrf2, apoptosis, and autophagy (Harding et al., 2003; Cullinan and Diehl, 2004).

PERK is a transmembrane protein with a C-terminal cytoplasmic domain with serine/threonine kinase activity, and an ER luminal domain that binds BiP in its inactivated state, similar to IRE1. BiP dissociates from PERK as the levels of

misfolded protein increases in the lumen of the ER, leading to autophosphorylation, oligomerisation and activation of the kinase domain. PERK signals downstream effectors such as GADD34 and CHOP. Activated PERK phosphorylates and inactivates eukaryotic translation initiation 2 α (eIF2 α). This is required for 80S ribosome assembly. As a consequence of this, a down regulation of protein synthesis occurs, decreasing the flow of newly synthesised unfolded protein into the ER. Interestingly, some mRNAs such as that encoding ATF4, a 39 kDa transcription factor, have a more efficient translation when eIF2 α is phosphorylated. ATF4 mRNA has a series of 5' open reading frames that result in inefficient translation under non-stressed conditions (Lu et al., 2004). Phosphorylated eIF2 α alters the reading dynamics of these open reading frames, resulting in increased ATF4 synthesis. ATF4 is a member of the cAMP-response element binding (CREB) family. It activates genes involved in the UPR such as the chaperones BiP and GRP94, genes involved in oxidative stress suppression, and genes involved in amino acid transport and metabolism. ATF4 also triggers the expression of CHOP (CCAAT/enhancer-binding protein homologous protein) which has been associated with ER-stress induced apoptosis (Zinszner et al., 1998).

CHOP is also known as growth arrest and DNA damage-inducible gene 153 (GADD153) and is a component of the ER stress apoptosis pathway. CHOP is a 29 kDa protein consisting of 169 amino acids in humans and 168 amino acids in rodents. The GADD genes are induced by genotoxic stress and growth arrest signals. C/EBP's form a family of transcription factors that regulate genes involved in physiological processes such as immune functions, cell proliferation and differentiation. CHOP protein consists of 2 functional domains – an N terminal transcriptional activation domain and a C terminal basic leucine zipper (bzip) domain, made up of a basic amino acid rich DNA binding region and a leucine zipper dimerization motif. CHOP contains 2 serines at positions 79 and 82 that are capable of acting as substrates of the p38 Map kinase family. The bzip domain is important for CHOP induced apoptosis. C/EBP members are capable of forming homodimers and heterodimers. CHOP is a heterodimer. *CHOP* is able to inhibit C/EBP's function and act as an activator of other genes.

CHOP is ubiquitously expressed at very low levels and is present in the cytosol. Under stress conditions, CHOP is induced and accumulates in the nucleus. CHOP has been identified in stress conditions such as UV radiation, genotoxic stress, and nutrient depletion. CHOP expression is mainly regulated at the transcriptional level. Transcriptional upregulation occurs in response to ER stress. BiP acts as a sensor of unfolded proteins. Under normal 'non-stressed' conditions, BiP binds to the luminal domains of the stress transducers PERK, IRE1 α and

IRE1 β to prevent homodimerisation transport to Golgi. During stress, BiP binds to the unfolded proteins instead thereby releasing the transducers into their active state.

The PERK/eIF2 α signalling pathway induces CHOP in ER stress and is dominant over ATF6 and IRE1/XBP1 signalling pathways. For maximum CHOP induction though, all three pathways are necessary. Activated PERK phosphorylates SER51 on Eif2 α which causes blocking of the Met-tRNA binding to ribosome by decreasing Eif2 β turnover, resulting in a decrease in the general translation due to decreased recognition of AUG initiation codon. ATF4 mRNA is still translated due to small upstream open reading frames (ORF's). ATF4 can bind to the ATF/CRE consensus sequence 5'-TGACGTCA-3' and the amino acid regulatory element (AARE) core sequence 5'-ATTGCATCA-3'. BiP-free Patf6 α (p) and pATF β (p) are transported the Golgi for cleavage by Site-1 and Site-2 proteases. The cleaved N-terminal domains Patf6 α (N) and Patf6 β (N) are transported to the nucleus, where they bind to the ERSE due to their bZip domains. This binding with ERSE activates NF-Y trimer. Activated IRE1 α and IRE1 β cleave XBP-1 mRNA, which removes a 26-nucleotide intron, triggering an ORF switch to yield bZip and transactivation domains, binding ERSE and UPRE sequences in interaction with NF-Y.

CHOP expression is also regulated by mRNA stability. CHOP mRNA 5' UTR consists of highly conserved UORF's which repress CHOP translation. CHOP undergoes phosphorylation by Map Kinases during ER stress. CHOP overexpression results in cell cycle arrest and/or apoptosis. BiP overexpression results in decreased CHOP induction and thus decreased apoptosis. CHOP null mice have reduced apoptosis in response to ER stress. All these show that CHOP is important in ER stress induced apoptosis.

The results (section 3.5.3) suggested that *Chop* is upregulated in Y64H mice (with the caveat mentioned in section 3.5.3). However, later work carried by Martin Barron as a continuation of the work described here showed that *Chop* is significantly upregulated in Y64H mice. This data strongly suggests activation of the PERK branch of the UPR in Y64H mice. Since *Chop* induces apoptosis it appears that the UPR acting in Y64H is unable to relieve ER stress via survival strategies and instead signals cell death as the final solution to the problem.

4.9.1.3 The ATF6 pathway

ATF6 is a 90 kDa transmembrane protein with a cytoplasmic domain which contains a transcription factor with a bZIP motif, and a luminal domain that binds to BiP. When an increase in unfolded protein in the ER lumen is detected, BiP dissociates and the Golgi-localisation sequences in the ER luminal domain of ATF6 are exposed (Shen et al., 2005). ATF6 then translocates to the Golgi where the protein is cleaved by site 1 and site 2 proteases (Ye et al., 2000). This releases the 50 kDa cytosolic domain as an active transcription factor, known as ATF6₅₀. ATF6₅₀ moves to the nucleus where it activates genes involved in ER quality control such as BiP, XBP1, ERAD components and apoptosis inducing *Chop*.

We have already discussed the upregulation of XBP1 and *Chop* with reference to the IRE1 and PERK pathways described above. That upregulation of BiP was also observed (page Figure 63 Section 3.5.3). Although not statistically significant in the data reported here, later analyses carried out by Dr Martin Barron, University of Manchester, (Brookes et al., 2014) showed that BiP upregulation was significant. This data strongly suggests activation of the ATF6 branch of the UPR in Y64H mice is activated. As described above BiP is bound to IRE1, PERK and ATF6 in non-stressed cells but the presence of misfolded proteins in the ER causes BiP to dissociate from IRE1, PERK and ATF6 resulting in their activation. Once free, BiP acts as a chaperone and binds to hydrophobic regions on the misfolded proteins in an attempt to reduce protein aggregation. Upregulation of BiP is another classic UPR response designed to relieve ER stress.

In summary, the UPR in the Y64H ameloblasts attempts to relieve the ER stress as evidenced by the upregulation of prosurvival factors (BiP, XBP1 and GRP94). However, the clear upregulated expression of *Chop* suggests that the UPR cannot rescue the cells from ER stress and commits the cells to apoptosis. It appears therefore that ameloblast ER stress and subsequent apoptosis is the pathological driver for this form of amelogenesis imperfecta. The validity of this hypothesis is explored in the next section by surveying the literature with regard to other connective tissue diseases caused by ER stress arising from protein mutations.

4.9.2 ER stress induced diseases

Mutations identified in ECM structural proteins and their associated post-translational processing enzymes show that the resulting pathology depends upon the function of the protein, the nature of the actual mutation (premature termination,

nonsense) and its distribution in the body's tissues. The most commonly explored ECM mutations and diseases focus on collagen and its associated proteins and enzymes; with emphasis on secretion, proteolytic cleavage of the teleopeptide and fibril formation. The effects on the ECM resulting from these mutations are due to intracellular degradation of the mutant protein prior to secretion and/or release of faulty proteins that disrupt the ECM.

Liang et al., 2014 investigated *Col2a1* mutations in 13 mouse models to study the resulting phenotypes and possible mechanisms involved in various chondrodysplasias (lethal such as hypochondrodysplasia or deforming such as Stickler syndrome) or hip and knee joint diseases. All of the above are triggered by mutations in the *Col2A1* gene encoding the $\alpha 1$ chain of procollagen type II and display the common symptoms of a disordered growth plate and slowed endochondral ossification. The researchers showed that the severity of the disease depended on the mutation type (large deletion vs. point deletion), mutation position (Y chromosome or X chromosome) and heterozygous or homozygous (i.e. whether some normal type II collagen remained). The mutations in the $\alpha 1$ chain of procollagen type II gene ultimately lead to apoptosis via a series the UPR in the cells. Gaiser et al., 2002, and Arita et al., 2002 reported accumulation of the mutated collagen in the endoplasmic reticulum with an associated decrease in the amount of collagen type II secreted into the ECM. Further investigations by Chung et al., 2009 and Esapa et al., 2012 showed that these retained mutant collagen II molecules could induce ER stress and activate the unfolded protein response (UPR) which works to remove the misfolded collagen and maintain homeostasis. This is a direct parallel to what is observed in the Y64H amelogenin mutation.

Osteogenesis imperfecta (OI) is a disorder of the connective tissues caused by mutation in the genes encoding collagen type 1 (*COL1A1* and *COL1A2*). Collagen 1 is the principal structural protein of bone and consists of fibrils of 2 collagen 1 alpha 1 chains $\alpha 1$ and 1 collagen 1 alpha 2 chain. The OI phenotype, like AI, depends upon the nature of the mutation and ranges from mild risk of bone fractures to perinatal lethality. Lisse et al., (2008) used an ENU-mouse model with a dominant mutation in the C-propeptide domain of collagen 1. Heterozygous mice displayed a severe to lethal phenotype associated with ER stress, and caspase 3 and 12 activation within the osteoblasts. Immunofluorescence studies showed retention of the pro alpha (1) collagen chains in the ER. QPCR studies using primary calvarial osteoblasts showed elevated levels of BiP (1.5 to 2.2 fold increase), HSP47 (1.5 to 2.28 fold increase) and CHOP (3.7 fold increase). Caspase 12 is a specific mediator of the ER stress induced UPR in skeletal tissues

(Nakagawa and Yuan, 2000) and its elevation in these models is an indicator for apoptosis.

There is also a growing body of evidence for the role of ER-stress and the UPR in age related disorders. The pathogenesis is the destruction of critical cells due to the formation of highly insoluble aggregated of the misfolded proteins and evidence has been shown for retinitis pigmentosa (Saliba et al., 2002), Alzheimer's disease (Mann et al., 1985), prion disease (Forloni et al., 1993), Huntington's disease (Zuleta et al., 2012) Parkinson's disease (Gorbatyuk et al., 2012), cancer (Mahadevan and Zanetti., 2011) and glaucoma (Anholt and Carbone, 2013). Some of these diseases will be discussed next.

Retinosis pigmentosa (RP) is a group of inherited diseases that, due to the progressive death of rod and cone photoreceptors, causes progressive blindness (Dryja et al., 1990). Autosomal dominant RP is caused by mutations in rhodopsin. The most common mutation in the US is a P23H mutation resulting in protein misfolding and the accumulation of retained protein in the ER (Mendes et al., 2005), sometimes causing aggregates to form visible intracellular inclusions (Saliba et al., 2002). This is comparable to the histidine substitution investigated in this thesis and the accumulation of amelogenin aggregates in the ameloblasts. Large amounts of rhodopsin is produced by the rod photoreceptors and mutant rhodopsin induces the UPR highlighting the use of this cascade in photoreceptors for dealing with misfolding stress (Lin et al., 2008; Athanisiou et al., 2013). Interestingly, the P23H mutation in rhodopsin activates both the UPR and the heat shock response (HSR); both of which activate the proteasome downstream for destruction of misfolded proteins (Kosmaoglou et al., 2009). Treatment of P23H mutants in rats with Arimaclomol, an inducer of the HSR, has been shown to improve vision and protect against photoreceptor destruction (Lewin et al., 1998; Parfit et al., 2014). Ablation of CHOP did not protect the photoreceptors against P23H mutant rhodopsin triggered cell death (Adekeye et al., 2014).

Primary open angle glaucoma (POAG) is the most common form of glaucoma and is a hereditary, autosomal dominant mutation linked to chromosome 1q23-q25, known as MYOC. (Anholt and Carbone, 2013). MYOC encodes a 55kDa secretory glycoprotein, myocilin, Myocilin, like amelogenin, is normally secreted into an ECM where it interacts with various ECM proteins such as fibronectin, laminin, collagen and fibrillin-1 (Myung et al., 2003). Mutant myocilin has been shown to accumulate in the ER and induce the UPR (Sidrauski et al., 1998; Mori et al., 2000). Myocilin secretion in adult eyes is normally at a low level but can be activated by stress, especially by high levels of circulating cortisol, a well-known risk factor for glaucoma and a link to diabetes (Anholt and Carbone, 2013). Excessive production of normal

myocilin, production of misfolded myocilin or any protein associated with MYOG, has been shown to form aggregates that in susceptible patients (those with a genetic predisposition to glaucoma) overwhelm the UPR to eliminate them via the proteasome. These causes ER stress and activate apoptosis of the TM cells that regulate intraocular pressure. Thus POAG may result in adult onset protein aggregation followed by neurodegeneration similar to Parkinson's, Alzheimer's and AI related to the Y64H amelogenin mutation. A transgenic mouse containing the common Y437H MYOC mutation was created to study POAG (Zode et al., 2014). Adult mice with the mutation showed the glaucoma phenotype such as increased intraocular pressure, retinal ganglion cell death and axonal degeneration. The resulting mutant myocilin was not secreted into the aqueous humor as normal myocilin is, but accumulated in the ER of the TM cells. This is comparable to the accumulation of the Y64H amelogenin in the ER of ameloblasts. Chronic persistent ER stress resulted in TM cell death and increased intraocular pressure. Using the chemical chaperone phenylbutyric acid (PBA) prevented the glaucoma phenotype in the transgenic Y437H mice. PBA works by promoting secretion of the mutant myocilin into the aqueous humor and by reducing accumulation of the protein in the ER, hence preventing TM cell death (Zode et al., 2014; Shepard et al., 2007).

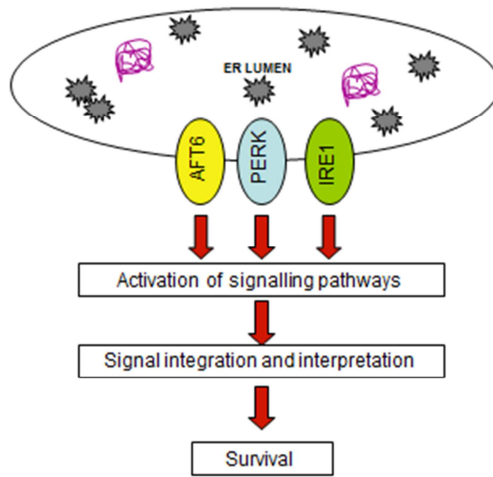
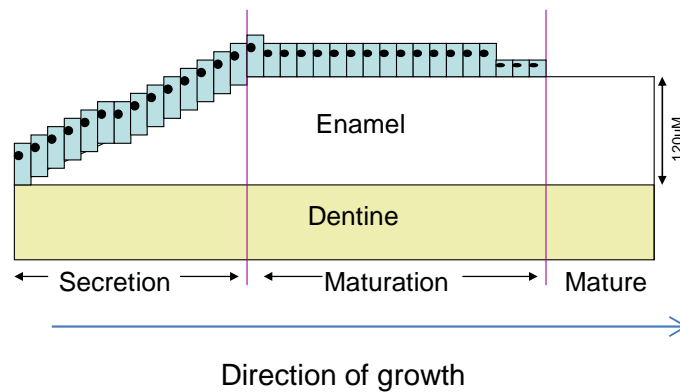
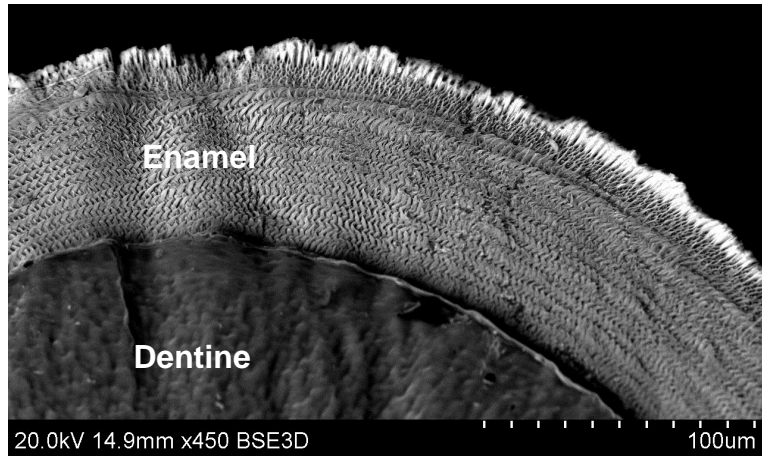
It is clear that in mutations in ECM proteins can result in potentially pronounced phenotypes associated with a range of pathologies. Interpreting the phenotype in the context of what is now understood of ER stress and its resulting consequences prompted an ultrastructural characterisation of the enamel phenotype in the mice affected by the Y64H amelogenin mutation to investigate whether this might provide further evidence of the etiology of the biomineralisation defects associated with the mutation.

4.10 Scanning Electron Microscopy of wild type and Y64H amelogenin mutant mouse incisors

To confirm whether the hypothesis that the ameloblasts in mice containing the Y64H amelogenin mutation do deal with the mutation via the UPR, the resulting effect impact upon the enamel phenotype, was investigated. It was hypothesized that the enamel in wild type mice incisors would appear completely normal, and that male mice homozygous for the Y64 mutation would have very poorly formed enamel. Female mice heterozygous for the Y64H mutation were expected to exhibit enamel, which at first was correctly formed, but then poorly formed once the switch from cell survival to apoptosis occurred in the UPR.

Imaging of transverse sections through erupted mice incisors corroborates the data from the immunohistochemistry staining and q-PCR analysis. The SEM in Figure 78

shows that in the wild-type tooth, enamel matured normally (see figures 63 and 64 in section 3.6). It can therefore be inferred that wild type amelogenin protein was secreted normally during the earlier secretory stage of amelogenesis. The enamel is secreted in an incremental fashion from the dentinenamel junction. The prisms exhibit the characteristic interwoven decussating pattern and the enamel is of normal thickness. The schematic shows the life history of the ameloblasts as they incrementally secrete enamel during secretion and enter the maturation stage. During this the UPR is helping the cell cope with the large secretory load of amelogenin by operating in prosurvival mode (as discussed in section 4.9).

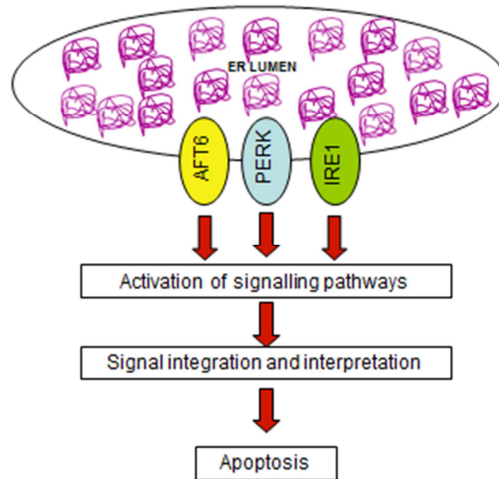
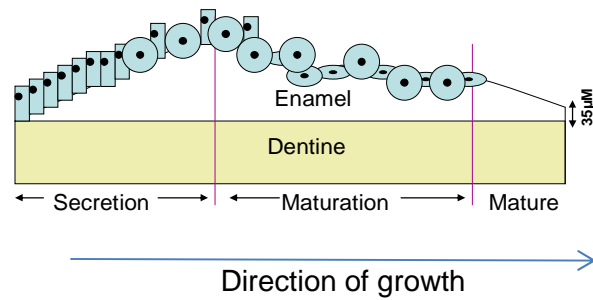
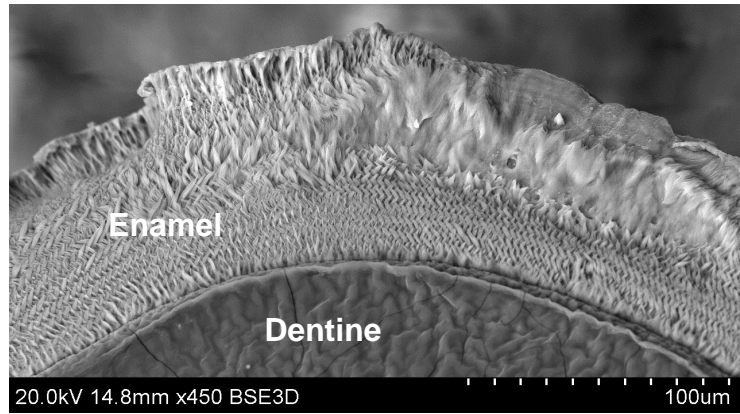


★ = Normally folded WT amelogenin

🌀 = Spontaneously misfolded WT amelogenin

Figure 78. Scanning electron microscopy image of a transverse section through a normal wild type mouse incisor (top panel). A corresponding schematic to show the progress of enamel formation is shown below (middle panel). Note that even in wild type ameloblasts some amelogenin misfolds and the UPR acts to promote cell survival. The UPR is active in wild type ameloblasts (Kubota et al., 2005).

By contrast, SEM analysis across a Y64H amelogenin female (heterozygous) mouse incisor displays the effects of the mutation on the phenotype (figure 79, and figures 65 and 66 in section 3.6). In heterozygous females about 50% of the ameloblast will be normal and 50% will be affected by the mutation (due to X-chromosome silencing) The initially secreted inner enamel closest to the dentinoenamel junction displays the characteristic interwoven pattern of prisms and looks normal; the affected ameloblasts are coping with the ER stress due to the UPR acting in pro-survival mode and are surviving (though their secretory activity is impaired as the Y64H amelogenin is accumulating intracellularly). However, their mere survival ensures the integrity of the ameloblast enamel layer and the unaffected ameloblasts evidently secrete enough amelogenin to produce normal looking enamel. Eventually the apparently normal enamel secretion is disturbed and the last enamel to be deposited (the outer enamel) is structurally abnormal and hypoplastic. It is hypothesised that the UPR switches from pro-survival to pro-apoptotic mode and affected ameloblasts die. This effectively destroys 50% of the ameloblasts and disrupts the ameloblast layer resulting in abnormal enamel secretion.



 = Misfolded mutated amelogenin

Figure 79. Scanning electron microscopy image of a transverse section through a female heterozygous mutant mouse incisor (top panel). A corresponding schematic to show the progress of enamel formation is shown below (middle panel). Note that in affected ameloblasts misfolded amelogenin stimulates the UPR. Initially the UPR promotes cell survival and the initial enamel layer appears normal. With time, the continuing ER stress switches the UPR to promote apoptosis which leads to disruption of the ameloblast layer and malformation of the outer enamel layer.

In males with the amelogenin mutation, all the ameloblasts are expressing the mutant amelogenin which isn't being secreted at all so there is very little enamel laid down. Any amelogenin that does get secreted is mutated so may not work properly in the matrix anyway (but the main point is that full length amelogenin is not even getting out of the cells to have a chance of forming the enamel). At first the ameloblasts are enduring the ER stress and the UPR is helping them to do this (e.g. by reducing amelogenin transcription). This is supported by figure 72 from Dr. Martin Barron where the ameloblasts in the early secretion stage look phenotypically normal apart from being engorged with vesicles. Eventually the UPR trips into apoptotic mode and all the ameloblasts die hence only a thin layer of enamel is produced that is far from normal in structure (because there is no full length amelogenin being secreted and the cells die early).

If these hypotheses are true, there are chemicals available that have been shown to have the ability to relieve ER stress by relieving the blockage in secretion or by inhibiting UPR induced apoptosis. If the mice were treated with such chemicals, it may free up the secretory pathway which would allow the ameloblasts to live but then we would see for the first time the effect of the mutation on how amelogenin behaves functionally once it is in the matrix. In males this would be a big question as all the amelogenin would be mutated. But it would remain to be seen if just restoring the secretory route would cure amelogenesis imperfecta. Other drugs might inhibit apoptosis and in the heterozygous females especially this would help by preventing the breakup of the ameloblast monolayer so leaving the 50% of the wild type ameloblasts to go on secreting a normal enamel layer (Brookes et al., 2014).

4.11 Summary

The work presented in this thesis was mainly concerned with the Y64H mutation in amelogenin, and how this impacted upon the normal structure-function status of the protein and results in amelogenesis imperfecta. The results presented in this thesis allow us to hypothesise that this single amino acid change caused a potential conformational change in amelogenin structure. Y64H amelogenin was shown to bind more strongly to itself. This in turn could cause the protein to aggregate abnormally in the ER, stall the secretory process and lead to ER stress. The normal structure of the ameloblast ER and Golgi apparatus is highly disturbed as a result with abnormal cytoplasmic vesicles packed with amelogenin. This triggers the unfolded protein response, which as indicated by the q-RT-PCR studies, reduced amelogenin transcription and elevated transcription of the UPR proapoptotic transcription factor *Chop*. Nucleation studies showed that the mutated amelogenin was able to nucleate hydroxyapatite mineral as well as the native protein. No significant difference was seen in the phosphate levels obtained for wild type or mutant amelogenin, alone or with 5 µg/mL enamelin, implying that the mutation in the amelogenin protein does not affect the proteins role in hydroxyapatite nucleation.

In vitro nucleation studies using a steady-state system showed that nucleation of hydroxyapatite mineral deposits was achieved with recombinant 32 kDa enamelin protein. Comparison to known hydroxyapatite nucleators showed that enamelin protein had some features in common, whereas amelogenin did not (Table 2). The amount of mineral deposited with wild type or Y64H mutant amelogenin under the same experimental conditions was similar, with or without the Y64H mutation and with or without the presence of recombinant 32 kDa enamelin. Therefore the overall conclusion from these *in vitro* nucleation experiments was that the amelogenin imperfecta phenotype observed in mice carrying the Y64H amelogenin mutation is not due to the Y64H amelogenin behaving differently from the wild type molecule in terms of its behaviour with respect to mineral nucleation.

Experiments were performed to investigate the importance of the 32 kDa enamelin processing product as a discrete entity during amelogenesis. The 32 kDa enamelin entity has been shown to be the predominant enamelin in pig enamel, and is the most widely studied enamelin protein due to its abundance and ease of collection. SDS-PAGE and western blot analysis of rat secretory enamel showed that the 32 kDa fragment was not the dominant enamelin species in the rat. Bioinformatics alignment of the amino acid sequences of enamelin from several

species showed that the cleavage sites for the 32 kDa enamelin are only present in the pig. Therefore, the 32 kDa enamelin fragment should be used with caution when investigating amelogenesis in general or in relation to other species.

Amelogenin has been well documented to assemble and form nanospheres, thought to be important for nucleation of hydroxyapatite. The presence of vacuoles full of unsecreted amelogenin in the ameloblasts of the Y64H amelogenin mutant mouse suggested premature/increased aggregation of the mutant protein (Barron et al., 2010). Protein-protein interaction studies *in vitro* using recombinant wild-type protein and Y64H mutant amelogenin showed that the Y64H amelogenin- Y64H amelogenin binding was 2 to 3 times greater than wild type amelogenin-wild type amelogenin binding. This led to the conclusion that the Y64H amelogenin molecules could aggregate within the ameloblasts and block the secretory pathway in mice carrying the mutation. This in turn would activate elevated levels of ER stress, triggering the UPR and driving the ameloblasts towards apoptosis. This hypothesis was supported by the data from quantitative PCR studies that showed that amelogenin was statistically significantly downregulated in the Y64H mutant mice, implying that the ER stress response and UPR is active, reducing protein synthesis to relieve ER stress and prevent apoptosis. The upregulation of *Chop* and *Bip* were also noted, although not statistically significant ($p < 0.05$) in this study (later shown to be, Brookes et al., 2014) indicating that the IRE1 and PERK pathways of the UPR were underway in the Y64H mice.

SEM analysis of the wild type and Y64H mice incisors showed that it was possible to identify where the UPR was unable to cope with the high levels of unsecreted, aggregated mutant amelogenin, and drives the ameloblasts towards apoptosis. This results in the structurally abnormal, hypoplastic enamel, typical of the AI phenotype.

The work presented in this thesis supports the work of Brookes et al., 2014 confirming that the Y64H amelogenin mutation is not a loss of function mutation but rather one that triggers ER stress, reduction of protein secretion and apoptosis of ameloblast cells. In the published study, mice with the Y64H mutation displayed the morphological characteristics of malformed tooth enamel displayed in the human equivalent amelogenesis imperfecta. The presence of the mutation caused the intracellular accumulation of the unsecreted protein, triggering apoptosis of the ameloblasts via ER stress and the UPR. They proposed that 4-phenylbutyrate, a drug already licensed for treatment of in-born errors of the urea cycle, could be a potential treatment for AI. Sodium phenylbutyrate is a histone deacetylase inhibitor

(HDACI). It is currently being investigated as a potential treatment for cystic fibrosis, cancer, motor neurone disease and haemoglobinopathies Sodium phenylbutyrate is a short chain aromatic fatty acid that undergoes β -oxidisation *in vivo* to form phenylacetate (PAA). PAA binds with glutamine to form phenacetylglutamine which is excreted via the urea cycle (Iannitti and Palmieri, 2011). It has also been proposed that sodium phenylbutyrate acts as a chemical chaperone. Kubota et al., 2006 investigating the signalling pathways involved in Parkinson disease, looked at the effects of phenylbutyrate on the accumulation of Parkin-associated endothelin receptor-like receptor (Pael-R). Several findings allowed the authors to conclude that phenylbutyrate was able to suppress ER stress by reducing the amount of misfolded protein collecting in the ER. These findings included; restoration of normal Pael-R expression and reduction of ER-stress with phenylbutyrate treatment, activation of ER-stress pathways and neuronal cell death with phenylbutyrate treatment, and the restoration of yeast viability in cells which failed to trigger an ER stress response under ER stress conditions following treatment with phenylbutyrate. Other studies investigating the effects of phenylbutyrate treatment include reversal of memory and learning deficits in Alzheimer disease mice models, proposing the use of phenylbutyrate to restore memory function in Alzheimer patients (Ricobaraza et al., 2009), the use of phenylbutyrate to prevent the accumulation of the toxic branched-chain amino acids and α -keto acids in Maple Syrup Urine disease (Brunetti-Pierri et al. 2011), efficacy of phenylbutyrate in the prevention of lipid-induced insulin resistance and β -cell dysfunction in overweight or obese men (Xiao et al., 2011). Phenylbutyric acid was also used to treat mice models for POAG with a Y437H mutation in MYOC (described in section 4.10.2).

A number of hypotheses were explored as part of this thesis.

Hypothesis 1: Is the 32 kDa enamel breakdown product conserved across all species? The majority of studies to date have used the porcine 32kDa enamel product due to its ready availability. To investigate this hypothesis, western blot analysis of porcine and rat enamel were used, as was a bioinformatics exploration of enamel sequences across many species. The data presented in this thesis showed that the 32 kDa enamel breakdown product was not the major fragment in rat enamel. A bioinformatics search of enamel sequences also revealed that the 32 kDa enamel product was not conserved across all species. This has significance for the use of the porcine 32 kDa enamel breakdown product as a model for full length enamel in *in vitro* studies.

Hypothesis 2: The AI phenotype generated as a result of the Y64H amelogenin mutation in mice is a result of the mutated protein behaving differently upon secretion. To investigate this hypothesis, *in vitro* nucleation studies were performed to explore the effect of the mutation on the ability of amelogenin, and amelogenin in conjunction with enamelin, to nucleate hydroxyapatite mineral. *In vitro* binding studies were also performed using the wild type and Y64H mutant amelogenin to investigate the effect of the mutation on protein-protein interactions. The steady state agarose gel nucleation studies showed that the Y64H mutation in amelogenin did not affect the way the amelogenin nucleated mineral, either alone or with the presence of 32 kDa enamelin. This implies that the mutant amelogenin does not behave differently with regards to ability to nucleate mineral in an *in vitro* system. The use of an *in vitro* microplate binding assay to investigate protein-protein interactions showed that the Y64H amelogenin bound with more affinity to itself and wild type amelogenin, than wild type amelogenin bound to itself. This may result in the Y64H mutant amelogenin forming aggregates that were contained in vesicles in the ameloblasts.

Hypothesis 3: The AI phenotype generated as a result of the Y64H amelogenin mutation in mice is a result of the mutated protein being retained in the ameloblast and not being secreted correctly. Similar mutations in other proteins have resulted in endoplasmic stress in cells, resulting in transcription and translation downregulation and ultimately apoptosis of the secretory cells. Quantitative PCR and SEM analysis of wild type and Y64H mutant mice incisors were performed to probe whether ER stress and the unfolded protein response could be responsible for the AI phenotype in Y64H mutant mice. The q-PCR data presented in this thesis showed that ER stress was a possible result of the AI genotype. A down-regulation in *Amelx* was noted, indicative of transcriptional and translational attenuation. Upregulation of genes involved in the UPR were also noted.

Future perspectives

In the 2014 paper, Brookes et al., performed *in vitro* transfection studies using COS-7 cells and wild-type or Y64H amelogenin. A significant increase in apoptosis was noted in the cells transfected with Y64H amelogenin. This was abolished by the addition of 0.5mM phenylbutyrate. *In vivo* studies conducted consisted of feeding wild type and Y64H mice a diet containing 7g/kg sodium – 4-phenylbutyrate. The appearance of incisor teeth in Y64H female mice improved with the poor quality enamel being replaced over the course of the experiment by translucent, orange coloured enamel similar to the wild type counterparts. Histological examination of the incisors showed that the wild-type mice exhibited tall secretory stage ameloblasts associated with an eosinophilic enamel ECM. Untreated female Y64H showed a reduced secretory zone and thickness of ECM with intracellular eosinophilic staining indicating retained matrix protein. Phenylbutyrate treated Y64H female incisors showed a reversal of these anomalies, with a return to the phenotype displayed by the wild type incisors. Western blot analysis of the phenylbutyrate treated male Y64H secretory stage ECM showed that amelogenin secretion was still impaired, indicating that the phenylbutyrate is unable to restore normal secretory function in affected ameloblasts. To probe whether the phenylbutyrate elicited an effect on the UPR, the levels of caspase-3, a marker for apoptosis, were compared in the ameloblasts of affected mice with and without treatment. No phenylbutyrate treatment resulted in large numbers of ameloblasts testing immunopositive for caspase-3, whereas treatment with phenylbutyrate reduced the caspase-3 levels to those observed in the wild type. This implies that the phenylbutyrate treatment worked by reducing apoptosis in the Y64H affected mice ameloblasts.

The study of hydroxyapatite nucleation *in vitro* has shown that amelogenin is incapable of nucleating hydroxyapatite, and that enamelin is capable of nucleating hydroxyapatite production. The two proteins together are capable of hydroxyapatite nucleation. The presence of the Y64H mutation in the recombinant amelogenin was shown to not effect hydroxyapatite nucleation. Further studies could use this *in vitro* nucleation system to investigate whether known mutations in the 32 kDa enamelin, shown in humans to trigger amelogenesis imperfecta, change the ability of the enamelin protein to nucleate hydroxyapatite. This would involve producing recombinant enamelin protein containing the mutations and repeating the

experimental work shown in this thesis with the mutated protein. It would also be interesting to see how other proteins identified *in vivo* in the ECM behave in the *in vitro* steady-state agarose gel nucleation system with regards to nucleating hydroxyapatite production. It would be interesting to include recombinant ameloblastin, alone and in conjunction with amelogenin and/or enamelin in the steady state agarose gel system. This could help elucidate the essential protein combination necessary for optimised hydroxyapatite production.

The q-RT-PCR experiments performed within this thesis have shown a decrease in the production of amelogenin in mouse incisors containing the Y64H amelogenin mutation. This could be due to activation of the Unfolded Protein Response (UPR) removing the mutated protein via apoptosis, or by the UPR switching off or slowing down production of the mutated protein while it deals with the mutated protein already produced. The q-RT-PCR experiments also showed an increase in the amount of CHOP, a stress protein in the UPR pathway. Further studies could be performed to investigate this down production of amelogenin, using histology and immunochemistry staining of slices of tooth. Q-RT-PCR experiments using other genes involved in the UPR pathways could give a fuller picture of what is happening to the mutated amelogenin protein.

Protein uptake and binding studies seemed to show that the mutated Y64H amelogenin protein is 'stickier', binding to itself and wild-type amelogenin protein more strongly. Expansion of these studies could elucidate what is actually happening to the protein once it is secreted. Surface Plasmon Resonance (SPR) would be able to identify differences in the binding strengths and affinities of these proteins. SEM studies could show any differences in nanosphere formation due to the amelogenin mutation.

Identification of a true molecular chaperone for amelogenin would be extremely useful for describing the secretory pathway for amelogenin in the ameloblast cells. Due to amelogenin and ameloblastin being co-localised on the same gene, and being located together, it is highly probable that ameloblastin is the molecular chaperone for amelogenin. Co-localisation studies using ELISA, IHC and histological staining would help to show if this is a realistic hypothesis.

It would be beneficial to repeat the proteolytic degradation studies with maturation stage enamel from rat incisors to see if the serine proteases present in the maturation stage enamel could lead to proteolytic processing and reveal the presence of the 32 kDa enamelin processing product in rat, and not just porcine enamel.

The work in this thesis helps us to understand better the role of the major ECM proteins, amelogenin and enamelin, in the development of tooth enamel. There is still a long way to go to fully understand the complex interplay of these proteins with each other, either in matrix formation or in a chaperoning role during protein secretion, and their interaction with hydroxyapatite mineral crystals to form mature enamel. The mature tooth enamel is a unique and amazing biomineralised tissue. Understanding as much as we can about its production can only help us in our quest to design and produce better products for its care and repair, and this affects nearly every one of us.

Bibliography

ABIKO Y., NAGAYASU H., TAKESHIMA M., YAMAZAKI M., NISHIMURA M. & KUSANO K. (2007) Ameloblastic carcinoma ex ameloblastoma: report of a case-possible involvement of CpG island hypermethylation of the p16 gene in malignant transformation. *Oral Surg Oral Med Oral Pathol Oral Radiol Endod*, 103, 72-6.

ADDADI L. & WEINER S. (1985) Interactions between acidic proteins and crystals: stereochemical requirements in biomineralisation. *PNAS*, 82, 4110-4114.

ADDADI L. & WEINER S. (1992) Control and design principles in biological mineralisation. *Angew. Chem. Int. Ed. Eng.*, 31, 153-169.

ADEKEYE A., HAERI M., SOLESSIO E. & KNOX B.E. (2014) Ablation of the proapoptotic genes CHOP or Ask1 does not prevent or delay loss of visual function in a P23H transgenic mouse model of retinitis pigmentosa. *PLoS One*. 9, e83871.

AGGELI A., BELL M., CARRICK L.M., FISHWICK C.W., HARDING R., MAWER P.J., RADFORD S.E., STRONG A.E. & BODEN N. (2003) pH as a trigger of peptide beta-sheet self-assembly and reversible switching between nematic and isotropic phases. *J Am Chem Soc* 125, 9619-9628.

AICHMAYER B., MARGOLIS H.C., SIGEL R., YAMAKOSHI Y., SIMMER J.P. & FRATZL P. (2005) The onset of amelogenin nanosphere aggregation studied by small-angle X-ray scattering and dynamic light scattering. *J Struct. Biol*, 151, 239-249.

ALDRED M.J. & CRAWFORD P.J. (1995) Amelogenesis imperfecta - towards a new classification. *Oral Diseases*, 1, 2-5.

AL-HASHIMI N., SIRE J.Y. & DELGADO S. (2009) Evolutionary analysis of mammalian enamelin, the largest enamel protein, supports a crucial role for the 32-kDa peptide and reveals selective adaptation in rodents and primates. *J Mol Evol.*, 69, 635-56.

AMIZUKA N., UCHIDA T., FUKAE M., YAMADA M. & OZAWA H. (1992) Ultrastructural observation of enamel tufts in human permanent teeth. *Arch. Histol. Cytol.* 55, 179-190.

ANELLI T. & SITIA R. (2008) Protein quality control in the early secretory pathway. *EMBO*, 27, 315-327.

ANGMAR B., CARLSTROM D. & GLAS J.E. (1963) The mineralization of normal human enamel. *J. Ultrastruct. Res.*, 8, 12-23.

ANHOLT R.R. & CARBONE M.A. (2013) A molecular mechanism for glaucoma: endoplasmic reticulum stress and the unfolded protein response. *Trends Mol Med.*, 19, 586-93.

ANTOINE D., DEAN C. & HILLSON S. (2000) The Periodicity of Incremental Structures in Dental Enamel Based on the Developing Dentition of Post-Medieval Known-Age Children. *Dental Morphology*, 48-55.

ANTOINE D., HILLSON S. & DEAN M.C. (2009) The developmental clock of dental enamel: a test for the periodicity of prism cross-striations in modern humans and an evaluation of the most likely sources of error in histological studies of this kind. *Journal of Anatomy*, 214, 45-55.

AOBA T., TANABE T. & MORENO E.C. (1987A) Function of amelogenins in porcine enamel mineralisation during the secretory stage of amelogenesis. *Adv Dent Res.*, 1.

AOBA T., FUKAE M., TANABE T., SHIMIZU M. & MORENO E.C. (1987B) Selective adsorption of porcine amelogenins onto hydroxyapatite and their inhibitory activity on Hydroxyapatite growth in supersaturated solutions. *Calcif Tissue Int.*, 41, 281-289.

AOBA T., TANABE T. & MORENO E.C. (1987C) Proteins in the enamel fluid of immature porcine teeth. *J. Dental Res.*, 66, 721-726.

AOBA T., SHIMODA S., AKITA H., HOLMBERG C. & TAUBMAN M.A. (1992 A) Antipeptide antibodies reactive with epitopic domains of porcine amelogenins at the C-terminus. *Archs Oral Biol*, 37, 249-255.

AOBA T., SHIMODA S., SHIMIKAWA H. & INAGE T. (1992B) Common epitopes of mammalian amelogenins at the C-terminus and possible functional roles of the corresponding domain in enamel mineralisation. *Calcif Tissue Int.*, 51, 85-91.

ARENDS J. & JONGEBLOED W.L. (1978) Crystallites dimensions of enamel. *J.Biol.Buccale*, 6, 161-171.

ARITA M., LI S.W., KOPEN G., ADACHI E., JIMENEZ S.A., FERTALA A. & . (2002) Skeletal abnormalities and ultrastructural changes of cartilage in transgenic mice expressing a collagen II gene (COL2A1) with a Cys for Arg-alpha1-519 substitution.. *Osteoarthritis Cartilage*. 2002 Oct;10(10):808-15, 10, 808-15.

ASH MAJOR M. & NELSON S.J. (2003) *Wheeler' dental anatomy, physiology and occlusion*, Elsevier.

ATHANASIOU D., AGUILÀ M., BEVILACQUA D., NOVOSELOV S.S., PARFITT D.A. & CHEETHAM M.E. (2013) The cell stress machinery and retinal degeneration. *FEBS Lett.* , 587, 2008-17.

AVERY, J. K. (2002) *Oral Development and Histology*.

AVERY, J. K. (2011) *Oral Development and Histology*, Thieme Medical Publishers.

BAEUERLE P.A. & BALTIMORE D. (1996) NF-kappa B: ten years after. *Cell*, 87, 13-20.

BALMER R., CAMERON A.C., ADÈS L. & ALDRED M.J. (2004) Enamel defects and Lyonization in focal dermal hypoplasia. *Oral Surg Oral Med Oral Pathol Oral Radiol Endod*, 98, 686-91.

BARKER D. & WELBURY R.R. (2000) Dental findings in Morquio syndrome (mucopolysaccharidoses type IVa). *ASDC J Dent Child*, 67, 431-433.

BARRALET, J. E., BEST, S. M. & BONFIELD, W. (1998) Carbonate Substitution in Precipitated Hydroxyapatite:an Investigation into the Effects of Reaction Temperature and Bicarbonate Ion Concentration. *J. Biomed. Mater. Res*, 41, 79-86.

BARRON M.J., BROOKES S.J., KIRKHAM J., SHORE R.C., HUNT C., MIRONOV A., KINGSWELL N.J., MAYCOCK J., SHUTTLEWORTH C.A. & DIXON M.J. (2010) A mutation in the mouse Amelx tri-tyrosyl domain results in impaired secretion of amelogenin and phenocopies human X-linked amelogenesis imperfecta. *Hum Mol Genet.* , 19, 1230-47.

BARTLETT J.D. & SIMMER J.P. (1999) Proteinases in developing dental enamel. *Crit Rev Oral Biol Med*, 10, 425-441.

BARTLETT J.D., ZHOU Z., SKOBE Z., DOBECK J.M. & TRYGGVASON K. (2003) Delayed tooth eruption in membrane type-1 matrix metalloproteinase deficient mice. *Connect Tissue Res.*, 44, 300-4.

BARTLETT J.D., BENIASH E., LEE D.H. & SMITH C.E. (2004) Decreased mineral content in MMP-20 null mouse enamel is prominent during the maturation stage. *J Dent Res*, 83, 909-913.

BARTLETT J.D., GANSS B., GOLDBERG M., MORADIAN-OLDAK J., PAINE M.L., SNEAD M.L., WEN X., WHITE S.N. & ZHOU Y.L. (2006) Protein-protein interactions of the developing enamel matrix. *Current topics in developmental biology*, 74, 57-115.

BATEMAN J.F., BOOT-HANDFORD R.P. & SHIREEN R. L. (2009) Genetic diseases of connective tissues: cellular and extracellular effects of ECM mutations. *Nature Reviews Genetics* 10, 173-183.

BEANAN M.J. & SARGENT T.D. (2000) Regulation and function of dlx3 in vertebrate development. . *Developmental Dynamics*, 218, 545-553.

BEAUSOLEIL S.A., JEDRYCHOWSKI M., SCHWARTZ D., ELIAS J.E., VILLEN J., LI J., COHN M.A., CANTLEY L.C. & GYGI S.P. (2004) Large scale characterisation of HeLa cell nuclear phosphoproteins. *PNAS*, 101, 12130-12135.

BEISSINGER M. & BUCHNER J. (1998) How chaperones fold proteins. *Biol Chem.*, 379, 245-59.

BENIASH, E., SIMMER, J. P. & MARGOLIS, H. C. (2005) The effect of recombinant mouse amelogenins on the formation and organization of hydroxyapatite crystals in vitro. *J Struct. Biol.*, 149, 182-190.

BERKOWITZ B.M.B, HOLLAND G.R. & MOXHAM B.J. (2009) *Oral anatomy, histology and embryology.*

BERNALES S., SCHUCK S. & WALTER P. (2007) ER-Phagy: Selective Autophagy of the Endoplasmic Reticulum. *Autophagy*, 3, 285-287.

BERTOLOTTI A., WANG X., NOVOA I., JUNGREIS R., SCHLESSINGER K., CHO J.H., WEST A.B. & RON D. (2001) Increased sensitivity to dextran sodium sulphate colitis in IRE1 beta-deficient mice. *J Clin. Invest.*, 107, 585-593.

BERTOLOTTI A., ZHANG Y., HENDERSHOT L.M., HARDING H.P. & RON D. (2009) Dynamic interaction of BiP and ER stress transducers in the unfolded protein response. *Nat. Cell Biol.*, 2, 326-332.

BETTS M.J. & RUSSELL R.B. (2003) Amino Acid Properties and Consequences of Substitutions. IN GRAY, M. R. B. A. I. C. (Ed.) *Bioinformatics for Geneticists*. Chichester, John Wiley & Sons, Ltd.

BEUST T.B. & (1932) Occurrence of enamel tufts. *J Dent Res* 12, 601-608.

BEYELER M., SCHILD C., LUTZ R., CHIQUET M. & TRUEB B. (2010) Identification of a fibronectin interaction site in the extracellular matrix protein ameloblastin. *Exp Cell Res.*, 316, 1202-12.

BEYNON A.D. & DEAN M.C. (1988) Distinct dental development patterns in early fossil hominids. *Nature*, 335, 509-514.

BOBOLA M.S, BERGER M.S., ELLENBOGEN R.S., ROBERTS T.S., GEYER J.R. & SILBER J.R. (2001) O6-Methylguanine-DNA Methyltransferase in Pediatric Primary Brain Tumors. *Clin Cancer Res* 7, 613.

BOIVIN, G. (2007) The hydroxyapatite crystal: a closer look. *Medicographia*, 29, 126-132.

BONASS W.A., KIRKHAM J., BROOKES S.J., SHORE R.C. & ROBINSON C. (1994) Molecular cloning and DNA sequence of rat amelogenin and a comparative analysis of mammalian amelogenin protein sequence divergence. *Biochem. Biophys. Res. Commun.*, 198, 755-763.

BOOT-HANDFORD R.P. & BRIGGS M.D. (2010) The unfolded protein response and its relevance to connective tissue diseases. *Cells Tissue Res.*, 339, 197-211.

BOSKEY A. L., MARESCA M., DOTY S., SABSAY B. & VEIS A. (1990) Concentration-dependent effects of dentin phosphophoryn in the regulation of in vitro hydroxyapatite formation and growth. *Bone Mineral*, 11, 55-65.

BOSKEY, A. L. (2003) Biomineralisation: An overview. *Connective Tissue Research*, 44, 5-9.

BOSSHARDT, D. D. & NANJI, A. (1997) Immunodetection of enamel- and cementum-related (bone) proteins at the enamel-free area and cervical portion of the tooth in rat molars. *J Bone Miner. Res.*, 12, 367-379.

BOUROPOULOS N. & MORADIAN-OLDAK J. (2004) Induction of Apatite by the cooperative effect of Amelogenin and the 32-kDa Enamelin. *J Dent Res*, 83, 278-282.

BOYDE A. (1989) *Teeth. Handbook of Microscopic Anatomy*, New York: Springer Verlag.

BOYDE A. (1990) *Developmental interpretations of dental microstructure*, New York, Wiley-Liss.

BRADFORD M.M. (1976) A rapid and sensitive method for the quantitation of microgram quantities of protein utilising the principle of protein-dye binding. *Analytical Biochemistry*, 7, 248-54.

BRODSKY J.L. (2007) The protective and destructive roles played by molecular chaperones during ERAD (Endoplasmic -reticulum-associated degradation). *J Biochem.*, 404, 352-362.

BROMAGE T.G. (1991) Enamel incremental periodicity in the pig-tailed macaque: a polychrome fluorescent labeling study of dental hard tissues. *Am J Phys Anthropol.*, 86, 205-214.

BROOKES S.J., ROBINSON C., KIRKHAM J. & BONASS W.A. (1995) Biochemistry and molecular biology of Amelogenin proteins of developing dental enamel. *Archs Oral Biol*, 40, 1-14.

BROOKES S.J., KIRKHAM J., SHORE R.C., WOOD S.R., SLABY I. & ROBINSON C. (2001) Amelin extracellular processing and aggregation during rat incisor amelogenesis. *Archives of Oral Biology*, 46, 201-208.

BROOKES S.J., LYGSTADAAS S.P., ROBINSON C., SHORE R.C. & KIRKHAM J. (2006) Intracellular nanosphere subunit assembly as revealed by amelogenin molecular cross-linking studies. *Eur J Oral Sci.* , 114, 280-4.

BROOKES S.J. , KINGSWELL N.J., BARRON, M. J., DIXON M. J. & KIRKHAM J. (2011) Is the 32kDa Fragment the Functional Enamelin Unit in all Species? *European Journal Oral Science*, 119, 345-350.

BROOKES S.J., BARRON M.J., BOOT-HANDFORD R., KIRKHAM J. & DIXON M.J. (2014) Endoplasmic reticulum stress in amelogenesis imperfecta and phenotypic rescue using 4-phenylbutyrate. *Hum Mol Genet.*, 23, 2468-2480.

BRUNETTI-PIERRI N., LANPHER B., EREZ A., ANANIEVA E.A., ISLAM M., MARINI J.C., SUN Q., YU C., HEGDE M., LI J., WYNN R.M., CHUANG D.T., HUTSON S. & LEE B. (2011) Phenylbutyrate therapy for maple syrup urine disease. *Hum Mol Genet.* , 20, 631-40.

BRUNTON P. A., DAVIES R. P. W., BURKE J. L. , SMITH A, AGGELI A., BROOKES S.J. & KIRKHAM J. (2013) Treatment of early caries lesions using biomimetic self-assembling peptides – a clinical safety trial. *British Dental Journal* 215.

BUKAU B., WEISSMAN J. & HORWICH A. (2006) Molecular chaperones and protein folding. *Cell* 125, 443-451.

BUSK M., PYTELA R. & SHEPPARD D. (1992) Characterization of the integrin alpha v beta 6 as a fibronectin-binding protein. *Journal of Biological Chemistry*, 267, 5790-5796.

CATERINA J.J., SKOBE Z., SHI J., DING Y., SIMMER J.P., BIRKEDAL-HANSEN H. & BARTLETT J.D. (2002) Enamelysin (Matrix Metalloproteinase 20) - deficient mice display an Amelogenesis Imperfecta phenotype. *JBC*, 277, 49598-49604.

CERNY R., SLABY I., HAMMERSTROM L. & WURTZ T. (1996) A novel gene expressed in rat ameloblasts codes for proteins with cell binding domains. *J Bone Miner Res.*, 11, 883-891.

CHENG P-T. & PRITZKER K.P.H. (1983) Solution Ca/P ratio affects calcium phosphate crystal phases. *Calcified Tissue International* 35, 596-601.

CHUNG H.J., JENSEN D.A., GAWRON K., STEPLEWSKI A. & FERTALA A. (2009) R992C (p.R1192C) Substitution in collagen II alters the structure of mutant molecules and induces the unfolded protein response. *J Mol Biol.* , 390, 306-18.

COBOURNE M.T. & SHARPE P.T. (2012) Diseases of the tooth: the genetic and molecular basis of inherited anomalies affecting the dentition. *WIREs Dev Biol*, 2, 183-212.

COGHILL E.L., HUGILL A., PARKINSON N., DAVISON C., GLENISTER P., CLEMENTS S., HUNTER J., COX R.D. & BROWN S.D. (2002) A gene-driven approach to the identification of ENU mutants in the mouse. *Nat Genet.* , 30, 255-6.

COLLIER P.M., SAUK J.J., ROSENBLOOM J., YUAN Z.A. & GIBSON C.W. (1997) An amelogenin gene defect associated with human X-linked Amelogenesis Imperfecta. *Archs Oral Biol*, 42, 235-242.

COOK N.R., ROW P.E. & DAVIDSON H.W. (2004) Lysosome associated membrane protein 1 (Lamp1) traffics directly from the TGN to early endosomes. *Traffic*, 5, 685-699.

COOPER T.G. & DE LEEUW N.H. (2004) A computer modeling study of the competitive adsorption of water and organic surfactants at surfaces of the mineral scheelite. *Langmuir*, 20, 3984-94.

CRAWFORD P.J.M., ALDRED M. & BLOCH-ZUPAN A. (2007) Amelogenesis imperfecta. *Orphanet Journal of Rare Diseases*, 2, 1-11.

CULLINAN S.B. & DIEHL J.A. (2004) PERK-dependent activation of Nrf2 contributes to redox homeostasis and cell survival following endoplasmic reticulum stress. *J Biol Chem.*, 279, 20108-17.

CURREY J. (1984) Effects of differences in mineralisation on the mechanical properties of bone. *Proc. R. Soc. London B*, 304, 509-518.

DACULSI G., MENANTEAU J., KREBEL L.M. & MITRE D. (1984) Enamel crystals: size, shape, length and growing process; high resolution TEM and biochemical study. *Tooth enamel 1V*.

DEAN M.C. (1987) Growth layers and incremental markings in hard tissues: a review of the literature and some preliminary observations about enamel structure in *Paranthropus boisei*. *J Hum Evol.*, 16, 157-172.

DEAN M.C. (1989) The developing dentition and tooth structure in hominoids. *Folia Primatol (Basel)*. 53, 160-176.

DEAN M.C. & SCANDRETT A.E. (1996) The relation between long-period incremental markings in dentine and daily cross-striations in enamel in human teeth. *Arch Oral Biol*, 41, 233-241.

DEAN M.C. (1998) A comparative study of cross striation spacings in cuspal enamel and of four methods of estimating the time taken to grow molar cuspal enamel in *Pan*, *Pongo* and *Homo*. *J Hum Evol.*, 35, 449-462.

DEUTSCH D, P. A., FISHER L.W., KOLODNY N., TERMINE J.D. YOUNG M.F. (1991) Sequencing of bovine enamelin ("tuftelin") a novel acidic enamel protein. *JBC*, 266, 16021-16028.

DEUTSCH D, P. A., DAFNI L., CATALANO-SHERMAN J., YOUNG M.F., FISHER L.W. (1995) The enamelin (tuftelin) gene. *Int. J. Dev. Biol.*, 39, 135-143.

DING Y., ESTRELLA M.R., HU Y.Y., CHAN H.L., ZHANG H.D., KIM J.W., SIMMER J.P. & HU J.C. (2009) Fam83h is associated with intracellular vesicles and adhcai. *Journal of Dental Research*, 88, 991-996.

DOHI, N., MURAKAMI C., TANABE T., YAMAKOSHI Y., FUKAE M., YAMAMOTO Y., WAKIDA K., SHIMIZU M., SIMMER J.P., KURIHARA H. &

- UCHIDA T. (1998) Immunocytochemical and immunochemical study of enamelin, using antibodies against porcine 89-kDa enamelin and its N-terminal synthetic peptide, in porcine tooth germs. *Cells Tissue Res.*, 293, 313-325.
- DOMINGUES M.G., JAEGER M.M., ARAÚJO V.C. & ARAÚJO N.S. (2000) Expression of cytokeratins in human enamel organ. *Eur J Oral Sci.*, 108, 43-7.
- DONG J., GU T.T., SIMMONS D. & MACDOUGALL M. (2000) Enamelin maps to human chromosome 4q21 within the autosomal dominant amelogenesis imperfecta locus. *Eur J Oral Sci.*, 108, 353-8.
- DONG J., AMOR D., ALDRED M.J., GU T., ESCAMILLA M. & MACDOUGALL M. (2005) Dlx3 mutation associated with autosomal dominant amelogenesis imperfecta with taurodontism. *American journal of medical genetics.*, 133A, 138-141.
- DOS SANTOS NEVES J., WAZEN R.M., KURODA S., ZALZAL S.F., MOFFATT P. & NANJI A. (2012) Odontogenic ameloblast-associated and amelotin are novel basal lamina components. *Histochemistry and Cell Biology* 137, 329-338.
- DRYJA T.P., MCGEE T.L., HAHN L.B., COWLEY G.S., OLSSON J.E., REICHEL E., SANDBERG M.A. & BERSON E.L. (1990) Mutations within the rhodopsin gene in patients with autosomal dominant retinitis pigmentosa. *N Engl J Med.*, 323, 1302-7.
- D'SOUZA, R. (2002) Development of the pulpdentinal complex. IN HARGREAVES K.M. (Ed.) *Seltzer and Bender's Dental Pulp*. Chicago, Quintessence Books.
- DU C., FALINI G., FERMANI S., ABBOTT C. & MORADIAN-OLDAK J. (2005) Supramolecular assembly of amelogenin nanospheres into birefringent microribbons. *Science*, 307, 1450-1454.
- DUFFIELD, A., KAMSTEEG, E. J., BROWN, A. N., PAGEL, P. & CAPLAN, M. J. (2003) The tetraspanin CD63 enhances the internalization of the H,K-ATPase beta-subunit. *PNAS*, 100, 15560-5.
- DUPONT B.R., HU C.C., REVELES X. & SIMMER J.P. (1999) Assignment of serine protease 17 (prss17) to human chromosome bands 19q13.3-q13.4 by in situ hybridization. *Cytogenetics and cell genetics*, 86, 212-213.
- EASTOE J.E. (1964) The chemical composition of bone and tooth. IN HARDWICK J.L., H. H. R., KONIG K.G. (Ed.) *Advances in fluorine research and dental caries prevention*. Oxford, Pergamon Press.
- ELLGAARD L. & HELENIUS A. (2003) Quality control in the endoplasmic reticulum. *Nature Reviews Molecular Cell Biology* 4, 181-191.

ELLIOTT J.C., ANDERSON P., GAO X.J., WONG F.S.L., DAVIS G.R. & DOWKER S.E.P. (1994) Application of scanning microradiography and X-ray microtomography to study bones and teeth. *Journal of X-ray Science and Technology*, 4, 102-117.

ELLIOTT J.C., WONG F. S., ANDERSON P., DAVIS G.R. & DOWKER S.E. (1998) Determination of mineral concentration in dental enamel from X-ray attenuation measurements. *Connect Tissue Res.*, 38, 61-72.

EL-SAYED W., PARRY D.A., SHORE R.C., AHMED M., JAFRI H., RASHID Y., AL-BAHLANI S., AL HARASI S., KIRKHAM J., INGLEHEARN C.F. & MIGHELL A.J. (2009) Mutations in the beta propeller wdr72 cause autosomal recessive hypomaturation amelogenesis imperfecta. . *American Journal of Human Genetics*, 85, 699-705.

EL-SAYED W., SHORE R.C., PARRY D.A., INGLEHEARN C.F. & MIGHELL A.J. (2010) Ultrastructural analyses of deciduous teeth affected by hypocalcified amelogenesis imperfecta from a family with a novel y458x fam83h nonsense mutation. *Cells, tissues, organs*, 191, 235-239.

EL-SAYED W., SHORE R.C., PARRY D.A., C. F. INGLEHEARN C.F. & MIGHELL A.J. (2011) Hypomaturation amelogenesis imperfecta due to wdr72 mutations: a novel mutation and ultrastructural analyses of deciduous teeth. . *Cells, tissues, organs*, 194, 60-66.

ESAPA C.T., HOUGH T.A., TESTORI S., HEAD R.A., CRANE E.A., CHAN C.P., EVANS H., BASSETT J.H., TYLZANOWSKI P., MCNALLY E.G., CARR A.J., BOYDE A., HOWELL P.G., CLARK A., WILLIAMS G.R., BROWN M.A., CROUCHER P.I., NESBIT M.A., BROWN S.D., COX R.D., CHEESEMAN M.T. & THAKKER R.V. (2012) A mouse model for spondyloepiphyseal dysplasia congenita with secondary osteoarthritis due to a Col2a1 mutation. *J Bone Miner Res.* , 27, 413-28.

FAN D., LAKSHMINARAYAN R. & MORADIAN-OLDAK J. (2008) The 32 kDa enamelin undergoes conformational transitions upon calcium binding. *J Struct. Biol*, 163, 109-115.

FAN D., DU C., SUN Z., LAKSHMINARAYAN, R. & MORADIAN-OLDAK J. (2009A) In vitro study on the interaction between the 32 kDa enamelin and amelogenin. *J Struct. Biol*, 166, 88-94.

FAN Y., SUN Z. & MORADIAN-OLDAK J. (2009B) Controlled remineralisation of enamel in the presence of amelogenin and fluoride. *Biomaterials*, 30, 478-483.

FAN D., IJIMA M., BROMLEY, K. M., YANG X., MATHEW S. & MORADIAN-OLDAK J. (2011) The Cooperation of Enamelin and Amelogenin in Controlling Octacalcium Phosphate Crystal Morphology. *Cells Tissues Organs*, 194, 194-198.

FARBER M.J. & MITTERMAIER A. (2008) Side chain burial and hydrophobic core packing in protein folding transition states. *Protein Science* 17, 644-651.

FINCHAM A.G., BELCOURT A.B. & TERMINE J.D. (1981) The molecular composition of bovine fetal enamel matrix. IN A., V. (Ed.) *The chemistry and biology of mineralised connective tissues*. Amsterdam, Elsevier.

FINCHAM A.G., MORADIAN-OLDAK J., SIMMER J.P., SARTE P., LAU E.C., DIEKWISCH T. & SLAVKIN H.C. (1994) Self-assembly of a recombinant amelogenin protein generates supramolecular structures. *J Struct. Biol.*, 112, 103-109.

FINCHAM A.G. & MORADIAN-OLDAK J. (1995) Recent advances in amelogenin biochemistry. *Connect Tissue Res.*, 32, 119-124.

FINCHAM A.G., MORADIAN-OLDAK J., DIEKWISCH T.G.H., LYARUU D.M., WRIGHT J.T., BRINGAS P. & SLAVKIN H.C. (1995) Evidence for amelogenin nanospheres as functional components of secretory-stage enamel matrix. *J. Struct. Biol.*, 115, 50-59.

FINCHAM A., LEUNG W., TAN J. & MORADIAN-OLDAK J. (1998) Does amelogenin nanosphere assembly proceed through intermediary-sized structures? *Connect Tissue Res.* , 38, 237-40.

FISCHER H., POLIKARPOV I. & CRAIEVICH A.F. (2004) Average protein density is a molecular-weight-dependent function. *Protein Science*, 13, 2825-2828.

FISHER L.W., HEEGAARD A.M., VETTER U., VOGEL W., JUST W., TERMINE J.D. & YOUNG M.F. (1991) Human biglycan gene: Putative promoter, intron-exon junctions and chromosomal localization. *JBC*, 266, 14371-14377.

FITZGERALD J. & VERVENIOLIS S.J. (1998) Morquio's syndrome. A case report and review of clinical findings. *N.Y. State Dent. J.*, 64, 48-50.

FOLK J.E. & FINLAYSON J.S. (1977) The epsilon-(gamma-glutamyl)lysine crosslink and the catalytic role of transglutaminases. *Adv Protein Chem.* , 31, 1-133.

FORLONI G., ANGERETTI N., CHIESA R., MONZANI E., SALMONA M., BUGIANI O. & TAGLIAVINI F. (1993) Neurotoxicity of a prion protein fragment. *Nature.* , 362, 543-6.

FRIBLEY A., ZHANG K. & KAUFMAN R.J. (2009) Regulation of apoptosis by the unfolded protein response. *Methods Mol Biol.* , 559, 191-204.

FUJISAWA R., WADA Y., NODASAKA Y. & KUBOKI Y. (1996) Acidic amino acid rich sequences as binding sites of osteonectin to HAP crystals. *Biochimica et Biophysica Acta*, 1292, 53-60.

FUKAE M., TANABE T., IJIRI H. & SHIMIZU M. (1980) Studies on porcine enamel proteins: A possible original enamel protein. *Tsurumi Univ. Dent. J.*, 6, 87-94.

FUKAE M., TANABE T. & SHIMIZU M. (1983) Amino acid sequence of the main component of porcine enamel proteins. *Jap. J. Oral Biol.*, 25, 29.

FUKAE M. & TANABE T. (1987) Nonamelogenin components of porcine enamel in the protein fraction free from the enamel crystals. *Calcif Tissue Int.*, 40, 286-293.

FUKAE M., TANABE T., MURAKAMI C., DOHI N., UCHIDA T. & SHIMIZU M. (1996) Primary structure of the porcine 89-kDa enamelin. *Adv Dent Res.*, 10, 111-8.

FUKUDA S., TOMATSU S., MASUE M., SUKEGAWA K., IWATA H., OGAWA T., NAKASHIMA Y., HORI T., YAMAGISHI A. & HANYU Y. (1992) Mucopolysaccharidosis type IVA. Nacetylgalactosamine-6-sulfate sulfatase exonic point mutations in classical Morquio and mild cases. *J Clin Invest.*, 90, 1049-1053.

FUKUMOTO S., KIBA T., HALL B., IEHARA N., NAKAMURA T., LONGENECKER G., KREBSBACH P.H., NANJI A., KULKARNI A.B. & YAMADA Y. (2004) Ameloblastin is a cell adhesion molecule required for maintaining the differentiation state of ameloblasts. *J. Cell Biol.*, 167, 973-983.

GAISER K.G., MADDOX B.K., BANN J.G., BOSWELL B.A., KEENE D.R., GAROFALO S. & HORTON W.A. (2002) Y-position collagen II mutation disrupts cartilage formation and skeletal development in a transgenic mouse model of spondyloepiphyseal dysplasia. *J Bone Miner Res.*, 17, 39-47.

GARANT, P. (2003) *Oral cells and tissues*, Quintessence Publishing.

GARDNER B.M., PINCUS D., GOTTHARDT K., GALLAGHER C.M. & WALTER P. (2013) Endoplasmic Reticulum Stress Sensing in the Unfolded Protein Response. *Cold Spring Harbor Perspectives in Biology*, 5.

GIANNAKIS E., JOKIRANTA T. S., MALE D. A., RANGANATHAN S., ORMSBY R. J., FISCHETTI V. A., MOLD C. & GORDON D. L. (2003) A common site within factor H SCR 7 responsible for binding heparin, C-reactive protein and streptococcal M protein. *Eur. J. Immunol.*, 33, 962-969.

GIBSON C.W., YUAN Z.A., HALL B., LONGENECKER G., CHEN E., THYAGARAJAN T., SREENATH T., WRIGHT J.T., DECKER S. & PIDDINGTON R. (2001) Amelogenin deficient mice display an amelogenesis imperfecta phenotype. *JBC*, 276, 31871-31875.

GOLDBERG M., FEINBERG J., RAINTEAU D., LECOLLE S., KAETZEL M.A., DEDMAN J.R. & WEINMAN S. (1990) Annexins I-VI in secretory ameloblasts and odontoblasts of rat incisor. *J Biol Buccale.*, 18, 289-98.

GOLDBERG M., VERMELIN L., MOSTERMANS P., LECOLLE S., SEPTIER D., GODEAU G. & LEGEROS R.Z. (1998) Fragmentation of the distal portion of Tomes' processes of secretory ameloblasts in the forming enamel of rat incisors. *Connect Tissue Res.*, 38, 159-169.

GOLDBERG M., LECOLLE S., VERMELIN L., BENGHEZAL A. & GODEAU G. (1999) [3H]choline uptake and turnover into membrane and extracellular matrix phospholipids, visualization and radioautography in rat incisor. *Calcif Tissue Int.*, 65, 66-72.

GOLDBERG M., RAPOPORT O., SEPTIER D., PALMIER K., HALL R., EMBERY G., YOUNG M. & AMEYE L. (2003) Proteoglycans in predentin: The last 15 micrometers before mineralization. *Connect Tissue Res.*, 44.

GOLDBERG M., SEPTIER D., RAPOPORT O., IOZZO R.V., YOUNG M.F. & AMEYE L.G. (2005) Targeted disruption of two small leucine-rich proteoglycans, biglycans and decorin, exerts divergent effects on enamel and dentin formation. *Calcif Tissue Int.*, 77, 297-310.

GOLDBERG M., KULKARNI A.B., YOUNG M. & BOSKEY A. L. (2011) Dentin: Structure, Composition and Mineralization: The role of dentin ECM in dentin formation and mineralization. *Front Biosci (Elite Ed)*, 3, 711-735.

GOPINATH V.K., YOONG T.P., YEAN C.Y. & RAVICHANDRAN M. (2008) Identifying polymorphism in enamelin gene in amelogenesis imperfecta (AI). *Archives of Oral Biology*.

GORBATYUK M.S., SHABASHVILI A., CHEN W., MEYERS C., SULLIVAN L.F., SALGANIK M., LIN J.H., LEWIN A.S., MUZYCZKA N. & GORBATYUK O.S. (2012) Glucose regulated protein 78 diminishes α -synuclein neurotoxicity in a rat model of Parkinson disease. *Mol Ther.*, 20, 1327-37.

GRZESCHIK K.H., BORNHOLDT D., OEFFNER F., KONIG A., DEL CARMEN BOENTE M., ENDERS H., FRITZ B., HERTL M., GRASSHOFF U., HOFLING K., OJI V., PARADISI M., SCHUCHARDT C., SZALAI Z., TADINI G., TRAUPE H. & HAPPLE R. (2007) Deficiency of PORCN, a regulator of Wnt signaling, is associated with focal dermal hypoplasia. *Nat Genet.*, 39, 833-835.

GUTIERREZ S.J., CHAVES M., TORRES D.M. & BRICENO I. (2007) Identification of a novel mutation in the *enamelin* gene in a family with autosomal-dominant amelogenesis imperfecta. *Archives of Oral Biology*, 52, 503-506.

HABELITZ S., DENBESTEN P.K., MARSHALL S.J., MARSHALL G.W. & LI W. (2006) Self-assembly and effect on crystal growth of the leucine-rich amelogenin peptide. *Eur J Oral Sci*, 114, 315-319.

HALLSWORTH A.S., ROBINSON C. & WEATHERELL J.A. (1972) Mineral and magnesium distribution within the approximal carious lesion of dental enamel. *Caries Research*, 6, 156-168.

HALLSWORTH A.S., WEATHERELL J.A. & ROBINSON C. (1973) Loss of carbonate during the first stages of enamel caries. *Caries Research*, 7, 345-8.

HAMMARSTRÖM L. (1997) Enamel matrix, cementum development and regeneration. *J Clin Periodontol.* , 24, 658-68.

HANKS S.K., QUINN A.M. & HUNTER T. (1988) The protein kinase family: conserved features and deduced phylogeny of the catalytic domains *Science* 214, 42-52.

HAO J., HE G., NARAYANAN K., ZOU B., LIN L., MUNI T., RAMACHANDRAN A. & GEORGE A. (2005) Identification of differentially expressed cDNA transcripts from a rat odontoblast cell line. *Bone* 37, 578-88.

HAO J., NARAYANAN K., MUNI T., RAMACHANDRAN A. & GEORGE, A. (2007) Dentin matrix protein 4, a novel secretory calcium-binding protein that modulates odontoblast differentiation. . *The Journal of biological chemistry*, 282, 15357-15365.

HARDING H.P., ZHANG Y. & RON D. (1999) Protein translation and folding are coupled by an endoplasmic-reticulum-resident kinase. *Nature*, 397, 271-4.

HARDING H.P., ZHANG Y., ZENG H., NOVOA I., LU P.D., CALFRON M., SADRI N., YUN C., POPKO B., PAULES R., STOJDL D.F., BELL J.C., HETTMANN T., LEIDEN J.M. & RON D. (2003) An integrated stress response regulates amino acid metabolism and resistance to oxidative stress. *Mol. Cell*, 11, 619-633.

HARMER I.J. & SAMUEL D. (1989) The FITC-anti-FITC system is a sensitive alternative to biotin-streptavidin ELISA. *Journal of Immunological Methods*, 122, 115-121.

HART P.S., ALDRED M.J., CRAWFORD P.J.M., WRIGHT N.J., HART T.C. & WRIGHT J.T. (2002) Amelogenesis imperfecta phenotype-geneotype correlations with two amelogenin gene mutations. *Arch Oral Biol.*, 47, 261-265.

HART P.S., MICHALEC M.D., SEOW W.K., HART T.C. & WRIGHT J.T. (2003) Identification of the enamelin (g.8344delG) mutation in a new kindred and presentation of a standardised ENAM nomenclature. *Arch Oral Biol.*, 48, 589-596.

HART P.S., HART T.C., MICHALEC M.D., RYU O.H., SIMMONS D., HONG S. & WRIGHT J.T. (2004) Mutation in kalikrein 4 causes autosomal recessive hypomaturation amelogenesis imperfecta. *J. Med. Genet.*, 41.

HART P.S., BECERIK S., COGULU D., EMINGIL G., OZDEMIR-OZENEN D., HAN S.T., SULIMA P.P., FIRATLI E. & HART T.C. (2009) Novel FAM83H mutations in Turkish families with autosomal dominant hypocalcified amelogenesis imperfecta. *Clin Genet.* , 75, 410-4.

HAUSCHKA P.V. (1986) Osteocalcin: the vitamin K-dependent Ca²⁺-binding protein of bone matrix. *Haemostasis.* 1986;16(3-4):258-72. *Review.*, 16, 258-72.

HE X., LI W. & HABELITZ S. (2008) The cooperative self-assembly of 25 and 23 kDa amelogenins. *J Struct. Biol*, 164, 314-21.

HETZ C. (2012) The unfolded protein response: controlling cell fate decisions under ER stress and beyond. *Nat Rev Mol Cell Biol*, 13, 89-102.

HILLSON S. (1986) *Teeth*, Cambridge, Cambridge University Press.

HODSON J.J., SHEFF B.D.S. & EDIN L.D.S. (1952) Micro dissection and other techniques for the investigation of human enamel. *Br Dent J*, 92 195-203.

HU C-C., FUKAE M., UCHIDA T., QIAN Q., ZHANG C.H., RYU O.H., TANABE T., YAMAKOSHI Y., MURAKAMI C., DOHI N., SHIMIZU M. & SIMMER J.P. (1997) Cloning and characterisation of porcine enamelin mRNA's. *J Dent Res*, 79, 1720-1729.

HU J.C., HART T.C., DUPONT B.R., CHEN J.J., SUN X. & QIAN Q. (2000) Cloning human enamelin cDNA chromosomal localisation and analysis of expression during tooth formation. *J Dent Res*, 79, 912-919.

HU J.C., ZHANG C., YANG Y., MARDH K.C., FORSMAN-SEMB K. & SIMMER J.P. (2001) Cloning and characterisation of the mouse and human enamelin genes. *J Dent Res*, 80.

HU J.C., SUN X., ZHANG C., LIU S., BARTLETT J.D. & SIMMER J.P. (2002) Enamelysin and kallikrein-4 mRNA expression in developing mouse molars. *E.J Oral Sci.*, 110, 307-315.

HU J.C. & YAMAKOSHI Y. (2003) Enamelin and autosomal-dominant amelogenesis imperfecta. *Crit Rev Oral Biol Med*, 14, 387-398.

HU J.C., YAMAKOSHI Y., YAMAKOSHI F., KREBSBACH P.H. & SIMMER J.P. (2005) Proteomics and genetics of dental enamel. *Cells Tissues Organs.* , 181, 219-31.

HU J.C., CHUN Y-H.P., HAZZAZZI T.A. & SIMMER J.P. (2007) Enamel formation and amelogenesis imperfecta. *Cells Tissues Organs.* , 186, 78-85.

HU J.C., HU Y., SMITH C.E., MCKEE M.D., WRIGHT J.T., YAMAKOSHI Y., PAPAGERAKIS P., HUNTER G.K., FENG J.Q., YAMAKOSHI F. & SIMMER J.P. (2008) Enamel defects and ameloblast-specific expression in Enam knock-out/lacZ knock-in mice. *JBC*, 283, 10858-10871.

HU J. C-C. , HU Y., LU Y., SMITH C.E., LERTLAM R., WRIGHT J.T., SUGGS C., MCKEE M.D., BENIASH E., KABIR M. & SIMMER J.P. (2014) Enamelin Is Critical for Ameloblast Integrity and Enamel Ultrastructure Formation. *PLoS One*.

HUNTER G.K., ALLEN B.L., GRYPNPAS M.D. & P.T., C. (1985) Inhibition of hydroxyapatite formation in collagen gels by chondroitin sulphate. *Biochem J.* , 2.

HUNTER G.K. & SZIGETY S.K. (1992) Effects of proteoglycan on hydroxyapatite formation under non-steady-state and pseudo-steady-state conditions. *Matrix.* 1992 Nov;12(5):362-8., 12, 362-8.

HUNTER G.K. & GOLDBERG H.A (1993) Nucleation of hydroxyapatite by bone sialoprotein. *PNAS*, 90, 8562-8565.

HUNTER G.K. & GOLDBERG H.A. (1994) Modulation of crystal formation by bone phosphoproteins: role of glutamic acid-rich sequences in the nucleation of hydroxyapatite by BSP. *Biochem. J.* , 302, 175-179.

HUNTER G.K., KYLE C.L. & GOLDBERG H.A. (1994) Modulation of crystal formation by bone phosphoproteins: structural specificity of the osteopontin mediated inhibition of hydroxyapatite formation. *Biochem. J.* , 300, 723-728.

HUNTER G.K., HAUSCHKA P.V., POOLE A.R., ROSENBERG L.C. & GOLDBERG H.A. (1996) Nucleation and inhibition of hydroxyapatite formation by mineralized tissue proteins. *Biochem. J.* , 317, 59-64.

HUNTER G.K., CURTIS H.A., GRYPNPAS M.D., SIMMER J.P. & FINCHAM A.G. (1999) Effects of recombinant amelogenin on hydroxyapatite formation in vitro. *Cal. Tissue Int.*, 65, 226-31.

HUNTER C.A., LAWSON K.R., PERKINSA J, M. & URCHB C.J. (2001) Aromatic interactions. *J. Chem. Soc.*, 651-669.

IANITTI T. & PALMIERI B. (2011) Clinical and Experimental Applications of Sodium Phenylbutyrate. *Drugs in R & D* 11, 227-249.

IJIMA M. & MORADIAN-OLDAK J. (2005) Control of apatite crystal growth in a fluoride containing amelogenin-rich matrix. . *Biomaterials*, 26, 1595–1603.

IIJIMA M., FAN D., BROMLEY K.M., SUN Z. & MORADIAN-OLDAK J. (2010) Tooth enamel proteins enamelin and amelogenin cooperate to regulate the growth morphology of octacalcium phosphate crystals. *Cryst Growth Des.*, 10, 4815-4822.

INOUE M., SAKURABA Y., MOTEGI H., KUBOTA N., TOKI H., MATSUI J., TOYODA Y., MIWA I., TERAUCHI Y., KADOWAKI T., SHIGEYAMA Y., KASUGA M., ADACHI T., FUJIMOTO N., MATSUMOTO R., TSUCHIHASHI K., KAGAMI T., INOUE A., KANEDA H., ISHIJIMA J., MASUYA H., SUZUKI T., WAKANA S., GONDO Y., MINOWA O., SHIROISHI T. & NODA T. (2004) A series of maturity onset diabetes of the young, type 2 (MODY2) mouse models generated by a large-scale ENU mutagenesis program. *Hum Mol Genet.*, 13, 1147-1157.

IOZZO, R. V. (1999) Functional network of interactive proteins. *J Biol Chem*, 274.

IWASAKI K., BAJENOVA E., SOMOGYI-GANSS E., MILLER M., NGUYEN V., NOURKEYHANI H., GAO Y., WENDEL M. & GANSS B. (2005) Amelotin - a novel secreted, ameloblast-specific protein. *J. Dental Res.*, 84, 1127-1132.

IWATA T., YAMAKOSHI Y., HU J.C., ISHIKAWA I., BARTLETT J.D. & KREBSBACH P.H. (2007) Processing of ameloblastin by MMP-20. *J Dent Res*, 86, 153-157.

JANONES D.S., MASSA L.F. & ARANA-CHAVEZ V.E. (2005) Immunocytochemical examination of the presence of amelogenin during the root development of rat molars. *Arch Oral Biol.* 50, 527-32.

JERNVALL J. & FORTELIUS M. (2002) Common mammals drive the evolutionary increase of hypsodonty in the Neogene. *Nature*, 417, 538-540.

KASPER M., KARSTENB U., STOSLEKA P. & MOLLIC R. (1989) Distribution of intermediate-filament proteins in the human enamel organ: unusually complex pattern of coexpression of cytokeratin polypeptides and vimentin. *Differentiation*, 40, 207-214.

KEREBEL B., DACULSI G. & KEREBEL L.M. (1979) Ultrastructural studies of enamel crystallites. *J Dent Res*, 58, 844-851.

KIDA M., ARIGA T., SHIRAKAWA T., OGUCHI H. & SAKIYAMA Y. (2002) Autosomal dominant hypoplastic form of amelogenesis imperfecta caused by an enamelin gene mutation at the exon-intron boundary. *J Dent Res*, 81, 738-742.

KIM J.W., SIMMER J.P., HU Y.Y., LIN B.P., BOYD C. & WRIGHT J.T. (2004) Amelogenin p.M1T and p.W4S mutations underlying hypoplastic X-linked amelogenesis imperfecta. *J Dent Res*, 83.

KIM J.W., SEYMAN F., LIN B.P., KIZILTAN B., GENÇAY K. & SIMMER J.P. (2005A) ENAM mutations in autosomal dominant amelogenesis imperfecta. *J Dent Res*, 84.

KIM J.W., SIMMER J.P., HART T.C., HART P.S., RAMASWAMI M.D. & BARTLETT J.D. (2005B) MMP-20 mutation in autosomal recessive pigmented hypomaturation amelogenesis imperfecta. *J Medical Genetics*.

KIM J.W., SIMMER J.P., LIN B.P., SEYMAN F., BARTLETT J.D. & HU J.C. (2006) Mutational analysis of candidate genes in 24 amelogenesis imperfecta families. *E.J Oral Sci.*, 114.

KIM J.W., LEE S.K., LEE Z.H., PARK J.C., LEE K.E., LEE M.H., PARK J.T., SEO B.M., HU J.C.C. & SIMMER J.P. (2008) *FAM83H* mutations in families with autosomal dominant hypocalcified amelogenesis imperfecta. *Am j human genetics*, 82, 489-494.

KINDELAN S., BROOK A., GANGEMI L., LENCH N., WONG F. & FEARNE J. (2000) Detection of a novel mutation in X-linked Amelogenesis Imperfecta. *J Dent Res*, 79.

KINIRONS M.J. & NELSON J. (1990) Dental findings in mucopolysaccharidosis type IV A (Morquio's disease type A). *Oral Surg Oral Med Oral Pathol Oral Radiol Endod*, 70, 176-9.

KIRKHAM J., ROBINSON C., WEATHERELL J.A., RICHARDS A, FEJERSKOV O. & JOSEPHSEN K. (1988) Maturation in Developing Permanent Porcine Enamel *J Dent Res*, 67, 1156.

KIRKHAM J., ZHANG J., BROOKES S.J., SHORE R.C., WOOD S.R., SMITH D.A., WALLWORK M.L., RYU O.H. & ROBINSON C. (2000) Evidence for charge density domains on developing enamel crystal surfaces. *J Dent Res*, 79, 1943-1947.

KITANAKA S., TAKEYAMA K., MURAYAMA A., SATO T., OKUMURA, K., NOGAMI M., HASEGAWA Y., NIIMI H., YANAGISAWA J., TANAKA T. & KATO S. (1998) Inactivating mutations in the 25-hydroxyvitamin D3 1 α -hydroxylase gene in patients with pseudovitamin D-deficiency rickets. *N Engl J Med.*, 228, 653-661.

KLEIN R. J., ZEISS C., CHEW E. Y., TSAI J. Y., SACKLER R. S., HAYNES C., HENNING A. K., SANGIOVANNI J. P., MANE S. M., MAYNE S. T., BRACKEN M. B., FERRIS F. L., OTT J., BARNSTABLE C. & HOH J. (2005) Complement factor H polymorphism in age-related macular degeneration. *Science*, 308, 385-389.

KODAKA T., OHOHARA Y. & DEBARI K. (1992) Scanning electron microscopy and energy-dispersive X-ray microanalysis studies of early dental calculus on resin plates exposed to human oral cavities. *Scanning Microsc.*, 6, 475-85.

KOHLSCHUTTER A., CHAPPUIS D., MEIER C., TONZ O., VASSELLA F. & HERSCHKOWITZ N. (1974) Familial epilepsy and yellow teeth—a disease of the CNS associated with enamel hypoplasia. *Helv Paediatr Acta*, 29, 283-294.

KOIKE T., IZUMIKAWA T., TAMURA J. & KITAGAWA H. (2009) Fam20b is a kinase that phosphorylates xylose in the glycosaminoglycan-protein linkage region. *The Biochemical journal*, 421, 157-162.

KOSMAOGLU M., KANUGA N., AGUILÀ M., GARRIGA P. & CHEETHAM M.E. (2009) A dual role for EDEM1 in the processing of rod opsin. *J Cell Sci.* 122, 4465-72.

KOUSSOULAKOU D.S., MARGARITIS L.H. & KOUSSOULAKOS S.L. (2009) A Curriculum Vitae of Teeth: Evolution, Generation, Regeneration. *Int J Biol Sci* , 5, 226-243.

KOUTSOUKOS P., AMJAD Z., TOMSON M.B. & NANCOLLAS G.H. (1980) Crystallization of calcium phosphates - constant composition study. *Journal of the American Chemical Society*, 102, 1552-1557.

KRAMER I.R., PINDBORG J.J. & SHEAR M. (1992) *Histological typing of odontogenic tumours (International Histological Classification of Tumours)*, Berlin, Springer-Verlag.

KREBSBACH P.H., LEE S.K., MATSUKI Y., KOZAC C., YAMADA K.M. & YAMADA Y. (1996) Full-length sequence, localisation and chromosome mapping of ameloblastin: A novel tooth-specific gene. *JBC*, 271, 4431-4435.

KUBOTA, K., LEE, D. H., TSUCHIYA, M., YOUNG, C., EVERETT, E. T., MARTINEZ-MIER, E. A., SNEAD M.L., NGUYEN L., URANO F. & BARTLETT J.D. (2005) Fluoride Induces Endoplasmic Reticulum Stress in Ameloblasts Responsible for Dental Enamel Formation. *JBC*, 280, 23194-23202.

KWEON Y.S., LEE K.E., KO J., HU J.C., SIMMER J.P., KIM J.W. & (2013) Effects of fam83h overexpression on enamel and dentine formation. *Archives of Oral Biology*, 58, 1148-1154.

LAEMMLI, U. K. (1970) Cleavage of the structural proteins during the assembly of the head bacteriophage T4. *Nature*, 227, 680-5.

LAGERSTROM M., DAHL N., NAKAHORI Y., NAKAGOME Y., BACKMAN B. & LANDEGREN U. (1991) A deletion in the amelogenin gene (AMG) causes X-linked amelogenesis imperfecta (AIH1). *Genomics*, 10, 971-975.

LAGERSTROM-FERMER M., NILSSON M., BACKMAN B., SALIDO E.C., SHAPIRO C. & PETTERSON U. (1995) Amelogenin signal peptide mutation: correlation between mutations in the amelogenin gene (AMGX) and manifestations of X-linked amelogenesis imperfecta. *Genomics*, 26, 159-162.

- LARSEN M.J. (1975) Degrees of saturation with respect to apatites in parotid saliva at various pH values. *Scand J Dent Res.*, 83, 7-12.
- LEE A.H., IWAKOSHI N.N. & GLIMCHER L.H. (2003) XBP-1 regulates a subset of endoplasmic reticulum resident chaperone genes in the unfolded protein response. *Mol Cell Biol.*, 23, 7448-59.
- LEE S.K., HU J.C.C., BARTLETT J.D., LEE K.E., LIN B.P.J., SIMMER J.P. & KIM J.W. (2008) Mutational spectrum of *FAM83H*: The C-terminal portion is required for tooth enamel calcification. *Human Mutations*, 1014, 95-99.
- LEE K.E., LEE S.K., JUNG S.E., SONG S.J., CHO S.H., LEE Z.H. & KIM J.W. (2011) A novel mutation in the *amelx* gene and multiple crown resorptions. *European journal of oral sciences*, 119, 324-328.
- LEGEROS R.Z. (1991) *Calcium phosphate* Basel, Karger.
- LEGFROS R.Z., SAKAE T., BAUTISTA C., RETINO M. & LEGEROS J.P. (1996) Magnesium and Carbonate in Enamel and Synthetic Apatites. *ADR*, 10, 225-231.
- LENCH N.J., BROOK A.H. & WINTER G.B. (1994) SSCP detection of a nonsense mutation in exon 5 of the amelogenin gene (*AMGX*) causing X-linked amelogenesis imperfecta. *Human Molecular Genetics*, 3.
- LENCH N.J. & WINTER G.B. (1995) Characterisation of molecular defects in X-linked amelogenesis imperfecta (*AIH1*). *Human Mutations*, 5, 251-259.
- LEVIN L.S., JORGENSON R.J. & SALINAS C.F. (1975) Oral findings in the Morquio syndrome (mucopolysaccharidosis IV). *Oral Surg Oral Med Oral Pathol Oral Radiol Endod*, 39, 390-395.
- LEWIN A.S., DRENSER K.A., HAUSWIRTH W.W., NISHIKAWA S., YASUMURA D., FLANNERY J.G. & LAVAIL M.M. (1998) Ribozyme rescue of photoreceptor cells in a transgenic rat model of autosomal dominant retinitis pigmentosa. *Nat Med.* 1998 Aug;4(8):967-71., 4, 967-71.
- LI W., GIBSON C.W., ABRAMS W.R., ANDREWS D.W. & DENBESTEN P.K. (2001) Reduced hydrolysis of amelogenin may result in X-linked amelogenesis imperfecta. *Matrix Biol.*, 19, 755-60.
- LIANG G., LIAN C., HUANG D., GAO W., LIANG A., PENG Y., YE W., WU Z., SU P. & HUANG D. (2014) Endoplasmic reticulum stress-unfolding protein response-apoptosis cascade causes chondrodysplasia in a *col2a1* p.Gly1170Ser mutated mouse model. *PLoS One.*, 9, 86894.
- LIN J.H., WALTER P. & YEN T.S. (2008) Endoplasmic reticulum stress in disease pathogenesis. *Annu. Rev. Pathol.*, 3, 399-425.
- LISSE T.S., THIELE F., FUCHS H., HANS W., PRZEMECK G.K.H., ABE K., RATHKOLB B., QUINTANILLA-MARTINEZ L., HOELZLWIMMER G.,

HELFICH M., WOLF E., RALSTON S.H. & ANGELIS M.H.DE (2008) ER stress-mediated apoptosis in a new mouse model of osteogenesis imperfecta. *PLoS Genet.*, 4, e7.

LIVAK K.J. & SCHMITTGEN T.D. (2001) Analysis of Relative Gene Expression Data Using RealTime Quantitative PCR and the 2⁻ΔΔCT Method. *Methods Mol Biol.*, 25, 402-408.

LLANO E., PENDAS A.M., KNAUPER V., SORSA T., SALO T., SALIDO E., MURPHY G., SIMMER J.P., BARTLETT J.D. & LOPEZ-OTIN C. (1997) Identification and structural and functional characterization of human enamelysin (mmp-20). *Biochemistry*, 36, 15101-15108.

LORAND L. & CONRAD S.M. (1984) Transglutaminases. *Mol. Cell Biochem.*, 58, 9-35.

LOWESTAM H.A. (1981) Minerals formed by organisms. *Science*, 211, 1126-1131.

LOWESTAM H.A. & WEINER S. (1989) *On biomineralisation*, Oxford University Press.

LU P.D, HARDING H.P & RON D. (2004) Translation reinitiation at alternative open reading frames regulates gene expression in an integrated stress response. *J Cell Biol.* , 167, 27-33.

LU Y., PAPAGERAKIS P., YAMAKOSHI Y., HU J.C., BARTLETT J.D. & SIMMER J.P. (2008) Functions of KLK4 and MMP-20 in dental enamel formation. *Biol Chem*, 389, 695-700.

LYNGSTADAAS S.P., RISNES S., NORDBØ H. & FLØNES A.G. (1990) Amelogenin gene similarity in vertebrates: DNA sequences encoding amelogenin seem to be conserved during evolution. *J Comp Physiol B.* , 160, 468-72.

MACDOUGALL, M., DUPONT, B. R., SIMMONS, D., REUS, B., KREBSBACH, P., KARRMAN, C., HOLMGREN, G., LEACH, R. J. & FORSMAN, K. (1997) Ameloblastin gene (AMBN) maps within the critical region for autosomal dominant amelogenesis imperfecta at chromosome 4q21. *Genomics*, 41, 115-118.

MACGIBBON, D. (1972) Generalized enamel hypoplasia and renal dysfunction. *Aust Dent J* 17, 61-63.

MAHADEVAN N.R. & ZANETTI M. (2011) Tumor stress inside out: cell-extrinsic effects of the unfolded protein response in tumor cells modulate the immunological landscape of the tumor microenvironment. *J Immunol.* 2011 187, 4403-9.

MANN D.M., YATES P.O. & MARCYNIUK B. (1985) Correlation between senile plaque and neurofibrillary tangle counts in cerebral cortex and

neuronal counts in cortex and subcortical structures in Alzheimer's disease. *Neurosci Lett.* , 56, 51-5.

MANN, S. (1988) Molecular recognition in biomineralisation. *Nature*, 332, 119-124.

MANN A., MONGE J. & LAMPI M. (1990) Dental caution. *Nature* 348, 202.

MANN, S. (2001) *Biomineralisation*, Oxford University Press.

MANN, S. (2007) Mineralization in biological systems. IN P.H. CONNETT, H. F., M. LAMMERS, S.MANN, J.D.ODOM, K.E.WETTERHAHN (Ed.) *Inorganic elements in biochemistry*. Heidelberg, Springer-Verlag.

MARDH C.K., BACKMAN B., HOLMGREN G., HU J.C.C., SIMMER J.P. & FORSMAN.-SEMB K.. (2002) A nonsense mutation in the enamelin gene causes local hypoplastic autosomal dominant amelogenesis imperfecta (AIH2). *Human Molecular Genetics*, 11, 1069-1074.

MARGOLIS H.C. & MORENO E.C. (1990) Physicochemical Perspectives on the Cariostatic Mechanisms of Systemic and Topical Fluorides. *J Dent Res*, 69, 606-613.

MARGOLIS H.C., BENIASH E. & FOWLER C.E., (2006) Role of macromolecular assembly of enamel matrix proteins in enamel formation. *J Dent Res*, 85, 775-793.

MARSON A., ROCK M.J., CAIN S.A., FREEMAN L.J., MORGAN A., MELLODY K., SHUTTLEWORTH C.A., BALDOCK C. & KIELTY C.M. (2005) Homotropic fibrillin-1 interactions in microfibril assembly. *J Biol. Chem.*, 280, 5013-21.

MASUYA H., SHIMIZU K., SEZUTSU H., SAKURABA Y., NAGANO J. & SHIMIZU A. (2005) Enamelin (Enam) is essential for amelogenesis: ENU-induced mouse mutants as models for different clinical subtypes of human amelogenesis imperfecta (AI). *Human Molecular Genetics*, 14, 575-583.

MAYRAN N., R.G. PARTON R.G. & GRUENBERG J. (2003) Annexin II regulates multivesicular endosome biogenesis in the degradation pathway of animal cells. *EMBO J*, 22, 3242-3253.

MENDES H.F., VAN DER SPUIJ J., CHAPPLE J.P. & CHEETHAM M.E. (2005) Mechanisms of cell death in rhodopsin retinitis pigmentosa: implications for therapy. *Trends Mol Med.* , 11, 177-85.

MEREDITH R.W., GATESY J., MURPHY W.J., RYDER O.A. & SPRINGER M.S. (2009) Molecular Decay of the Tooth Gene Enamelin (ENAM) Mirrors the Loss of Enamel in the Fossil Record of Placental Mammals. *PLoS Genet.*, 10.

MEYER T.S. & LAMBERTS B.L. (1965) Use of coomassie brilliant blue R250 for the electrophoresis of microgram quantities of parotid saliva proteins on acrylamide-gel strips. *Biochim Biophys Acta.* , 107, 144-5.

MIMURA T. (1939) The periodicity of growth lines seen in the enamel. *Kobyoshi*, 13, 454-455.

MORADIAN-OLDAK, J. (2001) Amelogenins: assembly, processing and control of crystal morphology. *Matrix Biology*, 20, 293-305.

MORADIAN-OLDAK J., JIMENEZ I., MALTBY D. & FINCHAM A.G. (2001) Controlled proteolysis of Amelogenins reveals exposure of both carboxyl- and amino-terminal regions. *Biopolymers*, 58, 606-616.

MORADIAN-OLDAK J., DU C. & FALINI G. (2006) On the formation of amelogenin microribbons. *Eur J Oral Sci*, 114, 289-296.

MORADIAN-OLDAK, J. (2007) The emergence of “nanospheres” as basic structural components adopted by amelogenin. . *J Dent Res*, 86, 487-490.

MORI K., OGAWA N., KAWAHARA T., YANAGI H. & YURA T. (2000) mRNA splicing-mediated C-terminal replacement of transcription factor Hac1p is required for efficient activation of the unfolded protein response. *Proc Natl Acad Sci U S A.* , 97, 4660-5.

MURPHY L.R., WALLQVIST A. & LEVY R.M. (2000) Simplified amino acid alphabets for protein fold recognition and implications for folding. *Protein Eng.*, 13, 149-152.

MYOUNG S., LEE J., CONSTANTINO P., LUCAS P., CHAI H. & LAWN B. (2009) Morphology and fracture of enamel. *J Biomech*, 42.

MYUNG K.J., SOHN S., HUR W., MOON Y., YOUNG R.C. & KEE C. (2003) Accumulation of mutant myocilins in ER leads to ER stress and potential cytotoxicity in human trabecular meshwork cells. *Biochemical and Biophysical Research Communications*, 312, 592-600.

NAGANO T., OIDA S., ANDO H., GOMI K., ARAI T. & FUKAE M. (2003) Relative levels of mRNA encoding enamel proteins in enamel organ epithelia and odontoblasts. *J Dent Res*, 82, 982-6.

NAKAGAWA, T. & YUAN, J. (2000) Cross-talk between two cysteine protease families. Activation of caspase-12 by calpain in apoptosis. *J. Cell Biol.* , 150, 887-894.

NANCI, A. & WARSHAWSKY, H. (1984) Characterisation of putative secretory sites on ameloblasts of the rat incisor. *Am. J. Anat.*, 171, 163-189.

NANCI, A., ZALZAL S. & KAN F.W.K. (1993) High-resolution Scanning Electron Microscopy of Rat Incisor Ameloblasts. *Scanning Microsc.*, 7, 165-175.

NANCI, A., FORTIN M. & GHITESCU L. (1996A) Endocytotic functions of ameloblasts and odontoblasts: Immunohistochemical and tracer studies on the uptake of plasma proteins. *Anat Rec.*, 245, 219-264.

NANCI A., HASHIMOTO J., ZALZAL S. & SMITH C.E. (1996B) Transient accumulation of proteins at interrod and rod enamel growth sites. *Adv Dent Res.*, 10, 135-149.

NANCI ,A. (2008) Oral Histology. IN TEN CATE, A. R. (Ed.) *Oral Histology*. Mosby.

NUÑEZ J., SANZ M., HOZ-RODRÍGUEZ L., ZEICHNER-DAVID M. & ARZATE H. (2010) Human cementoblasts express enamel-associated molecules in vitro and in vivo. *J Periodont Res*, 809-814.

OGATA M., HINO S., SAITO A., MORIKAWA K., KONDO S., KANEMOTO S., MURAKAMI T., TANIGUCHI M., TANII I., YOSHINAGA K., SHIOSAKA S., HAMMERBACK J.A., URANO F. & IMAIZUMI K. (2006) Autophagy is activated for cell survival after endoplasmic reticulum stress. *Mol. Cell Biol.*, 26, 9220-9231.

OH S.H. & LIM S.C. (2009) Endoplasmic reticulum stress-mediated autophagy/apoptosis induced by capsaicin (8-methyl-N-vanillyl-6-nonenamide) and dihydrocapsaicin is regulated by the extent of c-Jun NH2-terminal kinase/extracellular signal-regulated kinase activation in W138 lung epithelial fibroblast cells. *Pharmacol Exp Ther*, 329, 112-122.

OHH M., PARK C.W., IVAN M., HOFFMAN M.A., KIM T.Y., HUANG L.E., PAVLETICH N., CHAU V. & KAELIN W.G. (2000) Ubiquitination of hypoxia-inducible factor requires direct binding to the beta-domain of the von Hippel-Lindau protein. *Nat Cell Biol.* , 2, 423-7.

OLDBERG A., FRANZEN A. & HEINGARD D. (1988) The primary structure of a cell-binding bone sialoprotein. *JBC*, 263, 19433-19436.

OMARY, M. B., KU, N.-O., LIAO J. & PRICE D. (1998) Keratin modifications and solubility properties in epithelial cells and in vitro. *Subcell. Biochem*, 31, 105-140.

OSBORN J.W. & (1969). The 3-dimensional morphology of the tufts in human enamel. . *Acta Anat* 73, 481-495.

O'SULLIVAN J., BITU C.C., DALY S.B., URQUHART J.E., BARRON M.J., BHASKAR S.S., MARTELLI-JUNIOR H., DOS SANTOS NETO P.E., MANSILLA M.A., MURRAY J.C., COLETTA R.D., BLACK G.C. & DIXON M.J. (2011) Whole-exome sequencing identifies fam20a mutations as a cause of amelogenesis imperfecta and gingival hyperplasia syndrome. *American Journal of Human Genetics*, 88, 616-620.

OZDEMIR D., HART P.S., RYU O.H., CHOI S.J., OZDEMIR-KARATAS M., FIRATLI E., PIESCO N. & HART T.C. (2005) Mmp20 active-site mutation in hypomaturation amelogenesis imperfecta. *Journal of Dental Research*, 84, 1031-1035.

PAINE C.T., PAINE M.L., LUO W., OKAMOTO C.T., LYGSTADAAS S.P. & SNEAD M.L. (2000) A tuftelin-interacting protein (TIP39) localises to the apical secretory pole of mouse ameloblasts. *J. Biol. Chem.*, n275, 22284-22292.

PAINE, M. L., WHITE S.N., LUO W., FONG H., SARIKAYA M. & SNEAD M.L. (2001) Regulated gene expression dictates enamel structure and tooth function. *Matrix Biol.*, 20, 273-292.

PAINE, M. L., LOU, W., ZHU D.H., BRINGAS P. & SNEAD M.L. (2003) Functional domains for amelogenin revealed by compound genetic defects. *J Bone Miner. Res.*, 18, 466-472.

PALMER L.C., NEWCOMB C.J., KALTZ S.R., SPOERKE E.D. & STUPP S.L. (2008) Biomimetic systems for hydroxyapatite mineralisation inspired by bone and enamel. *Chem. Rev.*, 108, 4754-4783.

PARFITT D.A., AGUILA M., MCCULLEY C.H., BEVILACQUA D., MENDES H.F., ATHANASIOU D., NOVOSELOV S.S., KANUGA N., MUNRO P.M., COFFEY P.J., KALMAR B., GREENSMITH L. & CHEETHAM M.E. (2014) The heat-shock response co-inducer arimoclomol protects against retinal degeneration in rhodopsin retinitis pigmentosa. *Cell Death Dis.* 2014 May 22;5:e1236. , 22, 1236.

PARRY D.A., MIGHELL A.J., EL-SAYED W., SHORE R.C., JALILI I.K., DOLLFUS H., BLOCH-ZUPAN A., CARLOS R., CARR I.M., DOWNEY L.M., BLAIN K.M., MANSFIELD D.C., SHAHRABI M., HEIDARI M., AREF P., ABBASI M., MICHAELIDES M., MOORE A.T., KIRKHAM J. & INGLEHEARN C.F. (2009) Mutations in CNNM4 cause Jalili syndrome, consisting of autosomal-recessive cone-rod dystrophy and amelogenesis imperfecta. *Am J Hum Genet*, 84, 266-273.

PEARCE E.I., COOTE G.E. & LARSEN M.J. (1995) The distribution of fluoride in carious human enamel. *J Dent Res*, 74, 1775-82.

PERDIGAO, P. F., GOMEZ R.S., PIMENTA F.J.G.S. & DE MARCO L. (2004) Ameloblastin gene (AMBN) mutations associated with epithelial odontogenic tumors. *Oral Oncol.*, 40, 841-846.

PERNIOLA R., TAMBORRINO G., MARSIGLIANTE S. & DE RINALDIS, C. (1998) Assessment of enamel hypoplasia in autoimmune polyendocrinopathy-candidiasis-ectodermal dystrophy (APECED). *J Oral Pathol Med*, 27, 278-282.

PETERS B.P., EBISU S., GOLDSTEIN I.J. & FLASHNER M. (1979) Interaction of wheat germ agglutinin with sialic acid. *Biochemistry.*, 27, 5505-11.

PFEFFER S.R. & ROTHMAN J.E. (1987) Biosynthetic Protein Transport and Sorting by the Endoplasmic Reticulum and Golgi. *Annual Review of Biochemistry* 56, 829-852.

PISPA J. & THESLEFF I. (2003) Mechanisms of ectodermal organogenesis. *Developmental Biology*, 262, 195-205.

POLOK B., ESCHER P., AMBRESIN A., CHOUERY E., BOLAY S., MEUNIER I., NAN F., HAMEL C., MUNIER F.L., THILO B., MÉGARBANÉ A. & SCHORDERET D.F. (2009) Mutations in CNNM4 cause recessive cone-rod dystrophy with amelogenesis imperfecta. *Am J Hum Genet* 84, 259-265.

POULTER J, A., BROOKES S.J., SHORE R.C., SMITH C.E.L., FARRAJ L.A., KIRKHAM J., INGLEHEARN C.F. & MIGHELL A.J. (2014A) A missense mutation in ITGB6 causes pitted hypomineralized amelogenesis imperfecta. *Human Molecular Genetics*, 23, 2189-2197.

POULTER J.A., MURILLO G., BROOKES S.J., SMITH C.E.L., PARRY D.A., SILVA S., KIRKHAM J., INGLEHEARN C.F. & MIGHELL A.J. (2014B) Deletion of ameloblastin exon 6 is associated with amelogenesis imperfecta. *Hum Mol Genet.* , 23, 5317-5324.

PRICE J.A., BOWDEN D.W., WRIGHT J.T., PETTENATI M.J. & HART T.C. (1998) Identification of a mutation in DLX3 associated with tricho-dento-osseous (TDO) syndrome. *Hum Mol Genet.*, 7, 563-569.

PULKKINEN L., ROUAN F., BRUCKNER-TUDERMAN L., WALLERSTEIN R., GARZON M., BROWN T., SMITH L., CARTER W. & UITTO J. (1998) Novel ITGB4 Mutations in Lethal and Nonlethal Variants of Epidermolysis Bullosa with Pyloric Atresia: Missense versus Nonsense. *American Journal of Human Genetics*, 63, 1376-1387.

RAJPAR M.H., HARLEY K., LAING C., DAVIES R.M. & DIXON M.J. (2001) Mutation of the gene encoding the enamel-specific protein, enamelin, causes autosomal-dominant amelogenesis imperfecta. *Human Molecular Genetics*, 10, 1673-1677.

RAJPAR M.H., MCDERMOTT B., KUNG L., EARDLEY R., KNOWLES L., HEERAN M., THORNTON D.J., WILSON R., BATEMAN J.F., POULSOM R., ARVAN P., KADLER K.E., BRIGGS M.D. & BOOT-HANDFORD R.P. (2009) Targeted Induction of Endoplasmic Reticulum Stress Induces Cartilage Pathology. *PLoS Genet.*, 5, 1-15.

RAVINDRANATH R.M.H., MORADIAN-OLDAK J. & FINCHAM A.G. (1999) Tyrosyl Motif in Amelogenins Binds N-acetyl-D-glucosamine. *The Journal of Biological Chemistry*, 274, 2464-2471.

RAVINDRANATH R.M.H., TAM W-Y., NGUYEN P. & FINCHAM A.G. (2000) The Enamel Protein Amelogenin Binds to the N-Acetyl-D-glucosamine-mimicking Peptide Motif of Cytokeratins. *The Journal of Biological Chemistry*, 275, 39654-39661.

RAVINDRANATH R.M.H., TAM W-Y., BRINGAS P., SANTOS V. & FINCHAM A.G. (2001) Amelogenin-Cytokeratin 14 interaction in ameloblasts during Enamel Formation. *The Journal of Biological Chemistry*, 276, 36586-36597.

RAVINDRANATH R.M.H., BASILROSE R.M., RAVINDRANATH N.H. & VAITHEESVARAN B. (2003) Amelogenin interacts with Cytokeratin-5 in Ameloblast during enamel growth. *Journal of Biological Chemistry*, 278, 20293-20302.

RAVINDRANATH H.H., CHEN L-S., ZEICHNER-DAVID M., ISHIMA R. & RAVINDRANATH R.M.H. (2004) Interaction between the enamel matrix proteins amelogenin and ameloblastin. *BBRC*, 323, 1075-1083.

RAVINDRANATH R.M.H., DEVARANJAN A. & BRINGAS P. (2007) Enamel formation *in vitro* in mouse molar explants exposed to amelogenin polypeptides ATMP and LRAP on enamel development. *Archives of Oral Biology*.

REID D.J., BEYNON A.D. & RAMIREZ ROZZI F.V. (1998) Histological reconstruction of dental development in four individuals from a medieval site in Picardie, France. *J Hum Evol.*, 35, 463-477.

REID D.J. & FERRELL R.J. (2005) The relationship between number of striae of Retzius and their periodicity in imbricational enamel formation. *Journal of Human Evolution* 50, 195-202.

REITH, E. J. (1970) The stages of amelogenesis as observed in molar teeth of young rats. *J. Ultrastruct. Res.*, 30, 111-151.

RICOBARAZA A., CUADRADO-TEJEDOR M., PÉREZ-MEDIAVILLA A., FRECHILLA D., DEL RÍO J. & GARCÍA-OSTA A. (2009) Phenylbutyrate ameliorates cognitive deficit and reduces tau pathology in an Alzheimer's disease mouse model. *Neuropsychopharmacology.* , 34, 1721-32.

RISNES S. (1986) Enamel apposition rate and the prism periodicity in human teeth. *Scand J Dent Res.*, 94, 394-404.

RITCHIE H.H. & WANG L.H. (1996) Sequence determination of an extremely acidic rat dentin phosphoprotein. *J Biol Chem.* , 271, 21695-8.

ROBINSON C., LOWE N.R. & WEATHERELL J.A. (1975) Amino acid composition distribution and origin of tuft" protein in human and bovine dental enamel. . *Arch Oral Biol* 20, 29-42.

ROBINSON C., FUCHS P. & WEATHERALL J.A. (1981) The appearance of developing rat incisor enamel using freeze-fracture technique. *J. Crystal Growth*, 53, 160-165.

ROBINSON C., KIRKHAM J., STONEHOUSE N.J. & SHORE R.C. (1989) Extracellular Processing of enamel matrix and origin and function of tuft protein. . IN FEARNHEAD R.W. (Ed.) *Tooth Enamel V*. Yokohama, Florence Publishers.

ROBINSON C. & KIRKHAM J. (1986) Dental Enamel, its Formation and its Behaviour in the Oral Environment. *Perspectives in Public Health* 106, 5-7.

ROBINSON C., BROOKES S.J., SHORE R.C. & KIRKHAM J. (1998) The developing enamel matrix: nature and function. *Eur J Oral Sci.* , 106, 282-91.

ROBINSON C., KIRKHAM J., SHORE R.C., BROOKES S.J. & WOOD S.R. (2000) Enamel matrix function and the tuft enigma: a role in directing enamel tissue architecture: a partial sequence of human ameloblastin. IN GOLDBERG M., BOSKEY A. & ROBINSON C. (Eds.) *American academy of orthopaedic surgeons, chemistry and biology of mineralized tissues. Proc, 6th Int. Conf. Chem. Biol. Min. Tiss.*

ROBINSON C. & HUDSON J. (2011) Tuft protein: protein cross-linking in enamel development. *Eur J Oral Sci.*, 119, 50-54.

ROCK M.J., CAIN S.A., FREEMAN L.J., MORGAN A., MELLODY K., MARSON A., SHUTTLEWORTH C.A., WEISS A.S. & KIELTY C.M. (2004) Molecular basis of elastic fiber formation. Critical interactions and a tropoelastin-fibrillin-1 cross-link. *J Biol. Chem.*, 279, 23748-58.

RON, D. & HABENER, J. F. (1992) CHOP, a novel developmentally regulated nuclear protein that dimerizes with transcription factors C/EBP and LAP and functions as a dominant-negative inhibitor of gene transcription. *Genes Dev.*, 6, 439-453.

RON, D. (2002) Translational control in the endoplasmic reticulum stress response. *J.Clin. Investig.*, 110, 1383-1388.

RON D. & WALTER P. (2007) Signal transduction in the endoplasmic reticulum unfolded protein response. *Nat. Rev. Mol. Cell Biol.*, 8, 519-529.

RUCH J.V., LESOT H. & BÈGUE-KIRN C. (1995) Odontoblast Differentiation. *Int. J. Dev. Biol.*, 39, 51-68.

RUSSELL W.L., KELLY E.M., HUNSICKER P.R., BANGHAM J.W., MADDUX S.C. & PHIPPS E.L. (1979) Specific-locus test shows ethylnitrosourea to be the most potent mutagen in the mouse. *PNAS*, 76, 5818-5819.

- RUTKOWSKI D.T. & KAUFMAN R.J. (2007) That which does not kill me makes me stronger: adapting to chronic ER stress. *Trends in biochemical sciences*, 32, 469-476.
- RYU O.H., FINCHAM A.J., HU C.C., ZHANG C, QIAN Q., BARTLETT J.D. & SIMMER J.P. (1999) Characterisation of recombinant pig enamelysin activity and cleavage of recombinant pig and mouse amelogenins. *J Dent Res*, 78, 743-750.
- SALIBA R.S., MUNRO P.M., LUTHERT P.J. & CHEETHAM M.E. (2002) The cellular fate of mutant rhodopsin: quality control, degradation and aggresome formation. *J Cell Sci.* , 115, 2907-18.
- SALIDO E.C., YEN P.H., KOPRIVNIKAR K., YU L-C. & SHAPIRO L.J. (1992) The human enamel protein gene amelogenin is expressed from both the X and the Y chromosomes. *Am. J. Hum. Genet.*, 50, 303-316.
- SASAKI T. (1984) Endocytotic pathways at the ruffled borders of rat maturation ameloblasts. *Histochemistry*, 80, 263-8.
- SASAKI, T. & GARANT, P. (1986) A study of post-secretory maturation ameloblasts in the cat by transmission and freeze-fracture electron-microscopy. *Archives of Oral Biology*, 31, 587-596.
- SCHEUNER D., SONG B., MCEWAN E., LIU C., LAYBUTT R., GILLESPIE P., SAUNDERS T., BONNER-WEIR S. & KAUFMAN R.J. (2001) Translational control is required for the unfolded protein response and in vivo glucose homeostasis. *Mol. Cell*, 7, 1165-1176.
- SCHRODER M. & KAUFMAN R.J. (2005) ER stress and the unfolded protein response. *Mutation Research* 569, 29-63.
- SCHUBERT U., ANTON L.C., GIBBS J., NORBURY C.C., YEWDELL J.W. & BENNINK J.R. (2000) Rapid degradation of a large fraction of newly synthesized proteins by proteasomes. . *Nature* 404, 770-774.
- SEKIGUSHI H., ALALUUSUA S., MINAGUCHI K. & YAKUSHUI M. (2001) A new mutation in the amelogenin gene causes X-linked amelogenesis imperfecta. *J Dent Res*, 80, 617.
- SHEN X., ELLIS R.E., SAKAI K. & KAUFMAN R.J. (2005) Genetic interactions due to constitutive and inducible gene regulation mediated by the unfolded protein response. *PLoS Genet.*, 1, e37.
- SHEPARD A.R., JACOBSON N., MILLAR J.C., PANG I.H., STEELY H.T., SEARBY C.C., SHEFFIELD V.C., STONE E.M. & CLARK A.F. (2007) Glaucoma-causing myocilin mutants require the Peroxisomal targeting signal-1 receptor (PTS1R) to elevate intraocular pressure. *Hum. Mol. Genet.*, 16, 609-617.

SHIKHMAN A.R., GREENSPAN N.S. & CUNNINGHAM M.W. (1994) Cytokeratin peptide SFGSGFGGGY mimics N-acetyl-beta-D-glucosamine in reaction with antibodies and lectins, and induces in vivo anti-carbohydrate antibody response. *J. Immunology*, 154, 5593-5606.

SHORE R.C., BACKMAN B., ELCOCK C., BROOK A., BROOKES S.J. & KIRKHAM J. (2010) The structure and composition of deciduous enamel affected by local hypoplastic autosomal dominant amelogenesis imperfecta resulting from an ENAM mutation. *Cells Tissues Organs*, 191, 301-6.

SIDRAUSKI C., CHAPMAN R. & WALTER P. (1998) The unfolded protein response: an intracellular signalling pathway with many surprising features. *Trends Cell Biol.*, 8, 245-9.

SIMKISS K. & WILBUR K. (1989) *Biomineralisation: cell biology and mineral deposition*, San Diego, Academic Press.

SIMMER J. & FINCHAM A. (1995) Molecular mechanisms of dental enamel formation. *Crit Rev Oral Biol Med.*, 6, 84-108.

SIMMER J.P. & HU J.C. (2002) Expression, structure and function of enamel proteinases. *Connect Tissue Res.*, 43, 441-449.

SIMMER J.P., HU Y., LERTLAM R., YAMAKOSHI Y. & HU J.C. (2009) Hypomaturation enamel defects in *Klk4* knockout/*LacZ* knockin mice. *J Biol Chem*, 284, 19110-21.

SIMMER J.P., PAPAGERAKIS P., SMITH C.E., FISHER D.C., ROUNTREY A.N., ZHENG L. & HU J.C. (2010) Regulation of dental enamel shape and hardness. *J Dent Res.*, 89, 1024-38.

SIMMER S.G., ESTRELLA N.M.R.P., MILKOVICH R.N. & HUA J.C.C. (2013) Autosomal dominant amelogenesis imperfecta associated with ENAM frameshift mutation p.Asn361Ilefs56. *Clin Genet.*, 83, 195-197.

SIMMONS L.M., MONTGOMERY J., BEAUMONT J., DAVIS G.R. & AL-JAWAD M. (2013) Mapping the spatial and temporal progression of human dental enamel biomineralisation using synchrotron X-ray diffraction. *Arch. Oral Biol.*, 58, 1726-1734.

SIRE J.Y., VIT-BEAL T., DELGADO S. & GU X. (2007) The origin and evolution of enamel mineralisation genes. *Cells Tissues Organs*, 186, 25-48.

SLAGER R.E., NEWTON T.L., VLANGOS C.N., FINUCANE B. & ELSEA S.H. (2003) Mutations in *RAI1* associated with Smith-Magenis syndrome. *Nat Genet.*, 33, 466-468.

SMITH D.A. & AMES B. N (1966) Phosphoribosyladenosine Monophosphate, an Intermediate in Histidine Biosynthesis *JBC*, 240, 3056-3053.

SMITH, C. E. & NANJI A. (1989) A method for sampling the stages of amelogenesis on mandibular rat incisors using the molars as reference for dissection. *Anat. Rec.*, 225, 257-266.

SMITH C.E., CHEN W.Y., ISSAD M. & FAZEL A. (1995) Enamel matrix turnover during amelogenesis: Basic biochemical properties of short-lived sulfated enamel proteins. *Calcif Tissue Int.*, 57, 133-144.

SMITH C.E. & NANJI A. (1996) Protein dynamics of amelogenesis. *Anat Rec.*, 245, 186-207.

SMITH, C. E. (1998) Cellular and chemical events during enamel mineralisation. *Crit. Rev. Oral. Biol. Med.*, 9, 128-161.

SMITH T.M. (2006) Experimental determination of the periodicity of incremental features in enamel. *J Anat.*, 208, 99-113.

SNEAD M.L., LUO W., HSU D.D., MELROSE R.J., LAU E.C. & STENMAN G. (1992) Human ameloblastoma tumors express the amelogenin gene. *Oral Surg Oral Med Oral Pathol.* 1992 Jul;74(1):64-72. . Snead ML(1), Luo W, Hsu DD, Melrose RJ, 74, 64-72.

SNEAD M.L., PAINE M.L., CHEN L.S., YOSHIDA B., LUO W., ZHU D-H., LEI Y-P., LIU Y-H. & MAXSON R.E.JR. (1996) The murine amelogenin promoter: Developmentally regulated expression in transgenic animals. *Connect Tissue Res.*, 35, 41-47.

STERN K.H. (1954) The Liesegang Phenomenon. *Chem. Rev.*, 54, 79-99.

STEWART, R. E., MACARTHUR, M. W., LASKOWSKI, R. A. & THORNTON, J. M. (2003) Molecular basis of inherited diseases: a structural perspective. *Trends Genet.*, 19, 505-513.

SUGA S. (1989) Enamel hypomineralisation viewed from the pattern of progressive mineralisation of human and monkey developing enamel. *Adv Dent Res.*, 3, 188-98.

SUN, T.-T., EICHNER, R., SCHERMER, A., COOPER, D., NELSON, W. G. & WIESS, R. A. (1984) Classification, expression and possible mechanisms of evolution of mammalian epithelial keratins: A unifying model. IN (A.J. LEVINE, G. F. V. W., W.C. TOPP AND J.D. WATSON, & EDS) (Eds.) *In Cancer Cells: I. The Transformed Phenotype*. New York, Cold Spring Harbor.

SZEGEZDI E., LOGUE S.E., GORMAN A.M. & SAMALI A. (2006) Mediators of endoplasmic stress-induced apoptosis. *EMBO Rep*, 7, 880-885.

TABATA M.J., MATSUMURA T., LIU J.G., WAKISAKA S. & KURISU K. (1998) Expression of cytokeratin 14 in ameloblast-lineage cells of the developing tooth of rat, both in vivo and in vitro. *Arch Oral Biol.*, 41, 1019-27.

TAKANO Y. (1995) Enamel mineralization and the role of ameloblasts in calcium transport. *Connect Tissue Res.*, 33, 127-137.

TAMBURSTUEN M.V., RESELAND J.E., SPAHR A., BROOKES S.J., KVALHEIM G., SLABY I., SNEAD M.L. & LYGSTADAAS S.P. (2011) Ameloblastin expression and putative autoregulation in mesenchymal cells suggest a role in early bone formation and repair. *Bone*, 48, 406-13.

TAN J., LEUNG W., MORADIAN-OLDAK J., ZEICHNER-DAVID M. & FINCHAM A.G. (1998) Quantitative Analysis of Amelogenin Solubility. *J Dent Res* 77, 1388-1396.

TANABE T. (1984) Purification and characterisation of proteolytic enzyme in porcine immature enamel. *Tsurumi Univ. Dent. J*, 10, 443-452.

TANABE T., AOBA T., MORENO E.C., FUKAE M. & SHIMIZU M. (1990) Properties of phosphorylated 32 kd nonamelogenin proteins isolated from porcine secretory enamel. *Calcif. Tissue Int.*, 46, 205-215.

TARASEVICH B.J., HOWARD C.J., LARSON J.L., SNEAD M.L., SIMMER J.P., PAINE M.L. & SHAW W.J. (2007) The nucleation and growth of calcium phosphate by amelogenin. *J Crystal Growth*, 304, 407-415.

TEN CATE, J. & DUIJUSTERS, P. (1982) Alternating demineralization and remineralization of artificial enamel lesions. *Caries Research*, 16, 201-210.

TEN CATE, A. R. (1998) *Oral Histology: development, structure and function*.

TERMINE J.D., BELCOURT A.B., CHRISTNER P.J., CONN K.M. & NYLEN M.U. (1980A) Properties of Dissociately Extracted Fetal Tooth Matrix Proteins I. Principal molecular species in developing bovine enamel. *The Journal of Biological Chemistry*, 255, 9760-9768.

TERMINE J.D., BELCOURT A.B., MIYAMOTO M.S. & CONN K.M. (1980B) Properties of Dissociately Extracted Fetal Tooth Matrix Proteins II. Separation and purification of Fetal Bovine Dentin Phosphoprotein. *The Journal of Biological Chemistry*, 255, 9769-9772.

TODD D.J., LEE A-H. & GLIMCHER L.H. (2008) The endoplasmic reticulum stress response in immunity and autoimmunity. *Nat. Rev. Immunol.*, 8, 663-674.

TOMPKINS K., GEORGE A., VEIS A. & (2006) Characterization of a mouse amelogenin [A-4]/M59 cell surface receptor. *Bone*, 38, 172-180.

TOWBIN H., STAEBELIN T. & GORDON J. (1979) Electrophoretic transfer of proteins from polyacrylamide gels to nitrocellulose sheets: procedure and some applications. *PNAS*, 76, 4350-4354.

TSAI C.T. & WEISSMAN A.M. (2010) The unfolded protein response, degradation from the endoplasmic reticulum, and cancer. *Genes and Cancer*, 1, 764-778.

TSUCHIYA M., TYE C.E., SHARMA R., SMITH C.E. & BARTLETT J.D. (2008) XBP1 May Determine the Size of the Ameloblast Endoplasmic Reticulum. *J Dent Res.* , 87, 1058-1062.

TYE C.E., RATTAY K.R., WARNER K.J., GORDON J.A.R., SODEK J., HUNTER G.K. & GOLDBERG H.A. (2003) Delineation of the hydroxyapatite-nucleating domains of Bone sialoprotein. *JBC*, 278, 7949-7958.

UCHIDA T., TANABE T., FUKAE M. & SHIMIZU M. (1991 a) Immunocytochemical and immunochemical detection of a 32 kDa nonamelogenin and related proteins in porcine tooth germs. *Arch Histol Cytol.* , 54, 527-38.

UCHIDA T., TANABE T., FUKAE M., SHIMIZU M., YAMADA M., MIAKE K. & KOBAYASHI S. (1991 b) Immunochemical and immunohistochemical studies, using antisera against porcine 25 kDa amelogenin, 89 kDa enamelin and the 13-17 kDa nonamelogenins, on immature enamel of the pig and rat. *Histochemistry*, 96, 129-38.

UCHIDA T., MURAKAMI C., DOHI N., WAKIDA K., SATODA T. & TAKAHASHI O. (1997) Synthesis, secretion, degradation and fate of ameloblastin during the matrix formation stage of the rat incisor as shown by immunocytochemistry and immunochemistry using region-specific antibodies/. *J. Histochem. Cytochem.*, 45, 1329-1340.

VAN SLEGTENHORST M., DE HOOGT R., HERMANS C., NELLIST M., JANSSEN B., VERHOEF S., LINDHOUT D., VAN DEN OUWELAND A., HALLEY D., YOUNG J., BURLEY M., JEREMIAH S., WOODWARD K., NAHMIAS J., FOX M., EKONG R., OSBORNE J., WOLFE J., POVEY S., SNELL R.G., CHEADLE J.P., JONES A.C., TACHATAKI M., RAVINE D., SAMPSON J.R., REEVE M.P., RICHARDSON P., WILMER F., MUNRO C., HAWKINS T.L., SEPP T., ALI J.B., WARD S., GREEN A.J., YATES J.R., KWIATKOWSKA J., HENSKE E.P., SHORT M.P., HAINES J.H., JOZWIAK S. & KWIATKOWSKI D.J. (1997) Identification of the tuberous sclerosis gene TSC1 on chromosome 9q34. *Science*, 277, 805-808.

WADA Y., FUJISAWA R., NODASAKA Y. & KUBOKI Y. (1996) Electrophoretic gels of dentin matrix proteins as diffusion media for *in vitro* mineralisation. *J Dent Res*, 75, 1381-1387.

WANG, Y., SHEN, J., ARENZANA N., TIRASOPHON W., KAUFMAN R.J. & PRYWES R. (2000) Activation of ATF6 and an ATF6 DNA binding site by the endoplasmic reticulum stress response. *JBC*, 275, 27013-17020.

WARSHAWSKY H., BAI P. & NANCI A. (1984) Lack of evidence for the rhythmicity in enamel development.. IN BELCOURT A.B. & RUCH J.V. (Eds.) *Tooth Morphogenesis and Differentiation* Paris, Insern.

WARSHAWSKY H., BAI P. & NANCI A. (1987) Analysis of crystallite shape in rat incisor enamel. *Anat Rec.* , 218, 380-90.

WATABE N. & KINGSLEY R.J., (1989) Extra-, inter-, and intracellular mineralization in invertebrates and algae. IN CRICK R.E. (Ed.) *Origin, Evolution, and Modern Aspects of Biomineralization in Plants and Animals*. New York, Plenum.

WAZEN R.M., MOFFATT P., ZALZAL S.F., YAMADA Y., NANCI A. & (2009) A mouse model expressing a truncated form of ameloblastin exhibits dental and junctional epithelium defects. . *Matrix Biol.*, 28, 292-303.

WEATHERELL J.A., WEIDMANN S.M. & EYRE D.R. (1968) Histological appearance and chemical composition of enamel protein from mature human molars. . *Caries Res* 2, 281-293.

WEATHERELL, J. (1975) Composition of dental enamel. *British Medical Bulletin*, 31, 115-119.

WEINER S. & ADDADI L. (1991) Acidic macromolecules of mineralized tissues: the controllers of crystal formation. *Trends Biochem Sci.*, 16, 252-6.

WEN X., CAWTHORN W.P., MACDOUGALD O.A., STUPP S.I., SNEAD M.L. & ZHOU Y. (2011) The influence of Leucine-rich amelogenin peptide on MSC fate by inducing Wnt10b expression. *Biomaterials*, 32, 6478-6486.

WIESNER S., STIER G., SATTLER M. & MACIAS M.J. (2002) Solution Structure and Ligand Recognition of the WW Domain Pair of the Yeast Splicing Factor Prp40. *Journal of Molecular Biology*, 324, 897-822.

WITKOP, C. J. (1988) Amelogenesis imperfecta, dentinogenesis imperfecta and dentin dysplasia revisited: problems in classification. . *Journal of oral pathology*, 17, 547-553.

WOLFE S.A., GRANT R.A., ELROD-ERICKSON M. & PABO C.O. (2001) Beyond the "recognition code": structures of two Cys2His2 zinc finger/TATA box complexes. *Structure*, 9, 717-23.

WRIGHT C.S. (1984) Structural comparison of the two distinct sugar binding sites in wheat germ agglutinin isolectin II. *J Mol Biol.*, 178, 91-104.

WRIGHT J.T., HART P.S., ALDRED M.J., SEOW K., CRAWFORD P.J., HONG S.P., GIBSON C.W. & HART T.C. (2003) Relationship of phenotype and genotype in X-linked amelogenesis imperfecta. . *Connect. Tissue Res.*, 44, 72-78.

WRIGHT, J. T. (2006) The molecular etiologies and associated phenotypes of Amelogenesis Imperfecta. *Am j med genet a*, 140, 2547-2555.

WRIGHT J.T., HONG S.P., SIMMONS D., DALY B., UEBELHART D. & LUDER H.U. (2008) DLX3 c.561_562delCT mutation causes attenuated phenotype of tricho-dento-osseous syndrome. *Am J Med Genet A*, 146, 343-349.

WRIGHT J.T., FRAZIER-BOWERS S., SIMMONS D., ALEXANDER K., CRAWFORD P., HAN S.T., HART P.S. & HART T.C., (2009) Phenotypic variation in FAM83H-associated amelogenesis imperfecta. *J Dent Res*. 2009 Apr;88(4):356-60, 88, 356-60.

WU J. & KAUFMAN R.J. (2006) From acute ER stress to physiological roles of the Unfolded Protein Response. *Cell Death and Differentiation* 13, 374-384.

XIAO C., GIACCA A. & LEWIS G.F. (2011) Sodium phenylbutyrate, a drug with known capacity to reduce endoplasmic reticulum stress, partially alleviates lipid-induced insulin resistance and beta-cell dysfunction in humans. *Diabetes*. , 60, 918-24.

XU L., HARADA H. & TANIGUCHI A. (2008) The effects of LAMP1 and LAMP3 on M180 amelogenin uptake, localization and amelogenin mRNA induction by amelogenin protein. . *Journal of Biochemistry*, 114, 531-537.

YAGISHITA, H., TAYA Y., KANRI Y., MATSUO A., NONAKA H., FUJITA H. & AOBA T. (2001) The secretion of amelogenins is associated with the induction of enamel and dentinoid in an ameloblastic fibro-odontoma. *J. Oral Pathol. Med.*, 30, 499-503.

YAMAKOSHI Y., TANABE T., FUKAE M. & SHIMIZU M. (1994) Porcine amelogenins. *Calcif Tissue Int.*, 54, 69-75.

YAMAKOSHI, Y. (1995) Carbohydrate moieties of porcine 32 kDa enamelin. *Cal. Tissue Int.*, 56, 323-330.

YAMAKOSHI Y., PINHEIRO F.H., TANABE T., FUKAE M. & SHIMIZU M. (1998) Sites of asparagine-linked oligosaccharides in porcine 32 kDa enamelin. *Connect Tissue Res.*, 39, 39-46.

YAMAKOSHI, Y., TANABE, T., OIDA S., HU C.C., SIMMER J.P. & FUKAE M. (2001) Calcium binding of enamel proteins and their derivatives with emphasis on the calcium-binding domain of porcine sheathlin. *Arch. Oral Biol.*, 46, 1005-1014.

YAMAKOSHI Y., HU J.C.C., FUKAE M., YAMAKOSHI F. & SIMMER J.P. (2006) How do enamelysin and kallikrein 4 process the 32-Kda enamelin? *Eur J Oral Sci*, 114, 45-51.

YAMAKOSHI Y., SIMMER J.P., BARTLETT J.D., KARAKIDA T. & OIDA S. (2013) MMP20 and KLK4 activation and inactivation interactions in vitro. *Arch Oral Biol.* , 58, 1569-77.

YAMAMOTO K., OHTANI S., KATO S., SUGIMOTO H., MIAKE K. & NAKAMURA T. (1990) Morphological changes in human and animal enamel rods with heating--especially limits in temperature allowing discrimination between human and animal teeth. *Bull Kanagawa Dent Coll.* , 18, 55-61.

YE J., RAWSON R.B., KOMURO R., CHEN X., DAVE U.P., PRYWES R., BROWN M.S. & GOLDSTEIN J.L. (2000) ER stress induces cleavage of membrane bound ATF6 by the same proteases that process SREBPs. *Mol. Cell*, 6, 1355-1364.

YILDIRIM S. (2013) *Dental pulp stem cells*, Springer.

YOSHIDA, H., MATSUI, T., YAMAMOTO A., OKADA T. & MORI K. (2001) XBP1 mRNA is induced by ATF6 and spliced by IRE1 in response to ER stress to produce a highly active transcription factor. *Cell*, 107, 881-891.

YUNTA M. & LAZO P.A. (2003) Tetraspanin proteins as organisers of membrane microdomains and signalling complexes. *Cell Signal.*, 15, 559-564.

ZBAR B., KISHIDA T., CHEN F., SCHMIDT L., MAHER E.R., RICHARDS F.M., CROSSEY P.A., WEBSTER A.R., AFFARA N, A., FERGUSON-SMITH M.A., BRAUCH H., GLAVAC D., NEUMANN H.P.H., TISHERMAN S., MULVIHILL J.J., GROSS D.J., SHUIN T., WHALEY J., SEIZINGER B., KLEY N., OLSCHWANG S., BOISSON C., RICHARD S., LIPS C.H.M., LINEHAN W.M. & LERMAN M. (1996) Germline mutations in the Von Hippel-Lindau disease (VHL) gene in families from North America, Europe, and Japan. *Hum Mutat.* , 8, 348-57.

ZEICHNER-DAVID M. (2001) Is there more to enamel matrix proteins than biomineralisation? *Matrix Biology*, 20, 307-316.

ZHANG, P., MCGRATH, B., LI S., FRANK A., ZAMBITO F., REINERT J., GANNON M., MA K., MCNAUGHTON K. & CAVENER D.R. (2002) The PERK Eukaryotic Initiation Factor 2 alpha Kinase is Required for the Development of the Skeletal System, Postnatal Growth, and the Function and Viability of the Pancreas. *Molecular and Cellular Biology*, 22, 3864-3874.

ZHANG K. & KAUFMAN R.J. (2008) From endoplasmic-reticulum stress to the inflammatory response. *Nature*, 454, 455-462.

ZHANG, H., TOMPKINS, K., GARRIGUES, J., SNEAD, M. L., GIBSON, C. W. & SOMERMAN, M. J. (2010) Full length amelogenin binds to cell surface LAMP-1 on tooth root/periodontium associated cells. *Archives of Oral Biology*, 55, 417-425.

ZHANG, K. & CHEN, J. (2012) The regulation of integrin function by divalent cations. *Cell Adhesion Migration*, 6, 20-29.

ZHAO Z.P., WANG Z. & WANG S.C. (2003) Formation, charged characteristic and BSA adsorption behavior of carboxymethyl chitosan/PES composite MF membrane. *J Membrane Sci*, 217, 151–158.

ZHU W., ROBEY P.G. & BOSKEY A.L. (2007) *The regulatory role of matrix proteins in mineralization of bone*, New York, Elsevier.

ZINSZNER H., KURODA M., WANG X., BATCHVAROVA N., LIGHTFOOT R.T., REMOTTI H., STEVENS J.L. & RON D. (1998) CHOP is implicated in programmed cell death in response to impaired function of the endoplasmic reticulum. *Genes Dev.*, 12, 982-995.

ZODE G.S., SHARMA A.B., LIN X., SEARBY C.C., BUGGE K., KIM G.H., CLARK A.F. & SHEFFIELD V.C. (2014) Ocular-specific ER stress reduction rescues glaucoma in murine glucocorticoid-induced glaucoma. *J Clin Invest.*, 124, 1956-65.

ZOU, Y., WANG, H., SHAPIRO, J. L., OKAMOTO, C. T., BROOKES, S. J., LYGSTADAAS, S. P., SNEAD, M. L. & PAINE, M. L. (2007) Determination of protein regions responsible for interactions of amelogenin with CD63 and LAMP1. . *Journal of Biochemistry*, 408, 347-354.

ZULETA A., VIDAL R.L., ARMENTANO D., PARSONS G. & HETZ C. (2012) AAV-mediated delivery of the transcription factor XBP1s into the striatum reduces mutant Huntingtin aggregation in a mouse model of Huntington's disease. *Biochem Biophys Res Commun.* , 420, 558-63.

List of Abbreviations

ADJ	Amelodental junction
Ag	Silver
AI	Amelogenesis Imperfecta
ALB	Albumin
ALP	Alkaline phosphatase
AMBN	Ameloblastin
AMG	Amelogenin
APS	Ammonium persulphate
ATMP	Amelogenin trityrosyl motif peptide
BSA	Bovine Serum Albumin
CK	Cytokeratin
CT	Crossing Threshold
D	Daltons
DEJ	Dentino-enamel junction
DH ₂ O	Distilled water
DMSO	Dimethyl sulphoxide
DNA	Deoxyribonucleic acid
DPP	Dentinephosphoprotein
DTT	DL-dithiothreitol
ECM	Extracellular matrix
EDTA -Na ₂	Ethylenediaminetetra-acetic acid (disodium salt)
EDX	Energy dispersive X-ray
ELISA	Enzyme linked immunosorbant assay
EMD	Enamel matrix derivative
EMGs	Enamel matrix glycoproteins
ER	Endoplasmic Reticulum
ERAD	Endoplasmic Reticulum Associated Degradation

FITC	Fluorescein Isothiocyanate
GAG	Glycosaminoglycan
GlcNAc	N-Acetyl-D-glucosamine
Gmp1	GlcNAc mimicking peptide
HAP	Hydroxyapatite
HCl	Hydrochloric acid
HDPL	Human Dental Peridontal Ligament
HEPES	(4-(2-hydroxyethyl)-1-piperazineethanesulfonic acid
HERS	Hertwig's epithelial root sheath
HMW	High molecular weight
Hr	Hour
Hrs	Hours
IgG	Immunoglobulin G
kDa	Kilodaltons
KLK-4	Kallikrein-4
LAMP's	Lysosomal associated membrane proteins
LB	Loading buffer
LRAP	Leucine rich amelogenin peptide
Mg	Milligram
mL	Millilitre
MMP	Matrix Metalloproteinase
MMP-20	Matrix Metalloproteinase 20 – enamelysin
MUT	Mutant
MW	Molecular Weight
NaCl	Sodium chloride
Ng	Nanogram
PAGE	Polyacrylamide gel electrophoresis
PBS	Phosphate buffered salt
PCR	Polymerase chain reaction
PDL	Periodontal ligament

PGA	Poly L-glutamic acid
PTM	Post-translational modification
Q-RT-PCR	Quantitative real time polymerase chain reaction
RGD	Arginine-glycine-aspartate
RNA	Ribonucleic acid
Rpm	Revolutions per minute
RT	Room temperature
RT-PCR	Reverse transcriptase polymerase chain reaction
SDS	Sodium dodecyl sulphate
SEM	Scanning electron microscope
TBS	Tris buffered saline
TBS-T	Tris buffered saline – Tween 20 (0.05%)
TEM	Transmission electron microscope
TIMP's	Tissue inhibitors of metalloproteinases
TRAP	Tyrosine rich amelogenin peptide
Tris	Tris-(hydroxymethyl)-methylamine
µg	Microgram
µL	Microlitre
UPR	Unfolded Protein Response
UV	Ultraviolet
WT	Wild type

Appendix 1 Comparison of mineral nucleating systems

Protein	Conc. of protein	Optimal conc. for hydroxyapatite	Conditions	Buffers	Publication	Comments	Time/ temperature
BSP	1-10 µg/mL	2 µg/mL	2% agarose, 150 mM NaCl, 0.01% NaN ₃ , 10 mM Tris-HCl pH 7.4. Flow = 1 mL/h per gel.	CaCl ₂ and NaPo ₄ (5.5 mM and 7.5 mM each tested)	Hunter and Goldberg, PNAS (1994)		37°C for 5 days
Osteopontin	1-10 µg/mL	No HAP seen	2% agarose, 150mM NaCl, 0.01% NaN ₃ , 10 mM Tris-HCl pH 7.4. Flow = 1 mL/h per gel.	CaCl ₂ and NaPo ₄ (5.5mM and 7.5mM each tested)	Hunter and Goldberg, PNAS (1994)		37°C for 5 days
BSP	0.3 ng/mL- 100 µg/mL	0.3 µg/mL	1% agarose, 150mM NaCl, 20 mM Hepes pH 7.4, 0.01%NaN ₃	CaCl ₂ and NaPo ₄ (6.5 mM and 3.9 mM each tested)	Hunter and Goldberg, J. Biochem (1996)	3500 mwco dialysis membrane	37°C for 5 days

Protein	Conc. of protein	Optimal conc. for hydroxyapatite	Conditions	Buffers	Publication	Comments	Time/temperature
Osteopontin	0.3 ng/mL- 100 µg/ml	No HAP seen	1% agarose, 150mM NaCl, 20 mM Hepes pH 7.4, 0.01% NaN ₃	CaCl ₂ and NaPo ₄ (6.5 mM and 3.9 mM each tested)	Hunter and Goldberg J. Biochem (1996)	3500 mwco dialysis membrane	37°C for 5 days
DPP	0.3 ng/mL- 100 µg/mL	10 µg/mL	1% agarose, 150 mM NaCl, 20 mM Hepes pH 7.4, 0.01% NaN ₃	CaCl ₂ and NaPo ₄ (6.5mM and 3.9mM each tested)	Hunter and Goldberg J. Biochem (1996)	3500mwco dialysis membrane	37°C for 5 days
Osteocalcin	0.3 ng/mL- 100 µg/mL	No HAP seen	1% agarose, 150 mM NaCl, 20mM Hepes pH 7.4, 0.01% NaN ₃	CaCl ₂ and NaPo ₄ (6.5mM and 3.9mM each tested)	Hunter and Goldberg J. Biochem (1996)	3500mwco dialysis membrane	37°C for 5 days
BSP - untreated	5 µg/mL	higher calcium-phosphate levels seen	1% agarose, 150mM NaCl, 10mM Tris-HCl, 0.01% NaN ₃ flow= 1ml/h/gel	CaCl ₂ and NaPo ₄ (6.0mM each, pH7.4)	Hunter and Goldberg, J. Biochem (1994)	AP not needed for nucleation	37°C for 5 days

Protein	Conc. of protein	Optimal conc. for hydroxyapatite	Conditions	Buffers	Publication	Comments	Time/temperature
0	5 µg/mL		1% agarose, 150mM NaCl, 10mM Tris-HCl, 0.01% NaN ₃ flow= 1ml/h/gel	CaCl ₂ and NaPo ₄ (6.0mM each, pH7.4)	Hunter and Goldberg, J. Biochem (1994)		37°C for 5 days
Calreticulin	20 µg/mL	No HAP seen	1% agarose, 150mM NaCl, 10 mM Tris-HCl, 0.01% NaN ₃ flow= 1 mL/h/gel	CaCl ₂ and NaPo ₄ (6.0mM each, pH7.4)	Hunter and Goldberg, J. Biochem (1994)	No HAP nucleation	37°C for 5 days
Osteopontin	100 µg/mL	No HAP seen	1% agarose, 150mM NaCl, 10 mM Tris-HCl, 0.01% NaN ₃ flow= 1 mL/h/gel	CaCl ₂ and NaPo ₄)7.5mM each, pH 7.4)	Hunter GK, Kyle CL, Goldberg HA, J.Biochem (1994)	Osteopontin is effective inhibitor of HAP	37°C for 5 days
BSP - native	0.087 µg/mL	HAP seen	1% agarose, 150mM NaCl, 20mM Hepes pH 7.4, 0.01% NaN ₃	CaNO ₃ (7.1mM) and NaPo ₄ (4.3mM)	Tye CE, Hunter GK, Goldberg HA, JBC (2003)	Glutamic acid rich region of BSP maybe a requisite for HAP nucleation	37°C for 5 days

Protein	Conc. of protein	Optimal conc. for hydroxyapatite	Conditions	Buffers	Publication	Comments	Time/temperature
BSP- rat recombinant	1.7-3.4 µg/mL	Less HAP than native	1% agarose, 150mM NaCl, 20mM Hepes pH 7.4, 0.01% NaN ₃	CaNO ₃ (7.1mM) and NaPo ₄ (4.3mM)	Tye CE, Hunter GK, Goldberg HA, JBC (2003)	Glutamic acid rich region of BSP maybe a requisite for HAP nucleation	37°C for 5 days
BSP-poly E to poly A	3 µg/mL	Decreased HAP	1% agarose, 150mM NaCl, 20 mM Hepes pH 7.4, 0.01% NaN ₃	CaNO ₃ (7.1 mM) and NaPo ₄ (4.3 mM)	Tye CE, Hunter GK, Goldberg HA, JBC (2003),	Glutamic acid rich region of BSP maybe a requisite for HAP nucleation	37°C for 5 days
BSP - poly E to poly D	3 µg/mL		1% agarose, 150 mM NaCl, 20 mM Hepes pH 7.4, 0.01% NaN ₃	CaNO ₃ (7.1mM) and NaPo ₄ (4.3mM)	Tye CE, Hunter GK, Goldberg HA, JBC (2003)	Glutamic acid rich region of BSP maybe a requisite for HAP nucleation	37°C for 5 days

Protein	Conc. of protein	Optimal conc. for hydroxyapatite	Conditions	Buffers	Publication	Comments	Time/temperature
Osteocalcin	100 µg/mL	No HAP seen	1% agarose, 150 mM NaCl, 20 mM Hepes pH7.4, 0.01% NaN ₃ flow= 1 mL/h/gel	CaCl ₂ and NaPo ₄ (6.5mM and 3.9mM, pH 7.4)	Hunter GK, Goldberg HA , J.Biochem (1996)	3500mwco dialysis membrane + 10 µg/mL PGA used as positive control	37°C for 5 days
Osteopontin	100 µg/mL	No HAP seen - potent inhibitor	1% agarose, 150 mM NaCl, 20mM Hepes pH7.4, 0.01% NaN ₃ flow= 1 mL/h/gel	CaCl ₂ and NaPo ₄ (6.5mM and 3.9mM, pH 7.4)	Hunter GK, Goldberg HA, J.Biochem (1996)	3500mwco dialysis membrane + 10 µg/mL PGA used as positive control	37°C for 5 days
Osteonectin	100 µg/mL	No HAP seen	1% agarose, 150mM NaCl, 20mM Hepes pH7.4, 0.01% NaN ₃ flow= 1 mL/h/gel	CaCl ₂ and NaPo ₄ (6.5 mM and 3.9 mM, pH 7.4)	Hunter GK, Goldberg HA, J.Biochem (1996)	3500mwco dialysis membrane + 10 µg/mL PGA used as positive control	37°C for 5 days

Protein	Conc. of protein	Optimal conc. for hydroxyapatite	Conditions	Buffers	Publication	Comments	Time/temperature
BSP	0.3 µg/mL		1% agarose, 150mM NaCl, 20mM Hepes pH7.4, 0.01% NaN ₃ flow= 1 mL/h/gel	CaCl ₂ and NaPo ₄ (6.5mM and 3.9 mM, pH 7.4)	Hunter GK, Goldberg HA, J.Biochem (1996)	3500mwco dialysis membrane + 10 µg/mL PGA used as positive control	37°C for 5 days
DPP	10 µg/mL		1% agarose, 150mM NaCl, 20mM Hepes pH7.4, 0.01% NaN ₃ flow= 1 mL/h/gel	CaCl ₂ and NaPo ₄ (6.5 mM and 3.9 mM, pH 7.4)	Hunter GK, Goldberg HA, J.Biochem (1996)	3500mwco dialysis membrane + 10 µg/mL PGA used as positive control	37°C for 5 days
Chondrocalcin	100 µg/mL	No HAP seen	1% agarose, 150mM NaCl, 20mM Hepes pH7.4, 0.01%NaN ₃ flow= 1 mL/h/gel	CaCl ₂ and NaPo ₄ (6.5 mM and 3.9 mM, pH 7.4)	Hunter GK, Goldberg HA, J.Biochem (1996)	3500mwco dialysis membrane + 10 µg/mL PGA used as positive control	37°C for 5 days

Protein	Conc. of protein	Optimal conc. for hydroxyapatite	Conditions	Buffers	Publication	Comments	Time/ temperature
BSA	0-500 µg/mL	No HAP	96 well plate – 100 µl 0.5% agarose, 10mM Na ₂ HPO ₄ , 50 mM Hepes, 10mM CaCl ₂ , pH 7.4	150 µl of 150 mM NaCl, 50 mM Hepes, 10mM CaCl ₂ pH7.4	Couchoural D et al, J.Inorganic Biochem (1999)	96 well plate format with phosphate buffer in gel, overlaid with calcium	37°C for 4 hours
Type 1 collagen (calf skin)	0-500 µg/mL	No HAP	96 well plate – 100 µL 0.5% agarose, 10 mM Na ₂ HPO ₄ , 50 mM Hepes, 10 mM CaCl ₂ , pH 7.4	150 µL of 150 mM NaCl, 50 mM Hepes, 10 mM CaCl ₂ pH7.4	Couchoural D et al, J.Inorganic Biochem (1999)	96 well plate format with phosphate buffer in gel, overlaid with calcium	37°C for 4 hours
Fibronectin (human plasma)	0-100 µg/mL	No HAP	96 well plate – 100 µL 0.5% agarose, 10 mM Na ₂ HPO ₄ , 50mM Hepes, 10mM CaCl ₂ , pH 7.4	150 µL of 150 mM NaCl, 50 mM Hepes, 10 mM CaCl ₂ pH7.4	Couchoural D et al, J.Inorganic Biochem (1999)	96 well plate format with phosphate buffer in gel, overlaid with calcium	37°C for 4 hours

Protein	Conc. of protein	Optimal conc. for hydroxyapatite	Conditions	Buffers	Publication	Comments	Time/temperature
PGA (Sigma P-4886)	0-30 µg/mL	HAP at 5 µg/mL	96 well plate – 100 µL 0.5% agarose, 10 mM Na ₂ HPO ₄ , 50 mM Hepes, 10 mM CaCl ₂ , pH 7.4	150 µL of 150 mM NaCl, 50 mM Hepes, 10 mM CaCl ₂ , pH7.4	Couchoural D et al, J.Inorganic Biochem (1999)	96 well plate format with phosphate buffer in gel, overlaid with calcium	37°C for 4 hours
Phosphoryn	0-20 µg/mL	Increased HAP at 20 µg/mL	96 well plate – 50 µL 0.5% agarose, 150 mM NaCl, 50 mM Hepes, pH7.5, plus 10mM phosphate	100 µL of 150 mM NaCl, 50 mM Hepes, 10 mM CaCl ₂ , pH7.5	Fujisawa R et al, Biochimica et Biophysica (1996)	96 well plate format with phosphate buffer in gel, overlaid with calcium	25°C for 24 hours
Osteonectin (synthetic)	0-20 µg/mL	Increased HAP at 20 µg/mL	96 well plate – 50 µL 0.5% agarose, 150 mM NaCl, 50 mM Hepes, pH7.5, plus 10 mM phosphate	100 µL of 150 mM NaCl, 50 mM Hepes, 10 mM CaCl ₂ , pH7.5	Fujisawa R et al, Biochimica et Biophysica (1996)	96 well plate format with phosphate buffer in gel, overlaid with calcium	25°C for 24 hours

Protein	Conc. of protein	Optimal conc. for hydroxyapatite	Conditions	Buffers	Publication	Comments	Time/temperature
BSA	0-20 µg/mL	Decreased HAP	96 well plate – 50 µl 0.5% agarose, 150 mM NaCl, 50 mM Hepes, pH7.5, plus 10 mM phosphate	100 µL of 150 mM NaCl, 50 mM Hepes, 10 mM CaCl ₂ , pH7.5	Fujisawa R et al, Biochimica et Biophysica (1996)	96 well plate format with phosphate buffer in gel, overlaid with calcium	25°C for 24 hours
BSP - decarboxylated	5 µg/mL	Abolishes HAP formation	1% agarose, 150 mM NaCl, 10 mM Tris-HCl, 0.01% NaN ₃ flow= 1 mL/h/gel	CaCl ₂ and NaPo ₄ (6.0 mM each, pH7.4)	Hunter and Goldberg, Biochem (1994)	Modification of carboxylate groups abolishes HAP formation	37°C for 5 days

Appendix 2

Typical profile for Q-RT-PCR from the LightCycler



Nicky1

Experiment

Creation Date	12/10/2009 4:25:18 PM	Last Modified Date	12/10/2009 5:57:42 PM
Operator	System Admin	Owner	System Admin
Start Time	12/10/2009 4:26:55 PM	End Time	12/10/2009 5:37:07 PM
Run State	Completed	Software Version	LCS480 1.5.0.39
Macro		Macro Owner	
Macro Status			
Templates	Mono Color Hydrolysis Probe - UPL Probe 96-I	Plate ID	00985399
Test ID		Lot ID	
Color Comp ID			
Run Notes			

Abs Quant/2nd Derivative Max for All Samples (Abs Quant/2nd Derivative Max)

Results

Inc	Pos	Name	Type	CP	Concentration	Standard	Status
<input checked="" type="checkbox"/>	A1	WT 0 GAPDH	Standard				
<input checked="" type="checkbox"/>	A2	WT 1 GAPDH	Standard			1.00E0	
<input checked="" type="checkbox"/>	A3	WT 2 GAPDH	Standard			1.00E-1	
<input checked="" type="checkbox"/>	A4	WT 3 GAPDH	Standard			1.00E-2	
<input checked="" type="checkbox"/>	A5	WT 4 GAPDH	Standard			1.00E-3	
<input checked="" type="checkbox"/>	A6	WT 5 GAPDH	Standard			1.00E-4	
<input checked="" type="checkbox"/>	A7	Sample 7	Unknown				
<input checked="" type="checkbox"/>	A8	Sample 8	Unknown				
<input checked="" type="checkbox"/>	A9	Sample 9	Unknown				
<input checked="" type="checkbox"/>	A10	Sample 10	Unknown				
<input checked="" type="checkbox"/>	A11	Sample 11	Unknown				
<input checked="" type="checkbox"/>	A12	Sample 12	Unknown				
<input checked="" type="checkbox"/>	B1	WT 0 GAPDH	Standard				
<input checked="" type="checkbox"/>	B2	WT 1 GAPDH	Standard			1.00E0	
<input checked="" type="checkbox"/>	B3	WT 2 GAPDH	Standard			1.00E-1	
<input checked="" type="checkbox"/>	B4	WT 3 GAPDH	Standard			1.00E-2	
<input checked="" type="checkbox"/>	B5	WT 4 GAPDH	Standard			1.00E-3	
<input checked="" type="checkbox"/>	B6	WT 5 GAPDH	Standard			1.00E-4	
<input checked="" type="checkbox"/>	B7	Sample 19	Unknown				
<input checked="" type="checkbox"/>	B8	Sample 20	Unknown				

Results

Inc	Pos	Name	Type	CP	Concentration	Standard	Status
<input checked="" type="checkbox"/>	B9	Sample 21	Unknown				
<input checked="" type="checkbox"/>	B10	Sample 22	Unknown				
<input checked="" type="checkbox"/>	B11	Sample 23	Unknown				
<input checked="" type="checkbox"/>	B12	Sample 24	Unknown				
<input checked="" type="checkbox"/>	C1	WT 0 GAPDH	Standard				
<input checked="" type="checkbox"/>	C2	WT 1 GAPDH	Standard			1.00E0	
<input checked="" type="checkbox"/>	C3	WT 2 GAPDH	Standard			1.00E-1	
<input checked="" type="checkbox"/>	C4	WT 3 GAPDH	Standard			1.00E-2	
<input checked="" type="checkbox"/>	C5	WT 4 GAPDH	Standard			1.00E-3	
<input checked="" type="checkbox"/>	C6	WT 5 GAPDH	Standard			1.00E-4	
<input checked="" type="checkbox"/>	C7	Sample 31	Unknown				
<input checked="" type="checkbox"/>	C8	Sample 32	Unknown				
<input checked="" type="checkbox"/>	C9	Sample 33	Unknown				
<input checked="" type="checkbox"/>	C10	Sample 34	Unknown				
<input checked="" type="checkbox"/>	C11	Sample 35	Unknown				
<input checked="" type="checkbox"/>	C12	Sample 36	Unknown				
<input checked="" type="checkbox"/>	D1	WT 0 AMELX	Standard				
<input checked="" type="checkbox"/>	D2	WT 1 AMELX	Standard			1.00E0	
<input checked="" type="checkbox"/>	D3	WT 2 AMELX	Standard			1.00E-1	
<input checked="" type="checkbox"/>	D4	WT 4 AMELX	Standard			1.00E-2	
<input checked="" type="checkbox"/>	D5	WT 4 AMELX	Standard			1.00E-3	
<input checked="" type="checkbox"/>	D6	WT 5 AMELX	Standard			1.00E-4	
<input checked="" type="checkbox"/>	D7	Sample 43	Unknown				
<input checked="" type="checkbox"/>	D8	Sample 44	Unknown				
<input checked="" type="checkbox"/>	D9	Sample 45	Unknown				
<input checked="" type="checkbox"/>	D10	Sample 46	Unknown				
<input checked="" type="checkbox"/>	D11	Sample 47	Unknown				
<input checked="" type="checkbox"/>	D12	Sample 48	Unknown				
<input checked="" type="checkbox"/>	E1	WT 0 AMELX	Standard				
<input checked="" type="checkbox"/>	E2	WT 1 AMELX	Standard			1.00E0	
<input checked="" type="checkbox"/>	E3	WT 2 AMELX	Standard			1.00E-1	
<input checked="" type="checkbox"/>	E4	WT 4 AMELX	Standard			1.00E-2	
<input checked="" type="checkbox"/>	E5	WT 4 AMELX	Standard			1.00E-3	
<input checked="" type="checkbox"/>	E6	WT 5 AMELX	Standard			1.00E-4	
<input checked="" type="checkbox"/>	E7	Sample 55	Unknown				
<input checked="" type="checkbox"/>	E8	Sample 56	Unknown				
<input checked="" type="checkbox"/>	E9	Sample 57	Unknown				

Results

Inc	Pos	Name	Type	CP	Concentration	Standard	Status
<input checked="" type="checkbox"/>	E10	Sample 58	Unknown				
<input checked="" type="checkbox"/>	E11	Sample 59	Unknown				
<input checked="" type="checkbox"/>	E12	Sample 60	Unknown				
<input checked="" type="checkbox"/>	F1	WT 0 AMELX	Standard				
<input checked="" type="checkbox"/>	F2	WT 1 AMELX	Standard			1.00E0	
<input checked="" type="checkbox"/>	F3	WT 2 AMELX	Standard			1.00E-1	
<input checked="" type="checkbox"/>	F4	WT 4 AMELX	Standard			1.00E-2	
<input checked="" type="checkbox"/>	F5	WT 4 AMELX	Standard			1.00E-3	
<input checked="" type="checkbox"/>	F6	WT 5 AMELX	Standard			1.00E-4	
<input checked="" type="checkbox"/>	F7	Sample 67	Unknown				
<input checked="" type="checkbox"/>	F8	Sample 68	Unknown				
<input checked="" type="checkbox"/>	F9	Sample 69	Unknown				
<input checked="" type="checkbox"/>	F10	Sample 70	Unknown				
<input checked="" type="checkbox"/>	F11	Sample 71	Unknown				
<input checked="" type="checkbox"/>	F12	Sample 72	Unknown				
<input checked="" type="checkbox"/>	G1	Sample 73	Unknown				
<input checked="" type="checkbox"/>	G2	Sample 74	Unknown				
<input checked="" type="checkbox"/>	G3	Sample 75	Unknown				
<input checked="" type="checkbox"/>	G4	Sample 76	Unknown				
<input checked="" type="checkbox"/>	G5	Sample 77	Unknown				
<input checked="" type="checkbox"/>	G6	Sample 78	Unknown				
<input checked="" type="checkbox"/>	G7	Sample 79	Unknown				
<input checked="" type="checkbox"/>	G8	Sample 80	Unknown				
<input checked="" type="checkbox"/>	G9	Sample 81	Unknown				
<input checked="" type="checkbox"/>	G10	Sample 82	Unknown				
<input checked="" type="checkbox"/>	G11	Sample 83	Unknown				
<input checked="" type="checkbox"/>	G12	Sample 84	Unknown				
<input checked="" type="checkbox"/>	H1	Sample 85	Unknown				
<input checked="" type="checkbox"/>	H2	Sample 86	Unknown				
<input checked="" type="checkbox"/>	H3	Sample 87	Unknown				
<input checked="" type="checkbox"/>	H4	Sample 88	Unknown				
<input checked="" type="checkbox"/>	H5	Sample 89	Unknown				
<input checked="" type="checkbox"/>	H6	Sample 90	Unknown				
<input checked="" type="checkbox"/>	H7	Sample 91	Unknown				
<input checked="" type="checkbox"/>	H8	Sample 92	Unknown				
<input checked="" type="checkbox"/>	H9	Sample 93	Unknown				
<input checked="" type="checkbox"/>	H10	Sample 94	Unknown				

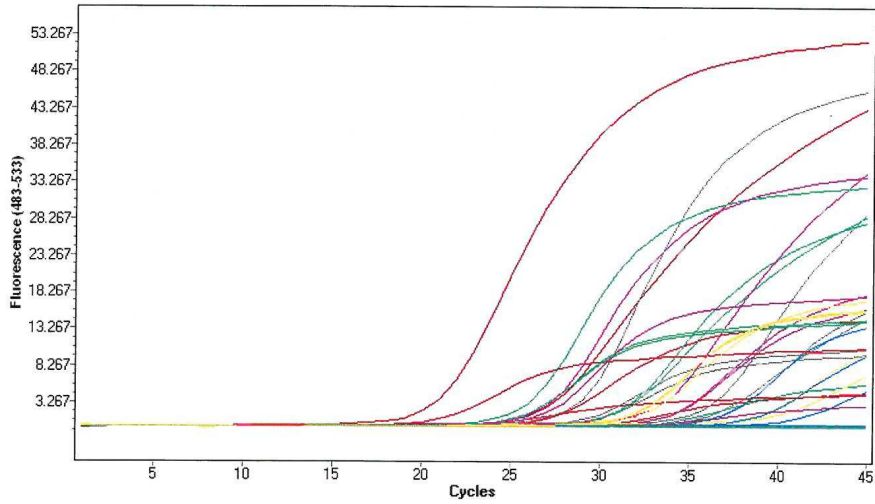
Results

Inc	Pos	Name	Type	CP	Concentration	Standard	Status
<input checked="" type="checkbox"/>	H11	Sample 95	Unknown				
<input checked="" type="checkbox"/>	H12	Sample 96	Unknown				

Statistics

Samples	Mean Cp	Std Cp	Mean conc	Std conc
A1, B1, C1				
A2, B2, C2				
A3, B3, C3				
A4, B4, C4				
A5, B5, C5				
A6, B6, C6				
D1, E1, F1				
D2, E2, F2				
D3, E3, F3				
D4, E4, F4				
D5, E5, F5				
D6, E6, F6				

Amplification Curves



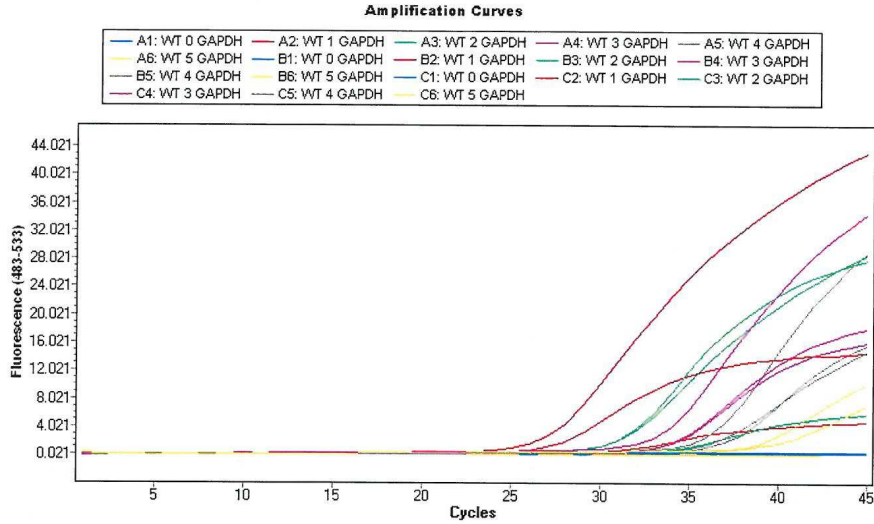
Abs Quant/2nd Derivative Max for New Subset 1 (Abs Quant/2nd Derivative Max)

Results

Inc	Pos	Name	Type	CP	Concentration	Standard	Status
<input type="checkbox"/>	A1	WT 0 GAPDH	Standard				
<input checked="" type="checkbox"/>	A2	WT 1 GAPDH	Standard			1.00E0	
<input checked="" type="checkbox"/>	A3	WT 2 GAPDH	Standard			1.00E-1	
<input checked="" type="checkbox"/>	A4	WT 3 GAPDH	Standard			1.00E-2	
<input checked="" type="checkbox"/>	A5	WT 4 GAPDH	Standard			1.00E-3	
<input checked="" type="checkbox"/>	A6	WT 5 GAPDH	Standard			1.00E-4	
<input type="checkbox"/>	B1	WT 0 GAPDH	Standard				
<input checked="" type="checkbox"/>	B2	WT 1 GAPDH	Standard			1.00E0	
<input checked="" type="checkbox"/>	B3	WT 2 GAPDH	Standard			1.00E-1	
<input checked="" type="checkbox"/>	B4	WT 3 GAPDH	Standard			1.00E-2	
<input checked="" type="checkbox"/>	B5	WT 4 GAPDH	Standard			1.00E-3	
<input checked="" type="checkbox"/>	B6	WT 5 GAPDH	Standard			1.00E-4	
<input type="checkbox"/>	C1	WT 0 GAPDH	Standard				
<input checked="" type="checkbox"/>	C2	WT 1 GAPDH	Standard			1.00E0	
<input checked="" type="checkbox"/>	C3	WT 2 GAPDH	Standard			1.00E-1	
<input checked="" type="checkbox"/>	C4	WT 3 GAPDH	Standard			1.00E-2	
<input checked="" type="checkbox"/>	C5	WT 4 GAPDH	Standard			1.00E-3	
<input checked="" type="checkbox"/>	C6	WT 5 GAPDH	Standard			1.00E-4	

Statistics

Samples	Mean Cp	Std Cp	Mean conc	Std conc
A1, B1, C1				
A2, B2, C2				
A3, B3, C3				
A4, B4, C4				
A5, B5, C5				
A6, B6, C6				



Abs Quant/2nd Derivative Max for New Subset 1 (1) (Abs Quant/2nd Derivative Max)

Results

Inc	Pos	Name	Type	CP	Concentration	Standard	Status
<input checked="" type="checkbox"/>	A1	WT 0 GAPDH	Standard				
<input checked="" type="checkbox"/>	A2	WT 1 GAPDH	Standard	30.49		1.00E0	
<input checked="" type="checkbox"/>	A3	WT 2 GAPDH	Standard	33.78		1.00E-1	
<input checked="" type="checkbox"/>	A4	WT 3 GAPDH	Standard	34.00		1.00E-2	
<input checked="" type="checkbox"/>	A5	WT 4 GAPDH	Standard	36.87		1.00E-3	
<input checked="" type="checkbox"/>	A6	WT 5 GAPDH	Standard			1.00E-4	
<input checked="" type="checkbox"/>	B1	WT 0 GAPDH	Standard				
<input checked="" type="checkbox"/>	B2	WT 1 GAPDH	Standard	27.21		1.00E0	
<input checked="" type="checkbox"/>	B3	WT 2 GAPDH	Standard	31.13		1.00E-1	
<input checked="" type="checkbox"/>	B4	WT 3 GAPDH	Standard	33.91		1.00E-2	
<input checked="" type="checkbox"/>	B5	WT 4 GAPDH	Standard	36.14		1.00E-3	
<input checked="" type="checkbox"/>	B6	WT 5 GAPDH	Standard	38.51		1.00E-4	
<input checked="" type="checkbox"/>	C1	WT 0 GAPDH	Standard				
<input checked="" type="checkbox"/>	C2	WT 1 GAPDH	Standard	27.16		1.00E0	
<input checked="" type="checkbox"/>	C3	WT 2 GAPDH	Standard	31.19		1.00E-1	
<input checked="" type="checkbox"/>	C4	WT 3 GAPDH	Standard	33.54		1.00E-2	

> - Late Cp call (last five cycles) has higher uncertainty

Results

Inc	Pos	Name	Type	CP	Concentration	Standard	Status
<input checked="" type="checkbox"/>	C5	WT 4 GAPDH	Standard	36.21		1.00E-3	
<input checked="" type="checkbox"/>	C6	WT 5 GAPDH	Standard	40.00		1.00E-4	>

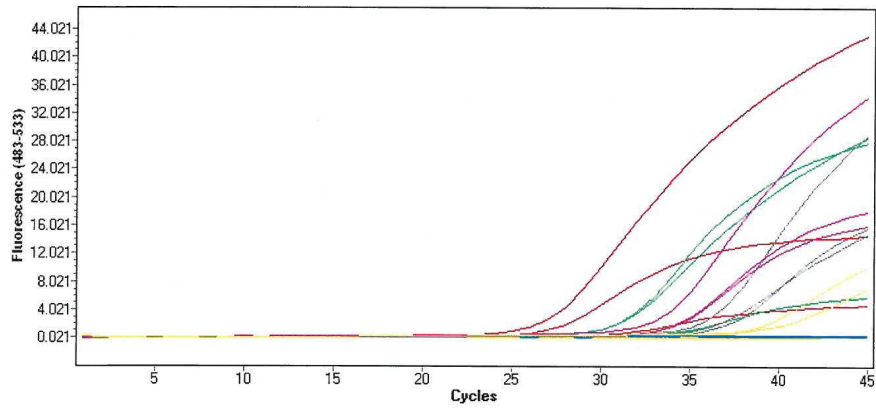
> - Late Cp call (last five cycles) has higher uncertainty

Statistics

Samples	Mean Cp	Std Cp	Mean conc	Std conc
A1, B1, C1				
A2, B2, C2	28.29	1.91		
A3, B3, C3	32.03	1.51		
A4, B4, C4	33.81	0.25		
A5, B5, C5	36.41	0.40		
A6, B6, C6	39.25	1.05		

Amplification Curves

A1: WT 0 GAPDH	A2: WT 1 GAPDH	A3: WT 2 GAPDH	A4: WT 3 GAPDH	A5: WT 4 GAPDH
A6: WT 5 GAPDH	B1: WT 0 GAPDH	B2: WT 1 GAPDH	B3: WT 2 GAPDH	B4: WT 3 GAPDH
B5: WT 4 GAPDH	B6: WT 5 GAPDH	C1: WT 0 GAPDH	C2: WT 1 GAPDH	C3: WT 2 GAPDH
C4: WT 3 GAPDH	C5: WT 4 GAPDH	C6: WT 5 GAPDH		



Abs Quant/2nd Derivative Max for New Subset 2 (Abs Quant/2nd Derivative Max)

Results

Inc	Pos	Name	Type	CP	Concentration	Standard	Status
<input checked="" type="checkbox"/>	D1	WT 0 AMELX	Standard	40.00			>
<input checked="" type="checkbox"/>	D2	WT 1 AMELX	Standard	23.88		1.00E0	
<input checked="" type="checkbox"/>	D3	WT 2 AMELX	Standard	25.48		1.00E-1	

> - Late Cp call (last five cycles) has higher uncertainty

Results

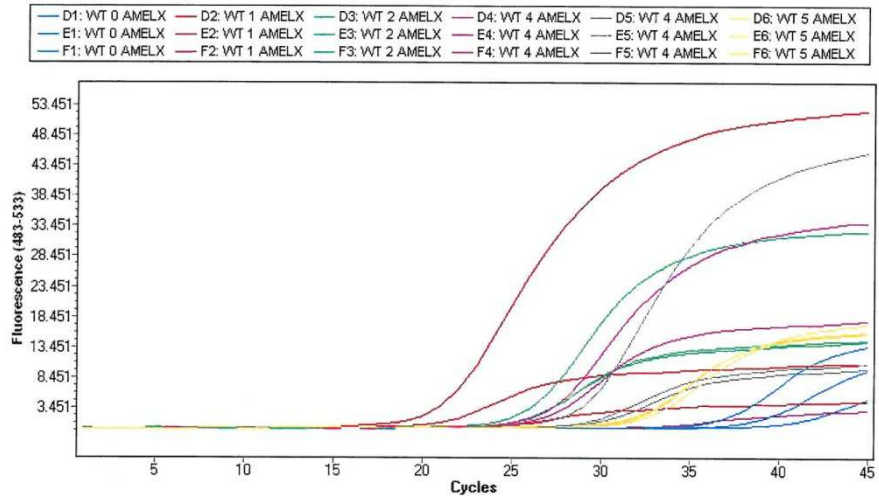
Inc	Pos	Name	Type	CP	Concentration	Standard	Status
<input checked="" type="checkbox"/>	D4	WT 4 AMELX	Standard	32.77		1.00E-2	
<input checked="" type="checkbox"/>	D5	WT 4 AMELX	Standard	29.65		1.00E-3	
<input checked="" type="checkbox"/>	D6	WT 5 AMELX	Standard	31.63		1.00E-4	
<input checked="" type="checkbox"/>	E1	WT 0 AMELX	Standard	36.60			
<input checked="" type="checkbox"/>	E2	WT 1 AMELX	Standard	20.94		1.00E0	
<input checked="" type="checkbox"/>	E3	WT 2 AMELX	Standard	25.44		1.00E-1	
<input checked="" type="checkbox"/>	E4	WT 4 AMELX	Standard	26.66		1.00E-2	
<input checked="" type="checkbox"/>	E5	WT 4 AMELX	Standard	29.01		1.00E-3	
<input checked="" type="checkbox"/>	E6	WT 5 AMELX	Standard	31.74		1.00E-4	
<input checked="" type="checkbox"/>	F1	WT 0 AMELX	Standard	38.75			
<input checked="" type="checkbox"/>	F2	WT 1 AMELX	Standard	21.13		1.00E0	
<input checked="" type="checkbox"/>	F3	WT 2 AMELX	Standard	25.72		1.00E-1	
<input checked="" type="checkbox"/>	F4	WT 4 AMELX	Standard	26.89		1.00E-2	
<input checked="" type="checkbox"/>	F5	WT 4 AMELX	Standard	28.95		1.00E-3	
<input checked="" type="checkbox"/>	F6	WT 5 AMELX	Standard	32.29		1.00E-4	

> - Late Cp call (last five cycles) has higher uncertainty

Statistics

Samples	Mean Cp	Std Cp	Mean conc	Std conc
D1, E1, F1	38.45	1.72		
D2, E2, F2	21.98	1.65		
D3, E3, F3	25.54	0.15		
D4, E4, F4	28.77	3.47		
D5, E5, F5	29.20	0.39		
D6, E6, F6	31.89	0.36		

Amplification Curves



Appendix 3

Bioinformatics data for 290 enamelin sequences

C-terminus and N-terminus highlighted

```
10/26/2014 www.uniprot.org/align/A2014102673FR3PFG6W.aln
TR|T2B3P2|T2B3P2_9EUTH -----
TR|T2B3N8|T2B3N8_9EUTH -----
TR|T2B1Z8|T2B1Z8_9EUTH -----
TR|T2B3X8|T2B3X8_9EUTH -----
TR|T2B2O8|T2B2O8_9EUTH -----
TR|T2B3Y2|T2B3Y2_9EUTH -----
TR|T2B3M8|T2B3M8_9EUTH -----
TR|T2B417|T2B417_9EUTH -----
TR|T2B2P0|T2B2P0_9EUTH -----
TR|T2B3X3|T2B3X3_9EUTH -----
TR|F7HPM2|F7HPM2_CALJA --PN-----QTQ-SK----KPPQKRPLKQP-----SH--T
144 -----
TR|B1ACV1|B1ACV1_EUBAS -----

SP|O97939|ENAM_PIG PTQP-E-EETQTPQAFPPFGNGLFPYQQPLWHVPHR-----
180 -----
SP|Q9NRM1|ENAM_HUMAN QQPQ--EEEAQPPQAFPPFGNGLFPYQQPPWQIPQR-----
179 -----
SP|O55196|ENAM_MOUSE AARA--KDDAQPPQFPFPFGNGLYPYQPPWPPIQR-----
184 -----
SP|P27628|TUFT1_BOVIN -----
TR|D3ZIB0|D3ZIB0_RAT AARA--KDEAQPPQFPFPFGNGLYPYQPPWPPIPQT-----
254 -----
TR|Q548P8|Q548P8_MOUSE AARA--KDDAQPPQFPFPFGNGLYPYQPPWPPIQR-----
184 -----
TR|G5BMZ8|G5BMZ8_HETGA PSKG--KVDTPPQFPFPFNGLFPYQQPPWPPIQR-----
174 -----
TR|B2L7U6|B2L7U6_PANTR QQPQ--EEEAQPPQAFPPFGNGLFPYQQPPWQIPQR-----
179 -----
TR|C8C1R6|C8C1R6_HORSE -----
TR|L5LI18|L5LI18_MYODS FTTP--QEEAQPPQAFPPFGNGIFHYQQPPWQVPHR-----
168 -----
TR|B9UIT7|B9UIT7_XENTR PPAP--DQQAQAPMMFPFNSIMNYPYQ--PYWQQPF-----
173 -----
TR|G5CXW7|G5CXW7_TARSY -----
TR|F1RUQ1|F1RUQ1_PIG PTQP-E-EETQTPQAFPPFGNGLFPYQQPLWHVPHR-----
180 -----
TR|G7P5N1|G7P5N1_MACFA PAQP--E-----EEAQPPQR-----
119 -----
TR|L5K8J3|L5K8J3_PTEAL PTQP--QEEAQTQAFSPFGNGLFPYQQPPWQVPHR-----
147 -----
TR|G3I4B5|G3I4B5_CRIGR AARA--KEEAQPPQFPFPFGNGLYPYQQPPWPPIQR-----
128 -----
TR|C8C1S5|C8C1S5_PROCA -----
TR|Q8IWP4|Q8IWP4_HUMAN QQPQ--EEEAQPPQAFPPFGNGLFPYQQPPWQIPQR-----
179 -----
TR|C8C1S4|C8C1S4_HETBR -----
TR|B2L7V9|B2L7V9_SAGLB -----
TR|C8C1Q4|C8C1Q4_VOMUR -----
TR|B2L7T7|B2L7T7_MACMU -----WQIPQR-----
21 -----
TR|C8C1R8|C8C1R8_AMBHO -----
TR|B2L7V2|B2L7V2_NASLA PAQP--EEEAQPPQAFPPFGNGLFLYQPPWPPIQR-----
104 -----
TR|B2L7U4|B2L7U4_COLAN -----
TR|C8C1R5|C8C1R5_LAMGL -----
TR|C8C1S2|C8C1S2_9EUTH -----
TR|B2L7V5|B2L7V5_LAGLA -----
TR|C8C1Q6|C8C1Q6_DELLE -----
TR|C8C1S9|C8C1S9_ERIEU -----
TR|C8C1R3|C8C1R3_HIPAM -----
TR|C8C1S3|C8C1S3_DUGDU -----
TR|B2L7U7|B2L7U7_PANTR -----
TR|C8C1S6|C8C1S6_ELEMA -----
TR|C8C1R7|C8C1R7_FELCA -----
TR|B2L7U0|B2L7U0_PAPAN -----R-----
```


10/26/2014

www.uniprot.org/align/A2014102673FR3PFG6W.aln

TR G5CXQ0 G5CXQ0_AEPRU	-----
TR G5CXR3 G5CXR3_ALLFU	-----
TR G5CXV6 G5CXV6_TUPMI	-----
TR G5CXQ1 G5CXQ1_HYPMS	-----
TR G5CXP8 G5CXP8_TRIVU	-----
TR G5CXU6 G5CXU6_GALVR	-----
TR G5CXR5 G5CXR5_SURSU	-----
TR G5CXP3 G5CXP3_ISOMA	-----
TR G5CXS9 G5CXS9_HIPCO	-----
TR G5CXS1 G5CXS1_ARCFO	-----
TR G5CXR6 G5CXR6_CROCR	-----
TR G5CXS4 G5CXS4_AILME	-----
TR G5CXP2 G5CXP2_RHYRA	-----
TR G5CXW5 G5CXW5_LEMCA	-----
TR G5CXW4 G5CXW4_PROVE	-----
TR G5CXP9 G5CXP9_PHACI	-----
TR G5CXS0 G5CXS0_9CARN	-----
TR G5CXS5 G5CXS5_GENGE	-----
TR G5CXN9 G5CXN9_DROGL	-----
TR G5CXT4 G5CXT4_HYSTU	-----
TR G5CXU4 G5CXU4_THYTR	-----
TR G5CXU0 G5CXU0_PTEGI	-----
TR B2L7T4 B2L7T4_MACNE	-----
TR G5CXQ9 G5CXQ9_9CETA	-----
TR G5CXY2 G5CXY2_9HYST	-----
TR G5CXX7 G5CXX7_CHILA	-----
TR G5CXZ6 G5CXZ6_9HYST	-----
TR G5CXY3 G5CXY3_JACJA	-----
TR G5CXZ0 G5CXZ0_GRAMU	-----
TR G5CXY7 G5CXY7_DIPHE	-----
TR G5CXZ3 G5CXZ3_9HYST	-----
TR G5CXZ5 G5CXZ5_THRSW	-----
TR G5CXX1 G5CXX1_APLRU	-----
TR G5CXY5 G5CXY5_EREDO	-----
TR G5CXW8 G5CXW8_ABRBE	-----
TR G5CXX5 G5CXX5_CASCN	-----
TR G5CXZ4 G5CXZ4_TAMST	-----
TR G5CXW9 G5CXW9_CUNTA	-----
TR G5CXZ2 G5CXZ2_PEDCA	-----
TR G5CXX4 G5CXX4_NYOCO	-----
TR G5CXY6 G5CXY6_CRACA	-----
TR G5CXY4 G5CXY4_HOPGY	-----
TR G5CXX8 G5CXX8_CRIGR	-----
TR G5CXZ1 G5CXZ1_OCTGL	-----
TR G5CXX2 G5CXX2_HETGA	-----
TR G5CXY9 G5CXY9_HYSBR	-----
TR Q8NFB4 Q8NFB4_HUMAN	-----R-----
1	
TR S9WRG8 S9WRG8_9CETA	PTQP-Q-EEAQTPEAFLPFGNGLFPYQPPWHVPHR-----
129	
TR G7MT52 G7MT52_MACMU	PAQP--E-----EEAQPQR-----
119	
TR L8IJZ2 L8IJZ2_9CETA	TAQP-QBEETQTPQAFPPFGNGLFPYQPPWHIPHK-----
168	
TR Q4R358 Q4R358_MACFA	-----
TR V8NY54 V8NY54_OPHHA	-----
TR B2L7V8 B2L7V8_SAGLB	-----R-----
1	
TR B2L7U2 B2L7U2_COLAN	-----
TR B2L7U3 B2L7U3_COLAN	-----AFPPFGNGLFLYQPPWQIPQ-----
21	
TR B2L7T9 B2L7T9_PAPAN	-----AFPPFGNGLFLYQPPWQIPQ-----
21	
TR B2L7V6 B2L7V6_SAGLB	-----
TR B2L7U9 B2L7U9_HYLSY	-----
TR A0A061IKW6 A0A061IKW6_CRIGR	AARA--KEEAQPPQFPFPFGNGLYPYQPPWPIPQR-----
185	

10/26/2014 www.uniprot.org/align/A2014102673FR3PFG6W.aln

TR|A0A061IJS1|A0A061IJS1_CRIGR AARA--KEEAQPPQAFPPFNGLYPYQQPPWQIPQR-----
171
SP|P02769|ALBU_BOVIN -----
TR|F1MKR5|F1MKR5_BOVIN TAQP--QEEETQTPQAFFPPFNGLFPYQQPPWHIPHK-----
184
TR|H2QPM0|H2QPM0_PANTR QQP--EEEAQPPQAFPPFNGLFPYQQPPWQIPQR-----
179
TR|G3X143|G3X143_SARHA EGPPRQKEEDEQPPQYPPFNGMFPFPQPPWQFPQ-----
188
TR|F7HPL6|F7HPL6_CALJA PAQP--KEEDQPPQAFPPFNGLFPYQQPPWQIPQR-----
178
TR|H2PDI6|H2PDI6_PONAB QAQP--KEEAQPPQAFPPFNGLFPYQQPPWQIPQR-----
179
TR|M3X473|M3X473_FELCA PAQP--EEEAQPPQAFPPFNGLFLYQQPPWQVPHR-----
183
TR|G1R843|G1R843_NOMLE -----QR-----
2
TR|G3RLI8|G3RLI8_GORGO QQP--EEEAQPPQAFPPFNGLFPYQQPPWQIPQR-----
179
TR|G1KW91|G1KW91_ANOCA FVQPPKGEKPPQQAFFPH-----PQQPPWQIPQI----FGH-----GGF
188
TR|T2B203|T2B203_9EUTH -----
TR|T2B2P6|T2B2P6_9EUTH -----
TR|T2B2M4|T2B2M4_9EUTH -----
TR|T2B431|T2B431_9EUTH -----
TR|T2B3N3|T2B3N3_9EUTH -----
TR|B1ACV5|B1ACV5_MESBI -----
TR|T2B2N6|T2B2N6_9EUTH -----
TR|T2B3W8|T2B3W8_9EUTH -----
TR|T2B410|T2B410_9EUTH -----
TR|T2B420|T2B420_9EUTH -----
TR|T2B3P2|T2B3P2_9EUTH -----
TR|T2B3N8|T2B3N8_9EUTH -----
TR|T2B1Z8|T2B1Z8_9EUTH -----
TR|T2B3X8|T2B3X8_9EUTH -----
TR|T2B208|T2B208_9EUTH -----
TR|T2B3Y2|T2B3Y2_9EUTH -----
TR|T2B3M8|T2B3M8_9EUTH -----
TR|T2B417|T2B417_9EUTH -----
TR|T2B2P0|T2B2P0_9EUTH -----
TR|T2B3X3|T2B3X3_9EUTH -----
TR|F7HPM2|F7HPM2_CALJA PAQP--KEEDQPPQAFPPFNGLFPYQQPPWQIPQR-----
178
TR|B1ACV1|B1ACV1_EUBAS -----

SP|O97939|ENAM_PIG -----IPPGYG--RPPTSNEEGNPFYFGYHGFGGRPPYYSEEMFEQ-DF
224
SP|Q9NRM1|ENAM_HUMAN -----LPPPGYG--RPPISENEEGNPFYFGYHGFGGRPPYYSEEMFEQ-DF
224
SP|O55196|ENAM_MOUSE -----GPPTAFG--RPKFSNEEG-NPYAFFGYHGFGGR-PYYSEEMFE--DY
226
SP|P27628|TUFT1_BOVIN -----
TR|D3ZIB0|D3ZIB0_RAT -----GPPTGFG--RPKFSNEEG-NPYAYFGYHGFGGR-PYYSEEMFE--DY
296
TR|Q548P8|Q548P8_MOUSE -----GPPTAFG--RPKFSNEEG-NPYAFFGYHGFGGR-PYYSEEMFE--DY
226
TR|G5BMZ8|G5BMZ8_HETGA -----MPPPGFG--RPPLSNEEGNPFYFGYHGFGGR-PYYSEE-IE--DY
216
TR|B2L7U6|B2L7U6_PANTR -----LPPPGYG--RPPMSNEEGNPFYFGYHGFGGRPPYYSEEMFEQ-DF
224
TR|C8C1R6|C8C1R6_HORSE -----RPPYYSEEMFE--DF
13
TR|L5LI18|L5LI18_MYODS -----VPPGYG--RPPVSNEEGNPFYFGYHGFGGRPPYYSEEMFEQ-DF
212
TR|B9UIT7|B9UIT7_XENTR -----MHGFG--RPPNSNEEGN---YFGFFGNGGRAPYNSEEINE--DE
211

10/28/2014

www.uniprot.org/align/A2014102673FR3PFG6W.aln

```

TR|G5CXX8|G5CXX8_CRIGR -----
TR|G5CXZ1|G5CXZ1_OCTGL -----
TR|G5CXX2|G5CXX2_HETGA -----
TR|G5CXY9|G5CXY9_HYSBR -----
TR|Q8NFB4|Q8NFB4_HUMAN -----
TR|S9WRG8|S9WRG8_9CETA -----
TR|G7MT52|G7MT52_MACMU -----
TR|L8IJZ2|L8IJZ2_9CETA -----
TR|Q4R358|Q4R358_MACFA -----
TR|V8NY54|V8NY54_OPHHA -----
TR|B2L7V8|B2L7V8_SAGLB -----
TR|B2L7U2|B2L7U2_COLAN -----
TR|B2L7U3|B2L7U3_COLAN -----
TR|B2L7T9|B2L7T9_PAPAN -----
TR|B2L7V6|B2L7V6_SAGLB -----
TR|B2L7U9|B2L7U9_HYLSY -----
TR|AOA061IKW6|AOA061IKW6_CRIGR -----
TR|AOA061IJS1|AOA061IJS1_CRIGR -----
SP|P02769|ALBU_BOVIN -----
TR|F1MKR5|F1MKR5_BOVIN -----
TR|H2QPM0|H2QPM0_PANTR -----
TR|G3X143|G3X143_SARHA -----
TR|F7HPL6|F7HPL6_CALJA -----
TR|H2PDI6|H2PDI6_PONAB -----
TR|M3X473|M3X473_FELCA -----
TR|G1R843|G1R843_NOMLE -----
TR|G3RLI8|G3RLI8_GORGO -----
TR|G1KW91|G1KW91_ANOCA -----G
275
TR|T2B203|T2B203_9EUTH -----
TR|T2B2P6|T2B2P6_9EUTH -----
TR|T2B2M4|T2B2M4_9EUTH -----
TR|T2B431|T2B431_9EUTH -----
TR|T2B3N3|T2B3N3_9EUTH -----
TR|B1ACV5|B1ACV5_MESBI -----
TR|T2B2N6|T2B2N6_9EUTH -----
TR|T2B3W8|T2B3W8_9EUTH -----
TR|T2B410|T2B410_9EUTH -----
TR|T2B420|T2B420_9EUTH -----
TR|T2B3P2|T2B3P2_9EUTH -----
TR|T2B3N8|T2B3N8_9EUTH -----
TR|T2B1Z8|T2B1Z8_9EUTH -----
TR|T2B3X8|T2B3X8_9EUTH -----
TR|T2B208|T2B208_9EUTH -----
TR|T2B3Y2|T2B3Y2_9EUTH -----
TR|T2B3M8|T2B3M8_9EUTH -----
TR|T2B417|T2B417_9EUTH -----
TR|T2B2P0|T2B2P0_9EUTH -----
TR|T2B3X3|T2B3X3_9EUTH -----
TR|F7HPM2|F7HPM2_CALJA -----
TR|B1ACV1|B1ACV1_EUBAS -----

SP|O97939|ENAM_PIG -----PTGTSGQGNPRSNPT-----GQNG---PA
289
SP|Q9NRM1|ENAM_HUMAN -----PTGNSTPGLNTGNNPP-----AQNGIGPLPA
294
SP|O55196|ENAM_MOUSE -----PIGNTGPGPNAGNNPT-----VQNGVFPPPK
298
SP|P27628|TUFT1_BOVIN -----
TR|D3ZIB0|D3ZIB0_RAT -----PVGNTGPGPNAGNNPT-----VLNGVFPLPK
371
TR|Q548P8|Q548P8_MOUSE -----PIGNTGPGPNAGNNPT-----VQNGVFPPPK
298
TR|G5BMZ8|G5BMZ8_HETGA -----PTLNNVPGLNTGNNPT-----AQNGIFPLPR
283
TR|B2L7U6|B2L7U6_PANTR -----PTGNSTPGLNTGNNPP-----AQNGIGPLPA

```

10/26/2014

www.uniprot.org/align/A2014102673FR3PFG6W.aln

```
294
TR|C8C1R6|C8C1R6_HORSE      --PTGNSGYGPNNTVSNRT-----VQNGVILPPT
86
TR|L5LI18|L5LI18_MYODS     --PTGNSGHGPNNTGGNPT-----AQNGVNPHPA
285
TR|B9UIT7|B9UIT7_XENTR     ESMAGDITQS-----STIALNAQNGHIEGPP
280
TR|G5CXW7|G5CXW7_TARSY     --PTGN-----AGSNPT-----VQNGVILPPT
77
TR|F1RUQ1|F1RUQ1_PIG       ---TGTSGQGPNPRSNPT-----GQNG---PA
288
TR|G7P5N1|G7P5N1_MACFA     --PTGNSIPGPNNTGNNPP-----AQNGIVPLPA
234
TR|L5K8J3|L5K8J3_PTEAL     --PTGNSHGGPNNTVSGPT-----AQNGAIPPPA
265
TR|G3I4B5|G3I4B5_CRIGR     --PVGNRGPGPNAGNNPT-----VQNGVFLPK
245
TR|C8C1S5|C8C1S5_PROCA     --LTGNS-HGPNLGSNPT-----AQNGVISPST
86
TR|Q8IWP4|Q8IWP4_HUMAN     --PTGNSTPGLNTGNNPP-----AQNGIGPLPA
294
TR|C8C1S4|C8C1S4_HETBR     --LTGNS-HGPNLGSNPT-----AQNGVISPST
86
TR|B2L7V9|B2L7V9_SAGLB     ---TGNSTPGPNNTGNNPP-----DQNGIGPVPA
25
TR|C8C1Q4|C8C1Q4_VOMUR     --PTGNDAQQPNPGNNQG-----VHPGVHSTPS
86
TR|B2L7T7|B2L7T7_MACMU     --PTGNSIPGPNNTGNNPP-----AQNGIVPLPA
136
TR|C8C1R8|C8C1R8_AMBHO     --PAGNS-NG---QNPT-----AQNGVISPPT
82
TR|B2L7V2|B2L7V2_NASLA     --PTGNSIPGLNTGNNPP-----AQNGIVPLPA
219
TR|B2L7U4|B2L7U4_COLAN     --PTGNSIPGPNNTGNNPP-----AQNGIVPLPA
98
TR|C8C1R5|C8C1R5_LAMGL     --PSGNSGGPNNTVSNPT-----AQNG---PV
81
TR|C8C1S2|C8C1S2_9EUTH     --PIGNG-HSPNPEGNPT-----AQNGVILPPT
86
TR|B2L7V5|B2L7V5_LAGLA     --PTGNSTPGPNNTGNNPP-----DQNGIGPVPA
28
TR|C8C1Q6|C8C1Q6_DELLE     --PTGNSVQGSNTVSNAT-----AQNS---PA
83
TR|C8C1S9|C8C1S9_ERIEU     --PAGNGGPGSNTVNNPA-----VQNP---SST
84
TR|C8C1R3|C8C1R3_HIPAM     --PTGNSVQRSNTVSNPT-----AQNS---PA
83
TR|C8C1S3|C8C1S3_DUGDU     --PTGNS-HDLNPGSNRT-----AQNGVISPST
86
TR|B2L7U7|B2L7U7_PANTR     -----
TR|C8C1S6|C8C1S6_ELEMA     --PTGNS-QGPNPGNDPT-----SQNGI-SPPT
85
TR|C8C1R7|C8C1R7_FELCA     --PTGNSGHGPNNTVSNPT-----AQNGVISPPT
85
TR|B2L7U0|B2L7U0_PAPAN     --XXXXXXPGPNNTGNNPP-----AQNGIVPLPA
116
TR|B2L7U8|B2L7U8_9PRIM     --PTGNSTPGLNTGNNPP-----VQNGIGPLPA
294
TR|B2L7V0|B2L7V0_HYLSY     --PTGNSTPGLNTGNNPP-----AQNGIGPLPA
238
TR|C8C1R4|C8C1R4_PIG       --PTGTSGQGPNPRSNPT-----GQNG---PA
79
TR|B2L7T5|B2L7T5_MACNE     --PTGNSIPGPNNTGNNPP-----AQNGIVPLPA
137
TR|G5CXR8|G5CXR8_MELME     --PTGNSGHGTNT-----AQNGVISPPT
82
TR|G5CXN7|G5CXN7_CALPD     --TTGKEAEMQNP-----GINLAPT
```

10/26/2014

www.uniprot.org/align/A2014102673FR3PFG6W.aln

```
78
TR|G5CXN8|G5CXN8_GLIVE      --TAGKEAEMPNP-----GIKLAPA
78
TR|D2KBL5|D2KBL5_TARRO     --PTGKEAQDQNPQNNQG-----VHPGVNSVPA
86
TR|G5CXR0|G5CXR0_TAYTA     --PTGNSGQGPNTGNSPT-----GQNS----PA
83
TR|D2KKB2|D2KKB2_PETBR     --PTGKEAQDQNPQNNQG-----VHPGVNSVPA
86
TR|G5CXQ8|G5CXQ8_OKAJO     --LAGNNGQGPNTASNPI-----VQNN----PV
82
TR|G5CXV3|G5CXV3_CERSI     --PTGNSGHGPNTGNSPT-----IQNGVIPPI
87
TR|G5CXU8|G5CXU8_OCHPR     --PTGNAGPQNTGGNPT-----AQNGVNSPPT
77
TR|G5CXP4|G5CXP4_MACLA     --PTGNDAQQNPQNNQG-----LYPGVHLSPT
86
TR|G5CXV4|G5CXV4_TAPIN     --PTGNNGHGPNVSNPT-----VQNGVIPPI
87
TR|G5CXP6|G5CXP6_CERNU     --PAGKETQAQNPENNQG-----VYPGVNSAPA
86
TR|D2KKB5|D2KKB5_PSEPE     --PTGKEAPDQNPQINQG-----VYPGVNSVPA
86
TR|G5CXN6|G5CXN6_DIDVI     --ITGKEAEVQNP-----GINLAPA
78
TR|G5CXP5|G5CXP5_ECHKA     --PTGNDAQQNPQNNQG-----LYPGVNLPT
86
TR|G5CXQ3|G5CXQ3_DASAL     --PTGNEAQAQNPQNNQG-----VYPGVNLAPT
86
TR|G5CXP1|G5CXP1_CAEFU     --TIGKETQAQDPGIDQA-----INPEINLAPT
86
TR|G5CXT0|G5CXT0_MEGLY     --PRGNSGHEPNTVNNPT-----AQNGVIPPPS
87
TR|G5CXR7|G5CXR7_MEPME     --PTGNSGLGPNT-----AQNGVISSPT
82
TR|G5CXS8|G5CXS8_FURHO     --PTGNSGPGPNTVGNPT-----AQNGVIPRPA
87
TR|G5CXT7|G5CXT7_NOCAL     --PTGNSGQGPNTVGNPA-----PPA
77
TR|G5CXV5|G5CXV5_9EUTH     --PR-NSGPGPNTGNSPT-----AQNGVITPPP
82
TR|G5CXP0|G5CXP0_NOTTY     --PTGKETQAQDPQNNQG-----ILPEVNLAPT
86
TR|G5CXV0|G5CXV0_SOLPA     --PTGS--NGPNTVGNPT-----AQNRVIP--A
83
TR|G5CXQ5|G5CXQ5_TRIMA     --PTGNS-HDLNPGSNHT-----AQNGVISHST
86
TR|G5CXV2|G5CXV2_TALAL     --PTGNSGHGPNAGSNPT-----AQNGVIPPPV
87
TR|G5CXT3|G5CXT3_PTEPA     --PTGNSGQGPNVGNPT-----AQNGVIPPPA
87
TR|G5CXU7|G5CXU7_RABIT     --PVGNGAPGQNTGNSPT-----AQNGVNSPPT
83
TR|G5CXP7|G5CXP7_MACEU     --PTGKEVPAQNPQNNQG-----VHPGVNLAPT
87
TR|G5CXX6|G5CXX6_CAVPO     --PTLNSIPGLNTGNNPT-----VQNGIFPLPT
79
TR|G5CXX9|G5CXX9_CTEGU     --PIRNPVPGPNTGSGPT-----AQNRLFPPPK
83
TR|G5CXY1|G5CXY1_9HYST     --PTLNSIPGLNTGNNPT-----AQNGIFPPPT
79
TR|G5CXY8|G5CXY8_HYDHY     --PTLNSIPGLNTGNNPT-----DQNGIFPPPT
79
TR|Q7M2M7|Q7M2M7_BOVIN     -----
TR|Q7M2M6|Q7M2M6_BOVIN     -----
TR|D2KKB9|D2KKB9_PSECU     --PTGKEAQDQNPQNNQG-----VHPGVNSIPS
86
```

10/26/2014

www.uniprot.org/align/A2014102673FR3PFG6W.aln

```
TR|G5CXV1|G5CXV1_SORAR 72 --TTGNPA-----NNPQSGIIPSPT
TR|G5CXT1|G5CXT1_9CHIR 87 --PTGNSGHGPNPTVSNPT-----VQNGGNPPPA
TR|G5CXT6|G5CXT6_NATST 87 --PTGNSGHGPNNTANNPT-----ARNGVNPSPA
TR|G5CXW0|G5CXW0_MACMU 83 --PTGNSIPGPNNTGNNPP-----AQNGVPLPA
TR|G5CXT8|G5CXT8_NYCTH 87 --PTGNSGHGPNNTANNPT-----TQNGVIPPPT
TR|G5CXU3|G5CXU3_RHIHA 87 --PRGNSGHGPNPTVSNPT-----AQNGVIPPPT
TR|G5CXR2|G5CXR2_PRILI 85 --PTGNSGHGPNPTVSNPT-----AQNGVIPPPT
TR|G5CXT9|G5CXT9_ARTJA 88 --PTGNSGQGNPTVDNPT-----AKNGVDPPPA
TR|G5CXS6|G5CXS6_CRATH 68 --PRGNSGHGPNPTVSNPT-----AQNRVVPPT
TR|G5CXU2|G5CXU2_RHICR 87 --PTGNSGHGPNNTASNPT-----TQNGVIPPPT
TR|G5CXR1|G5CXR1_TRANA 82 --PIGNNGQGNPTMNSHPT-----AQNN---PT
TR|G5CXU1|G5CXU1_NYCAL 86 --PTGNSGHGLNTVSGPT-----AQNAAIPPPA
TR|G5CXT5|G5CXT5_MYZAU 84 --PTGNGGHXKNTGNSPT-----AQNGVIPPPT
TR|G5CXS7|G5CXS7_SACBI 87 --PTGNSGQGNPAANNPT-----VQNGVIPPPT
TR|G5CXX3|G5CXX3_CAPPI 79 --PTLSNVXGLNTGNNPT-----TQNGIFPLPT
TR|G5CXZ7|G5CXZ7_SPAEH 82 --TIGNRGPGPNPGNNPT-----IQNGVFLPK
TR|G5CXX0|G5CXX0_9RODE 74 --TTGKGAPGSNTGNSPT-----VQNGVFPPI
TR|G5CXY0|G5CXY0_CTEBO 79 --PTLSNVFGLNTGNNPS-----TQNGIFPLPT
TR|G5CXZ8|G5CXZ8_9RODE 87 --PIGNRGPGPNAGNDPT-----VQNGVFLPK
TR|K9FYQ0|K9FYQ0_PEND1 522 ITSLKNNNNGPAAGSITFRRRAYAPTRDADIGGGTAIGGPGDDG-----SAFSAPT
TR|K9G341|K9G341_PEND2 834 ITSLKNNNNGPAAGSITFRRRAYAPTRDADIGGGTAIGGPGDDG-----SAFSAPT
TR|C8C1R1|C8C1R1_MESBI 83 --LTGNTVQGSNTVSNPT-----AQNS---PA
TR|C8C1R0|C8C1R0_PONBL 83 --PTGNSVQGSNTVSNPT-----AQNS---PA
TR|C8C1Q9|C8C1Q9_INIGE 83 --PTGNSVQGSNTVSNPT-----AQNS---PA
TR|C8C1S1|C8C1S1_ELERU 84 --PAGNG-PGPNPGSNP-----QHGVISPAT
TR|C8C1R2|C8C1R2_PLAMN 83 --PTGDSVQGSNTVSNPT-----AQNS---PA
TR|C8C1Q5|C8C1Q5_PHYCD 83 --PTGNTVQGSNTVSNPT-----AQNS---PA
TR|B2L7U5|B2L7U5_PANPA 294 --PTGNSTPGLNTGNNPP-----AQNGIGPLPA
TR|C8C1Q8|C8C1Q8_TURTR 83 --PTGNSVQGSNTVSNPT-----AQNS---PA
TR|C8C1S7|C8C1S7_LOXAF 85 --PTGNS-QGNPNPNPT-----AQNGI-SPPT
TR|C8C1R9|C8C1R9_CHRAS 82 --PAGNS-NG---PNPT-----AQNGVISPPT
TR|C8C1Q7|C8C1Q7_PHOPH 83 --PTGNSVQGSNTVSNPT-----AQNS---PA
TR|C8C1S8|C8C1S8_MYOLU 87 --PTGNSGHGPNNTGGNPT-----AQNGVNPHPA
TR|C8C1S0|C8C1S0_ECHTE --TPGH---GPGANPT-----AQDGVGSPPA
```

10/26/2014

www.uniprot.org/align/A2014102673FR3PFG6W.aln

```
82
TR|D8WUT7|D8WUT7_CRONI      VSAGSGTSPSQNPENKPA-----VENGTTPSPT
319
TR|D8WMZ4|D8WMZ4_ANOCA      LSEKATGANS PG-----LQNNMFSGNA
297
TR|D2KBL2|D2KBL2_9META      --PTGKEAQDQNPGINQG-----VYPGVNAIPA
86
TR|S7NIH4|S7NIH4_NYOBR      --PTGNSGHGPNTGNNPT-----AQNGVNPSPA
485
TR|D2KBL3|D2KBL3_9META      --PTGKEAQDQNPGINQG-----VYPGVNSIPA
86
TR|F5CIN2|F5CIN2_ORCOR      -----
TR|D2KBJ7|D2KBJ7_DISPE      --PTGNDAQQNPGNNGQ-----VHPGVHSTPS
86
TR|F5CIN3|F5CIN3_ZIPCA      -----
TR|D2KBK4|D2KBK4_9META      --PTGKEAQDQNPGNNGQ-----VHPGVNSIPS
86
TR|D2KBK7|D2KBK7_9META      --PTGKEAQDQNPGNNGQ-----VHPGVNSIPT
86
TR|D2KBL0|D2KBL0_9META      --PTGKEAQDQNPGINQG-----VYPGVNSIPA
86
TR|D2KBL1|D2KBL1_9META      --PTGKEAQDQNPGINQG-----VYPGVNSIPA
86
TR|D2KBK8|D2KBK8_9META      --PTGKEAQDQNPGNNGQ-----VHPGVNVIPS
86
TR|D2KBJ8|D2KBJ8_GYMLE      --PTGKEAQDQNPGNNGQ-----VHPGVNSVPA
86
TR|D2KBJ6|D2KBJ6_DACTR      --PTGKEAQDQNPGNNGQ-----VHPGVNSIPA
86
TR|D2KBJ9|D2KBJ9_9META      --PTGKEAQDQNPGISQG-----VYPGVNAVPA
86
TR|D2KBK6|D2KBK6_9META      --PTGKEAQDQNPGNNGQ-----VHPGVNSIPS
86
TR|D2KBK3|D2KBK3_PETNO      --PTGKEAQDQNPGNNGQ-----VHPGVNSVPA
86
TR|D2KBJ5|D2KBJ5_DACPA      --PTGKEAQDQNPGNNGQ-----VLPGVNSIPA
86
TR|D2KBJ4|D2KBJ4_ACRPY      --PTGKEAQVQNPGNNGQ-----VHPGVNSAPA
86
TR|D2KBK1|D2KBK1_9META      --PTGKEAQDQNPGNNGQ-----VHPGVNSVPA
86
TR|D2KBK0|D2KBK0_9META      --PTGKEAQDQNPGISQG-----VYPGVNSVPA
86
TR|D2KBL4|D2KBL4_9META      --PTGKEAQDQNPGINQG-----VYPGVNSIPA
86
TR|B2L7V7|B2L7V7_SAGLB      -----
TR|G5CXT2|G5CXT2_TADBR      --PTGNSGHGPNTVVRNPT-----AQNGVNPSPPT
87
TR|B2L7T6|B2L7T6_MACMU      -----
TR|G5CXV8|G5CXV8_CALJA      --PTVNSTPGPNTGNNPP-----GQNGIGPVPA
80
TR|B2L7V1|B2L7V1_NASLA      -----
TR|G5CXW6|G5CXW6_NYCCO      --PTGNGGLGPS-----PG-----TPNGVTPPPA
81
TR|B2L7U1|B2L7U1_COLAN      -----
TR|G5CXW2|G5CXW2_DAUMA      --PTGNSGPGQNNGGSPA-----APNGDIPPPV
83
TR|L9L5K7|L9L5K7_TUPCH      --PR-NSGPGPNTGSNPT-----AQNGGITPPP
240
TR|G5CXQ7|G5CXQ7_CERNT      --PVGNGQGPNPTVGNPT-----VQNN----PV
82
TR|B2L7V3|B2L7V3_LAGLA      -----
TR|B2L7V4|B2L7V4_LAGLA      -----
TR|G5XS2|G5XS2_PHOVI        --PTGNSGHGPNT-----AQNRVISPT
81
TR|G5XS3|G5XS3_PROLO        --PTGNSGHGPNN-----AQNGVISPTPT
82
```

10/28/2014

www.uniprot.org/align/A2014102673FR3PFG6W.aln

```
TR|G5CXW3|G5CXW3_OTOGA 83 --PAGNGGPGPSTGGSPA-----TPNGVTPPPA
TR|G5CXR4|G5CXR4_FOSFO 85 --PTGNSSRGPNPTVSNPT-----AQNGVISPPT
TR|G5CXV9|G5CXV9_CEBAL 80 --PTGNSTPGPNTGNNPP-----DQNGTRPVPA
TR|G5CXR9|G5CXR9_NANBI 87 --STGNSGHGSNTVNNPT-----AQNGVISPPI
TR|G5CXQ4|G5CXQ4_MYRFA 84 --PTGKEA--QNPQNNQG-----VYPGVNVAPA
TR|G5CXU9|G5CXU9_9EUTH 84 --PVGNGGPGSNTGNNPA-----AQNP---SPT
TR|B2L7T8|B2L7T8_PAPAN 82 -----
TR|G5CXW1|G5CXW1_MICMU 80 --PTGNSTPGPNTGNNPP-----DQXGIGPVPA
TR|G5CXQ6|G5CXQ6_ANTAM 82 --PAGNNGQGPNPTVSNPT-----VQNN---PV
TR|G5CXU5|G5CXU5_CYNVO 83 --PTGNSTPGPNTGNSPT-----TQNGVTQSPA
TR|G5CXQ0|G5CXQ0_AEPRU 87 --PTGKEAPAQNPQNNQG-----VHPGVNLAPT
TR|G5CXR3|G5CXR3_AILFU 82 --PTGNSGHGANT-----AQNGVLSPTT
TR|G5CXV6|G5CXV6_TUPMI 82 --PR-NSGPGPNPTGNSPT-----APNGGITPPP
TR|G5CXQ1|G5CXQ1_HYPMS 87 --PTGKEAPAQNPQNNQG-----VHPGVNLAPT
TR|G5CXP8|G5CXP8_TRIVU 86 --PAGKEAQAQNPQNNQG-----VHPGVNLAPA
TR|G5CXU6|G5CXU6_GALVR 83 --PTGNAGPQNPNTGNSPT-----TQNGVTQSPA
TR|G5CXR5|G5CXR5_SURSU 85 --PTGNSGHGPNPTVSNPT-----AQNGVISPPT
TR|G5CXP3|G5CXP3_ISOMA 86 --PTGNDAQQNPQNNQG-----LYPGANLPPT
TR|G5CXS9|G5CXS9_HIPCO 87 --TTGNSGGQPNPTASNPT-----TQNGXVPAPA
TR|G5CXS1|G5CXS1_ARCFO 80 --PTGNS--GPNT-----AQNGVISPST
TR|G5CXR6|G5CXR6_CROCR 85 --PTGNSGHGPNPTVSNPM-----AQNGVISPPT
TR|G5CXS4|G5CXS4_AILME 77 --PT-----GPNM-----AQNGVNSPPT
TR|G5CXP2|G5CXP2_RHYRA 86 --IIGKETQAQDPGINQA-----INPEIHLAPT
TR|G5CXW5|G5CXW5_LEMCA 83 --PTGNGGPGVNTGGSPT-----TQNSVIPSAPA
TR|G5CXW4|G5CXW4_PROVE 107 --PTGNGGPGVNTGGSPTTQNGGSPT-----TQNGGSPTTQNGGSPTTQNGVVPXPA
TR|G5CXP9|G5CXP9_PHACI 87 --PTGNDAQQNPQNNQG-----VHPGVHSAPT
TR|G5CXS0|G5CXS0_9CARN 80 --PTGNS--GPNT-----DQNGVISPST
TR|G5CXS5|G5CXS5_GENGE 85 --PTGNNGHGPNTMSNPT-----AQNGVVSPTT
TR|G5CXN9|G5CXN9_DROGL 86 --PTGKEAQDQNPQNNQG-----VHPGINLAPT
TR|G5CXT4|G5CXT4_MYSTU 87 --PTGNSGQPNPTGGNPT-----GPNGAIPAPA
TR|G5CXU4|G5CXU4_THYTR 87 --PTGNSGHGPNNAAGNPT-----AQNGVIPSAPA
TR|G5CXU0|G5CXU0_PTEGI 88 --PTGNSAHGPNPTVSGPT-----AQNGAIPPPA
TR|B2L7T4|B2L7T4_MACNE 82 -----
TR|G5CXQ9|G5CXQ9_9CETA 82 --PTGNGGQPNPTVSNPT-----VQNN---PV
```

10/26/2014

www.uniprot.org/align/A2014102673FR3PF6W.aln

```

TR|G5CXY2|G5CXY2_9HYST 79 --PTLPSPGLSTGNSPA-----VQSGIFPLPT
TR|G5CXX7|G5CXX7_CHILA 79 --PTLTNPGLNTGNNPT-----APNGIFPLPT
TR|G5CXZ6|G5CXZ6_9HYST 83 --PIRNSVPGPNTGNNPT-----AQNRIFFLPK
TR|G5CXY3|G5CXY3_JACJA 77 --VVGGRTPGPSTGSTPT-----VQLGVFPPT
TR|G5CXZ0|G5CXZ0_GRAMU 82 --PTGINPPGPNTGSNPT-----AQNGVLPAPT
TR|G5CXY7|G5CXY7_DIPHE 82 --TTGNSAPGQNPGSNPT-----PQNRVFP LPR
TR|G5CXZ3|G5CXZ3_9HYST 78 --PTLSSVPLNPGNIP I-----VPSRIFFLP R
TR|G5CXZ5|G5CXZ5_THRSW 71 --PTLSTVPGINP-----NRIFPIPR
TR|G5CXX1|G5CXX1_APLRU 83 --PTGNNAPGPNTASNPT-----TQNGALPPPL
TR|G5CXY5|G5CXY5_EREDO 79 --PTLNNLPGLNAGNNPT-----AQGGVFP PRT
TR|G5CXW8|G5CXW8_ABRBE 79 --PTLNNLPGLNTGNNPT-----AQNGIFPLPT
TR|G5CXX5|G5CXX5_CASCN 75 --TTGNSAPGRNTGSNPT-----GQNRVLQPVV
TR|G5CXZ4|G5CXZ4_TAMST 82 --PTGNNAPGPNI GNNPT-----AKNGVFP PPS
TR|G5CXW9|G5CXW9_CUNTA 79 --PTLNSIPGLNTGNNPT-----AQNGIFFPPT
TR|G5CXZ2|G5CXZ2_PEDCA 82 --TTGNSVPGSNTRSNPT-----AQNGILP PPI
TR|G5CXX4|G5CXX4_MYOCO 79 --PTLSNVPGLNTGNNPT-----TQNGIFPLPT
TR|G5CXY6|G5CXY6_CRACA 82 --TTGNSAPGRNTGSNPT-----AQNRVFP LPR
TR|G5CXY4|G5CXY4_HOPGY 79 --PILSNVPGMNTGNNPT-----AQNGIFPLPT
TR|G5CXX8|G5CXX8_CRIGR 87 --PVGNRGPGPNAGNNPT-----VQNGVFP LPK
TR|G5CXZ1|G5CXZ1_OCTGL 79 --PTLSNVPGLNTGNNPI-----GQNGIFPLPT
TR|G5CXX2|G5CXX2_HETGA 78 --PTLNNVPGLNTGNNPT-----AQNGIFPLPR
TR|G5CXY9|G5CXY9_HYSBR 79 --PTLSNVPGLNTGNNPT-----AQNGIFFPPT
TR|Q8NFB4|Q8NFB4_HUMAN 240 --PSGNSGQGPNTVSNPT-----AQNG----PV
TR|G7MT52|G7MT52_MACMU 234 --PTGNSIPGPNTGNNPP-----AQNGIVPLPA
TR|L8IJZ2|L8IJZ2_9CETA 280 --PAGNNGQDPNTVSNPT-----VQNN----PV
TR|Q4R358|Q4R358_MACFA 76 --PTGNSIPGPNTGNNPP-----AQNGIVPLPA
TR|V8NY54|V8NY54_OPHHA 98 I STTNNEANFPGLSKK-----IV-----SGNGI-PTPS
TR|B2L7V8|B2L7V8_SAGLB -----
TR|B2L7U2|B2L7U2_COLAN -----
TR|B2L7U3|B2L7U3_COLAN -----
TR|B2L7T9|B2L7T9_PAPAN -----
TR|B2L7V6|B2L7V6_SAGLB -----
TR|B2L7U9|B2L7U9_HYLSY -----
TR|A0A061IKW6|A0A061IKW6_CRIGR 302 --PVGNRGPGPNAGNNPT-----VQNGVFP LPK
TR|A0A061IJS1|A0A061IJS1_CRIGR 288 --PVGNRGPGPNAGNNPT-----VQNGVFP LPK
SP|P02769|ALBU_BOVIN -----
TR|F1MKR5|F1MKR5_BOVIN -----PAGNNGQDPNTVSNPT-----VQNN----PV

```

10/26/2014

www.uniprot.org/align/A2014102673FR3PFG6W.aln

```

296
TR|H2QPM0|H2QPM0_PANTR          --PTGNSTPGLNTGNNPP-----AQNIGPLPA
294
TR|G3X143|G3X143_SARHA          --PTGNEAQAQNPNGNQ-----VYPGVNLAPS
306
TR|F7HPL6|F7HPL6_CALJA         --PTVNSTPGPNTGNNPP-----GQNGIGPVPA
290
TR|H2PDI6|H2PDI6_PONAB         --PTGNSTPGLNTGNNPP-----AQNIGPLPA
294
TR|M3X473|M3X473_FELCA         --PTGNSGHGPNNTVSNPT-----AQNIGVISPT
298
TR|G1R843|G1R843_NOMLE         --PTGNSTPGLNTGNNPP-----AQNIGPLPA
117
TR|G3RLI8|G3RLI8_GORGO         --PTGNSTPGLNTGNNPP-----VQNGIGPLPA
294
TR|G1KW91|G1KW91_ANOCA         LSEKATGANS PG-----LQNNMFSGNA
297
TR|T2B203|T2B203_9EUTH         --PIGNG-HSPNPEGNPT-----AQNIGVLPPT
75
TR|T2B2P6|T2B2P6_9EUTH         --PIGNG-HSPNPEGNPT-----AQNIGVLPPT
72
TR|T2B2M4|T2B2M4_9EUTH         --PIGNG-HSPNPEGNPT-----AQNIGVLPPT
75
TR|T2B431|T2B431_9EUTH         --PIGNG-HSPNPEGNPT-----AQNIGVLPPT
70
TR|T2B3N3|T2B3N3_9EUTH         --PIGNG-HSPNPEGNPT-----AQNIGVLPPT
75
TR|B1ACV5|B1ACV5_MESBI         -----
TR|T2B2N6|T2B2N6_9EUTH         --PIGNG-HSPNPEGNPT-----AQNIGVLPPT
74
TR|T2B3W8|T2B3W8_9EUTH         --PIGNG-HSPNPEGNPT-----AQNIGVLPPT
73
TR|T2B410|T2B410_9EUTH         --PIGNG-HSPNPEGNPT-----AQNIGVLPPT
70
TR|T2B420|T2B420_9EUTH         --PIGNG-HSPNPEGNPT-----AQNIGVLPPT
74
TR|T2B3P2|T2B3P2_9EUTH         --PIGNG-HSPNPEGNPT-----AQNIGVLPPT
74
TR|T2B3N8|T2B3N8_9EUTH         --PIGNG-HSPNPEGNPT-----AQNIGVLPPT
71
TR|T2B1Z8|T2B1Z8_9EUTH         --PIGNG-HSPNPEGNPT-----AQNIGVLPPT
61
TR|T2B3X8|T2B3X8_9EUTH         --PIGNG-HSPNPEGNPT-----AQNIGVLPPT
75
TR|T2B208|T2B208_9EUTH         --PIGNG-HSPNPEGNPT-----AQNIGVLPPT
73
TR|T2B3Y2|T2B3Y2_9EUTH         --PIGNG-HSPNPEGNPT-----AQNIGVLPPT
68
TR|T2B3M8|T2B3M8_9EUTH         --PIGNG-HSPNPEGNPT-----AQNIGVLPPT
75
TR|T2B417|T2B417_9EUTH         --PIGNG-HSPNPEGNPT-----AQNIGVLPPT
75
TR|T2B2P0|T2B2P0_9EUTH         --PIGNG-HSPNPEGNPT-----AQNIGVLPPT
65
TR|T2B3X3|T2B3X3_9EUTH         --PIGNG-HSPNPEGNPT-----AQNIGVLPPT
75
TR|F7HPM2|F7HPM2_CALJA         --PTVNSTPGPNTGNNPP-----GQNGIGPVPA
290
TR|B1ACV1|B1ACV1_EUBAS         -----

SP|O97939|ENAM_PIG             VN-----VSGQGVPRSQS--P-----WGPRQTIIH--ENYPN--PNIRGFPARRQW
329
SP|Q9NRM1|ENAM_HUMAN           VN-----ASGQGGPGSQI--P-----WRPSQPNIR--ENHPY--PNIRNFPSGRQW
334
SP|O55196|ENAM_MOUSE           VN-----VSGQGVPKSQI--P-----WRPSQPNIIY--ENYPY--PN---YPSEKQW
335

```

Appendix 4

Poster presentation at Faculty of Medicine Postgraduate Research day at Weetwood Hall November 4th 2009. Winner of best laboratory poster and peoples choice award.

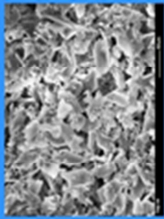


MEND YOUR OWN TEETH

Nicola Kingswell, Oral Biology, Leeds Dental Institute

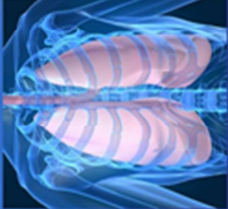


1. Tooth enamel is the hardest substance in the human body. Unlike bone, tooth enamel cannot repair itself after damage. More than a third of British 5-year olds have suffered tooth decay. New materials for tooth repair are needed, but wouldn't it be great if there was a way to encourage your own body to aid the repair?



The mineral crystals in tooth enamel consist of calcium and phosphate and are known as hydroxyapatite (HAP) $\text{Ca}_{10}(\text{PO}_4)_6(\text{OH})_2$

2. Biomineralisation is when organic compounds (such as proteins) interact with inorganic compounds (such as mineral crystals) to create tough substances in the body (such as teeth and bone, and shells on snails and shellfish).



My research is to investigate tooth formation. I am particularly interested in how the proteins in tooth enamel form the matrix, how they interact with one another and the mineral crystals. This research could lead to developing new treatments for caries.

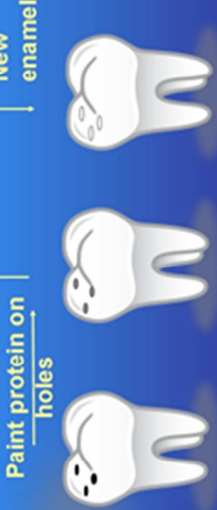
3. When tooth enamel is first made by the body, the HAP crystals grow on a protein net called the extracellular matrix (ECM). This net is removed as the tooth matures so the enamel erupting in our mouths contains >90% HAP. This makes it difficult to repair damaged enamel, as there is no protein net for new HAP crystals to grow on.

4. Tooth decay involves acid dissolving millions of little holes in enamel. Proteins that encourage HAP crystal growth could be applied to these holes so that the holes are repaired using natural tooth material. This could mean the end of the dentists' drill and amalgam fillings!

Paint protein on holes

HAP growth

New enamel



UNIVERSITY OF LEEDS

Poster presentation at Leeds Dental Institute Research day November 18th 2009.
Winner of best poster prize.

Leeds Dental Institute
FACULTY OF MEDICINE AND HEALTH

UNIVERSITY OF LEEDS

32 KDa Recombinant Enamelin Induces Hydroxyapatite Nucleation *In Vitro*

N. J. Kingswell^{1*}, S. J. Brookes¹, J. Maycock¹, C. A. Shuttleworth², R. C. Shore¹, J. Kirkham¹

¹Department of Oral Biology, Leeds Dental Institute, University of Leeds
²School of Biological Sciences, University of Manchester

1. Introduction

Dental enamel is the most highly mineralised of all the skeletal tissues. Proteins of the developing enamel matrix are thought to control mineral deposition and growth within the tissue. Enamelin is a minor protein component of the developing matrix, constituting < 1% of all enamel matrix proteins and present mainly as a 32 kDa fragment. Mutations in the *ENAM* gene are associated with inherited enamel defects ('amelogenesis imperfecta (AI)') - see Figure 1), suggesting that enamelin plays a fundamental role in enamel biomineralisation.



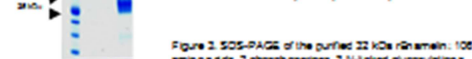
2. Aims

To identify a role for enamelin in enamel biomineralisation by expressing human 32 kDa enamelin as a recombinant protein and characterising its ability to control mineral growth *in vitro* in a steady state system.

3. Methods and Materials

Recombinant 32 kDa enamelin

rEnamelin was expressed in a eukaryotic system (cDNA clone - pCep-PU expression vector - 293-EBNA cells) and purified prior to use.



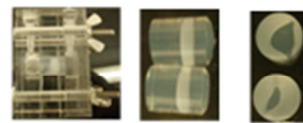
Steady-State Agarose Gel System



rEnamelin (1 µg/mL - 10 µg/mL), or poly glutamic acid (PGA - 10 µg/mL) in agarose were placed in a modified dialysis cell. Buffers containing 3.9 mM P and 6.5 mM Ca were pumped counter-currently at 1 mL/cell/hour for 7 days at 37°C. (Hunter and Goldberg, PNAS 1993).

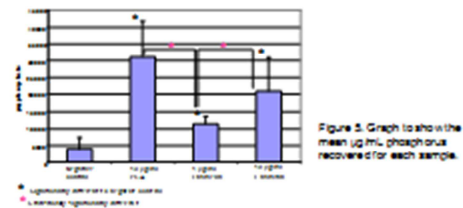
4. Results

Visual



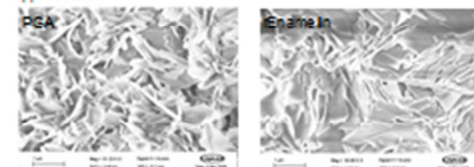
Phosphorus Assay

The gel plugs were washed in nitric acid and used in the colorimetric phosphomolybdate assay (Chen et al. Analytical Chemistry 1956) to determine the phosphorus content of the gels.



Scanning Electron Microscopy

SEM suggested that that crystals nucleated by PGA had a rosette formation while those nucleated by rEnamelin had a large, planar appearance.



EDX analysis of the crystals gave a Ca:P ratio of 1.65 for enamelin and 1.62 for PGA nucleated crystals. The theoretical ratio for hydroxyapatite is 1.66.

5. Conclusions

Recombinant 32 kDa enamelin is able to nucleate and support the growth of mineral crystals under the steady state conditions *in vitro* supporting a possible role for enamelin in enamel biomineralisation.

This work is supported by the Wellcome Trust programme 075945